National Aeronautics and Space Administration

Glenn Research Center at Lewis Field
Cleveland • Ohio

NASA/TM—2006-214016

# R&T RESEARCH AND TECHNOLOGY

# 2005

# ABOUT THE COVER:

Top left: At this year's Desert Research and Technology Studies (Desert RATS) field outing in Meteor Crater, Arizona, Glenn researchers provided integrated communications and data systems for two space-suited subjects as well as interaction with NASA Johnson Space Center's Science Crew Operations and Utility Testbed (SCOUT) rover (p. 27).

Top right: This 4- by 6-m offset-parabolic inflatable membrane reflector developed by Glenn and SRS Technologies produced a gain of about 48 dB at 8.4 GHz at Glenn's near-field antenna range. This corresponds to about 51 percent efficiency when compared with an ideal antenna, and 67 percent efficiency when the effect of the feed horn is considered. The goal is to develop large antennas for deep-space (Moon and Mars) applications that have very low mass, lower cost, and improved deployment reliability while maintaining very accurate surface tolerances during long missions (p. 16).

Center left: Closeup of a state-of-the-art active clearance control test rig showing internal components. The new rig, which was fabricated and installed at Glenn, employs a fast-acting mechanical actuation system designed to improve on existing clearance-control methods in the high-pressure turbine section of a modern jet engine (p. 108).

Bottom left: Researchers preparing to conduct an impact test on a space shuttle external tank panel in Glenn's Ballistic Impact Laboratory. As a result of Glenn's testing, the design of the space shuttle orbiter windows was changed, the external tank was cleared as safe to fly, and a previously unavailable physics-based impact analysis capability was established for the space shuttle program (p. 93).

Bottom right: A Glenn researcher examines a reaction control system thruster for cracking in the relief radius. Because hot combustion gases might leak through such cracks and damage the space shuttle orbiter, in-depth analyses and mechanical tests were conducted to determine the cause of the cracking. Results supported the conclusion that hydrogen embrittlement, not stress corrosion or hot-salt cracking, was the likely cause (p. 102).

# RESEARCH & TECHNOLOGY 2005


National Aeronautics and
Space Administration

**Glenn Research Center**
Cleveland, Ohio 44135–3191

NASA/TM—2006-214016

Trade names or manufacturers' names are used in this report for identification only. This usage does not constitute an official endorsement, either expressed or implied, by the National Aeronautics and Space Administration.



Available from

NASA Center for Aerospace Information
7121 Standard Drive
Hanover, MD 21076

National Technical Information Service
5285 Port Royal Road
Springfield, VA 22100

Available electronically at http://www.grc.nasa.gov/WWW/RT/

# Introduction

At the NASA Glenn Research Center, in partnership with U.S. industry, universities, and other Government institutions, we develop critical systems technologies and capabilities that address national priorities. Our world-class research, technology, and capability development efforts are keys to advancing space exploration of our solar system and beyond while maintaining global leadership in aeronautics. Our work is focused on technological advancements in space flight systems development, aeropropulsion, space propulsion, power systems, nuclear systems, communications, and human-related systems.

Glenn's main campus is situated on 350 acres adjacent to the Cleveland Hopkins International Airport. It has more than 140 buildings that include 24 major facilities and over 500 specialized research and test facilities. In addition, Plum Brook Station, located 50 miles west of Cleveland, offers four large, world-class facilities for space technology and capability development on a 6400-acre installation. All Center capabilities are available for Government and industry programs through Interagency or Space Act Agreements.

The Glenn team consists of over 3100 civil service employees and support service contractor personnel. Scientists and engineers comprise more than half of our workforce, while technical specialists, skilled workers, and an administrative staff support them. We aggressively strive for technical excellence through continuing education, increased diversity in our workforce, and continuous improvement in our management and business practices so that we can expand the boundaries of space and aeronautics technology.

The Center's activities support all NASA missions and the major programs of our Agency. We contribute to economic growth and national security by developing technology for safe, superior, and environmentally compatible U.S. aircraft propulsion systems. Glenn leads NASA's research in the fields of fluids, combustion, and reacting flow systems, including gravity variation. Glenn also leads in the testing and evaluation of materials and structures for atmospheric and space environments by utilizing our first-rate facilities and world-class researchers. Almost every space shuttle science mission has had an experiment managed by Glenn, and we have conducted a wide array of experiments on the International Space Station.

Knowledge generation and management are among our most important activities. Our annual Research & Technology report helps make this knowledge available to potential users in the technical community. This report is organized such that a broad cross section of people can readily use it. Each article begins with a short introductory paragraph and continues with a summary of the progress made during the year in various scientific and technical areas.

I hope that this information is useful to you. If additional information is desired, you are encouraged to contact the researchers identified at the end of each article and to visit Glenn's Web site at www.grc.nasa.gov.

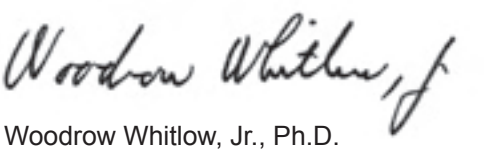

Woodrow Whitlow, Jr., Ph.D.
Director

# NASA Glenn Research Center Senior Management

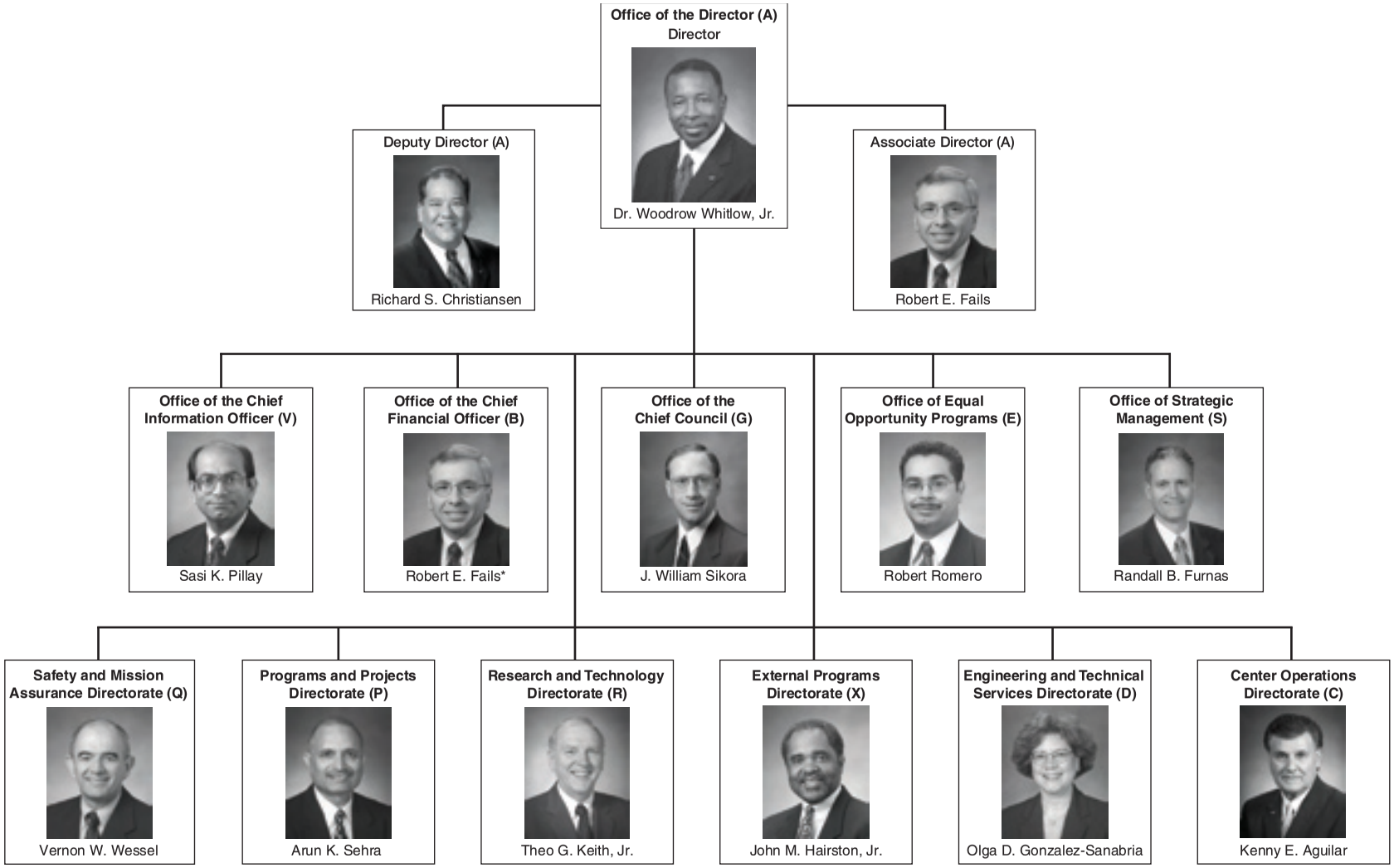


*Acting

CD–48534
February 9, 2006

# NASA Glenn Research Center at Lewis Field

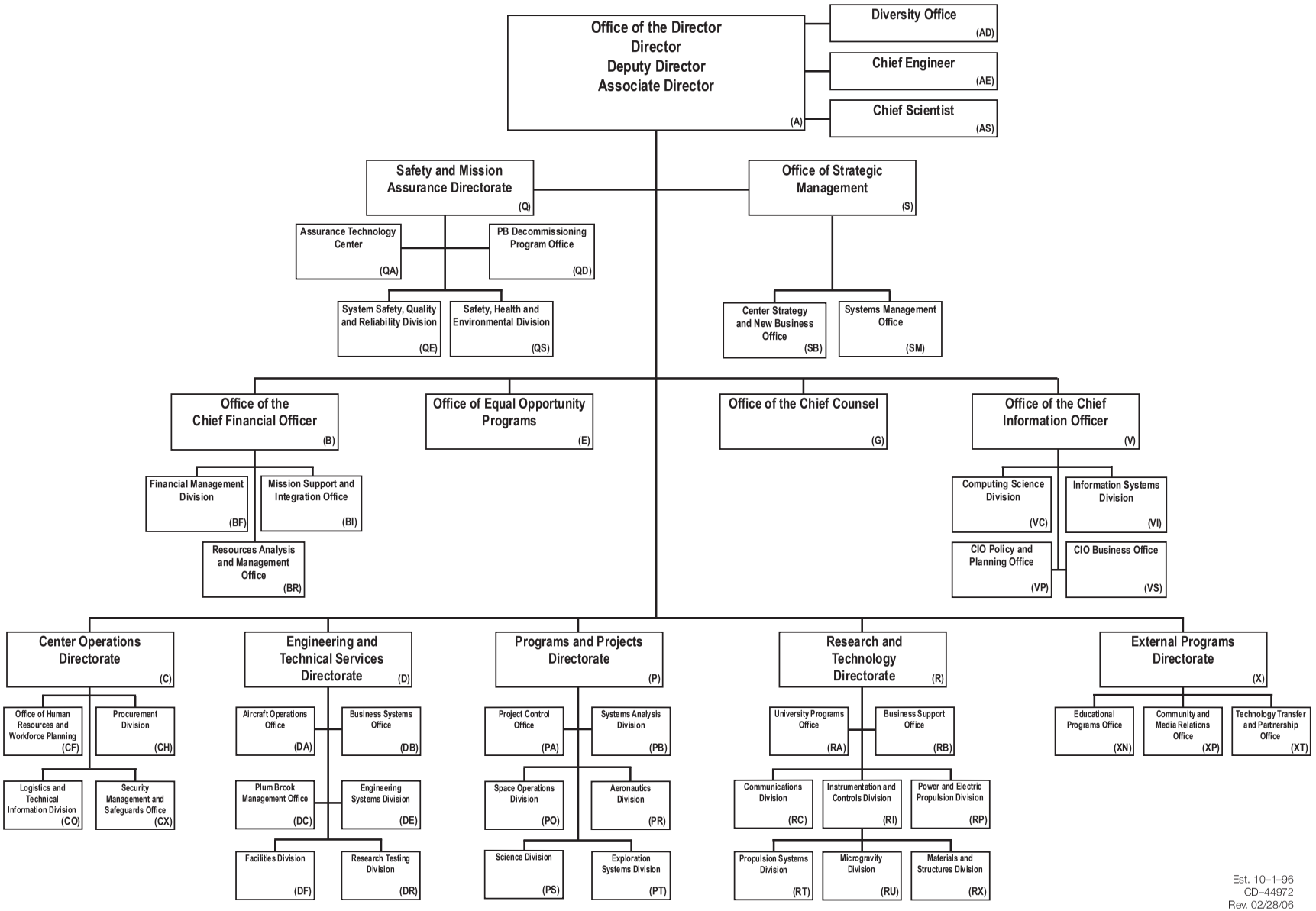


Est. 10–1–96
CD–44972
Rev. 02/28/06

# CONTENTS

## Programs and Projects

### Systems Analysis



### Exploration Systems



## Research and Technology

### Communications



### Instrumentation and Controls

## Power and Electric Propulsion



## Propulsion Systems



## Materials and Structures

# Engineering and Technical Services

## Engineering Systems



# Appendixes

# PROGRAMS AND PROJECTS

## SYSTEMS ANALYSIS
## EXPLORATION SYSTEMS

# Analytical Core Noise Model Improved for Modern Turbofan Engines

Dramatic reductions in civilian aircraft noise have been achieved since the introduction of the turbojet and low-bypass turbofan commercial engines in the late 1950s. A major contributing factor to this decline in noise has been major NASA-sponsored noise-reduction research programs. Over the past two decades, cooperative NASA/industry technology programs—such as the Advanced Subsonic Technology Program, the High-Speed Research Program, and the Vehicle Systems Program—have supported engine noise-reduction research. Recently, a robust, generalized method for predicting aircraft engine core noise was developed and coded into NASA's computer programs used for aircraft noise prediction.

Primary emphasis has historically been directed to the principal turbofan engine noise sources: the jet and the fan. With NASA's 20-year goal to develop technologies for reducing aircraft noise by 20 EPNdB (effective perceived noise in decibels) relative to the 1997 state of the art, this focus has been appropriate. However, as fan and jet noise are reduced, other engine noise sources, albeit lesser, are "uncovered" and become important.

The noise of the engine "core," classified principally as noise emanating from the unsteady heat release of the combustion process, is perhaps the most important of these other propulsion-related sources. Now that many fan and jet noise-reduction technologies have been successful, core noise needs to be addressed in order to meet the Agency's aggressive noise-reduction goal, especially with the advent of modern, high-pressure and high-temperature cores. It is, therefore, important that core noise be better understood and more accurately predicted.

Therefore, NASA sponsored GE Aircraft Engines to conduct acoustic engine measurements and subsequent analytical core noise modeling under a Revolutionary Aerospace Engine Research task order (ref. 1). In this task, which was awarded and monitored by the NASA Glenn Research Center, GE collected static acoustic data from four turbofan engines—the CF34, the CFM56, the CF6, and the GE90—representing an extremely wide span of thrust classes (see the photograph). Modern Technologies Corporation was subcontracted to develop semiempirical core-noise relationships for each of the engine classes.

*Outdoor engine acoustic ground testing conducted at GE Aircraft Engine's Peebles Test Facility.*

The results from the preliminary core-noise models were encouraging, but since correlating core noise is quite complex, there was a need for further improvement. For example, the calibration coefficients and the spectral character of the initial model changed from engine to engine, resulting in a noise-prediction method that was valid only for the individual engine type, rather than a general method for engines of all types and thrust classes. Modern Technologies was subsequently contracted to perform a follow-on task funded by NASA's Quiet Aircraft Technology project (ref. 2). In this effort, Modern Technologies discerned the internal geometric combustor design factors and thermodynamic parameters that influence the core's spectral content and levels. This resulted in a robust, generalized, and more physics-based core-noise-prediction method, which was subsequently coded into NASA's computer programs used for aircraft noise prediction.

**References**

1. Data-Based Core Noise Prediction Models by Modern Technologies Corporation. GEAE–NASA RASER Task Order 21: Modern Propulsion System Core Noise Evaluation, 2005 (to be published as a NASA CR).
2. Stone, J.R.; Krejsa, E.A.; and Clark, B.J.: Enhanced Core Noise Modeling for Turbofan Engines. NASA Contract NAS3–00178, Task Order 15, 2005 (to be published as a NASA CR).

**Glenn contact:**
Jeffrey J. Berton, 216–977–7031, Jeffrey.J.Berton@nasa.gov

**Author:**
Jeffrey J. Berton

**Headquarters program office:**
VSP

**Programs/Projects:**
QAT, RASER

# Cruise-Efficient, Low-Noise, Short-Takeoff-and-Landing Vehicle Studied for the Revolutionary System Concepts for Aeronautics Project

A novel, low-noise, short-takeoff-and-landing vehicle concept with a distributed propulsion system is being investigated to meet the growing future aviation market. For this concept, the blended-wing body configuration was selected for its cruise-efficient airframe with sufficient wing volume available for an embedded-wing, distributed propulsion system.

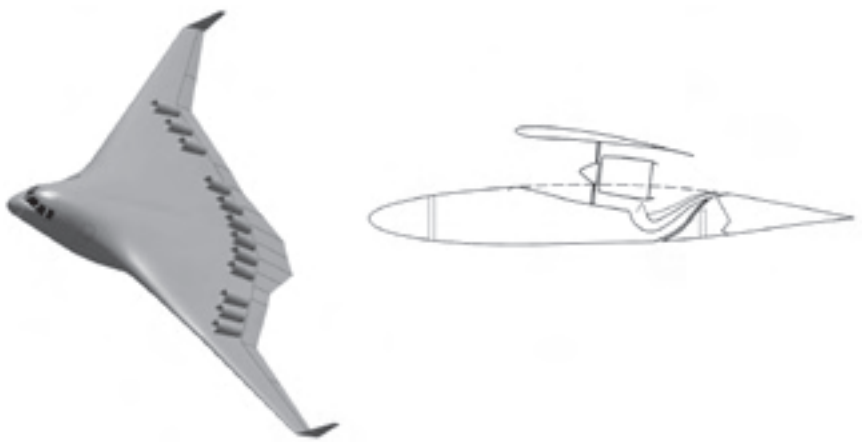

*Cruise-efficient, low-noise, short-takeoff-and-landing vehicle concept.*

The saturation of airports and the impact to the surrounding airspace and terrestrial communities are rapidly increasing limits to world aviation travel. Breakthrough concepts that enable increased air traffic and performance and decreased noise are required for growing future aviation markets. Subsonic commercial concepts appearing on the 25-year horizon must facilitate an increase in air traffic more than 4 times greater than current levels, while complying with more stringent respect for the surrounding communities across the expanding world market. Attacking these issues holistically is the concept of a short-takeoff-and-landing high-speed subsonic transport, which enables 24-hr expanded use of the untapped regional airspace. The concept is a high-lift-capable airframe, which employs embedded-wing, spanwise-distributed propulsion to meet rigorously defined airport operation requirements while maintaining efficient cruise capability.

The initial concept was conceived by NASA Glenn Research Center's Aeropropulsion System Analysis Office, and a proposal was submitted to NASA Headquarters' Revolutionary System Concepts for Aeronautics project. The proposal was competed among NASA's aeronautics centers and selected for funding. For the vehicle configuration, Boeing's Phantom Works Division (Huntington Beach, CA) was selected to develop a conceptual aircraft. The current vehicle concept has a 40,000-lb payload capability with a 3000-nautical mile range at a cruise mach number of 0.8. Because of its short-takeoff-and-landing characteristics, the vehicle will be able to take off and land within a 5000-ft field length, which captures 84 percent of all U.S. regional airports. For the noise study of distributed propulsion concepts and the new vehicle configuration, Diversitech, Inc. (Cincinnati, OH), is investigating the benefits of distributed propulsion systems and the effect of the vehicle on the airport community. To reduce the aircraft noise well below the current requirements, designers have employed noise shielding using the large blended-wing body upper surface, acoustic treatment of inlets and nozzles, and distribution of the thrust streams next to each other to attenuate noise propagation.

At the end of this conceptual study, a final report will be written and presented at NASA Headquarters. The report will include a technology assessment to determine technology gaps and to identify relevant technology challenges and investments for future research.

**Glenn contacts:**
Hyun D. Kim, 216–433–8344, Hyun.D.Kim@nasa.gov;
Jeffrey J. Berton, 216–977–7031, Jeffrey.J.Berton@nasa.gov; and
Scott M. Jones, 216–977–7015, Scott.M.Jones@nasa.gov

**Authors:**
Hyun D. Kim, Jeffrey J. Berton, and Scott M. Jones

**Headquarters program office:**
Aeronautics Research

**Programs/Projects:**
Revolutionary System Concepts for Aeronautics

# Water Injection in Commercial Aircraft Investigated for Increasing Engine Life and Reducing Costs and Emissions

Water-injection technology has historically been used in aviation to increase jet engine thrust and is presently used for ground power applications to increase gas turbine power and life, and to reduce the emissions of oxides of nitrogen ($NO_x$). Analytical systems studies were performed at the NASA Glenn Research Center to estimate the effects of water injection on a commercial turbofan engine to reduce specific fuel consumption (SFC), $NO_x$ emissions, and engine hot-section temperatures while maintaining constant thrust. The subsequent reduction in hot-section temperatures could increase engine life and reduce maintenance costs. In-house efforts included engine cycle modeling and mission analysis. Contracted efforts repeated and verified the in-house results. The researchers also developed preliminary schematics with the hardware required to implement this technology and estimated the changes to engine life and maintenance cost.

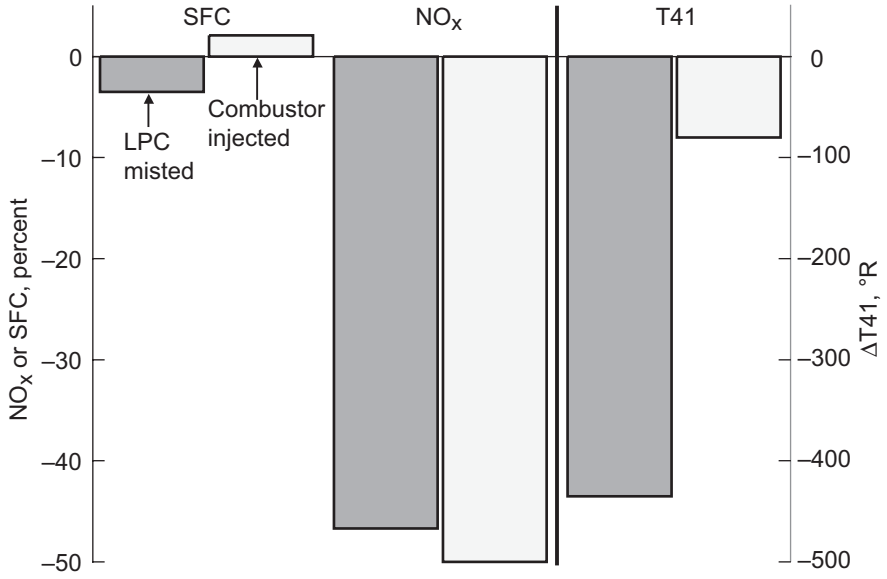


*The LPC water-misting system achieved lower SFC rates, $NO_x$ emissions, and turbine rotor inlet temperatures (T41) for 59 °F standard-day conditions.*

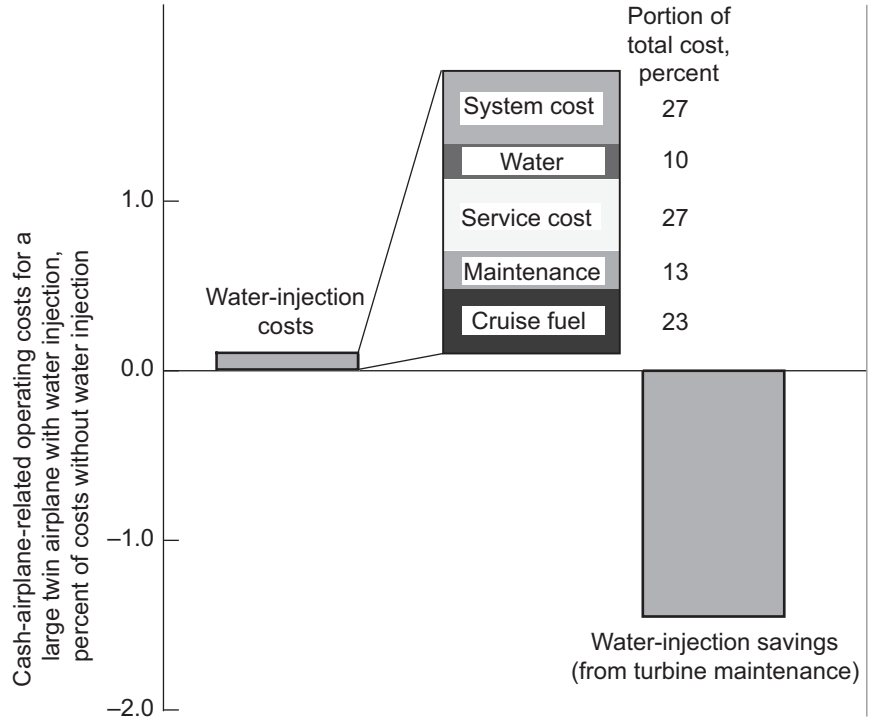


*Maintenance savings offset water-injection costs.*

The baseline vehicle was a 300-passenger aircraft using two high-bypass turbofan engines. Water injection before the low-pressure compressor (LPC) yielded greater reductions in maximum temperature and fuel consumption than combustor water injection, but it required almost twice as much water during the takeoff cycle. Water could be used through top-of-climb for continued reduction of the maximum cycle temperature and emissions, but this would require large amounts of water.

Estimates of hot-section life improvement from the lower temperatures with water injection would vary depending on engine type (for engines that experience higher removal or maintenance rates because of turbine blade temperature distress, water injection would be of more value). However, a breakdown of water-injection costs with average estimated engine maintenance savings suggests that savings could well offset the added costs of water injection.

Even though water injection is quite successful in reducing $NO_x$ emissions during takeoff, low-emission combustors are still needed for the cruise and climb portions of the flight. Although the $NO_x$ emission rate is high during takeoff and initial climbout,

most $NO_X$ is generated during the long cruise and climb periods where water injection is impractical because of the large quantity of water that would be required. Other considerations are potentially reduced smoke emissions but potentially increased hydrocarbon and carbon monoxide emissions, depending on the engine cycle. This will require further investigation if water injection is to be incorporated in new or existing engines.

**Bibliography**

Daggett, D.L., et al.: Water Injection: Disruptive Technology to Reduce Airline Emissions and Maintenance Costs. SAE Paper 2004–01–3108, 2004.

Daggett, David L.; and Hendricks, Robert C.: Water Misting and Injection of Commercial Aircraft Engines to Reduce Airport $NO_x$. NASA/CR—2004-212957, 2004. http://gltrs.grc.nasa.gov/cgi-bin/GLTRS/browse.pl?2004/CR-2004-212957.html

**Find out more about this research:**

**Propulsion and Power Project:**
http://www.grc.nasa.gov/WWW/AERO/base/psbase.htm

**Society of Automotive Engineers Environmental Excellence in Transportation Awards:** http://www.sae.org/news/releases/05transportation_award.htm

**Glenn contacts:**
Christopher A. Snyder, 216–977–7018, Christopher.A.Snyder@nasa.gov;
Jeffrey J. Berton, 216–977–7031, Jeffrey.J.Berton@nasa.gov; and
Robert C. Hendricks, 216–977–7507, Robert.C.Hendricks@nasa.gov

**Author:**
Christopher A. Snyder

**Headquarters program office:**
Aeronautics Research

**Programs/Projects:**
Future Propulsion Systems Research

**Special recognition:**
Runner-up, Society of Automotive Engineers (SAE) 2004 Environmental Excellence in Transportation Award

## XLerator Software Released

XLerator, a command-line program integration add-in for Microsoft Excel (Microsoft Corporation, Redmond, WA), was made available for download on NASA Glenn Research Center's software repository in 2005. Many scientists and engineers find themselves working with legacy software tools, with more current tools that have unintuitive text file interfaces, or with a feature set that does not completely fill their needs. XLerator allows command-line programs to be used as simple functions from within a spreadsheet environment that is familiar to a large number of people in scientific and engineering fields.

With XLerator, Excel's optimization and targeting capabilities can be wrapped around existing tools, spreadsheet-based graphical interfaces can be created, and tools can be integrated into Excel-based collaborative engineering environments such as Glenn's Global Integrated Design Environment (GLIDE) and the Jet Propulsion Laboratory's Team-X. Multiple command-line tools can be integrated to generate a system model. For instance, the results of a propulsion analysis tool can be fed into a trajectory optimization tool, and the results can be fed back into the propulsion tool automatically until sizing or performance criteria converge. The time and cost required to create an Excel-based version of an existing software routine can be avoided, and in cases where a mathematically intensive algorithm results in slow performance within Excel/Visual Basic, faster languages such as C or Fortran can be utilized, thereby reducing run time. The figure shows an example of the XLerator interface and how it is used to incorporate command-line programs into the Microsoft Excel environment.

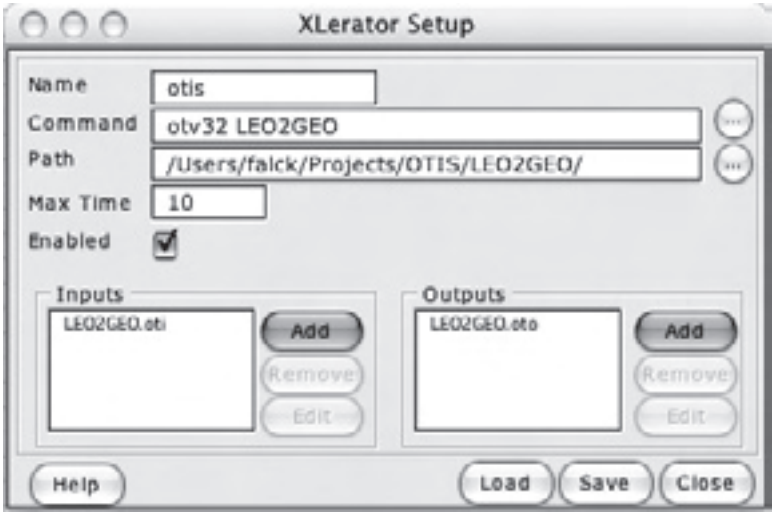


*XLerator Setup form.*

XLerator, which was developed by Glenn's Space Propulsion and Mission Analysis Office during the past 2 years, has been used for a wide range of

analyses. Initially developed as a proof-of-concept for applying Excel's optimization and goal-seeking capabilities to the SNAP trajectory propagation program, XLerator has since evolved into a utility capable of integrating almost any program that uses plain text files for input and output into a spreadsheet environment. For example, it was used in the Jupiter Icy Moons Orbiter program to integrate low-thrust trajectory optimization tools and Fortran database interpolators into the mission design portion of the Jupiter Icy Moons Orbiter systems model. In addition, XLerator was used in conjunction with the SNAP trajectory propagation tool and Excel's solver utility to optimize trajectories, providing an entirely new level of functionality.

XLerator is written in a combination of the Microsoft Visual Basic and Python (Python Software Foundation, Ipswich, MA) languages. Installation packages for Microsoft Windows 2000 or XP (Microsoft Office 2000 or later) and Macintosh OS X (Apple, Cupertino, CA; Microsoft Office X or later) are available. Support may be provided on a limited basis as time permits.

**Find out more about the research of Glenn's Space Propulsion and Mission Analysis Office:**
http://trajectory.grc.nasa.gov

**Glenn contacts:**
Robert D. Falck, 216–433–2295, Robert.D.Falck@nasa.gov; and
Leon P. Gefert, 216–977–7117, Leon.P.Gefert@nasa.gov

**Authors:**
Robert D. Falck and Laura M. Burke

**Headquarters program office:**
Exploration Systems

**Programs/Projects:**
Exploration Systems, In-Space Systems

## Global Integrated Design Environment (GLIDE) v.1.1 Software Released

One aspect of collaborative engineering is facilitated through the use of parameter-exchange software. Collaborative design efforts usually require the definition of a set of shared parameters that summarize the current state of design or that affect the overall design of the system. The Global Integrated Design Environment (GLIDE) facilitates easy passing and sharing of parameters between engineers from remote locations. GLIDE uses a common Web-based MySQL server (MySQL AB, Uppsala, Sweden) that is accessed using PHP scripts (the PHP Group). GLIDE's Web-served database allows secure and controlled access to design data by using firewall-friendly secure-sockets-layer- (SSL-) based user authentication. Data can be queried and published to the GLIDE database via a Microsoft Excel (Microsoft Corporation, Redmond, WA) interface. The training of engineers on GLIDE goes quickly because most users are familiar with Excel. Another benefit of using Excel as an interface is that optimization and other legacy tool integration developments like XLerator (ref. 1) can be used. The following diagram shows the data flow and interfaces that enable parameter exchange within GLIDE.

GLIDE was originally developed for the In-Space Propulsion program to support multicenter studies for the prioritization of technology-development funds. Recently, GLIDE was used by the NASA Engineering Design Team (NEDT), a 2005 Intramural Call for Proposals (ICP)-awarded project. The team was composed of many NASA centers—including the Ames Research Center, Glenn Research Center, Goddard Space Flight Center, Jet Propulsion

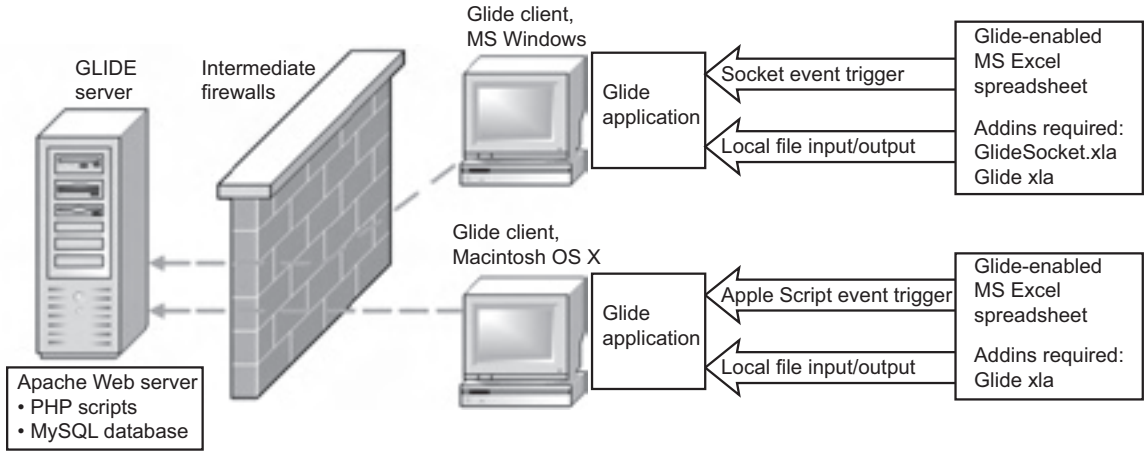


*GLIDE interfaces and data flow.*

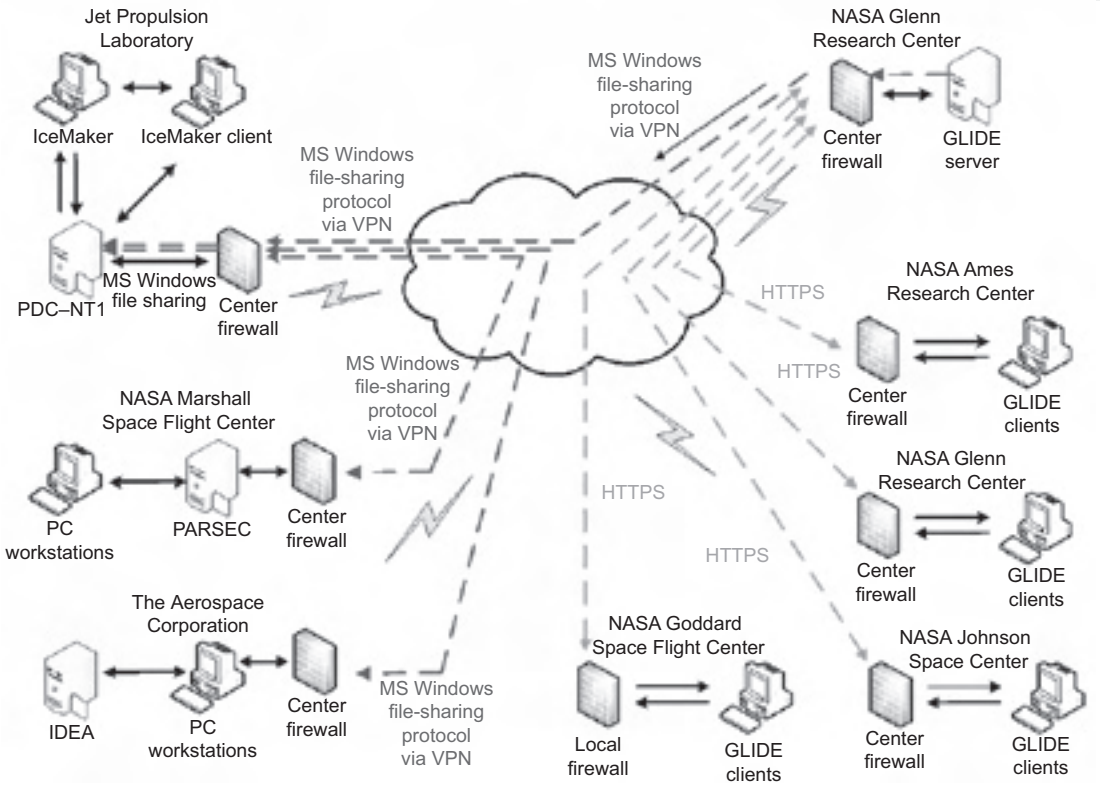


*NEDT data flow and interfaces. IceMaker (California Institute of Technology, Pasadena, CA), PARSEC (NASA Marshall Space Flight Center, AL), and IDEA (Aerospace Corporation, Segundo, CA) are other collaboration environments. VPN, virtual private networks; PDC–NT1, server at the Jet Propulsion Laboratory used to run Icemaker.*

Laboratory, Johnson Space Center, and Langley Research Center—and the Aerospace Corporation, an industry partner. The NEDT examined possible designs for a 2022 Mars sample return mission. The mission design used several different parameter-exchange solutions, including GLIDE, as well as other collaborative technologies such as Jabber-based text messaging (Jabber, Inc., Denver, CO), encrypted video conferencing, Asterisk-based multichannel voice conferencing, and WebEx screen-sharing software (WebEX Communications, Inc., Santa Clara, CA).

GLIDE was selected and used as the preferred parameter-exchange solution by Ames, Glenn, Goddard, and Johnson. Langley also demonstrated parameter exchange using GLIDE, but Langley's role within the Mars sample return study did not require parameter exchange. The final diagram shows the infrastructure data flow and protocol used by the NEDT.

GLIDE is written in a compilation of several programming languages, including REALbasic (REAL Software, Inc., Austin, TX), PHP, and Microsoft Visual Basic. GLIDE client installers are available to download for both Microsoft Windows and Macintosh systems (Apple, Cupertino, CA). The GLIDE client software is compatible with Microsoft Excel 2000 or later on Windows systems and with Microsoft Excel X or later on Macintosh systems.

**Reference**

1. Falck, Robert D.; and Burke, Laura M.: XLerator Software Released. Research & Technology 2005, NASA/TM—2006-214016, 2006, pp. 5–6. http://www.grc.nasa.gov/WWW/RT/RT2005/PB/PBM-falck.html

**Find out more about this research:**

**GLIDE:**
http://glide.grc.nasa.gov

**Space Propulsion and Mission Analysis Office:**
http://trajectory.grc.nasa.gov

**Glenn contacts:**
Leon P. Gefert, 216–977–7117, Leon.P.Gefert@nasa.gov; and
Bob A. Zalewski, 216–433–8014, Robert.A.Zalewski@nasa.gov

**RSIS contact:**
Matt R. Kunkel, 216–433–2535, Matthew.R.Kunkel@nasa.gov

**Authors:**
Leon P. Gefert and Matthew R. Kunkel

**Headquarters program office:**
Exploration Systems

**Programs/Projects:**
NEDT

## Leak Sensor Project Achieved a Major Milestone—a Miniaturized Leak Sensor System With an Integrated Wireless Antenna

An entire launch may be aborted if there is a possibility of oxygen or fuel leaks of any size on a spacecraft's surface because such leaks pose a high risk for an explosion. At the very least, discovered leaks result in schedule delays and timing issues for those supporting the launch. In support of NASA's ongoing efforts to promote safety throughout the Agency, the NASA Glenn Research Center has been developing leak sensors to detect potential fuel and oxygen leaks and help make the launch process go more smoothly. In spring 2005, the project achieved a major accomplishment by successfully integrating the wireless antenna into the postage-stamp-sized board unit as well as further decreasing the size and power consumption of the system.

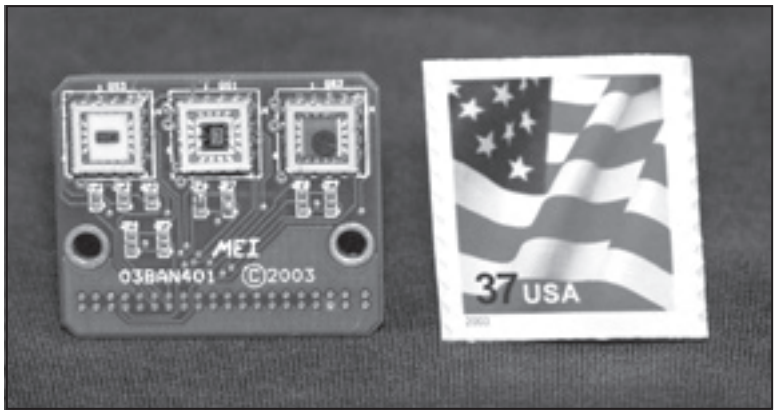


*"Lick and stick" leak-detection system.*

Glenn's leak sensor technology manager, Dr. Gary Hunter, worked with Case Western Reserve University on the invention and fabrication of the leak sensor. Makel Engineering, Inc., was involved in the integration and demonstration of the hardware, and product testing was conducted at the NASA Kennedy Space Center.

The leak sensor unit is composed of three different sensors: hydrogen, oxygen, and hydrocarbon. The recently integrated antenna, which used to be an attached component, enables wireless telemetry. This feature allows the unit to transmit leak rate data wirelessly to the remote central processing unit controlled by the user.

NASA leak sensor technology has been recognized with an R&D 100 Award, with NASA's Turning Goals into Reality Award, and, most importantly, with an increasing acceptance in multiple applications. In addition to preventing explosions, leak sensor technology can be used for safer, more efficient fuel management and chemical processing in space.

On Earth, leak sensors have been used to automatically check valves and fittings on automotive assembly lines and to improve the safety of hydrogen-powered vehicles. Other potential ground applications include fuel cells, hydrogen storage tanks, emission sensors, and advanced fire detection.

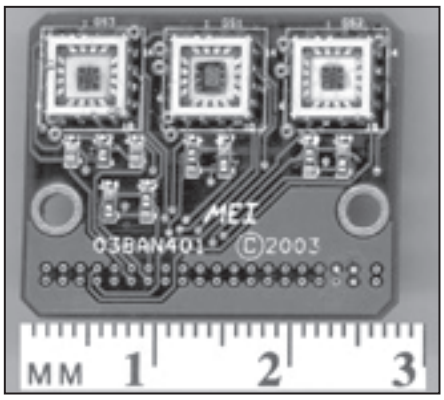


*Closeup view of the leak sensor board, including the hydrogen, oxygen, and hydrocarbon sensors.*

Long-term goals of the leak sensor project at Glenn include miniaturizing the unit while minimizing power consumption to extend its battery life. Miniaturization involves reducing the size of the entire leak sensor system (three sensors, signal conditioning, power, and telemetry) to fit onto the surface area of a postage stamp. Such a complete system would function as a "lick and stick" device, which could be transferred as easily as a postage stamp to any surface on the space vehicle or other leak-sensitive equipment.

**Find out more about this research:**

**Chemical species gas sensors:**
http://www.grc.nasa.gov/WWW/chemsensors/

**Glenn contact:**
Dr. Gary W. Hunter, 216–433–6459, Gary.W.Hunter@nasa.gov

**Author:**
Emily R. Groh

**Headquarters program office:**
Exploration Systems

**Programs/Projects:**
Constellation Systems

**Special recognition:**
R&D 100 Award (1995), NASA's Turning Goals into Reality Award (2003)

# 12-kW Proton-Exchange-Membrane Fuel Tested at Glenn

In summer 2005, a significant milestone in technology development for space exploration was achieved with the start of testing of a proton-exchange-membrane fuel cell (PEMFC) engineering model (EM) powerplant in the new state-of-the-art fuel cell test facility at the NASA Glenn Research Center. The PEMFC powerplant (see the following photograph) is the first high-fidelity 12-kW PEMFC hardware to be evaluated in a simulated launch environment for space applications. The facility, capable of testing various fuel cell types with power levels from 1 to 125 kW, brings new and unique capabilities to NASA for the evaluation of fuel cells and regenerative fuel cells for future missions.

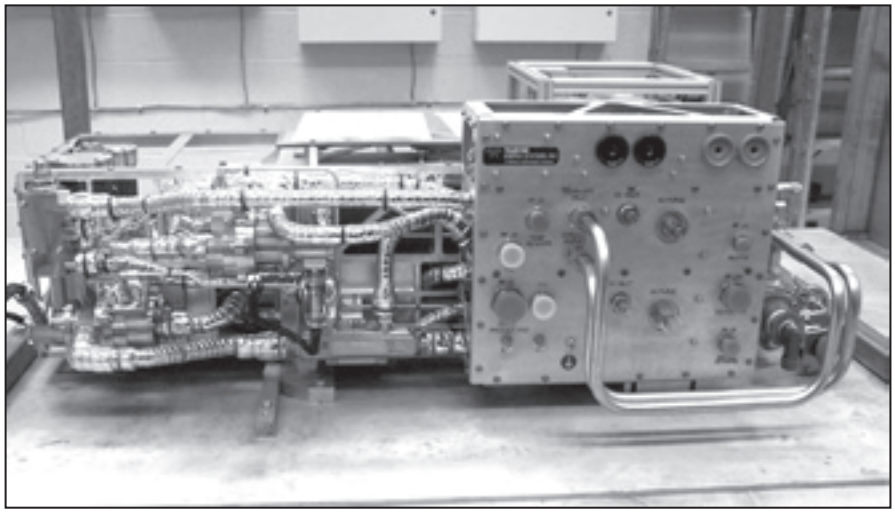

*12-kW PEMFC engineering model.*

The PEMFC is an electrochemical power-generation device that converts hydrogen and oxygen reactants into electrical power, heat, and water. Because the hydrogen and oxygen can be shared with propulsion systems and the water can be shared with crew life-support systems, fuel cells are an attractive primary power source for human space missions. When fuel cells are coupled with an electrolyzer to form a regenerative fuel cell system, the technology becomes an attractive energy storage alternative to battery systems, especially for lunar missions where the day-night cycles are much longer than those in low Earth orbit.

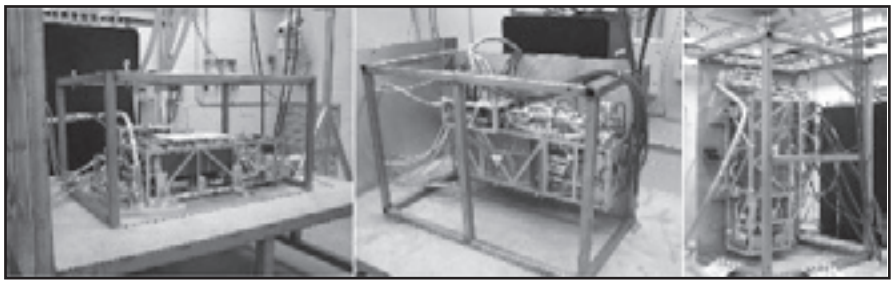

*PEMFC engineering model performance testing in three different orientations.*

The PEMFC EM successfully completed performance testing in three orthogonal orientations (see the final photograph). Following the completion of testing at Glenn, including mission profile simulation testing, the EM will undergo vibration and thermal vacuum testing at the NASA Johnson Space Center. At the conclusion of the test program, NASA will have demonstrated in a simulated space environment that the technology is ready to be considered for future missions.

PEMFC EM development and testing is being performed in support of Constellation Advanced Development Projects. Glenn is part of a team of NASA centers (Johnson Space Center, Kennedy Space Center, and Marshall Space Flight Center) that has been developing PEM fuel cell powerplant technology for future space missions. The PEMFC EM was designed and built under contract by Teledyne Energy Systems, Inc.

**Find out more about this research:**

**Glenn's Electrochemistry Branch:**
http://www.grc.nasa.gov/WWW/Electrochemistry/

**Exploration Systems at Glenn:**
http://exploration.grc.nasa.gov/

**Glenn contacts:**
Nang T. Pham, 216–433–6165, Nang.T.Pham@nasa.gov;
Mark A. Hoberecht, 216–433–5362, Mark.A.Hoberecht@nasa.gov; and
Scott R. Graham, 216–977–7123, Scott.R.Graham@nasa.gov

**Authors:**
Sally V. Harrington, Emily R. Groh, Mark A. Hoberecht, Nang T. Pham, and Scott R. Graham

**Headquarters program office:**
Exploration Systems

**Programs/Projects:**
Constellation Systems

# Nontoxic Turbine Power Unit Demonstrated Successfully

The first 100-kW-class pulse-controlled, nontoxic turbine power unit (TPU) has been built and demonstrated for space transportation flight control system applications. In space transportation vehicles, auxiliary power is used to provide short-duration high power for applications such as thrust vectoring, aerodynamic controls, brakes, and engine throttling. The space shuttle orbiter auxiliary power is provided by hydrazine-fueled auxiliary power units. Unlike the shuttle auxiliary power unit that uses toxic propellants to drive a hydraulic pump, this TPU (see the photograph to the right) uses nontoxic reactants to drive a generator to produce 270-Vdc electrical power. Applications of the TPU include power for high-horsepower, all-electric actuation systems and for electric-pump-powered hydraulic systems for launch vehicle flight controls.

The prototype nontoxic TPU includes a shaft-speed turboalternator, gas-cooled foil bearings, a high-reactance permanent magnet generator, and hydrogen and oxygen propellants with catalytic reaction that are pulsed on-off for speed control. A flight unit version is envisioned to be self-cooled using regenerative cooling with prognostic health monitoring and integrated power-processing modules wrapped around the TPU housing. The potential advantages of the new TPU concept include the elimination of toxic propellants, reduced ground processing, improved reliability, and reduced critical failure modes.

The prototype, also known as the brassboard TPU, has been successfully demonstrated with both cold and hot gases (see the following photograph). Cold gases include nitrogen and helium. A laboratory gas generator was used to generate the hot gas by the catalytic reaction of gaseous hydrogen and oxygen. The brassboard TPU has demonstrated 135-kW output with a designed electrical power output of 142 kW. TPU components such as seals and foil bearings have been demonstrated separately in simulated launch environments with no observable wear.

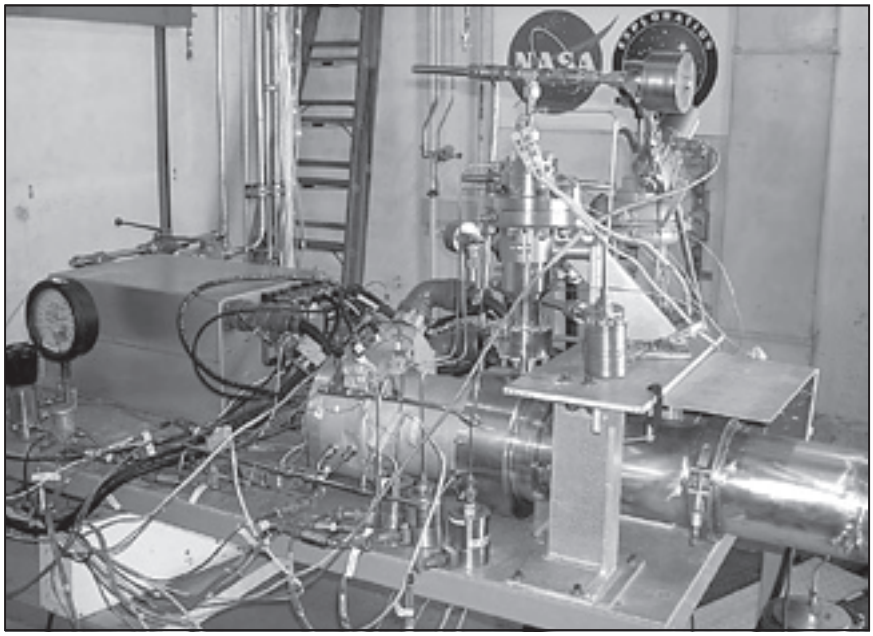


*Brassboard turbine power unit, power control and conditioning unit, and laboratory gas generator configured in a test cell for hot gas testing.*

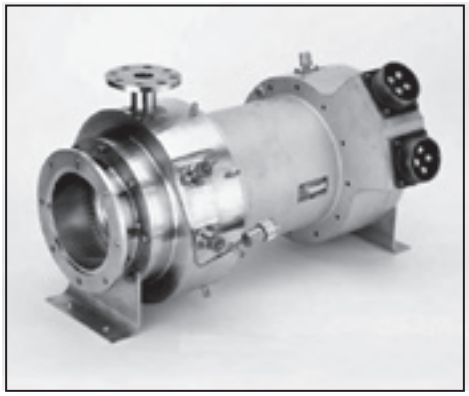

*Brassboard turbine power unit.*

The TPU effort is led by the NASA Glenn Research Center with a Lockheed Martin Corporation prime contract and a subcontract with Honeywell for hardware development and testing. The last phase of this task, which is currently underway, is to develop and test a new design brassboard hydrogen/oxygen gas generator with the goal of increased life and performance. The new gas generator will be integrated with the brassboard TPU and tested.

**Find out more about exploration systems research at Glenn:**
http://exploration.grc.nasa.gov

**Glenn contacts:**
Nang T. Pham, 216–433–6165,
Nang.T.Pham@nasa.gov;
Clint B. Ensworth, 216–433–6297,
Clinton.B.Ensworth@nasa.gov; and
Scott R. Graham, 216–977–7123,
Scott.R.Graham@nasa.gov

**Authors:**
Nang T. Pham, Clinton B. Ensworth,
Scott R. Graham, and Emily R. Groh

**Headquarters program office:**
Exploration Systems

**Programs/Projects:**
Constellation Systems

# New Tools Developed for Bioscience Experiments on the *International Space Station*

During the past year, much of NASA's research efforts have been focused on the promotion of astronaut health and safety. The NASA Glenn Research Center manages several projects involved in developing countermeasures to reduce health problems caused by prolonged exposure to microgravity. Under contract with Glenn, Physical Sciences Inc. is working on the low-power, confocal imaging of protein localization in living cells to better understand osteoporosis in astronauts. Currently in Phase II, the project utilizes a compact laser and fluorescence microscopy to study the activity of bone cells.

The project was initiated 2 years ago when Glenn identified the need for better tools to facilitate biological research experiments using the Light Microscopy Module (LMM) on the *International Space Station*. The LMM is a computerized microscope that is part of the Fluids Integrated Rack (FIR) and was developed to study fluid physics in microgravity. Through a Small Business Innovation Research (SBIR) solicitation, Physical Sciences Inc. was selected to perform the work.

The basic requirements for the new LMM tools were a compact laser (with a wavelength of approximately 600 nm) and fluorescent agents. The laser had to be reliable, yet small enough to meet the strict weight, power, and size requirements for space station flight hardware. Fluorescent agents, along with a line of bone cells with clearly visible markers, are necessary for fluorescence microscopy. This technique monitors cellular activity and protein interaction by sending out a colored beam of light to the bone cells, which return the light in a different color.

Confocal imaging technology will improve scientists' understanding of the effects of osteoporosis as it occurs in astronauts at accelerated rates. In the absence of gravity, osteoblasts do not readily rebuild bone cells. According to the project's contracting officer, Dr. DeVon Griffin, astronauts typically lose about 1 to 2 percent of their bone mass each month in the weight-bearing areas of their bodies. If this bone loss were to occur throughout a long-duration spaceflight to Mars, the astronauts would likely land on Mars or return to Earth with a severely damaged skeletal system.

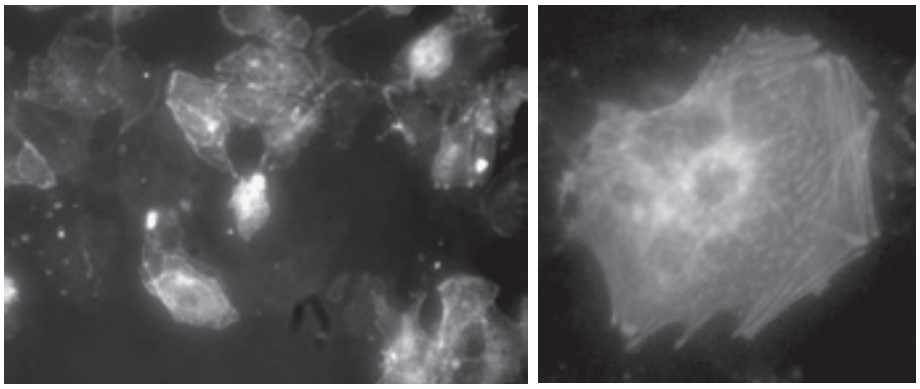

*Fluorescent images of the two types of cells being studied. Left: HEK 293, human kidney transfected with the HcRed-β-actin fusion protein construct. Right: UMR106-01, rat osteosarcoma cells transfected with the HcRed-β-actin fusion protein construct. The method for fusing the fluorophore to the cells was developed under this SBIR award. These images are shown in color in the online version of this article (http://www.grc.nasa.gov/WWW/RT/2005/PT/PTH-griffin.html).*

Phase II of the imaging project began in January 2005. So far, Physical Sciences Inc. has procured the compact laser and successfully established a stable cell line using DNA from protein fusion. After manipulating the genetic structures of the cells, the company has been photographing and analyzing images of cell activity. Physical Sciences Inc. also is integrating and testing a second laser to be added to the imaging system. As this research continues, increased knowledge of bone cell activity will result in more efficient countermeasures to protect astronaut health and may even help medical researchers prevent osteoporosis in people living on Earth.

**Find out more about exploration systems and human system research and technology development at Glenn:**
http://exploration.grc.nasa.gov/hsrt/

**Glenn contacts:**
Dr. DeVon W. Griffin, 216–433–8109, Devon.W.Griffin@nasa.gov; and Marsha M. Nall, 216–433–5374, Marsha.M.Nall@nasa.gov

**Author:**
Emily R. Groh

**Headquarters program office:**
Exploration Systems

**Programs/Projects:**
Human Health and Performance

# High-Power Space Traveling-Wave Tube Demonstrated Record Power Levels

The NASA Glenn Research Center, the Jet Propulsion Laboratory, and L–3 Communications Electron Technologies are pushing the limits on efficiently transmitting more data to the ground for NASA's space exploration missions. Earlier in 2005, L–3 Communications successfully completed performance testing of a high-power, high-efficiency Ka-band space traveling-wave tube (TWT) at 250 W through a 3-year project within Glenn's Exploration Systems Division. The completion of this milestone marks the highest power Ka-band space TWT ever manufactured and tested.

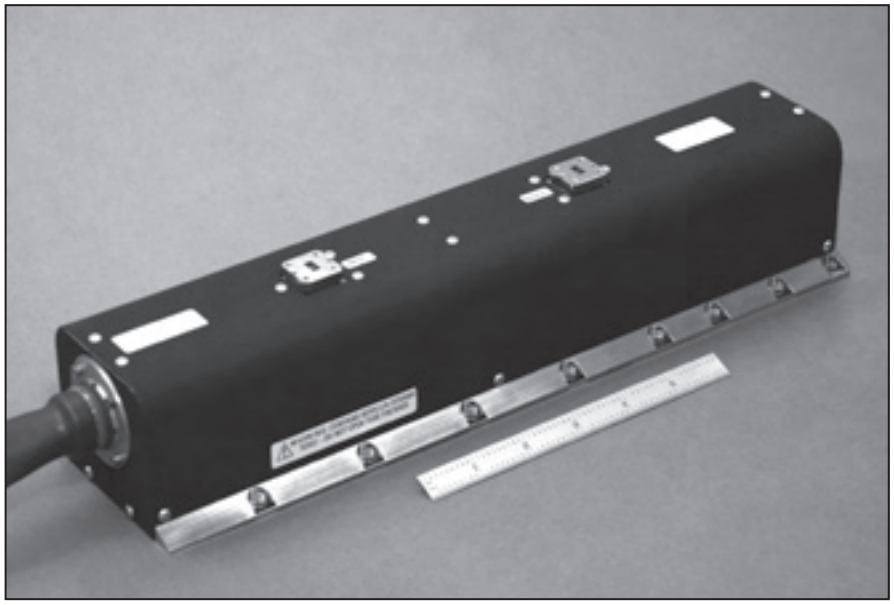

*Packaged high-power, high-efficiency Ka-band TWT; L–3 Communications Electron Technologies, Inc., Model 999HA. (Photograph courtesy of L–3 Communications Electron Technologies, Inc.; used with permission.)*

TWTs are attractive for deep-space applications because their construction is radiation tolerant and their power and efficiency levels are significantly higher than those of solid-state amplifiers. Although this new high-power TWT weighs only 1.5 kg, it is 7 times more powerful than the previous highest power Ka-band space TWT. Also, it is over 20 times more powerful than the Cassini TWT, which has been orbiting Saturn since July 2004. This increase in power capability directly translates into higher data transmission rates from greater distances, more flexibility, and more channels available for space communications.

This advance in TWT technology will improve the speed and efficiency of data communications, enabling real-time, high-resolution video transmission from space. High-power TWTs align with the President's vision for space exploration by increasing the science data rate-of-return for exploration missions by a factor of 7, enabling deeper, more sophisticated exploration of the solar system. This work will result in a flight-qualified model that can be used to design spacecraft for future deep-space missions. The TWT team also is developing and testing technology that combines two or more TWT devices to obtain even higher power.

**Find out more about exploration systems research at Glenn:**
http://exploration.grc.nasa.gov

**Glenn contacts:**
Dr. Jeffrey D. Wilson, 216–433–3513, Jeffrey.D.Wilson@nasa.gov; and
Dr. Rainee N. Simons, 216–433–3462, Rainee.N.Simons@nasa.gov

**L–3 Communications Electron Technologies, Inc., contact:**
Neal R. Robbins, 310–517–7548, Neal.Robbins@L-3com.com

**Author:**
Dr. Jeffrey D. Wilson

**Headquarters program office:**
Exploration Systems

**Programs/Projects:**
Nuclear Technology and Demonstration

# High-Fidelity *International Space Station* Flight Training Hardware Shipped to the NASA Johnson Space Center

NASA's astronauts must engage in years of rigorous training prior to becoming crew members of an actual space flight. Aside from being equipped for the physical demands of space travel, they must be equipped to handle the complex equipment and experiments designed for use while in orbit. Crews preparing for future missions on the *International Space Station* are no exception. Astronauts bound for the space station will soon receive state-of-the-art training on NASA Glenn Research Center's new Fluids and Combustion Facility (FCF) crew training units (CTUs). In spring 2005, the racks were delivered to the NASA Johnson Space Center and were added to the space station Mockup Training Facility's *Destiny* science module. The racks are designed to simulate the actual FCF equipment so crew members will be able to successfully operate the flight hardware to study fluid physics and combustion science in microgravity while onboard the space station.

*FCF CTUs deployed at Johnson. Right: Combustion Integrated Rack. Left: Fluids Integrated Rack.*

Glenn's Mission Operation and Integration Projects Office has been managing the development of the CTUs for 1 1/2 years. Hernandez Engineering Inc. designed and built the training racks. Glenn was responsible for the hardware requirements, the training rack integration, and the crew training. The NASA Marshall Space Flight Center was responsible for verifying training hardware readiness and procedure verification, and Johnson handled the training facility setup, trainer integration, and operation of the space station Mockup Training Facility.

The CTUs are detailed, high-fidelity, yet lightweight, versions of the two-rack FCF flight hardware, which is composed of the Fluids Integration Rack and the Combustion Integration Rack. They are made from a variety of materials including aluminum, steel, composite, and plastic. Each component has been tested for safety, maintainability, and structural integrity to ensure that they will last for up to 15 years.

The CTU design team's work was especially important because it provided a means to validate the flight hardware design and to verify operational procedures early in the development process, which resulted in cost and schedule savings for the entire FCF program. Beginning in spring 2006, two crews per year will be trained on the CTUs in preparation for flights on the space station. Members of the FCF training team at Glenn will work with the astronauts at Johnson prior to launch.

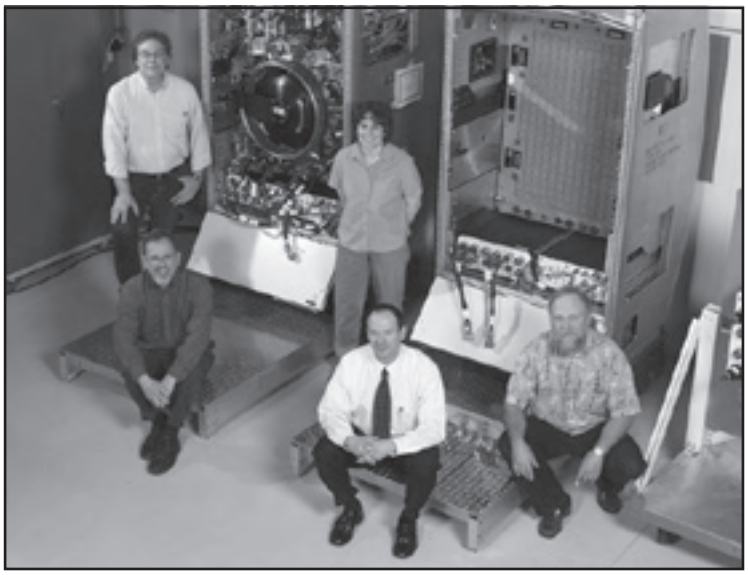

*FCF CTU development team. Seated left to right: Dave Lamar, FCF training manager; Tony Johnson, FCF CTU project manager; and Jim Imburgia, FCF CTU technician. Standing left to right: Warren Holt, FCF CTU technician, and Tracy Neff, FCF CTU lead engineer.*

*Fluids Integration Rack CTU being transported to the Payload Development Laboratory II at Johnson.*

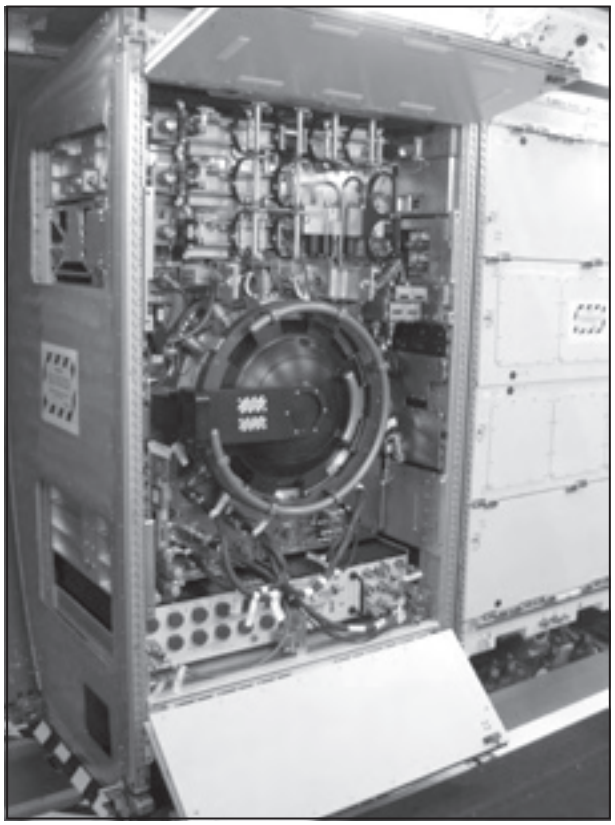

*Both training units are shown installed side-by-side in Payload Development Laboratory II. The rack doors open to display the Combustion Integrated Rack CTU interior.*

**Glenn contact:**
David A. Lamar, 216–433–6020, David.Lamar@nasa.gov

**Hernandez Engineering Inc. (HEI) contacts:**
Tony Johnson, 216–925–1056, tjohnson@mrdoc.cc; and Tracy A. Neff, 216–925–1173, tneff@mrdoc.cc (Tracy.A.Neff@nasa.gov)

**Author:**
Emily R. Groh

**Headquarters program office:**
Exploration Systems

**Programs/Projects:**
Mission Operation and Integration

**Special recognition:**
2005 Silver Snoopy Awards were given to three members of the FCF CTU team: Tracy A. Neff, Warren L. Holt, and James A. Imburgia.

# RESEARCH AND TECHNOLOGY

COMMUNICATIONS
INSTRUMENTATION AND CONTROLS
POWER AND ELECTRIC PROPULSION
PROPULSION SYSTEMS
MATERIALS AND STRUCTURES

# COMMUNICATIONS

## Inflatable Membrane Reflector and Shape-Memory Polymer Antenna Developed for Space and Ground Communications Applications

Communications requirements derived from the human and robotic exploration vision dictate a sophisticated, layered architecture that is dramatically different than what was required for the low-rate, point-to-point communications of the Apollo era. Emerging, but relatively near-term, exploration initiative needs include teleoperation and autonomous robotic missions, lunar reconnaissance and orbiting relay satellites, cooperative spacecraft, lunar surface wireless local area networks, extremely wide bandwidth links to support hyperspectral imaging, synthetic aperture radar, and other novel applications, such as high-definition television and telemedicine. For example, data rates on the order of 1 gigabit per second may be required from Mars areostationary relay satellites. Such enormous data rates and extreme link distances will require 10-meter-class microwave antennas, likely operating at Ka-band frequencies. The NASA Glenn Research Center has been involved in several efforts to meet these requirements. This year, Glenn and SRS Technologies developed a 4- by 6-m offset-parabolic inflatable membrane reflector. Glenn, SRS, and the Georgia Institute of Technology developed test apparatus and software to demonstrate that a novel ground station composed of an array of relatively small apertures can economically replace a single, expensive tracking ground station. In addition, Johns Hopkins University delivered a prototype 2-m version of an antenna based on a novel shape-memory composite structure.

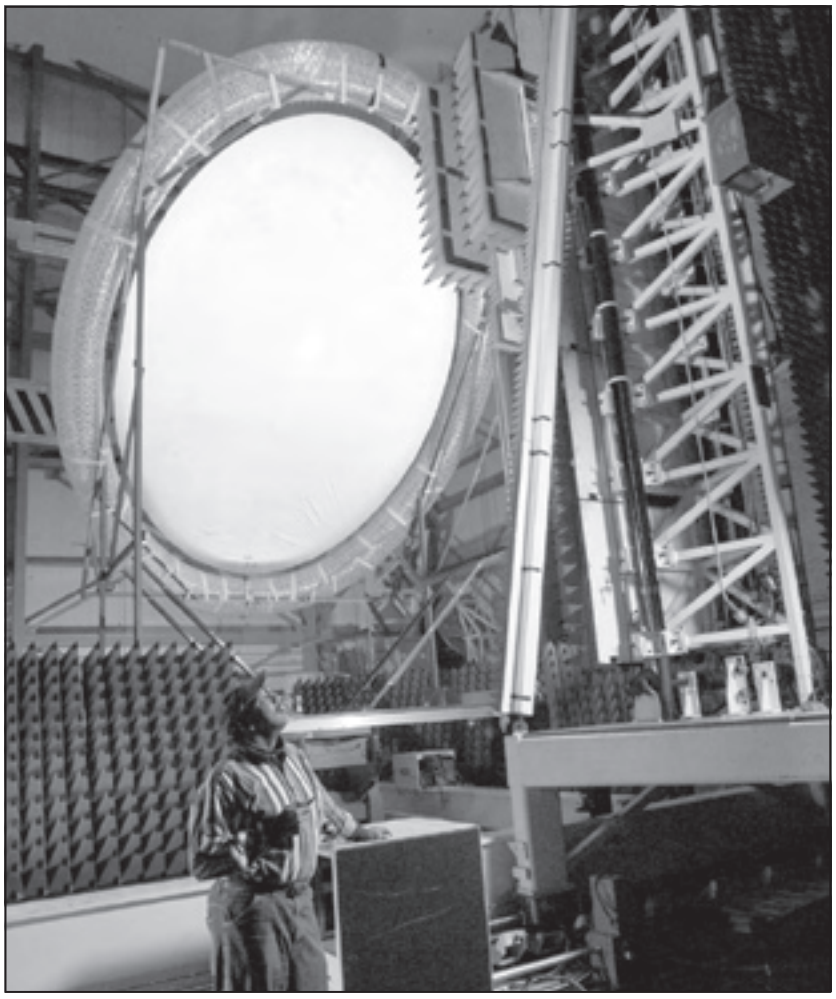

*SRS 4- by 6-m inflatable reflector in Glenn's near-field antenna range.*

Critical performance specifications for the very large antennas needed include low aerial density (~1 kg/m$^2$), high packaging efficiency (i.e., a ratio of deployed-to-stowed volume greater than 10:1), accurate surface geometry to ensure high reflector efficiency (root mean square surface errors of less than 1/20th of the operating wavelength), and of course reliable deployment. The NASA Glenn Research Center is developing two parallel approaches: inflatable membranes with a rigidized torus and a hybrid shape-memory composite approach that incorporates a fixed central reflector that serves as a backup antenna in case of deployment problems with the main aperture. Glenn is partnering with SRS Technologies (Huntsville, AL) on the former and with Johns Hopkins University (Laurel, MD) and ILC Dover (Frederica, DE) on the latter. The goal is to develop large gossamer antennas for deep-space, Moon, and Mars applications that have very low mass, lower cost, and improved deployment reliability while maintaining very accurate surface tolerances over long deployed durations.

The 4- by 6-m offset-parabolic inflatable membrane reflector developed by Glenn and SRS Technologies (see the photograph on the previous page) produced a gain of about 48 dB at 8.4 GHz at Glenn's near-field range. This corresponds to about 67-percent efficiency when compared with an ideal antenna using the same feed. Phase plots of the aperture more or less agree with the measured 3.5-mm average accuracy of the surface shape. The extreme antenna edges show some significant phase changes that are implicit with an inflatable lenticular geometry (i.e., flattened edges). Surface-shape accuracy can be improved through inflation pressure adjustment and/or perimeter attachment (catenary) tension adjustment.

During the late summer of 2005, Glenn, SRS, and the Georgia Institute of Technology developed a test apparatus and software to validate an adaptive beam-forming algorithm that synthesizes correlated aperture channels into a single signal. The goal is to demonstrate that an array of relatively small apertures can economically replace a single, expensive tracking ground station. The experiment involved an array of four inflatable 1-m-diameter membrane reflectors mounted onto a very low cost tracking pedestal (see the final photograph). The novel ground station successfully collected data from the SAC–C low-Earth-orbiting satellite. Data analysis is underway.

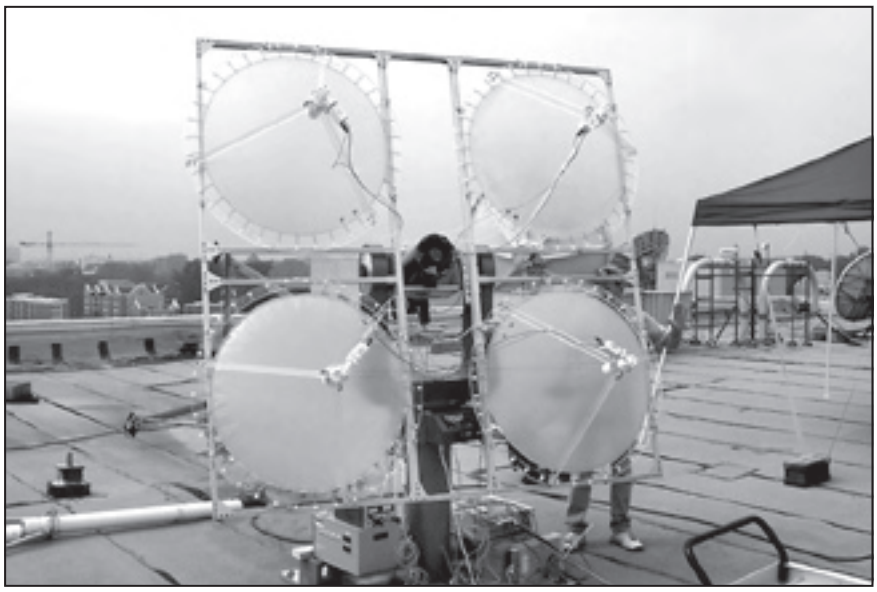

*Four-element inflatable membrane reflector array on a tracking pedestal at Georgia Tech as it prepares to track the SAC–C low-Earth-orbiting satellite.*

The shape-memory antenna system combines a fixed parabolic dish with an inflatable reflector annulus. This antenna, based on a novel shape-memory composite structure, provides a scaleable high-gain antenna architecture and is competitive with mesh and membrane reflectors in terms of cost, aerial density, and packing volume. The prototype 2-m antenna was delivered by Johns Hopkins University to Glenn in April 2005. The dish surface profile was validated with a coherent laser radar capable of mapping the surface shape to $\pm$25-$\mu$m accuracy. This proved to be a low-cost and highly accurate method to quickly validate the reflector and tune the perimeter attachments (catenaries) before proceeding with other tests. Initially, some wrinkling was observed near the inner ring and rim, but most wrinkles were eliminated upon retensioning and inflating the reflector to a pressure of about 5 in. of water. Testing indicated a root mean square surface error of 0.106 in. Removing problem areas near the outer rim resulted in a root mean square error of about 0.035 in.

**Bibliography**

Pearson, J.; and Romanofsky, R.: Thin Film Antenna Development and Optimization. AIAA–2006–2229, 2006 (to be published).

Ingram, M., et al.: Optimizing Satellite Communications With Adaptive and Phased Arrays. Presented at ESTC 2004, Palo Alto, CA, 2004.

**Glenn contacts:**

Dr. Robert R. Romanofsky, 216–433–3507, Robert.R.Romanofsky@nasa.gov; and
Dr. Félix A. Miranda, 216–433–6589, Felix.A.Miranda@nasa.gov

**Author:**

Dr. Robert R. Romanofsky

**Headquarters Program Office:**
Space Operations

**Programs/Projects:**
SCDS

# Software-Defined Radio Architecture Framework Developed for Space-Based Radios

The NASA Glenn Research Center, along with General Dynamics Decision Systems, has defined an open-architecture framework for space-based software-defined radios. Software-defined radio is a collection of hardware and software technologies that enable reconfigurable system architectures for wireless networks and user terminals. Software-defined radio enables multiband, multifunctional wireless devices that can be dynamically enhanced by software upgrades. They include technologies that are applicable across a wide range of wireless use. Software-enabled devices and equipment can be dynamically programmed to reconfigure the characteristics of radio equipment.

The framework developed by Glenn and General Dynamics consists of an architecture structure, the associated waveform parameters, and interface descriptions. Elements of software-defined radios are divided into different layers representing the hardware and software portions of the radio system. Open architectures allow technology insertion at certain layers without affecting other layers as technology changes and improves. Layering promotes and enables multiple vendor solutions and interoperability between independent hardware and software technologies.

This new architecture allows for flexibility and change and promotes the sharing and integration of software from a variety of sources. Software portability and design reuse play significant roles in containing the cost of software-defined radio developments. An open-architecture software design enables the separation of software from hardware, enabling the software to be ported to future platforms. The ability to reuse components is accomplished by defining various hardware and software interfaces and by defining the layers of the architecture framework to abstract the software from the hardware. By consistently specifying these interfaces and publishing them as part of the architecture, various hardware and software modules can be replaced and updated with a minimum amount of changes, since the interface is specified and rules are provided for each component.

A radio runs applications referred to as "waveforms" that include all the functions necessary to transmit information from one radio to another. The figure illustrates an example of the software abstraction definition between the waveform application and the radio operating environment. The application programming interface layer just below the waveform includes both a uniquely defined set of interfaces and an Institute of Electrical and Electronics Engineers, Inc. (IEEE), standard subset of the Portable Operating System Interface (POSIX) between the waveform applications and the radio's operating environment. The hardware abstraction layer and the associated lower-level software elements abstract the hardware from the operating system and software infrastructure. The architecture framework requires that vendors publish a hardware interface definition to provide a physical definition of the hardware interfaces for subsequent module integration.

The architecture development at Glenn is part of a larger NASA effort to develop a common radio architecture. Beginning with the baseline architecture, future work will evolve the architecture as it is applied to specific mission cases and will continue to leverage the Joint Tactical Radio System's Software Communications Architecture, a Department of Defense software radio architecture that was analyzed during this architecture development effort. The new architecture is intended to enable greater interoperability, to reduce cost through software reuse, and to minimize spacecraft resources (e.g., by combining radio functions to reduce radio count) as the architecture provides enhanced operations.

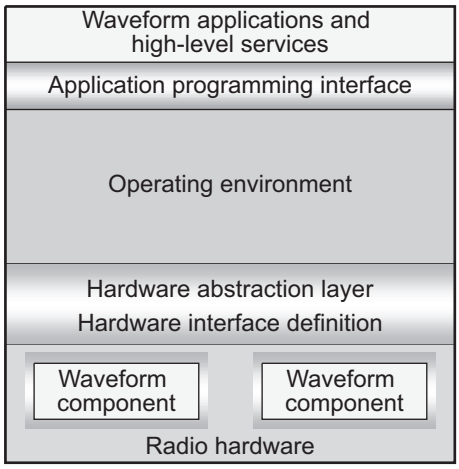


*Layered elements of an open architecture for software-defined radio.*

**Bibliography**

Johnson, Sandra K.; Kacpura, Thomas J.; and Reinhart, Richard C.: Software-Defined Radio Technology Analyzed for Space Exploration Scenario. Research & Technology 2005, NASA/TM—2006-214016, 2006, p. 19. http://www.grc.nasa.gov/WWW/RT/2005/RC/RCD-reinhart2.html

Kacpura, Thomas J.; Reinhart, Richard C.; and Johnson, Sandra K.: Reconfigurable, Software-Defined Waveform Developed on the Basis of the Software Communications Architecture. Research & Technology 2005, NASA/TM—2006-214016, 2006, pp. 20–21. http://www.grc.nasa.gov/WWW/RT/2005/RC/RCD-reinhart3.html

**Glenn contacts:**
Richard C. Reinhart, 216–433–6588, Richard.C.Reinhart@nasa.gov; and Sandra K. Johnson, 216–433–8016, Sandra.K.Johnson@nasa.gov

**Zin Technologies contact:**
Thomas J. Kacpura, 216–925–1266, thomas.kacpura@zin-tech.com

**Authors:**
Richard C. Reinhart, Thomas J. Kacpura, and Sandra K. Johnson

**Headquarters program office:**
Space Operations

**Programs/Projects:**
SCDS

# Software-Defined Radio Technology Analyzed for Space Exploration Scenario

Software-defined radio technology will benefit missions (1) that are expected to have a long operational life where enhancements and communication with assets not defined at launch are possible, (2) that communicate with different assets during different stages of operation, and (3) that will require enhanced capabilities such as autonomous operation and integrated navigation. The Space Telecommunications Radio System (STRS) project at the NASA Glenn Research Center analyzed the Crew Return Vehicle mission scenario, which exhibits many of these criteria. The Crew Return Vehicle was intended to function as a "lifeboat" for the International Space Station, providing an emergency, highly automated, escape mechanism. The Crew Return Vehicle scenario includes communications with many assets during its mission including the International Space Station, Tracking and Data Relay Satellite (TDRS), the Global Positioning System (GPS), and possibly the space shuttles for space operation and air traffic control for landing. Although the Crew Return Vehicle mission is no longer being considered, its communication architecture is similar to that of the planned Crew Exploration Vehicle mission, and the analysis and conclusions apply to the Crew Exploration Vehicle mission.

Two major tradeoffs were analyzed for this scenario: (1) the impact of allocating the transceiver functions in space-reconfigurable devices and (2) the estimated spacecraft resources needed to implement an open architecture. The potential of software-defined radio to reduce the number of radios and increase capability was also evaluated.

Waveform implementation in processor software is limited by the ability of general-purpose processors and shared-bus architectures to provide significant throughput for high-rate needs. High-speed signal processing can be implemented in field-programmable gate arrays (FPGAs) or in application-specific integrated circuits (ASICs). Reconfigurable FPGAs are extremely flexible but are less power efficient than ASICs or nonreconfigurable FPGAs. The analysis targeted FPGA implementations that would reduce power consumption. An analysis tool developed by the program was used to evaluate the communications requirements by waveform components and mission phase, and a vendor-provided tool was used to estimate power dissipation for the expected clock rates of the design.

The analysis compared the cost of implementing the scenario with three different software radio architectures: the Department of Defense's Software Communication Architecture (SCA), an optimized version of the SCA, and a proposed STRS architecture. Each was compared with an optimal nonreconfigurable radio solution. The modeling analysis showed that the software-defined radio architectures increased power from 10 to 40 percent and increased mass from approximately 10 to 30 percent, with the STRS architecture having the least impact and full SCA consuming the most resources. Reconfigurable technology allows a number of waveforms to operate at different times over different mission phases using the same hardware (a likely scenario for Crew Exploration Vehicle operation); thus, radio reduction is possible. Reducing the number of radios reduces mass and power resources, helping to offset the increased resources needed to adhere to a common open architecture, such as STRS or SCA. Further work will continue to quantify the benefit of radio reductions, operational improvements, and other considerations of using software radio technology for space exploration.

**Bibliography**

Reinhart, Richard C.; Kacpura, Thomas J.; and Johnson, Sandra K.: Software-Defined Radio Architecture Framework Developed for Space-Based Radios. Research & Technology 2005, NASA/TM—2006-214016, 2006, p.18. http://www.grc.nasa.gov/WWW/RT/2005/RC/RCD-reinhart1.html

Kacpura, Thomas J.; Reinhart, Richard C.; and Johnson, Sandra K.: Reconfigurable, Software-Defined Waveform Developed on the Basis of the Software Communications Architecture. Research & Technology 2005, NASA/TM—2006-214016, 2006, pp. 20–21. http://www.grc.nasa.gov/WWW/RT/2005/RC/RCD-reinhart3.html

**Glenn contacts:**
Richard C. Reinhart, 216–433–6588, Richard.C.Reinhart@nasa.gov; and Sandra K. Johnson, 216–433–8016, Sandra.K.Johnson@nasa.gov

**Zin Technologies contact:**
Thomas J. Kacpura, 216–925–1266, thomas.kacpura@zin-tech.com

**Authors:**
Sandra K. Johnson, Thomas J. Kacpura, and Richard C. Reinhart

**Headquarters program office:**
Space Operations

**Programs/Projects:**
SCDS

# Reconfigurable, Software-Defined Waveform Developed on the Basis of the Software Communications Architecture

A waveform compliant with the Software Communications Architecture (SCA) has been developed at the NASA Glenn Research Center. This development is part of the larger Space Telecommunications Radio System project currently underway to define a communications system architecture for future space-based reconfigurable transceivers and software-defined radios. Software-defined radios are becoming more common because of the capabilities of reconfigurable digital signal-processing technologies, such as field-programmable gate arrays (FPGA) and digital processors, placing radio functions in firmware and software that were traditionally performed with analog hardware components. The entire set of these radio functions running in software comprise the waveform, which is run as a software application by the radio processing elements.

The waveform was developed using the SCA framework of rules and requirements that the Department of Defense uses as the standard for the Joint Tactical Radio System. The Department of Defense envisions that their future radios will be SCA compliant. Although the use of the current SCA as a reference has increased our understanding of the architecture, the approach may be impractical for today's space applications because of its high consumption of processing resources. However, by developing an SCA-compliant waveform, one has direct insight into the resources required to support the reconfigurability offered by this architecture approach. The evolution of NASA's architecture will continue to identify areas where the SCA should be adapted, with the goal of converging to a common architecture. This will leverage the Department of Defense's significant investment in software-defined radio technology and software communications architectures.

The waveform was defined using existing telemetry link characteristics and space exploration initiative scenarios. The basic parameters defined were data rate, modulation, coding scheme, symbol rate, baseband data interface, intermediate frequency interface, scrambling scheme, and bandwidth. The waveform was designed from both signal-processing and software component perspectives. Running the waveform at a data rate of 1 megabit per second (Mbps) allowed the majority of signal-processing functions to be implemented in software. In addition, most functions could be implemented in the general-purpose processor, making the waveform ideal for portability and SCA implementation. However, since most applications require higher data rates, several higher rate signal-processing functions were targeted for FPGA implementation. This approach provides options for future waveform scalability.

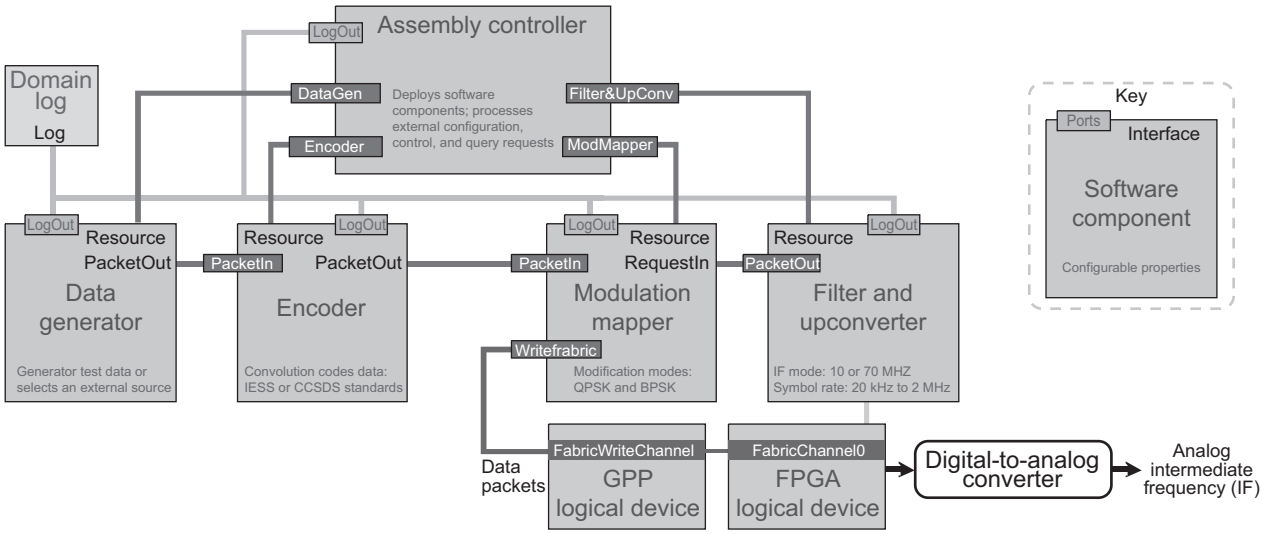


*Waveform transmit functions and top-level SCA components and interfaces. IESS, Intelsat Earth Station Standards; CCSDS, Consultative Committee Space Data Standards; GPP, generic packetized protocol; QPSK quaternary phase shift keying; BPSK, binary phase shift keying.*

The final step of the waveform development was integrating the waveform with the SCA infrastructure. The figure illustrates the complexity of waveform transmit functions (e.g., data generator, encoder, modulation, filtering and digital upconversion, and digital-to-analog converter) mapped across the software elements or components (logging function, logical connection ports, and interprocess communication transport mechanisms) of the SCA architecture.

The completed waveform will serve as a tool in the software-defined radio testbed to support further architecture tradeoffs for the space environment. The waveform routines can be scaled for data rates, frequencies, and alternative architectures to examine the range of communications commonly employed by NASA for space.

**Bibliography**

Reinhart, Richard C.; Kacpura, Thomas J.; and Johnson, Sandra K.: Software-Defined Radio Architecture Framework Developed for Space-Based Radios. Research & Technology 2005, NASA/TM—2006-214016, 2006, p. 18. http://www.grc.nasa.gov/WWW/RT/2005/RC/RCD-reinhart1.html

Johnson, Sandra K.; Kacpura, Thomas J.; and Reinhart, Richard C.: Software-Defined Radio Technology Analyzed for Space Exploration Scenario. Research & Technology 2005, NASA/TM—2006-214016, 2006, p. 19. http://www.grc.nasa.gov/WWW/RT/2005/RC/RCD-reinhart2.html

**Glenn contacts:**
Richard C. Reinhart, 216–433–6588, Richard.C.Reinhart@nasa.gov; and Sandra K. Johnson, 216–433–8016, Sandra.K.Johnson@nasa.gov

**Zin Technologies contacts:**
Dale J. Mortensen, 216–925–1267, Dale.J.Mortensen@nasa.gov; and Thomas J. Kacpura, 216–925–1266, thomas.kacpura@zin-tech.com

**Authors:**
Thomas J. Kacpura, Richard C. Reinhart, and Sandra K. Johnson

**Headquarters program office:**
Space Operations

**Programs/Projects:**

SCDS

## Multifocal Flat Lens Demonstrated With Left-Handed Metamaterial

Left-handed metamaterials (LHMs), also known as negative-index materials, are a new media engineered to provide an effective negative index of refraction over a selected frequency range. This characteristic enables LHMs to exhibit physical properties never before observed. In particular, a negative index of refraction causes electromagnetic radiation to refract or bend at a negative angle when entering and leaving an LHM as shown in this schematic. This enables radiation to be focused with a flat LHM lens. With a flat lens, unlike a conventional curved lens, the focal length can be varied simply by adjusting the distance between the lens and the electromagnetic wave source. Researchers at the NASA Glenn Research Center developed computational models for LHMs with commercial three-dimensional electromagnetic simulation codes (ref. 1), constructed an LHM flat lens, and used it to experimentally demonstrate reversed refraction and multifocal flat lens focusing of microwave radiation (ref. 2).

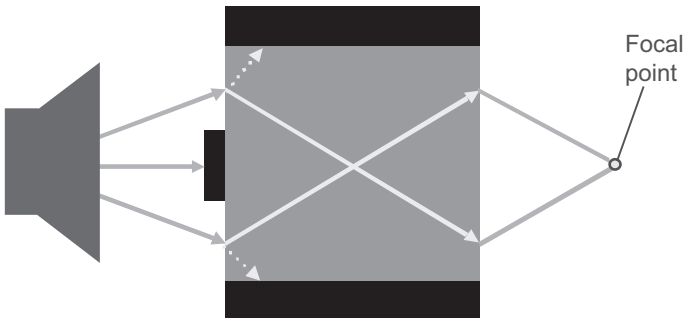


*The dashed lines represent the refracted path of radiation entering a conventional material with a positive index of refraction. Electromagnetic radiation refracts or bends at a negative angle when entering and leaving a slab of material with a negative index of refraction as indicated by the solid lines. The negative refraction angles enable radiation to converge to a focal point.*

The LHM configuration used in this experiment is a periodic array of metallic rings and wires based on work by researchers at the University of California at San Diego (refs. 3 and 4). The photograph on the next page shows part of the flat lens array of LHM cells that Glenn researchers constructed. For the focusing experiment, the metamaterial slab was placed inside a parallel-plate waveguide. On the source side, microwaves were emitted from a dipole antenna and directed into the metamaterial array.

On the other side of the array, a computer-controlled detecting probe measured the power distribution in the x-y plane.

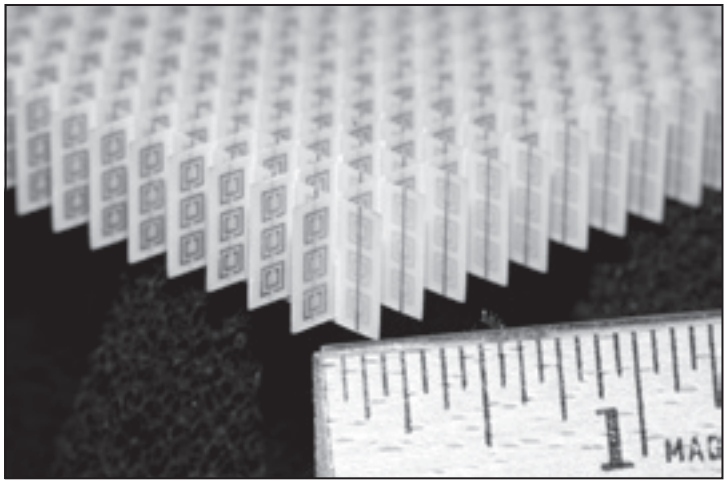

*Part of the left-handed metamaterial array configuration, which was constructed of copper split-ring resonators and wires mounted on interlocking sheets of fiberglass circuit board. The total array consists of 3 by 20 by 20 unit cells with overall dimensions of 10 by 100 by 100 mm.*

The graphs show the measured power beyond the metamaterial array. These results indicate the effects of negative refraction and demonstrate the feasibility of a multifocal left-handed metamaterial flat lens. Because of the high attenuation with the ring and wire geometry, approaches that could be more promising for practical applications are being investigated. A low-loss flat lens could enable objects positioned at different distances from the lens to be recorded by simply moving a recorder toward or away from the lens. If such a lens can be developed with ultrahigh resolution, it could have tremendous impact on a wide range of applications including wireless communications, integrated circuit manufacturing, biomedical imaging, detection of low levels of biological and chemical elements, and molecular viewing and manipulation.

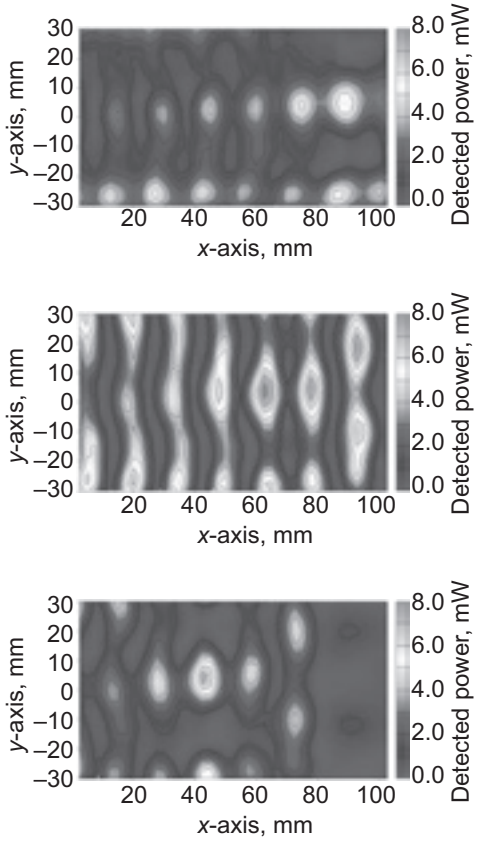


*Measured power beyond the metamaterial array with a microwave source located distances of 30 mm (top), 50 mm (center), and 70 mm (bottom) in front of the array. The corresponding focal points are indicated by the maxima in power and are positioned at 87.5 mm (top), 60 mm (center), and 40 mm (bottom) beyond the metamaterial array. As the source was moved farther from the array, the focal point occurred closer to the array. This figure is shown in color in the online version of this article (http://www.grc.nasa.gov/WWW/RT/2005/RC/RCE-wilson1.html).*


**References**

1. Chevalier, Christine T.; and Wilson, Jeffrey D.: Frequency Bandwidth Optimization of Left-Handed Metamaterial. NASA/TM—2004-213403, 2004. http://gltrs.grc.nasa.gov/cgi-bin/GLTRS/browse.pl?2004/TM-2004-213403.html
2. Wilson, Jeffrey D.; and Schwartz, Zachary D.: Multifocal Flat Lens With Left-Handed Metamaterial. Appl. Phys. Lett., vol. 86, no. 2, 2005. http://scitation.aip.org/getabs/servlet/GetabsServlet?prog=normal&id=APPLAB000086000002021113000001&idtype=cvips&gifs=yes or http://physics.ucsd.edu/~tdriscol/flib/papers/LHM/2004%20wilson%20schwartz%20flat%20LHM%20focus.pdf
3. Smith, D.R., et al.: Composite Medium With Simultaneously Negative Permeability and Permittivity. Phys. Rev. Lett., vol. 84, no. 18, 2000.
4. Shelby, R.A., et al.: Microwave Transmission Through a Two-Dimensional, Isotropic, Left-Handed Metamaterial. Appl. Phys. Lett., vol. 78, no. 4, 2001.


**Find out more about this research:**

**Glenn's Communications Division:**
http://ctd.grc.nasa.gov

**Glenn's Independent Research & Development Fund:**
http://www.grc.nasa.gov/WWW/5000/IRD/


**Glenn contact:**
Dr. Jeffrey D. Wilson, 216–433–3513, Jeffrey.D.Wilson@nasa.gov

**Analex Corporation contact:**
Christine T. Chevalier, 216–433–6082, Christine.T.Chevalier@nasa.gov

**Authors:**
Dr. Jeffrey D. Wilson, Zachary D. Schwartz, and Christine T. Chevalier


**Headquarters program office:**
Space Operations

**Programs/Projects:**
Glenn's IR&D, BEGIN

# Robust Circuit Designs Developed for High-Frequency Vacuum Electronics Amplifiers

At millimeter-wave and terahertz frequencies, vacuum electronics amplifiers have promising potential for high-data-rate secure communications, surveillance, and remote-sensing applications. However, the power and efficiency of vacuum electronic slow-wave circuits at these high frequencies is limited by the small size of the slow-wave circuit. Relatively small dimensional variations resulting from conventional micromachining techniques that are adequate for lower frequency operation can be large enough to cause serious degradation and variation of performance at higher frequencies. To alleviate this problem, a new design procedure for significantly improving the power, efficiency, and robustness of high-frequency vacuum electronic amplifiers was created and developed in an in-house research effort at the NASA Glenn Research Center.

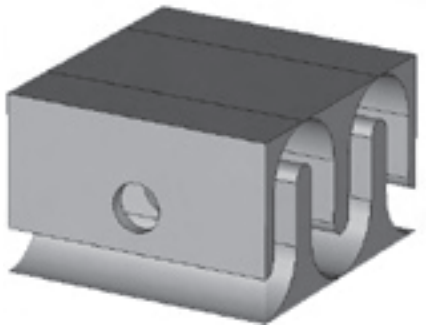

*Four periods, consisting of vacuum between copper walls, of a folded waveguide slow-wave circuit are shown. The entire copper circuit consists of several hundred periods with varying lengths. Amplification is obtained as the millimeter wave or terahertz wave travels through the serpentine path of the folded waveguide while interacting with an electron beam passing through the circular apertures. The length of a single period is approximately 500 μm for the 94-GHz circuit and 150 μm for the 400-GHz circuit.*

Several vacuum electronics slow-wave circuit geometries were investigated with a commercial three-dimensional electromagnetics simulation code (ref. 1) at frequencies of 94 and 400 GHz, and the folded waveguide geometry shown in the preceding illustration was found to be the most robust with respect to currently available manufacturing tolerances. A number of micromachining techniques were investigated and compared with respect to applicability, expected tolerances, and cost. Wire electrodischarge machining appears to be the best currently available technique for manufacturing folded waveguide circuits at these frequencies.

A robust optimization algorithm based on simulated annealing (refs. 2 and 3) was created to design slow-wave circuits consisting of a series of several hundred folded waveguide periods with varying lengths. This algorithm differs from previous slow-wave circuit design techniques in that the dimensional tolerances are taken into account during the optimization. Designs optimized for robustness were developed for folded waveguide circuits at 94 and 400 GHz.

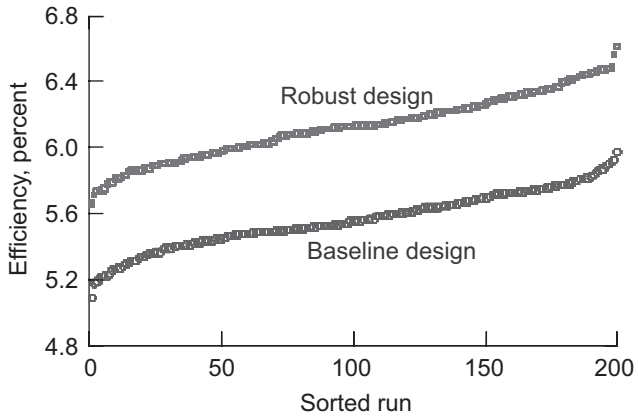


*Simulated efficiency values of a 94-GHz circuit design obtained with the new robust optimization algorithm compared with those for a baseline design obtained with a standard simulated annealing algorithm. For each design, 200 runs with pseudorandom dimensional variations were performed.*

The graph shows the simulated statistical performance of a 94-GHz circuit design obtained with the new robust optimization algorithm compared with that of a baseline design obtained with a standard simulated annealing optimization algorithm (ref. 2). For each design, 200 runs with pseudorandom dimensional variations were performed. The results show that the efficiency distribution is significantly improved with the new algorithm; similar results were obtained with the 400-GHz design. These results also indicate that this design procedure can significantly alleviate the performance degradation caused by manufacturing tolerance variations in high-frequency vacuum electronics amplifiers.

**References**

1. Chevalier, Christine T., et al.: Three-Dimensional Simulation of Traveling-Wave Tube Cold-Test Characteristics Using CST MICROWAVE STUDIO. NASA/TM—2003-212486, 2003. http://gltrs.grc.nasa.gov/cgi-bin/GLTRS/browse.pl?2003/TM-2003-212486.html

2. Wilson, Jeffrey D.: A Simulated Annealing Algorithm for Optimizing RF Power Efficiency in Coupled-Cavity Traveling-Wave Tubes. IEEE Trans. Electron Devices, vol. 44, issue 12, 1997, pp. 2295–2299. http://ieeexplore.ieee.org/iel3/16/14065/00644656.pdf?arnumber=644656

3. Wilson, Jeffrey D.: Design of High-Efficiency Wide-Bandwidth Coupled-Cavity Traveling-Wave Tube Phase Velocity Tapers With Simulated Annealing Algorithms. IEEE Trans. Electron Devices, vol. 48, 2001, pp. 95–100. http://ieeexplore.ieee.org/iel5/16/19304/00892174.pdf?arnumber=892174

**Find out more about the research of Glenn's Communications Division:**
http://ctd.grc.nasa.gov

**Glenn contact:**
Dr. Jeffrey D. Wilson, 216–433–3513, Jeffrey.D.Wilson@nasa.gov

**Analex Corporation contacts:**
Christine T. Chevalier, 216–433–6082, Christine.T.Chevalier@nasa.gov; and Dr. Carol L. Kory, 216–433–3512, Carol.L.Kory@nasa.gov

**Authors:**
Dr. Jeffrey D. Wilson, Christine T. Chevalier, and Dr. Carol L. Kory

**Headquarters program office:**
Space Operations

**Programs/Projects:**
Space Operations Mission Directorate

# High-Efficiency Power Combining of Ka-Band Traveling-WaveTubes Demonstrated for High-Data-Rate Space Communications

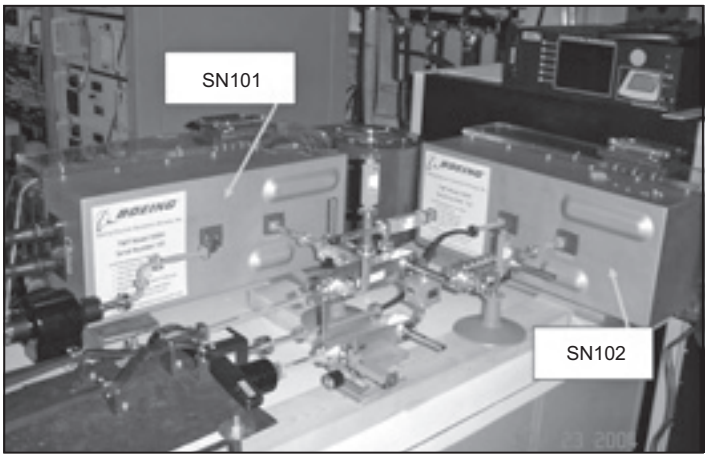


*Power-combiner testbed for 100-W space TWTs (serial numbers 101 and 102).*

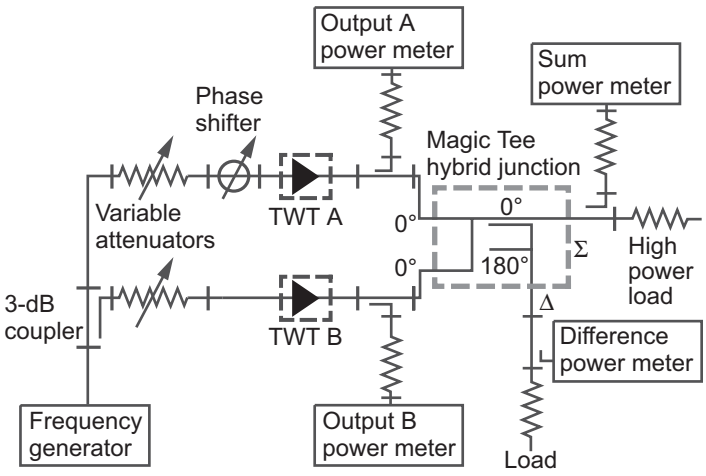


*Two-way power-combiner test circuit.*

High-efficiency (greater than 90 percent) microwave power combining and high-data-rate transmission (622 megabits/sec) were both successfully demonstrated for the first time at the NASA Glenn Research Center using a novel two-way power-combiner waveguide circuit with two 100-W state-of-the-art space traveling-wave tubes (TWTs) The TWTs were designed specifically for efficient operation (greater than 55 percent) over the Deep Space Network Ka-band frequency range of 31.8 to 32.3 GHz (refs. 1 to 3). The power-combining testbed for the two TWTs (SN101 and SN102, Boeing Model 999H, Boeing Company, Chicago, IL) is shown in the photograph on the left.

The two-way power-combining circuit, shown schematically in this diagram, was based on a four-port hybrid junction known as a Magic Tee, the basic operation of which is illustrated in the top figure on the next page. The TWT input powers (ports 1 and 4) add in phase at the output port (port 2) and cancel in phase at the opposite coplanar port (port 3). For optimum combining efficiency, the powers and phases of the two TWTs at the input ports must be balanced, which ideally results in double the power at the sum port (assuming no power losses in the junction).

The geometries of the Magic Tee and alternative hybrid junction were modeled by computer, leading to designs with improved efficiency and power handling (ref. 4). Two designs, which potentially offer combining efficiencies above 95 percent, are shown in the final figure. Successful transmission through the Magic Tee of the 622-megabits/second digital signal, which was

quaternary phase-shift-keying (QPSK) modulated, required maintaining a close phase balance over the 311-MHz signal bandwidth. It was thus necessary to appropriately modify the waveguide circuitry to compensate for the widely disparate rates of change of phase with frequency of the two TWTs and corresponding circuit paths. Initially, the phase differences were about 1°/MHz with no signal synchronization. This was subsequently reduced by a factor of more than 6, resulting in an observed low bit error rate of $2.4 \times 10^{-8}$. An additional benefit of the circuit modification was an extension of the useful bandwidth of the Magic Tee to more than 3 GHz.

Future NASA deep-space exploration missions may, in some cases, require telecommunication systems capable of operating at very high data rates (potentially 1 gigabit/sec or more) for efficiently transmitting large volumes of scientific data back to Earth. This would require high-frequency microwave transmitters (Ka-band) with large bandwidth. The large distances and the use of practical antenna sizes would dictate the need for transmitter power as high as 1 kW and possibly more. High electrical efficiency would also be a requirement. The high-efficiency, wide-band two-way combiner approach verified here, which can readily be extended to combining $2^n$ TWTs, where $n$ is an integer, also demonstrates the feasibility of meeting these high power, data rate, and efficiency requirements.

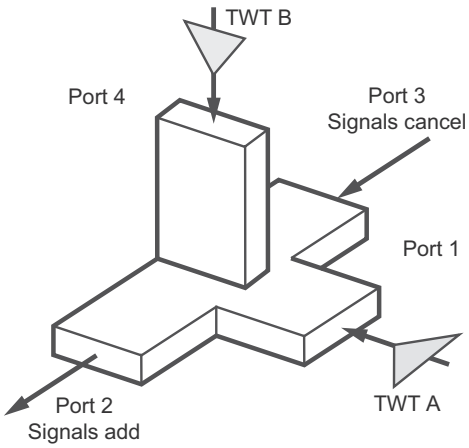


*Wave-guide hybrid Magic Tee showing input and output port functions.*

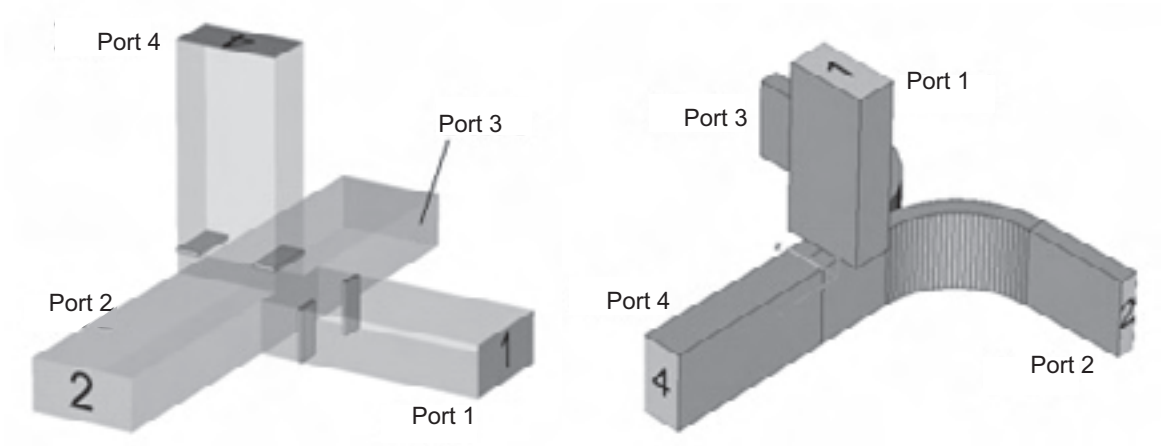


*Computer-modeled hybrid junctions. Left: Magic Tee matched by inductive windows. Right: Folded E-plane tee with split colinear arms.*

**References**

1. Bibyk, Irene; Romanofsky, Robert; and Wintucky, Ed: RF Technologies for Advancing Communication Infrastructure. 2006 IEEE Aerospace Conference, Big Sky, MT, 2006.
2. Wintucky, E., et al.: High-Power Combining of Ka-Band TWTs for Deep Space Communications. IVEC 2006, Monterey, CA, 2006.
3. Robbins, N.R., et al.: High Power, High Efficiency 32 GHz Space Traveling Wave Tube. Proceedings of the Fifth IEEE International Vacuum Electronics Conference, Monterey, CA, 2004, pp. 261–262.
4. Vaden, K.R.; and Simons, R.N.: Computer Aided Design of Ka-Band Waveguide Power Combiner Architectures for Interplanetary Spacecraft. 2005 IEEE Antennas and Propagation Society International Symposium, vol. 1A, 2005, pp. 635–638.

**Glenn contacts:**
Edwin G. Wintucky, 216–433–3510, Edwin.G.Wintucky@nasa.gov; and Karl R. Vaden, 216–433–8131, Karl.R.Vaden@nasa.gov

**Authors:**
Edwin G. Wintucky and Karl R. Vaden

**Headquarters program office:**
Exploration Systems

**Programs/Projects:**
Project Prometheus

# Mobile Router Technology Investigated for Space Radiation Effects

The NASA Glenn Research Center is involved in defining next-generation communication architectures for space exploration. These architectures are examining the use of commercial-off-the-shelf (COTS) mobile router hardware to provide communication networking interoperability among space systems. To be fully successful, COTS electronics and software require rigorous analysis and testing to determine if they can be used in extreme space environments. Glenn's Satellite Networks and Architectures Branch in conjunction with Zin Technologies performed radiation susceptibility testing and analyzed results to determine the feasibility of COTS mobile-router hardware for space applications.

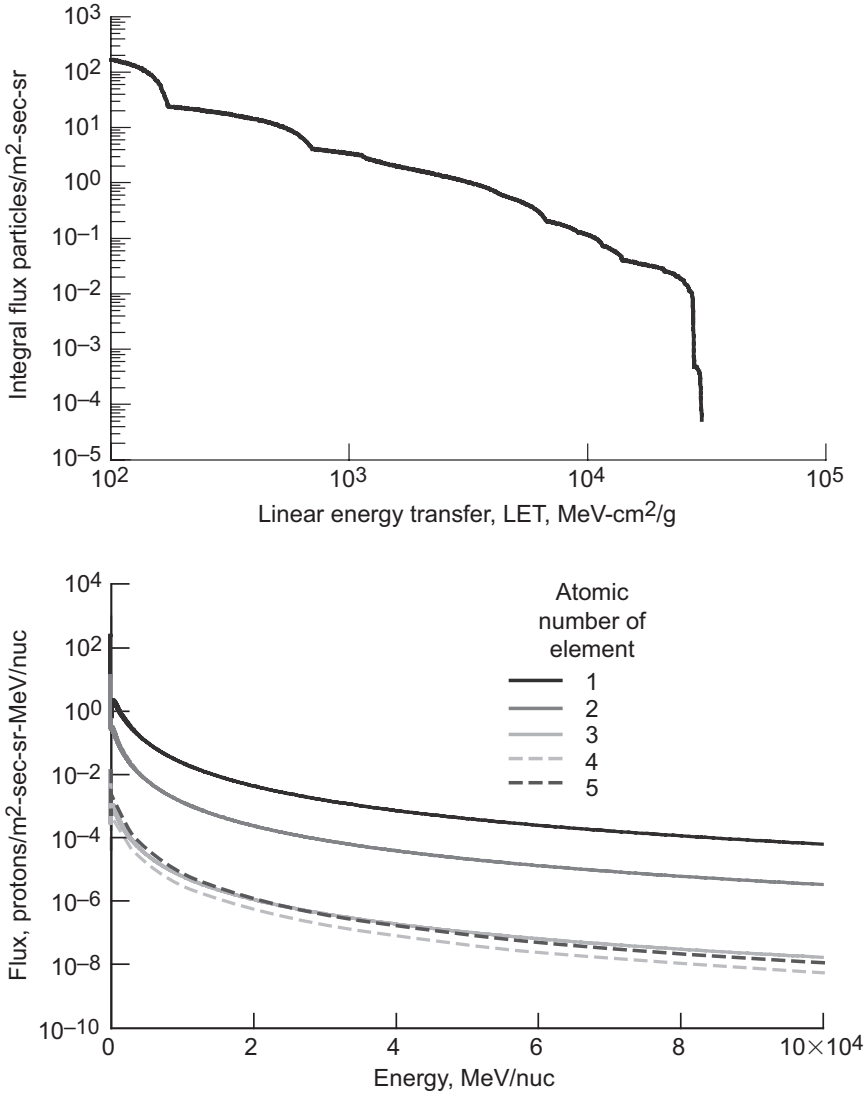


*Analytical radiation exposure for lunar orbit mission scenario—one of the space mission scenarios analyzed for radiation exposure levels.*

Of all electronic components, semiconductors are the most sensitive to radiation. Radiation can cause both permanent and temporary damage to a semiconductor device. The most effective way to determine the effects of radiation on microelectronics is to test the devices in radiation environments. Analyses were completed to determine radiation exposure levels to various sensitive electronic components of the mobile router hardware for a number of space mission scenarios (see the graphs). These analytical levels were used when the electronics were exposed to a proton beam at the cyclotron facility at Indiana University (photograph on the next page). During the test, failure data were used to statistically calculate the mean time between failures. With the exception of one component, the mobile router electronics demonstrated a high immunity to radiation exposure. If alternatives are found for the poorly performing component, the mobile router could prove to be a good candidate for noncritical space applications. It should be noted that software was not verified in this research. The demands for the verification and validation of space-rated software systems could limit the use of many COTS products in high-reliability space applications. COTS software reliability requires further investigation.

The analysis and testing of commercial mobile router technology has demonstrated that this technology, with appropriate component replacement, could be a strong candidate for distributing general data among space assets. This could be applied to onboard data systems for habitat and research modules in future space exploration initiatives.

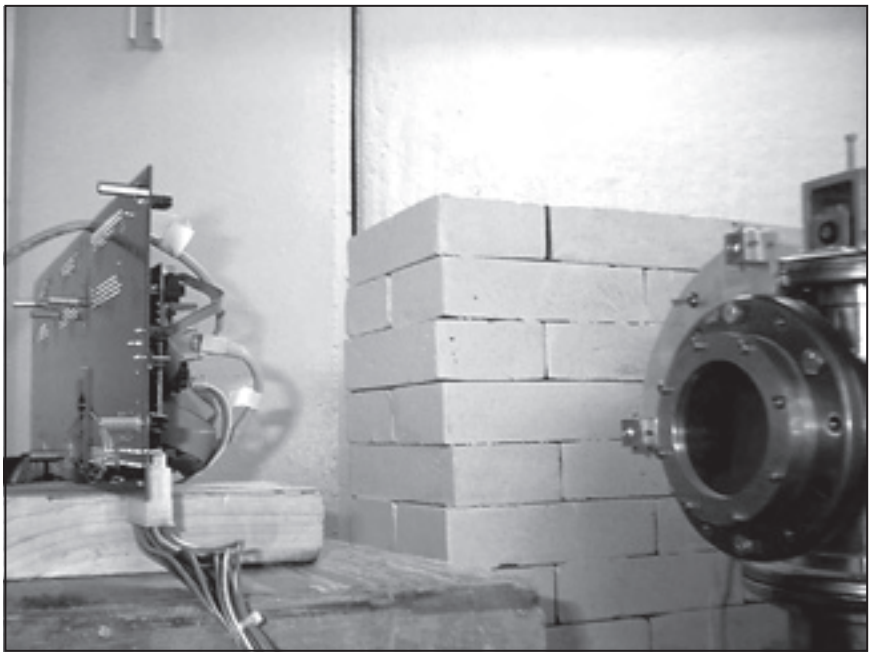

*Mobile router hardware test setup in front of the proton beam.*

The mobile-router feasibility study was funded by the NASA Electronics Parts Program and the Space Communications Applied Systems & Technologies Program of the former Space Communications Office.

**Glenn contact:**
David Andrew Carek, 216–433–8396, David.A.Carek@nasa.gov

**Zin Technologies contact:**
Alan J. Chmiel, 216–925–1291, Alan.J.Chmiel@nasa.gov

**Author:**
David Andrew Carek

**Headquarters program office:**
Office of Space Flight

**Programs/Projects:**
ISS, Earth Science, Space Shuttle, Exploration Systems

## Advanced Extravehicular Activity Subsystems Tested at Desert Research and Technology Studies Field Outing

As part of the Advanced Extravehicular Activity program, the NASA Glenn Research Center is responsible for communications, avionics, and informatics (CAI) subsystems for next-generation exploration spacesuits. Part of this effort involves testing operational concepts at the Desert Research and Technology Studies (Desert RATS) field outings. Desert RATS is a partnership of several NASA centers and outside industry involved in developing technologies applicable to the manned exploration of a planetary surface (the Moon and Mars). Individual teams work throughout the year on promising new technologies, which are candidates for demonstration at the outing.

The Desert RATS field outing is an opportunity to evaluate various concept technologies in a location selected to closely mimic characteristics of the Moon and Mars surface. The field outing is a laboratory for learning how to live and work during a human and robotic surface exploration mission. This year's exercise took place in a highly remote desert area near Meteor Crater, Arizona. The site was chosen for its terrain, lack of vegetation, and powdery soil. Held in September 2005, this year's outing involved integrated communications and data systems for two spacesuited subjects as well as interaction with the NASA Johnson Space Center Science Crew Operations and Utility Testbed (SCOUT) rover (see the photograph on the right). Approximately 120 individuals (9 from Glenn) participated at the test site.

*Two spacesuits being tested in conjunction with the SCOUT rover.*

Glenn developed the voice- and data-communications systems for the field outings. The communications system included both proximity voice and data networking (see the preceding photograph on the right) among surface assets. It also included satellite communications (see the lower photograph on the left) to the Exploration Planning Operations Center located at Johnson Mission Control. In addition, Glenn developed two CAI packs, which provided the communications, avionics, and informatics subsystems for each spacesuit (see the lower photograph on the right). These packs mount on the back of the portable life-support system and house the computer, radios, and other scientific instrumentation for the suit. The computer system in the CAI pack allowed the demonstration of advanced informatics software concepts. The NASA Ames Research Center worked in collaboration with Glenn to provide prototype software including voice recognition and productivity software integrated with helmet-mounted displays. Glenn also developed an audio subsystem to evaluate concept helmet-mounted audio interfaces. Digital signal processing techniques were used to clean up the audio from the suited subjects to make their vocalizations more intelligible. This research was funded by the Human Systems Research and Technology Program of the Exploration Systems Mission Directorate.

**Find out more about how Glenn's support of Desert RATS benefits space exploration:**
http://exploration.grc.nasa.gov/Exploration/outreach_articles/articles/Article-DRATS.html

**Glenn contacts:**
David Andrew Carek, 216–433–8396, David.A.Carek@nasa.gov;
Michael A. Cauley, 216–433–3483, Michael.A.Cauley@nasa.gov; and
Alan N. Downey, 216–433–3508, Alan.N.Downey@nasa.gov

**Authors:**
David Andrew Carek and Michael A. Cauley

**Headquarters program office:**
HSRT

**Programs/Projects:**
Exploration Systems

*Glenn communications engineer Michael Cauley checking out the satellite communications terminal.*

*Glenn engineers and contractors deploying a surface proximity networking relay station.*

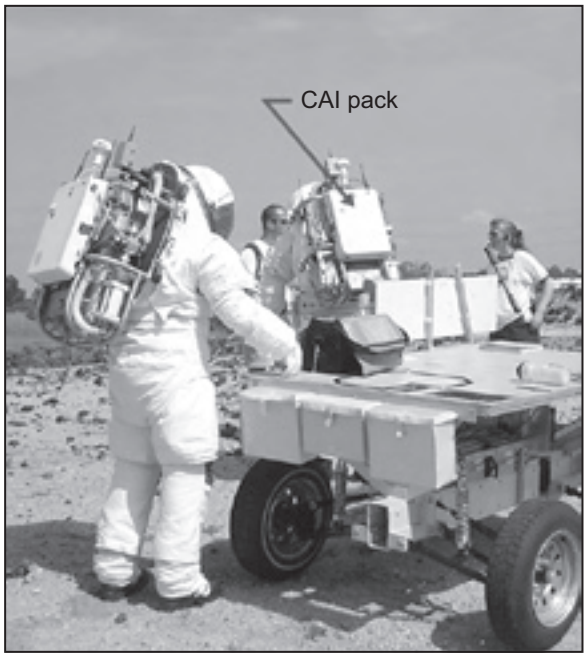


*Two CAI packs mounted on each of the advance spacesuits during dry run testing at Johnson.*

# Architectures and Protocols Assessed for Optical Networks Deployed on Aircraft Communication Systems

Most commercial aircraft require more antennas than in the past to accommodate a variety of required operating frequencies. As more antenna elements are deployed on an aircraft, existing electronics-based networking systems may not be the best way to route digital and analog signals because of the significant volume of electronic cables required to accommodate each antenna. The higher mass of cables would reduce fuel efficiency, increase electromagnetic interference, and make cable repair and maintenance more difficult. As an alternative, NASA Glenn Research Center's Satellite Network and Architecture Branch developed a radiofrequency/optical networking subsystem for data and voice transmission that reduces the adverse effects caused by conventional electronic subsystems.

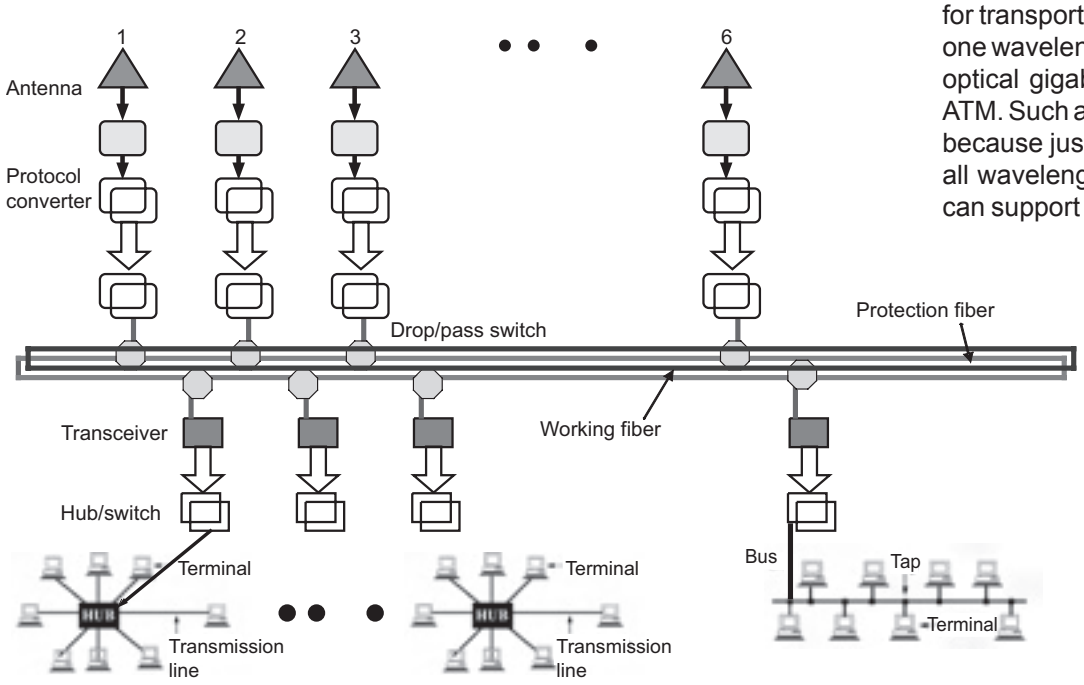


*Architecture of radiofrequency/optical backbone network suitable for supporting numerous antenna elements on an aircraft.*

The diagram shows the architecture of a radiofrequency/optical backbone network for supporting multiple antenna elements on an aircraft. There are six physical layers constructed in this architecture: the antenna, the protocol converter, a transceiver, protection and working fibers, another transceiver, and the hub and switch module. Protection and restoration data paths are used to prevent data loss in case of cable failure, port failure, or catastrophic failures. The architecture is based on the optical wavelength division multiplexing approach, which can support different types of protocols such as synchronous optical network (SONET)/synchronous digital hierarchy (SDH) time-division multiplexing, Ethernet system, and asynchronous-transfer-mode-(ATM-) packaging-based or cell multiplexing systems.

Two popular transport protocols proposed for the aircraft's networking backbones are SONET and wavelength division multiplexing (WDM). SONET has a number of advantages over other optical protocols, such as (1) less equipment needed, (2) increased network reliability, (3) easy access for switching and multiplexing, and (4) a flexible architecture to accommodate future requirements.

WDM relies on the fact that an increased number of wavelengths on a fiber tends to enhance the bit rate of network systems. A major attractive feature of the WDM structure is that each individual wavelength can use a different protocol for transport. For example, we could use one wavelength for SONET, a second for optical gigabit Ethernet, and a third for ATM. Such a WDM structure saves costs because just one amplifier can act upon all wavelengths. Most WDM equipment can support different types of interfaces, such as SONET, Ethernet (1 gigabit per second (Gbps), 10 Gbps, and fast), fiber channel, and ATM.

**Glenn contacts:**
Dr. Hung D. Nguyen, 216–433–6590, Hung.D.Nguyen@nasa.gov; and
Calvin T. Ramos, 216–433–9391, Calvin.T.Ramos@nasa.gov

**Author:**
Dr. Hung Nguyen

**Headquarters program office:**
Aeronautics Research

**Programs/Projects:**
Advanced communications, navigation, and surveillance architectures and system technologies

# Phase I Space Communications Testbed Developed

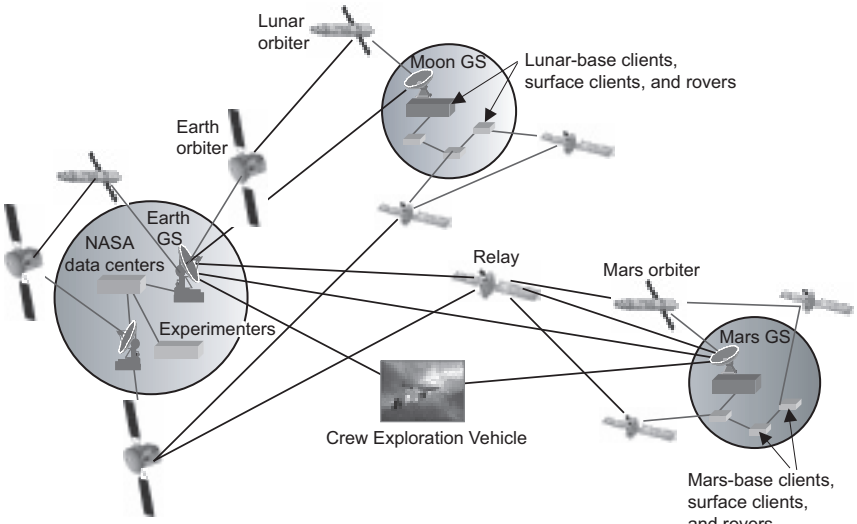


*Space communications architecture. GS, ground station.*

The Space Communications Testbed (SCT) is one of the defining projects of the Space Exploration Initiative that was awarded in April 2005. The SCT team is composed of ViaSat/Comsat (prime contractor) with Glenn Research Center, Goddard Space Flight Center, Langley Research Center, and the Jet Propulsion Laboratory as participating NASA centers.

The SCT is an integrated communications testbed focused on detailed testing of advanced space and ground communication networks, technologies, and client applications that are essential for future space exploration. Missions will utilize the testbed from development to operations for defining and validating mission requirements, testing communication schedules and patterns, testing and validating mission protocols, and verifying operational software. The testbed will function in an end-to-end environment where communications can occur continuously and seamlessly from a base station on the Moon to a computer connected to the Internet on Earth and, potentially, hopping through a series of relay satellites, as shown in the diagram. Customized, user-defined scenarios will specify the entities of the system, such as satellite and ground stations, and their properties, such as antennas and data rates.

SCT is divided into two phases. Phase I, a 1-year effort (April 2005 to 2006), will define a proof-of-concept system that NASA will use and evaluate. Phase II, a 3-year effort (2006 to 2009), will consist of system development and testing. In phase I, Glenn has the following responsibilities:

(1) **Lunar Relay Satellite system development**—The Lunar Relay Satellite is a satellite constellation system that will orbit the Moon. It will communicate with land entities on the Moon and satellite entities in space and will have cross-linking capabilities between individual satellites in the system. Orbital characteristics were based on the results of the Space Communications Architecture Working Group.

(2) **Link emulator development**—The link emulator provides bit-error-rate characteristics, link delays, data rates, and data loss. In phase II, the development will include aspects such as Doppler shift. The link emulator will use a technique called virtual large-area networks (LANs) to emulate multiple antennas on a satellite or ground station. Internally to the emulator, the connections will be dynamically bridged in an on-demand fashion. The number of connections to the emulator will be based on the number of ports available.

(3) **Protocol tradeoff study**—This year Glenn studied, tested, and evaluated a number of publicly and commercially available space-based protocols. The Glenn SCT team conducted a static analysis by evaluating code and documentation for parameters, such as the features and highlights of the protocol, assessment of the technology readiness level, the amount and thoroughness of protocol testing, and an identification of any known issues with the protocol. In addition, the team will conduct a dynamic test through the Protocol Research Evaluation Environment Testbed. The handbook from the protocol tradeoff study will serve as an operations guide for protocol integration in the SCT.

(4) **Monitor and controller**—The monitor and controller provide an interface for the main SCT controller located at ViaSat, to direct, manage, and control Glenn's regional testbed. Glenn's monitor and controller is responsible for configuring entities, starting and stopping the emulation, and providing health monitoring and statistics of the testbed. It will report warnings and errors to the main testbed at ViaSat.

**Find out more about Glenn's Satellite Networks & Architectures Branch:**
http://ctd.grc.nasa.gov/5610/5610.html

**Glenn contact:**
Richard A. Slywczak, 216–433–3493,
Richard.A.Slywczak@nasa.gov

**Author:**
Richard A.Slywczak

**Headquarters program office:**
Exploration Systems

**Programs/Projects:**
CEV, Life Support & Habitation, NGLT, RTF, Vehicle Systems, Satellite Missions

# INSTRUMENTATION AND CONTROLS

## Closed-Loop Actuation Concepts Investigated for Active Clearance Control

Active clearance control systems in the high-pressure turbine section of commercial aircraft engines are used to close the gap that exists between the turbine blades and shroud, minimizing leakage flow over the blade tip. Reducing this leakage flow will benefit specific fuel consumption, potentially saving the airline industry millions of dollars every year and lowering environmentally harmful nitrous oxide ($NO_x$) emissions, and it will also benefit the exhaust gas temperature overshoot that occurs during takeoff, improving the on-wing life of hot-section components and the time between overhauls. Current clearance control systems onboard modern engines only yield modest benefits because they rely on slow-response case cooling to match the thermal deflections of high-pressure turbine components. Significant gains may be realized by employing an active control system consisting of clearance probes and fast-response actuators to maintain tight clearances throughout the entirety of flight.

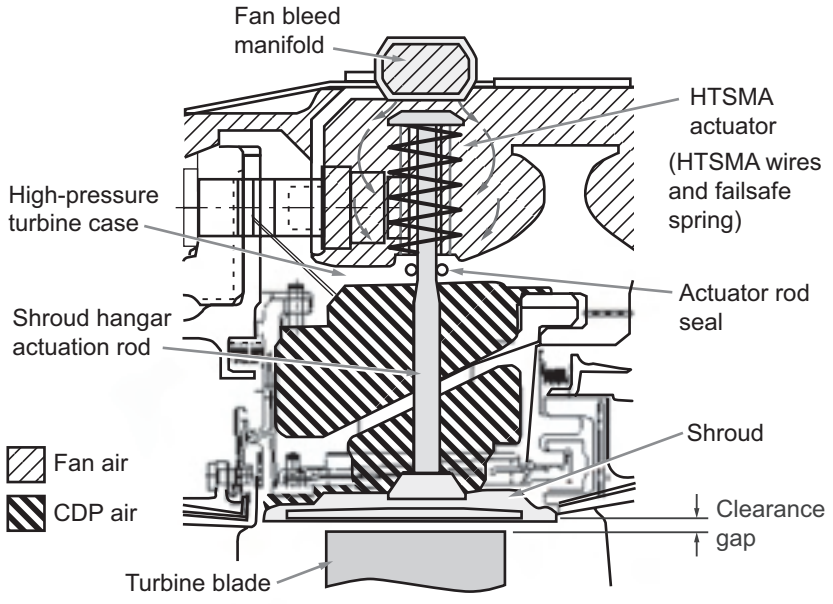


*HTSMA active clearance control actuator concept. CDP, compressor discharge pressure.*

COMPARISON OF CANDIDATE ACTUATORS

| Actuator | Approximate system weight, lb | Rate capability, in./sec | Maximum temperature, °F | Power consumption |
|---|---|---|---|---|
| Shape-memory alloy | 0.9 | ~ 0.1 | 930 | Low |
| Piezoceramic (PZT) | 43 | 200 | 400 | Moderate |
| Servohydraulic | 58 | 0.5 | 600 | High |

In-house researchers at the NASA Glenn Research Center are developing a high-temperature shape-memory alloy (HTSMA) actuator that is demonstrated to have the physical robustness necessary to withstand the extreme temperatures of the high-pressure turbine. Shape-memory alloys are promising actuation candidates because they have energy densities an order of magnitude higher than other candidate actuators, an attractive characteristic in meeting the stringent weight and size goals of a flight-worthy actuator package. They are also preferred because they can potentially operate without the addition of bulky power amplifiers, thereby minimizing energy consumption and weight of the actuation system. A viable HTSMA actuator concept was developed for application in the Active Clearance Control Test Rig at Glenn. The concept consists of several parallel HTSMA wires ($Ni_{30}Pt_{20}Ti_{50}$) that longitudinally expand or contract with changes in temperature, moving the shroud inward or outward relative to the blades. For implementation in a high-bypass turbofan engine, each actuator must displace at least 0.033 in. against large time-varying loads up to 2200 lbf and wide variations in the ambient temperature.

For evaluation of the HTSMA concept, a high-fidelity model of the actuation system was developed, the design was optimized, and the actuators were simulated to verify controllability across the engine's operating envelope. Transient simulations in a testbed engine simulation (see the graphs) revealed that a design consisting of ten 0.09-in.-diameter wires can provide rub-free tracking during rapid operating point transitions. It also showed that only a small amount of bleed coolant air from the fan is necessary for actuation and that a linear proportional-integral-derivative control law with anti-windup protection is sufficient for precise shroud control with the nonlinear actuator across the operating envelope.

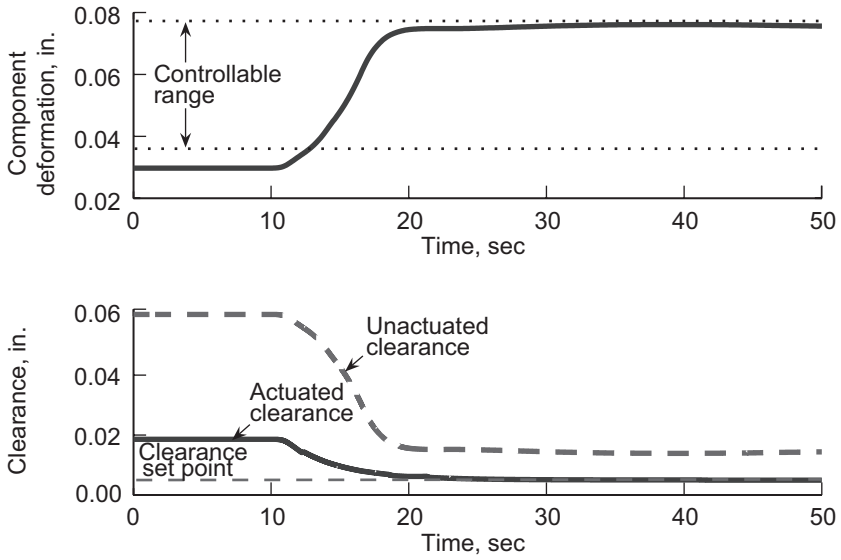


*High-pressure turbine component deformation and simulated active clearance control scenarios during takeoff.*

Shape-memory alloys, along with conventional servohydraulics and piezoelectric stacks are part of a broad feasibility study of active clearance control actuators. Servohydraulic actuators are a low-risk conventional technology, but resulting designs are high in weight and require large hydraulic power draw to operate. On the other hand, the two smart material actuators—piezoelectrics and shape-memory alloys—are high-reward technologies with greater energy densities but are considered to be of lower technological maturity and, therefore, higher-risk. The ultimate goal of this ongoing effort is to design, build, and demonstrate conventional and smart material actuation devices on the Active Clearance Control Test Rig.

This in-house study was conducted by Glenn's Controls and Dynamics Branch and the QSS Group, Inc., in collaboration with Glenn's Mechanical Components and Advanced Metallics Branches.

**Bibliography**

DeCastro, J.; and Melcher, K.: A Study on the Requirements for Fast Active Turbine Tip Clearance Control Systems. AIAA–2004–4176, 2004.

DeCastro, J.; Melcher, K.; and Noebe, R.: System-Level Design of a Shape Memory Alloy Actuator for Active Clearance Control in the High Pressure Turbine. AIAA–2005–3988, 2005.

**QSS Group, Inc., contact:**
Jonathan A. DeCastro, 216–433–3946, Jonathan.A.DeCastro@nasa.gov

**Glenn contact:**
Kevin J. Melcher, 216–433–3743, Kevin.J.Melcher@nasa.gov

**Authors:**
Jonathan A. DeCastro and Kevin J. Melcher

**Headquarters program office:**
Aeronautics Research

**Programs/Projects:**
VSP

## Hybrid-Fuel-Cell Power System Modeling and Controls Design Being Developed

Dynamic modeling and control methodologies are being developed to control the hybrid solid oxide fuel cell (SOFC) power system throughout its operating envelope and to develop subsystem integration processes, flow-down approaches for specifications, and corresponding analysis tools. As the aviation industry moves toward higher efficiency electrical power generation, all-electric aircraft (zero emissions), and more quiet aircraft, fuel cells are being sought as the technology that can deliver on these high expectations. The hybrid solid oxide fuel cell system combines a fuel cell with a microturbine to obtain up to 70-percent cycle efficiency and then distribute the electrical power to the loads via a power-distribution system. The challenge is to understand the dynamics of this complex multidisciplinary system, specify the subsystem interfaces, and design distributed controls that take the system through its operating scenarios in a stable and safe manner. All this needs to be accomplished while the overall system behaves much like a traditional power system in terms of its specifications and expected performance.

In this modeling and analysis approach, high-fidelity models are being developed for the distributed control designs, interface specification, and stability analysis; whereas low-fidelity models are being developed for longer time transient response analysis and to develop system control strategies. The high-fidelity models extend to frequencies that are up to the subharmonic frequency (i.e., half the switching frequency of the power processors), typically tens of kilohertz. In this regard, the power management and distribution system dictates the frequencies that need to be included in the

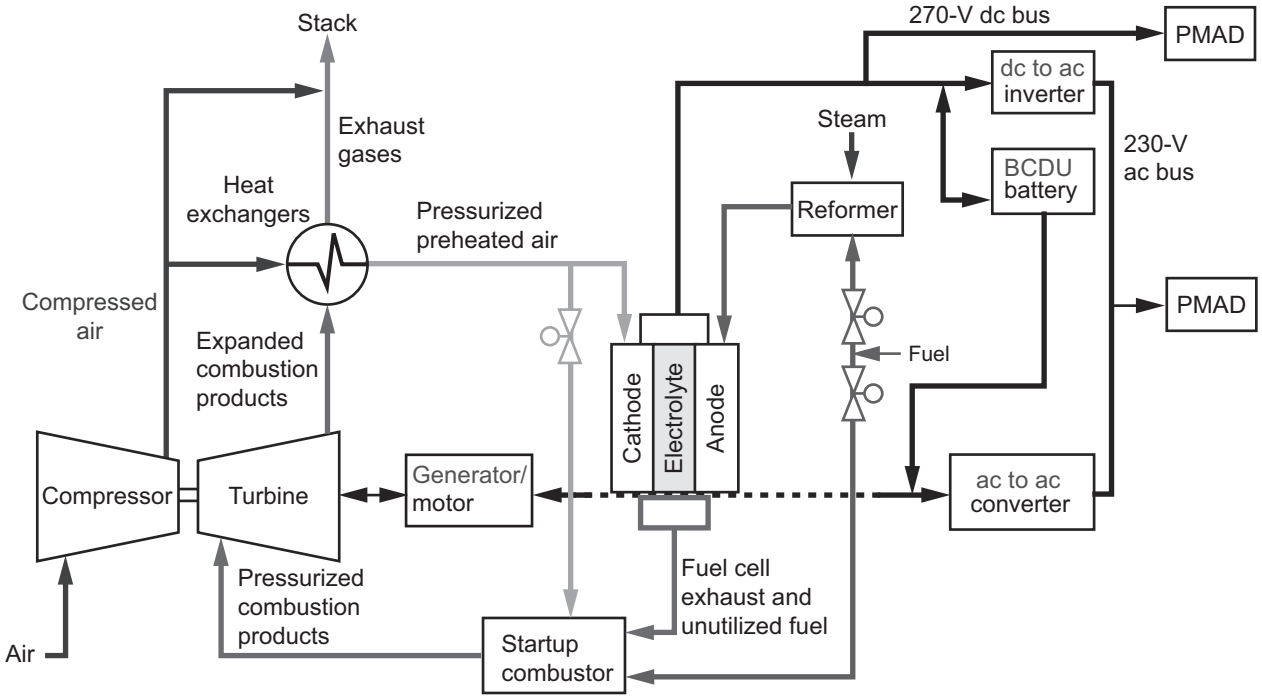


*Hybrid SOFC power system design. PMAD, power management and distribution; BCDU, battery charge discharge unit; ac, alternating current; dc, direct current.*

power source models so that the hybrid fuel cell properly interfaces with the dynamics of a typical power system. A preliminary detailed SOFC model has been developed for this analysis, which includes the conservation equation dynamics, ion diffusion, charge transfer kinetics, and inherent impedances.

It has been determined that the fuel cell mathematical model needs to include the following: the fuel cell voltage relation based on the Gibbs free energy and the Nernst potential, lumped volume conservation equations modeling that includes steady-state electrochemistry and the enthalpies of formation, ion diffusion modeling, charge transfer kinetics modeling, and the inherent electron flow impedances. This mathematical model derivation can be improved and calibrated by impedance spectroscopy testing.

The fuel cell model developed so far covers most of the modeling areas mentioned, including the development of simplified low-fidelity models. For the power system, certain key components, such as converters and inverters, are modeled with the *d-q* axes approach (i.e., in

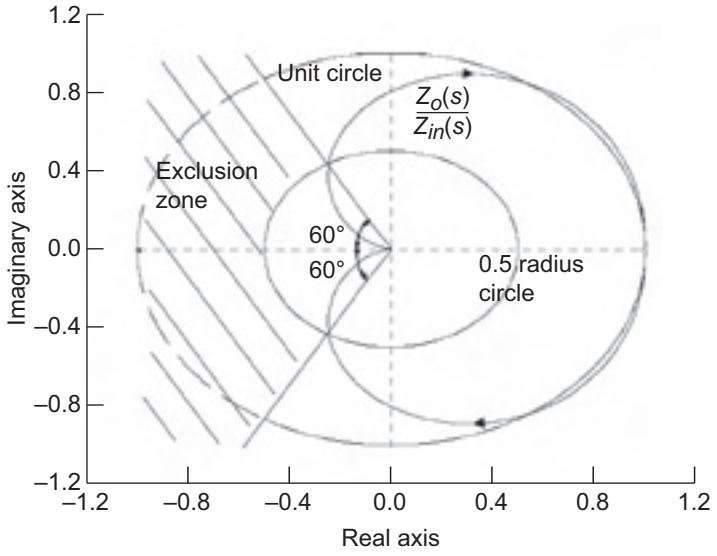


*Nyquist stability interface impedance specification. $Z_o$, power source output impedance; $Z_{in}$, power load input impedance; G(s), transfer function (s-function of frequency).*

a stationary reference frame). So far, most of the power-distribution components that interface with the hybrid fuel cell system have been modeled. This modeling approach will allow researchers to study and specify the dynamics of these interfaces and to design system operations and control. So far, system operations and control designs have been conceived, such as (1) using a battery to temporarily divert the load current in case of a load loss (which presents a safety issue) until the fuel supply to the fuel cell can be cut off or (2) using the battery for load transients to allow time to rebalance the source power of the microturbine and the fuel cell and match it to the load demand. The microturbine model is currently based on a steady-state spreadsheet model where reduced-order dynamics are added. A high-fidelity microturbine model based on conservation equations will be developed for the hybrid fuel cell. These equations also will be used to model other auxiliary components like diffusers, heat exchangers, heaters, and humidifiers.

The stability specification methodology calls for using the models developed, after they have been calibrated with test data, to determine the power source (fuel cell and microturbine) output impedances at the various system operating points involving voltage, temperature, and pressures. A preliminary top-level Nyquist stability specification is in the process of being developed. On the basis of this specification and the knowledge of the source impedances, the limits on the power-distribution load impedances will be determined at the fuel cell and microturbine interfaces. This will allow the system design to be stable with quantifiable stability margins. The resulting methodology will start by modeling the hybrid system components on the basis of the individual component designs, testing to calibrate the models, designing stable power source-distributed controls, determining the source impedances, and finally (on the basis of these impedances) specifying the power-distribution components that will interface with the source at these system interfaces. In addition, the methodology will specify the closed-loop control designs and, eventually, the inrush current and the voltage/current spectral densities that limit the life of the fuel cell. Once the system is shown to be stable, the reduced-order models will be used to design and verify the system operation controls and to conduct transient analysis.

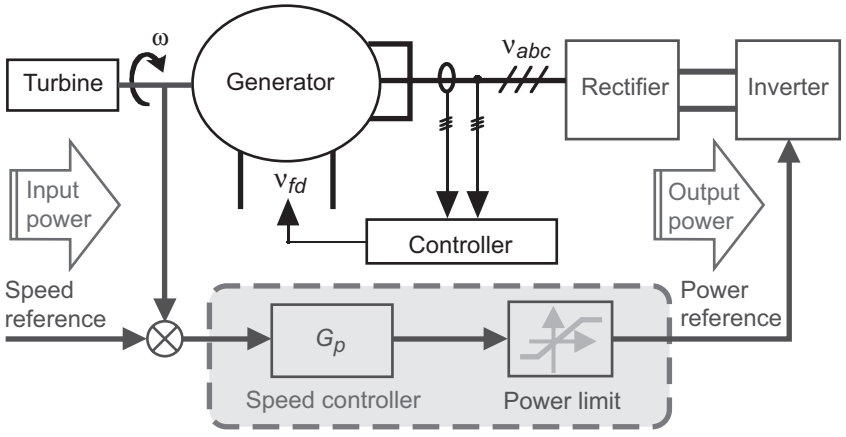


*Turbine speed-control diagram. ω, turbine speed; $v_{abc}$, three-phase voltage; $v_{fd}$, field winding terminal voltage; $G_p$, speed controller transfer function.*


**Bibliography**

Kopasakis, George, et al.: A Theoretical Solid Oxide Fuel Cell Model for System Controls and Stability Design. Proceedings of GT2006 ASME Turbo Expo 2006: Power for Land, Sea and Air. GT2006–91247, 2006.



**Glenn contact:**
George Kopasakis, 216–433–5327, George.Kopasakis-1@nasa.gov

**Author:**
George Kopasakis


**Headquarters program office:**
Aeronautics Research

**Programs/Projects:**
LEAP, AFCPS

# Retrofit Architecture for Intelligent Propulsion Control Demonstrated to Compensate for Thrust Asymmetry Due to Engine Degradation

A typical engine inner-loop control architecture uses fuel flow to control fan speed, which is assumed to be highly correlated to engine thrust. However, as the engine ages the relationship between fan speed and thrust changes, thus changing the thrust response to throttle input. If all engines on a multi-engine aircraft do not have the same throttle-to-thrust relationship, a thrust imbalance can result, producing unwanted yaw, which requires pilot intervention to correct. To overcome this problem, researchers at the NASA Glenn Research Center developed and demonstrated a retrofit architecture for intelligent turbofan engine control and diagnostics that changes the outer-loop fan-speed reference signal to account for changes in the fan speed-to-thrust relationship. This architecture includes a thrust estimator, the output of which is compared with the thrust response of a "nominal" engine to generate the corrected fan speed reference.

For a two-engine aircraft, as in the example, the intelligent control system evaluates the safety, performance, and capabilities of the engines. It takes input from both engines (control signals, sensed variables, thrust estimate, etc.) to determine each engine's current health and fitness for the mission. It also generates the outer-loop thrust command that both engines follow. If the intelligent control determines that the condition of an engine is such that corrective action is beyond the scope of the propulsion control (for example, a problem that might compromise the mission), it communicates this information to the mission manager. The intelligent retrofit architecture was demonstrated to compensate for thrust imbalance in a fixed-base piloted flight simulator for a commercial aircraft/engine simulation with one of the two engines severely degraded. With the intelligent control adjustment on, the pilot did not have to retrim the plane or adjust the throttles individually to maintain heading, thus resulting in reduced pilot workload. The thrust estimator tracked the actual thrust of the degraded engine and enabled direct thrust control. The work was performed in-house at Glenn.

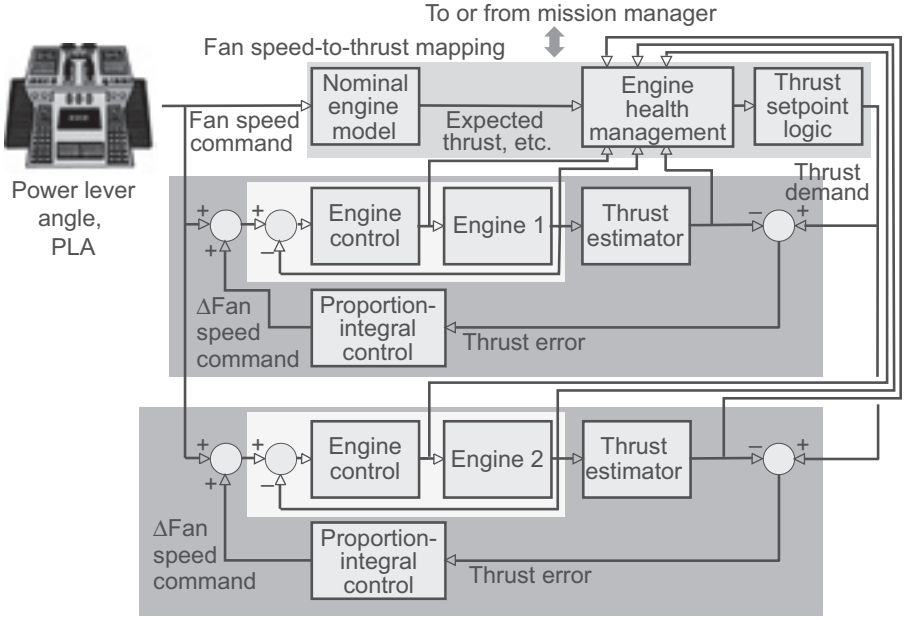


*Hierarchical intelligent control architecture consisting of the direct control level (the two small rectangles with light shading including engine control and engines 1 and 2), which controls the engine fan speed to a setpoint; the outer-loop control level (the two large rectangles with dark shading in the center and bottom of the figure), which adjusts the fan-speed reference signal to the direct control level to set thrust; and the intelligent control level (the large shaded rectangle at the top of the figure), which performs diagnostics and health management and sets the thrust reference for the outer-loop control.*

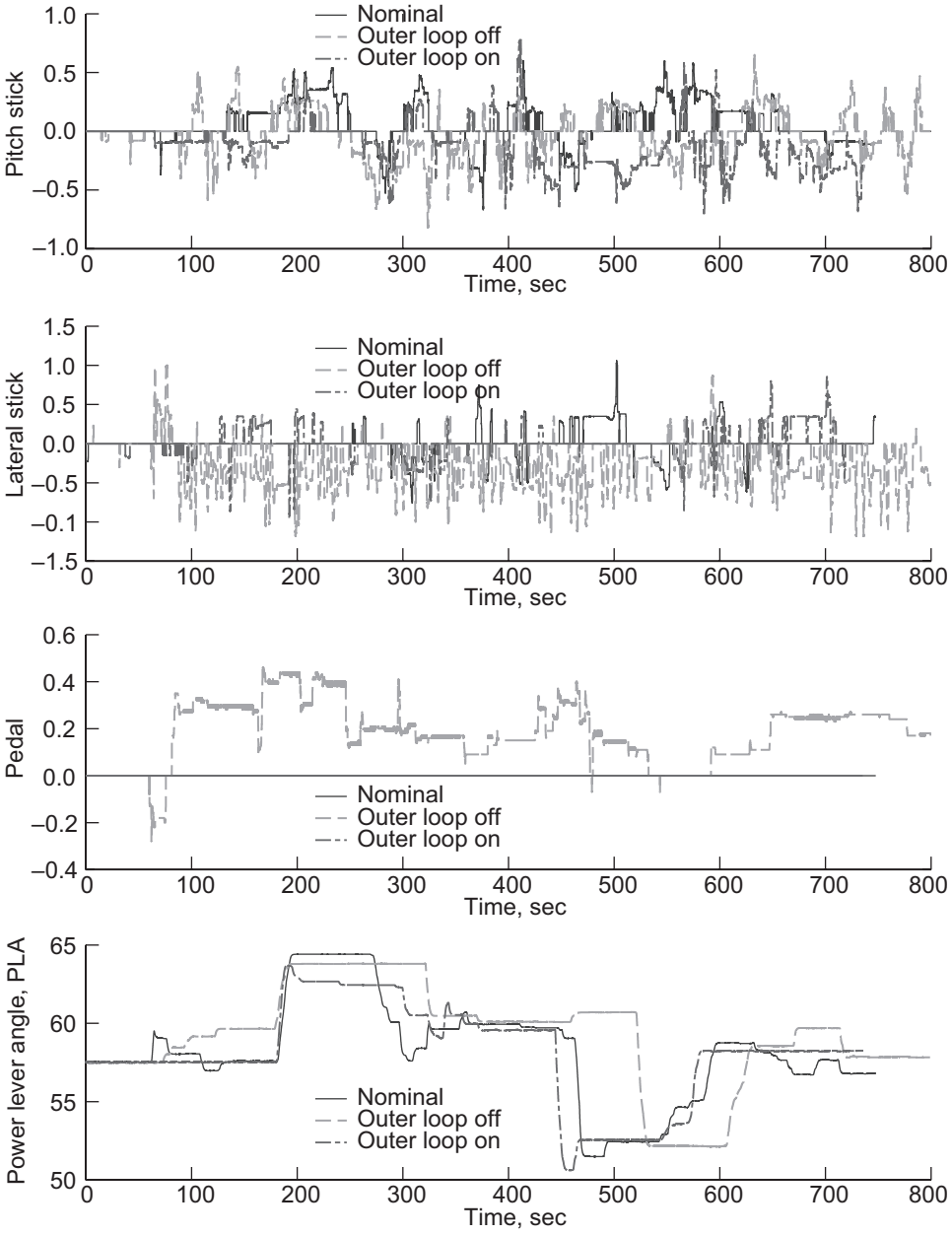


*Plots showing pilot workload in three cases: (1) both engines nominal, (2) one engine degraded with no outer-loop control, and (3) one engine degraded with outer-loop control on. The variables are the four pilot input devices: pitch stick, lateral stick, rudder pedals, and throttle or power lever angle. It is clear that the nominal and degraded cases under intelligent control were similar in terms of pilot workload (the amount of control movement the pilot needed to use to maintain the flight path). The degraded case with no intelligent control (no outer loop control) required much more effort by the pilot in terms of both lateral stick (which affects roll) and rudder pedals (which affect yaw).*

**Bibliography**

Litt, Jonathan S., et al.: A Demonstration of a Retrofit Architecture for Intelligent Control and Diagnostics of a Turbofan Engine. AIAA–2005–6905, 2005 (NASA/TM—2005-214019. ARL–TR–3667). http://gltrs.grc.nasa.gov/cgi-bin/GLTRS/browse.pl?2005/TM-2005-214019.html

**U.S. Army Research Laboratory at Glenn contact:**

Jonathan S. Litt, 216–433–3748, Jonathan.S.Litt@nasa.gov

**Author:**

Jonathan S. Litt

**Headquarters program office:**

Aeronautics Research

**Programs/Projects:**

Propulsion 21

# Data Qualification and Validation Testbed—New Tool Developed and Demonstrated for Evaluating the Performance of Engine Health Management Systems

Online data validation is a performance-enhancing component of modern engine control and health management systems. It is essential that the performance of a data-validation system be verified prior to its use in a flight-rated engine control and health management system. A new Data Qualification and Validation (DQV) Testbed application was developed and demonstrated. This testbed provides a systematic test environment for that performance verification. It was used to evaluate a model-based data-validation package being employed as the data-validation component of a rocket engine health management system. The DQV Testbed was developed and evaluated through an in-house effort at the NASA Glenn Research Center in collaboration with Christian Brothers University and Expert Microsystems, Inc.

The DQV Testbed is composed of four major modules: the test manager module, the data source module, the data-validation module, and the analysis and reporting module. The functionality of these modules and the information flow between them is illustrated in the diagram. The test manager module is used to define the test conditions, and it controls the overall execution of the test sequence. The data source module generates test data for the data-validation module. The data-validation module acts as an interface between the testbed and the health management system being evaluated. The analysis and reporting module evaluates the output from the system being tested with the known test conditions and generates a series of reports summarizing the results.

The primary benefit of the DQV Testbed is its ability to execute numerous health management system evaluations and to present results in a concise, yet informative manner. The reporting of results can be customized for a particular health management system as in the sample report shown in the table. Alternatively, a broad-based report can provide evaluation results in a histogram format using five generic categories:

(1) **Correct fault detection and isolation**—A fault condition was detected and isolated to the one correct fault.

(2) **Fault detection and partially correct isolation**—A fault condition was detected and isolated to a fault candidate list that included the correct fault.

(3) **Fault detection, but incorrect isolation**—A fault condition was detected, but it was isolated to a fault candidate list that did not include the correct fault.

(4) **No fault detection**—A fault condition was not detected.

(5) **False fault detection**—A fault condition was incorrectly detected when a fault was not inserted.

Results like these provide a means for developers to characterize the performance of and assess tradeoffs for a given health management system.

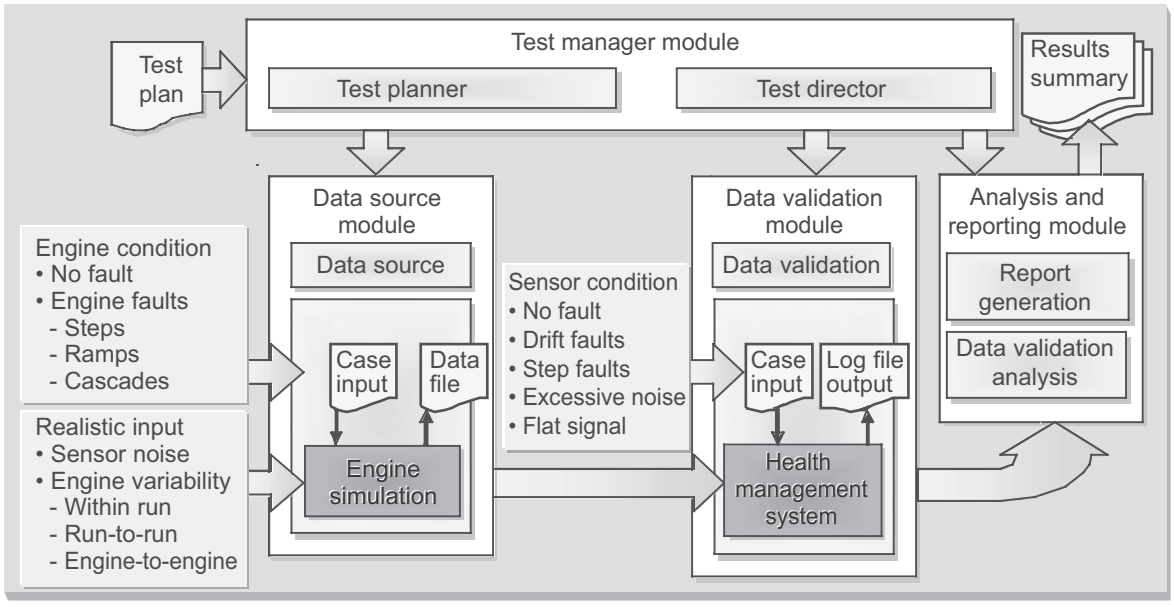


*Functionality and information flow within the DQV Testbed.*

SAMPLE REPORT GENERATED BY DQV TESTBED

| Result | Sensor fault detection and isolation method | | | | | | | |
|---|---|---|---|---|---|---|---|---|
| | Engine build variation disabled | | | | Engine build variation enabled | | | |
| | Version 1 | | Version 2 | | Version 1 | | Version 2 | |
| | Test series 1 | Test series 2 | Test series 1 | Test series 2 | Test series 1 | Test series 2 | Test series 1 | Test series 2 |
| Threshold limit exceeded | 25.35 | 24.12 | 18.90 | 19.12 | 23.90 | 25.10 | 20.67 | 20.62 |
| Relationship failed | 10.92 | 10.88 | 8.05 | 8.07 | 10.57 | 10.78 | 7.84 | 8.05 |

During initial studies, the DQV Testbed was shown to be an effective tool for cost-effective and comprehensive testing of health-monitoring systems. It provides an efficient avenue for assessing the strengths and weaknesses of prototype data-validation and fault-detection systems by improving the understanding of those systems' capabilities and tradeoffs. The testbed provides a potentially useful and important element of the infrastructure needed to iteratively develop and flight-qualify future propulsion health-monitoring systems.

**Bibliography**
Sowers, T.; Santi, L.; and Bickford, R.: Performance Evaluation of a Data Validation System. AIAA–2005–4486, 2005.

**Analex Corporation contact:**
T. Shane Sowers, 216–433–3405, Thomas.S.Sowers@nasa.gov

**Glenn contact:**
Kevin J. Melcher, 216–433–3743, Kevin.J.Melcher@nasa.gov

**Authors:**
T. Shane Sowers and Kevin J. Melcher

**Headquarters program office:**
Exploration Systems

**Programs/Projects:**
NGLT

**Special recognition:**
2005 Software Release Award from the Technology Transfer and Partnership Office; 2005 Space Act Award

## Fiber Bragg Gratings Operated at 1000 °C

Fiber Bragg gratings are formed by periodic variations of the refractive index in the core of an optical fiber. These periodic variations allow a fiber Bragg grating to pass the majority of light propagating through a fiber while reflecting back a narrow band of the incident light with a particular peak wavelength called the Bragg wavelength. In response to induced disturbances, the Bragg wavelength changes, making the grating a versatile sensing device. However, because they are "written" in germano-silicate fibers, the gratings are expected to fail at high temperatures because of the devitrification (crystallization) of the host material and the dissipation of the gratings themselves.

To assess the stability of Bragg gratings at high temperatures, researchers at the NASA Glenn Research Center evaluated the performance of the devices at temperatures up to 1000 °C using commercially available polyimide-coated high-temperature gratings annealed by the manufacturer to 300 °C. The gratings were placed in a furnace, and the signals generated by them were sent to photodetectors and, from there, to a spectrum analyzer. After that, the signals were fed into a computer equipped with LabVIEW software. This software was used to control and monitor the equipment as well as to process the data.

The tests included thermal cycling from room temperature to 750 and 1000 °C as well as prolonged exposure of the gratings to 1000 °C. The thermal limits of the tests were restricted by the test configuration and could be extended to even higher temperatures.

The top left graph on the next page shows test results from continuous operation of Bragg gratings at 1000 °C for over 400 hr. The top right graph describes events that happened during the first 25 hr of testing. It also shows the transition from degradation in the grating reflectivity to a formation of a stable response after 15 to 16 hr. The final graph demonstrates test results from continuous thermal cycling of Bragg gratings from room temperature to 1000 °C. It clearly shows the first run (cycle) during which the transient phenomenon and the formation of the stable response occur. After that, the consequent runs show very high repeatability. During the tests, the gratings were able to track the temperature measured by reference s-type thermocouples within 3-percent accuracy.

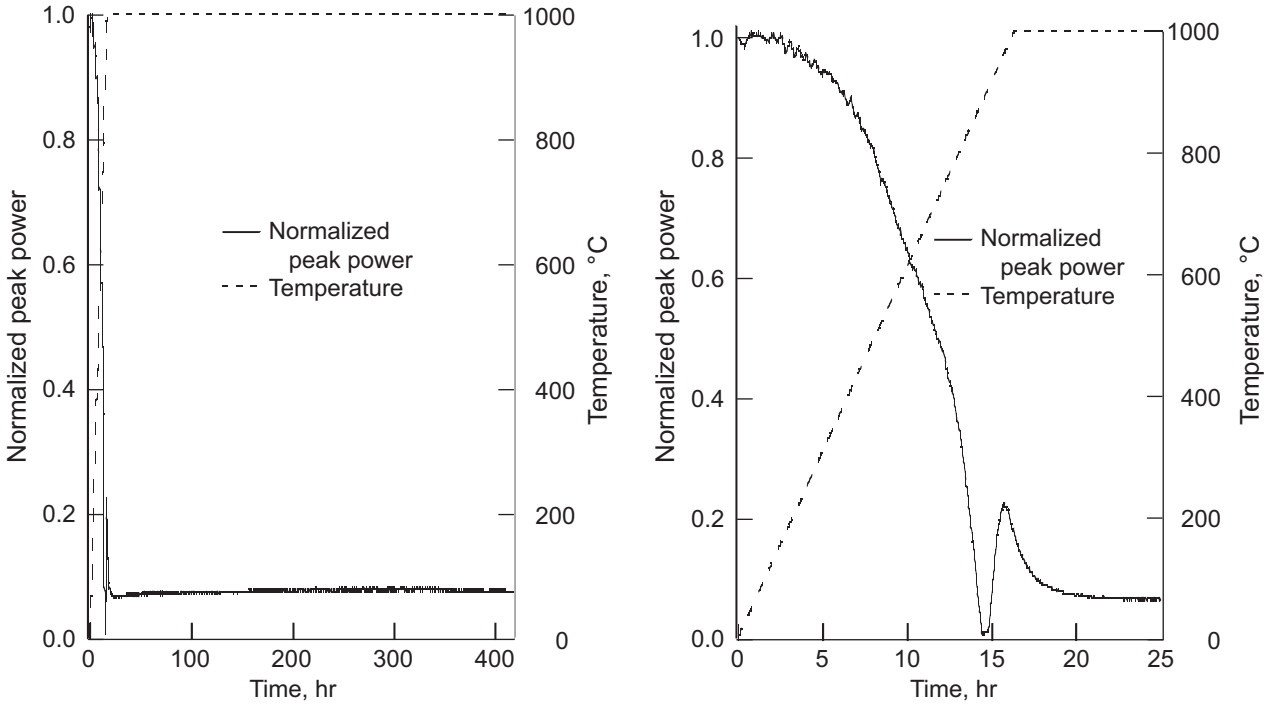


*Left: Test results from continuous operation of Bragg gratings at 1000 °C after 400 hr. Right: Formation of a stable response during the first 25 hr.*

The tests confirmed the formation, at high temperatures, of secondary thermally stable gratings in the germania-doped glasses. These secondary gratings were formed in place of the primary ones originally written by the ultraviolet light. Our results were corroborated by similar data obtained independently and simultaneously by other research groups, including Sabeus Photonics, United States; Royal Institute of Technology, Sweden; and Communication Research Center, Canada.

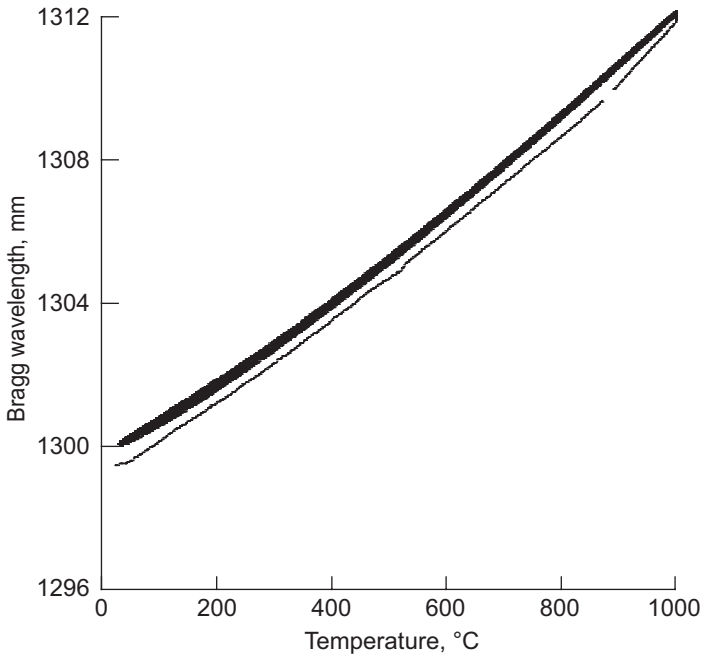


*Test results from thermal cycling of Bragg gratings from room temperature to 1000 °C.*

**Bibliography**

Juergens, J., et al.: Thermal Evaluation of Fiber Bragg Gratings at Extreme Temperatures. AIAA–2005–1214, 2005.

Juergens, Jeffrey, et al.: Thermal Evaluation of Fiber Bragg Gratings at Extreme Temperatures. NASA/TM—2005-213560 (AIAA–2005–1214), 2005. http://gltrs.grc.nasa.gov/cgi-bin/GLTRS/browse.pl?2005/TM-2005-213560.html

**Glenn contact:**
Dr. Grigory Adamovsky, 216–433–3736,
Grigory.Adamovsky-1@nasa.gov

**Author:**
Dr. Grigory Adamovsky

**Headquarters program office:**
Aeronautics Research, VSP

**Programs/Projects:**
LEAP, AEFT

# In-Plane Biaxial Loading Tests Used to Develop and Optimize a Heater Head Pressure Vessel Design

Testing capabilities recently developed at the NASA Glenn Research Center are being used to conduct highly vital tests in support of major and significant components of the Stirling Radioisotope Generator (SRG). These tests help in the development of an analytical life-prediction methodology and assist in verifying the life of flight-design components. Key components within the SRG undergo very harsh operating environmental conditions. For example, the heater head pressure vessel must bear high-temperature loads for an extended period of time. Such conditions are very worrisome since they impose life-limiting material creep and a slow gradual increase in strain, which will lead to an eventual breakdown. Efforts are ongoing to design an optimized heater head vessel that meets engine operation requirements. Substantial progress has been made.

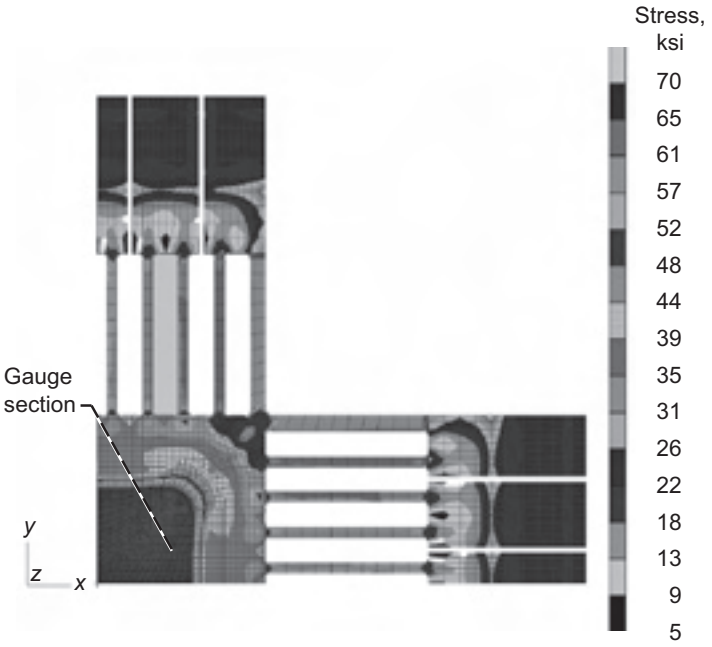


*Von Mises stress distribution under equibiaxial loading conditions.*

Experimental testing under biaxial loading is generally the appropriate approach for properly evaluating the performance, assisting in the design, and understanding the material behavior of heater head components under complex stress states (refs. 1 to 4). Furthermore, the structurally critical cylindrical heater head is made of thin-section wrought Inconel 718 but must operate at temperatures as high as 650 °C. Creep resistance is the primary durability limitation. Experiments under equibiaxial and nonequibiaxial loadings are being performed using cruciform-type specimens at combined thermomechanical loading conditions emulating a creep environment. This is followed by detailed three-dimensional finite-element analyses of the specimen under both elastic and steady-state creep conditions. It is to model the high-temperature creep, to calibrate the accuracy of the specimen's geometry, and to plan for the biaxial testing.

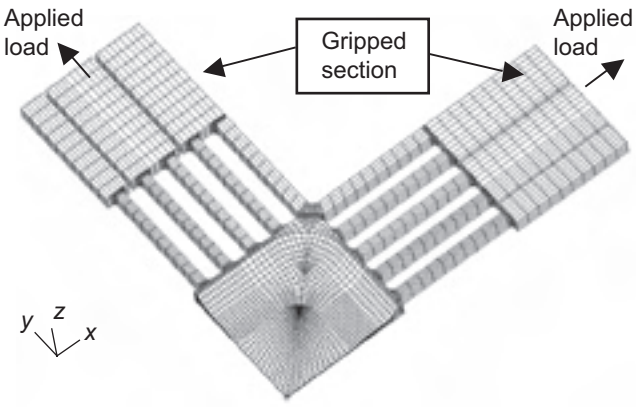


*Finite element model of the cruciform specimen and applied loading conditions.*

A cruciform plate test specimen design was successfully developed and optimized with overall dimensions of 12 by 12 by 0.625 in. (30.48 by 30.48 by 1.5875 cm) and a gauge area of 2.3 by 2.3 by 0.050 in. (5.842 by 5.842 by 0.127 cm) (ref. 1). The most important feature of the design was the four sets of flexures that were incorporated to partially decouple the applied biaxial loading. Detailed dimensions of the specimen are shown in the preceding figure. This design was tested and checked for compatibility with the in-plane biaxial testing systems installed at Glenn (ref. 1). The desired uniform stress state was achieved in the gauge region (see the figure above). This indicates that this cruciform specimen is suitable for biaxial testing and that these analyses will have a relevant role in evaluating the performance of this key component.

The benchmark testing was performed in collaboration with Glenn's Thermal Energy Conversion Branch as part of a Glenn in-house project supporting the development of the SRG110. NASA's Science Mission Directorate provided funding for this effort. The overall SRG110 project is managed by the Department of Energy. Lockheed Martin and Infinia Corporation are developing the SRG110 for the Department of Energy. Glenn is providing supporting technology development for the SRG110, independent verification and validation testing, and advanced technology efforts.

**References**

1. Bartolotta, Paul A.; Ellis, J. Rodney; and Abdul-Aziz, Ali: Structural Test Facility for In-Plane Biaxial Testing of Advanced Materials. Proceedings of the 1995 Symposium on Multiaxial Fatigue and Deformation Testing Techniques, ASTM, no. 1280, 1997, pp. 25–42.

2. Johnson, A.E.: Creep Under Complex Stress Systems at Elevated Temperatures. The Institution of Mechanical Engineers Proceedings, vol. 164, 1951, pp. 432–447.
3. Ellis, John R.; and Abdul-Aziz, Ali: Specimen Designs for Testing Advanced Aeropropulsion Materials Under In-Plane Biaxial Loading. NASA/TM—2003-212090, 2003. http://gltrs.grc.nasa.gov/cgi-bin/GLTRS/browse.pl?2003/TM-2003-212090.html
4. MSC/PATRAN Graphics and Finite Element Package, Vols. I and II, McNeal-Schwendler Corporation, Costa Mesa, CA, 1997.

**Cleveland State University contact:**
Dr. Ali Abdul-Aziz, 216–433–6729, Ali.Abdul-aziz@nasa.gov

**Glenn contact:**
David L. Krause, 216–433–5465, David.L.Krause@nasa.gov

**Authors:**
Dr. Ali Abdul-Aziz and David L. Krause

**Headquarters program office:**
Science Mission

**Programs/Projects:**
SRG110

## Finite Element Analysis Used to Study a Rotating Disk Subject to Cracking Under Typical Turbine Engine Loading Conditions

Health management development for advanced propulsion systems and ultrasafe engine technologies continues to be one of NASA's aviation safety program's goals. Such health management systems will assist in predicting, detecting, preventing, and overseeing safety-significant propulsion malfunctions. The primary goal is to minimize the number of propulsion system faults that lead to or contribute to civil aircraft accidents. Moreover, the health monitoring of essential and key components in aircraft engines, such as rotors, is gaining increased interest among engine makers and government institutions involved in aviation safety because it is becoming necessary to impose safety conditions during operation and to lower maintenance costs. In summary, having reliable diagnostic tools for the damage detection and health monitoring of rotating components is important in maintaining engine safety and reliability.

The NASA Glenn Research Center's role in supporting the NASA Aviation Safety Program involves providing finite-element analytical studies to study the durability issues of a rotor disk for a propulsion system. This led to carrying out analyses under representative engine loading conditions to investigate the application, performance, and functionality of an in-house crack-detection system. Rotational speeds in the range of 2000 to 10,000 rpm were used. Several key

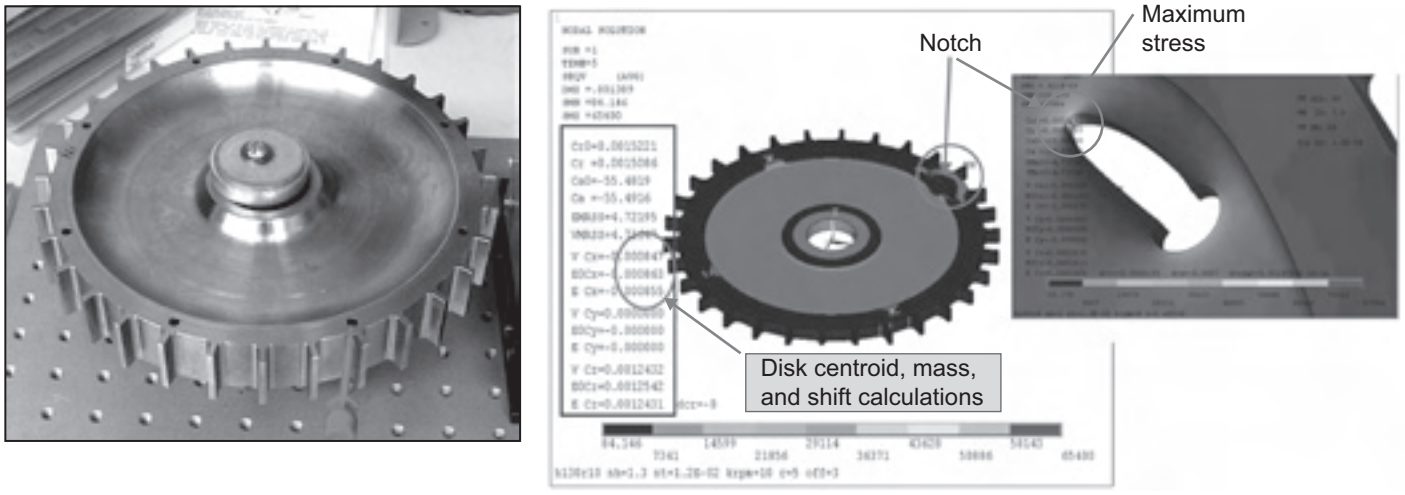


*Left: Rotor disk with attachment blades. Right: Von Mises stress distribution at 10,000 rpm for a 1.3-in. notch located in the rim region. Results for nickel CM–400 with the blade-hole aligned.*

design parameters, such as center-of-mass shift, induced cracks that ranged in length from 0.2 to 2.0 in. (1 to 5 cm), attachment blades, and typical holes within the disk, were explored to study their influence on the crack-detection system performance. Additional activities included comparing analytically derived results with those obtained from the experiment to verify the effectiveness and applicability of the system. The figures display typical results showing the relevant influence of these parameters on the performance of the disk and the crack-detection system. Furthermore, the results indicate that adding notches to the disk will allow systematic evaluation of crack-detection techniques by implementing highly controlled crack-initiation and crack-growth tests on a subscale, cost-effective spinning rotor.

**Bibliography**

Abdul-Aziz, Ali; Trudel, Jeffrey J.; and Baaklini, George Y.: Finite Element Design Study of a Bladed, Flat Rotating Disk to Simulate Cracking in a Typical Turbine Disk. Proceedings of the SPIE Symposium on Nondestructive Evaluation and Health Monitoring of Aerospace Materials, Composites, and Civil Infrastructure IV, vol. 5767, 2005, pp. 298–307.

ANSYS Finite Element Program. ANSYS Release 7.1, ANSYS, Inc., Canonsburg, PA, 2003.

**Cleveland State University contact:**
Dr. Ali Abdul-Aziz, 216–433–6729, Ali.Abdul-aziz@nasa.gov

**Glenn contacts:**
Dr. George Y. Baaklini, 216–433–6016, George.Y.Baaklini@nasa.gov; and Dr. Don J. Roth, 216–433–6017, Donald.J.Roth@nasa.gov

**Authors:**
Dr. Ali Abdul-Aziz, Dr. George Y. Baaklini, and Dr. Don J. Roth

**Headquarters program office:**
Aeronautics Research

**Programs/Projects:**
Aviation Safety

## Impact Damage in SiC/SiC Composite Materials Characterized With Pulsed Thermography

Because of their high-temperature strength properties, silicon carbide/silicon carbide (SiC/SiC) composite materials targeted for use in turbine components were developed at the NASA Glenn Research Center. Impact damage that occurs in hostile combustion environments reduces the strength properties of components made from these materials. Therefore, it was necessary to develop nondestructive evaluation (NDE) methods to detect and characterize impact damage in SiC/SiC composite materials for material development and future inspection purposes. The complex nature of the composite weave and the amount of porosity in ceramic matrix composites makes investigation with ultrasonic methods extremely challenging. Conventional x-ray methods are not able to detect planar defects, such as delaminations. Although microfocused computed tomography has been useful in detecting damage depth in small SiC/SiC composite samples, it has significant limitations with respect to inspection time, costs, and sample size. All these limitations necessitated the research and improvement of other inspection methods, such as pulsed thermography, for SiC/SiC composite materials.

Therefore, impact damage in 2.4-mm-thick SiC/SiC composite materials was investigated and characterized at Glenn with pulsed thermography (ref. 1). Pulsed thermography is an NDE technique that monitors the thermal response of a material over time. The surface of a component is heated with an instantaneous, uniform pulse of heat. As heat flows toward the back side of the material, disruptions in heat flow, due to subsurface discontinuities, result in localized surface temperature variations that are detected with an infrared camera.

In order to examine impact damage, researchers impacted SiC/SiC coupons with 1.59-mm-diameter steel spheres at velocities from 115 to 400 m/sec. Damage that went undetected optically was detected with pulsed thermography at impact velocities as low as 220 m/sec. A flat-bottom-hole thermal standard was fabricated to determine defect resolution limits and impact damage depth in these materials. Holes with hole-diameter-to-depth aspect ratios above 2.5 were detectable. Although detectable in the thermal image sequence, the edges of flat-bottom holes with depths 1.93 mm from the interrogation surface were not readily resolved because of their proximity to the back surface. The information acquired from the thermal standard was compared with thermal data acquired from an impacted SiC/SiC sample with known damage to determine the impact damage depth.

An illustration of how the depth of damage analysis can be applied follows. The figure shows a thermal image of an impacted sample with the cooling curves for an averaged 13- by 13-pixel area reference region and a delaminated 1- by 1-pixel area. The sample, impacted at 300 m/sec, had clearly identifiable damaged and undamaged regions in the thermal image. As shown on the cooling curve, the time of departure from the reference region is 0.031 sec. According to an equation derived from the analysis of the SiC/SiC standard (ref. 1), this time corresponds to a depth of 2.03 mm from the surface, which has an 8.5-percent error when compared with the depth of the delamination of 1.87 mm, as measured from a computed tomography image.

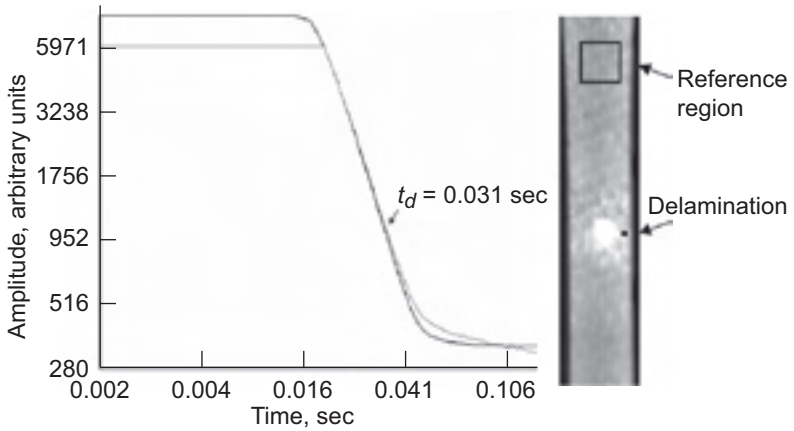


*Cooling behavior for an impacted SiC/SiC sample with $t_d$ representing the time of departure from the reference region, where the reference region represents an average 13- by 13-pixel area and the damaged region is a 1- by 1-pixel region.*

In addition to impact damage, these results can be utilized to characterize manufacturing defects in samples and components made from SiC/SiC materials with thicknesses of approximately 2.4 mm. This research represents a portion of a larger effort to develop and improve pulsed thermography for the detection and characterization of impact damage in uncoated and environmental-barrier-coated SiC/SiC composite materials. Research of impact damage in environmental-barrier-coated SiC/SiC composite materials with pulsed thermography is ongoing.

**Reference**

1. Cosgriff, Laura M., et al.: Thermographic Characterization of Impact Damage in SiC/SiC Composite Materials. Proceedings of the SPIE Symposium on Nondestructive Evaluation and Health Monitoring of Aerospace Materials, Composites, and Civil Infrastructure IV, vol. 5767, 2005, pp. 363–372.

**Cleveland State University contact:**
Laura M. Cosgriff, 216–433–3866,
Laura.M.Cosgriff@nasa.gov

**U.S. Army Research Laboratory at Glenn contact:**
Dr. Ramakrishna T. Bhatt, 216–433–5513,
Ramakrishna.T.Bhatt@nasa.gov

**Authors:**
Laura M. Cosgriff and
Dr. Ramakrishna T. Bhatt

**Headquarters program office:**
Aeronautics Research

**Programs/Projects:**
UEET

# Broadband, Capacitive-Based Wireless Slip Ring Designed and Fabricated for Application in Turbomachinery

Rotor health monitoring and online damage detection are increasingly gaining the interest of aircraft engine manufacturers. This is primarily due to the need to improve safety during operation as well as to lower maintenance costs. Applied techniques for detecting damage in and monitoring the health of rotors are essential for engine safety, reliability, and life prediction. A few years ago, the United States set the ambitious goal of reducing the fatal accident rate for commercial aviation by 80 percent within 10 years (ref. 1). In turn, NASA, in collaboration with the Federal Aviation Administration and other federal agencies, universities, and airline and aircraft industries, responded by developing the Aviation Safety Program. The program provides research and technology products needed to help the aerospace industry improve aviation safety. Researchers within NASA Glenn Research Center's Optical Instrumentation and Nondestructive Evaluation Technology Branch are developing propulsion-system-specific technologies intended to detect damage prior to catastrophe under the propulsion health management task.

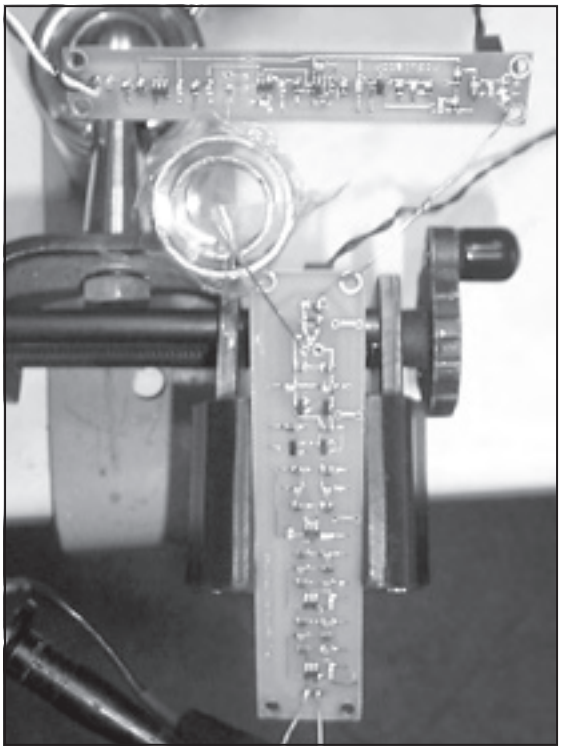

*Prototype wireless slip ring, showing modulator (top), wireless slip rings (center), and analog demodulator (bottom).*

Sensors that locally "ride" on the rotor are deemed a necessary choice for sensitive, high-resolution structural health monitoring of turbine engines because of the limited resolution of vibration-based methodologies. One such system being developed utilizes either traditional ultrasonic transducers or robust piezoelectric patches for real-time, continuous monitoring of acoustic emissions in the hopes of recognizing damage prior to catastrophe. In order to implement such a system, concerns regarding broadband data transfer from the rotor (location of the sensor) to the stator (location of signal-processing equipment) need to be addressed. As a result, a new 1-MHz broadband wireless slip ring was designed and fabricated at the NASA Glenn Research Center. The wireless communication between the rotor and the stator is accomplished through capacitive coupling. The antennas are fashioned as a ring-within-a-ring setup. In the current form, both the modulator and the demodulator use a 3-V battery supply, although both can function within the range of 2 to 7 V. Current draws at 3 V are 25 mA for the modulator and 10 mA for the demodulator. Future systems will aim to eliminate battery usage by power harvesting. Power harvesting converts ambient energy (such as normal structural vibrations and temperature gradients) into electrical power.

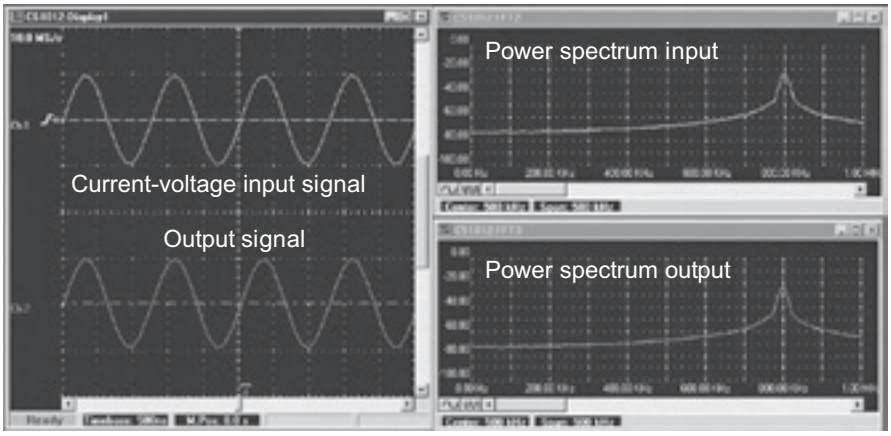


*Comparison of input and output signals.*

Tests were conducted at Glenn under static conditions in order to document the signal accuracy of the system after modulation and demodulation. Results showed that the wireless slip ring was able to accurately recreate the input signal, generated with a pulse-function generator, in the frequency range of approximately 375 Hz to 1 MHz. Success was achieved for sinusoidal waves as well as square waves with amplitudes ranging from 50 mV to 1 V. The preceding figure shows the results for an 800-kHz sine wave input. The next step

for verification tests involves subscale rotor tests, followed by further hardware refinements and finally full-scale tests in turbine engines.

**Reference**
1. Shin, J.: The NASA Aviation Safety Program—Overview. Proceedings of ASME Turbo Expo 2000, Munich, Germany, 2000.

**Ohio Aerospace Institute (OAI) contact:**
Dr. Andrew L. Gyekenyesi, 216–433–8155, Andrew.L.Gyekenyesi@nasa.gov

**Summit Safety, Inc., contact:**
Dr. Wayne C. Haase, 978–772–9909 (ext. 104), whaase@summitsafetyinc.com

**Cleveland State University contact:**
Dr. Jerzy T. Sawicki, 216–433–2467, Jerzy.T.Sawicki@nasa.gov

**Glenn contact:**
Dr. George Y. Baaklini, 216–433–6016, George.Y.Baaklini@nasa.gov

**Authors:**
Dr. Andrew L. Gyekenyesi, Dr. Wayne C. Haase, Dr. Jerzy T. Sawicki, and Dr. George Y. Baaklini

**Headquarters program office:**
Aeronautics Research

**Program/Project:**
Aviation Safety

## Quantum Optical System Developed for Ultra-Low-Power Communications

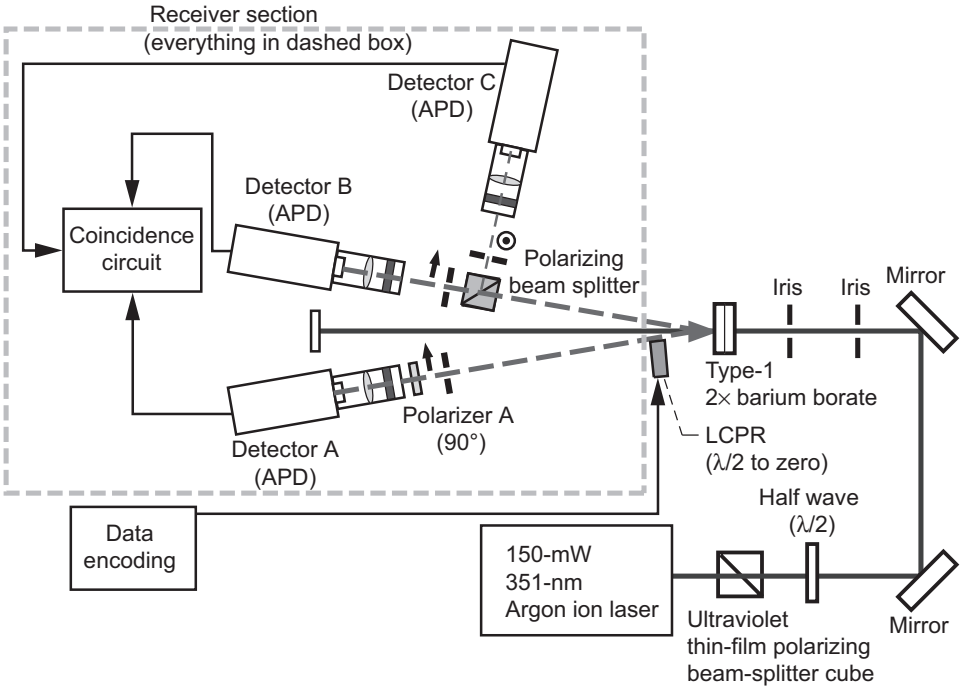


*Quantum optical communication system. Bit modulation coding: for state "0," the coincident (A,B) polarizing state is $H_1H_2$, with the liquid-crystal phase retarder (LCPR) set at zero; for state "1," the coincident (A,C) polarizing state is $V_1V_2$, with LCPR set at λ/2. APD, avalanche photodiode.*

A quantum communications system for the demonstration of optical communication at ultra-low-power levels was developed this year at the NASA Glenn Research Center. This system is meant as a precursor for a micro-optical transmitter that will work with microwatts or less of power. The experimental implementation of this architecture is shown schematically in the figure. Here, the beam from a 351-nm (<150-mW) single-frequency argon-ion laser passes through two thin (0.69-mm), optically contacted, orthogonally aligned Type-I beta barium borate crystals to generate two beams of polarized entangled photons through spontaneous parametric down conversion. One of the beams then passes through a digital-logic-controllable liquid-crystal phase modulator set to act as a bistate half-wave plate (0 or λ/2) that encodes information onto the beam via polarization rotation, either horizontal *H* or vertical *V*.

For the receiver, photon detectors A and B are set to detect only *H* polarization photons, whereas

detector C is set to detect only *V* polarization photons through the use of a polarizing filter and a polarizing beam splitter. Binary data modulate a variable-phase retarder, keeping the *H* and *V* photons intact under state "1" and changing the *H* photons into *V* and the *V* photons into *H* under state "0." As a result, photon detectors A and B trigger *H* photon coincidences in coincidence detector 1 when state "1" is transmitted, and detectors A and C trigger *V* photon coincidences in coincidence detector 2 when state "0" is transmitted. Decisions are made by comparing the number of coincidences per data bit from the two coincidence detectors. If the count from coincidence detector 1 is greater than that for coincidence detector 2, the receiver records a "1"; if not, the receiver records a "0." Accidental coincidences due to ambient light and unentangled photons from the laser source have been found to be much smaller than signal coincidences, affording reliable communications under very low signal-to-noise ratios.

Through the use of quantum-entangled photons, we have shown that reliable communication is possible at remarkably low received-energy levels (on the order of 1 picojoule per bit in the presence of an overwhelming background light, resulting in exceptionally low optical signal-to-noise ratios. With this system, we have demonstrated communication with the coincident-photon count to single-photon count ratio at –26.6 dB.

**Glenn contacts:**
John D. Lekki, 216–433–5650, John.D.Lekki@nasa.gov;
Dr. Quang-Viet Nguyen, 216–433–3574, QuangViet.Nguyen-1@nasa.gov;
Binh V. Nguyen, 216–433–8338, Binh.V.Nguyen@nasa.gov; and
Tom P. Bizon, 216–433–8121, Thomas.P.Bizon@nasa.gov;

**NASA Kennedy Space Center contact:**
Quang K. Tran, 321–867–3259, Quang.K.Tran@nasa.gov

**Cleveland State University contact:**
Murad Hizlan, 216–687–4826, M.Hizlan@csuohio.edu

**Authors:**
John D. Lekki, Dr. Quang-Viet Nguyen, Binh V. Nguyen, Thomas P. Bizon, Marc A. Seibert, Quang K. Tran, and Murad Hizlan

**Headquarters program office:**
Aeronautics Research

**Programs/Projects:**
AEFT

## Molecular Rayleigh Scattering Technique Developed to Measure Temperature Fluctuations in Heated Gas Flows

A nonintrusive optical point-wise measurement technique utilizing the principles of molecular Rayleigh scattering was developed at the NASA Glenn Research Center to obtain turbulent temperature fluctuation measurements in unseeded gas flows. This type of information is necessary for validating computational fluid dynamics and computational aeroacoustic codes. Dynamic temperature measurements allow the calculation of statistical quantities such as power spectra and mean square fluctuations. These types of measurements are used for jet noise studies in which sound pressure fluctuations are correlated with temperature fluctuations to ascertain the sources of noise in free jet flows.

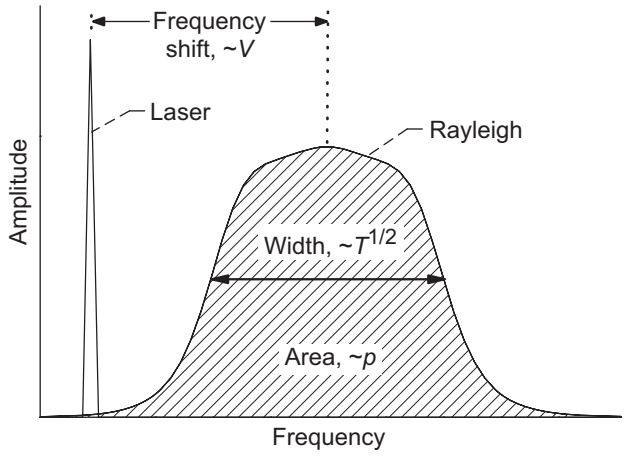


*Rayleigh scattering spectrum.*

Molecular Rayleigh scattering is the result of elastic light scattering from gas molecules. When light from a single-frequency laser beam passes through a gas, the scattered light is shifted in frequency by the Doppler effect because of the bulk motion of the molecules. The optical frequency spectrum of Rayleigh-scattered light contains information

about the gas density, bulk velocity, and temperature. The graph to the left shows a Rayleigh-scattering spectrum containing the narrow laser line and the broadened Rayleigh spectral peak. If the gas composition is known, the total intensity of the Rayleigh spectrum is directly proportional to the gas density. The frequency shift between the laser peak and the Rayleigh peak is proportional to the bulk flow velocity. The width of the spectral peak is broadened by thermal motion of the molecules and, hence, is related to gas temperature. A Fabry-Perot interferometer (see the next figure) operated in the static imaging mode is used to analyze the spectra of the laser light and the Rayleigh scattered light. The resulting circular fringe pattern contains spectral information about the light (see the final figure).

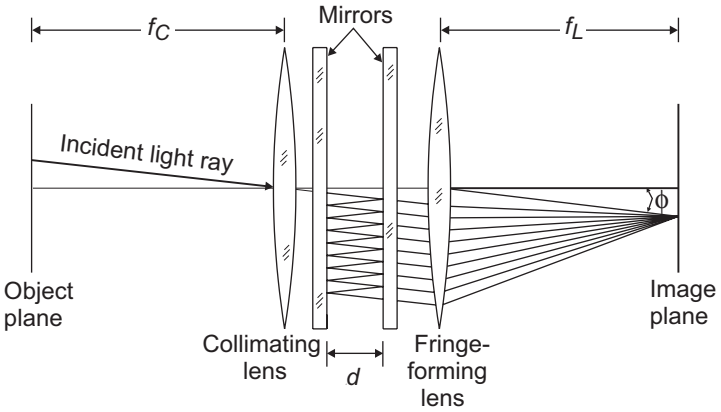


*Fabry-Perot interferometer; $f_C$, collimating lens focal length; $f_L$, fringe-forming lens focal length.*

A series of mirrors angled with respect to one another are used to divide the interference fringe pattern containing spectral information into four concentric regions (see the final figure). Light from each of these regions is directed toward photomultiplier tubes and sampled at 10 kHz using photon-counting electronics. Monitoring the relative change in intensity within each region allows for measurement of the gas temperature. Independently monitoring the total scattered intensity provides a measure of gas density. In addition, this technique has the potential to simultaneously measure a single component of flow velocity by monitoring the spectral peak location. Gas temperature and density were measured using a low-speed heated air jet surrounded by an unheated air coflow.

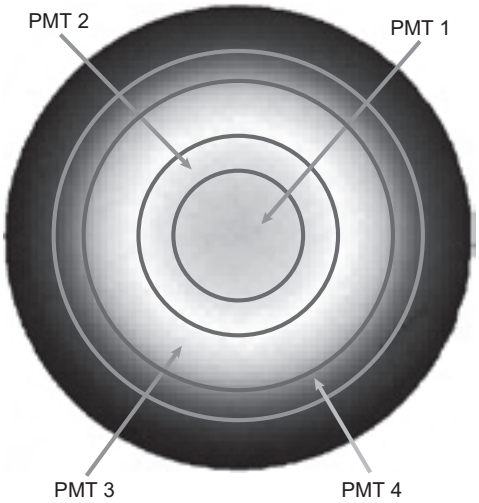


*Dissection of Fabry-Perot fringe pattern into four annular regions. PMT, photomultiplier tube.*

**Bibliography**

Mielke, A.F.; and Elam, K.A.: Molecular Rayleigh Scattering Diagnostic for Measurement of High Frequency Temperature Fluctuations. Proceedings of SPIE Optics and Photonics Conference, vol. 5880, 2005.

Mielke, Amy F., et al.: Time-Average Measurement of Velocity, Density, Temperature, and Turbulence Velocity Fluctuations Using Rayleigh and Mie Scattering. Exp. Fluids, vol. 39, no. 2, 2005, pp. 441–454.

Panda, J., et al.: Time-Averaged Velocity, Temperature and Density Surveys of Supersonic Free Jets. Proceedings of the ASME Heat Transfer/Fluids Engineering Summer Conference 2004, Charlotte, NC, 2004, pp. 811–817.

Panda, J., et al.: Effect of Heating on Turbulent Density Fluctuations and Noise Generation From High Speed Jets. AIAA–2004–3016, 2004.

Mielke, A.; and Seasholtz, R.: Time-Average Molecular Rayleigh Scattering Technique for Measurement of Velocity, Density, Temperature, and Turbulence Intensity in High Speed Nozzle Flows. AIAA–2004–0706, 2004.

Panda, J.; Seasholtz, R.; and Elam, K.: Further Progress in Noise Source Identification in High Speed Jets Via Causality Principle. AIAA–2003–3126, 2003.

Panda, J.; and Seasholtz, R.G.: Experimental Investigation of Density Fluctuations in High-Speed Jets and Correlation With Generated Noise. J. Fluid Mech., vol. 450, 2002, pp. 97–130.

Seasholtz, R.G.; Panda, J.; and Elam, K.A.: Rayleigh Scattering Diagnostic for Measurement of Velocity and Density Fluctuation Spectra. AIAA–2002–0827, 2002.

**Glenn contact:**
Amy F. Mielke, 216–433–6757,
Amy.F.Mielke@nasa.gov

**Author:**
Amy F. Mielke

**Headquarters program office:**
Aeronautics Research

**Programs/Projects:**
QAT, IR&D

# Particle Image Velocimetry Used Successfully to Nonintrusively Capture Novel Features of Steady and Unsteady Exhaust Flows

Particle image velocimetry (PIV) was successfully used to capture the evolution of steady and unsteady exhaust flows from test hardware operated within several facilities at the NASA Glenn Research Center. In the Small Hot Jet Acoustic Rig at Glenn's AeroAcoustic Propulsion Laboratory, the flows from numerous exhaust nozzles equipped with chevrons, or serrated edges, which are being investigated as passive jet-noise-reduction devices, were examined to evaluate their mixing performance. In a test cell at Glenn's Rocket Laboratory, the exhaust flows from a pulse detonation

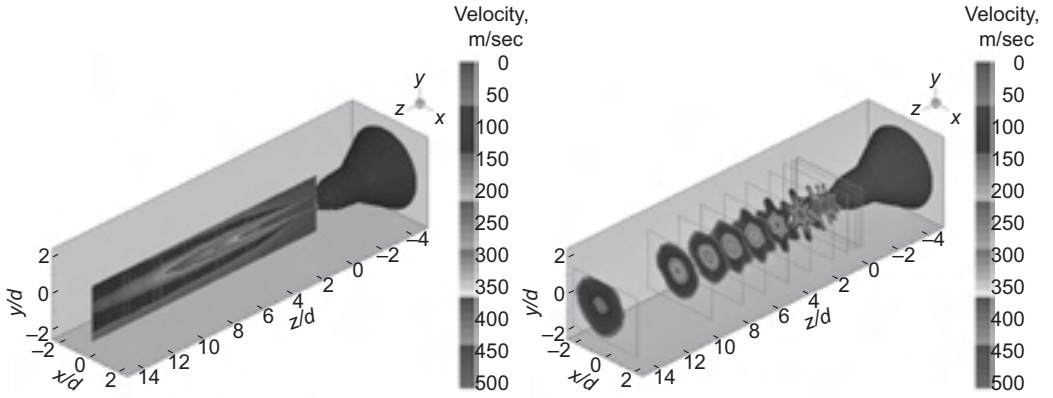


*Mean velocity fields evaluated from stereoscopic PIV data at several measurement stations downstream of chevron nozzles. Left: Axial plane. Right: Cross plane.*

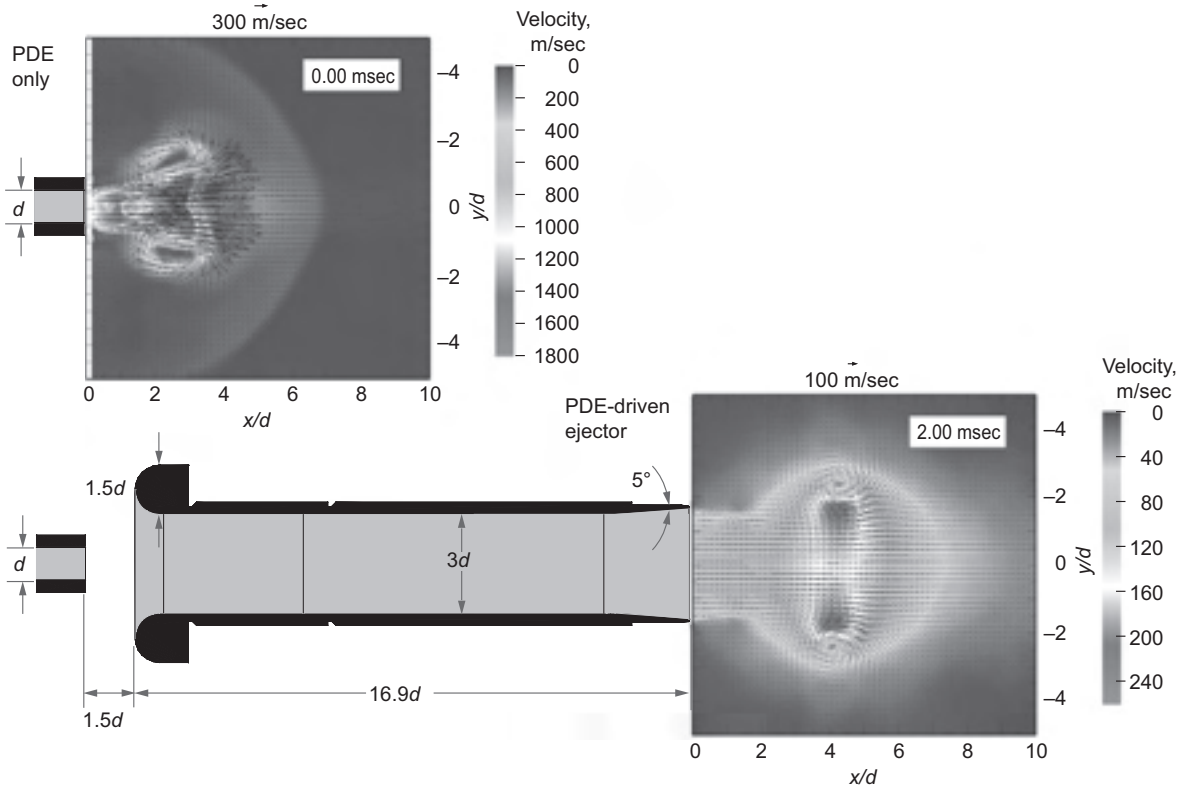


*Ensemble-averaged exhaust flow fields measured at several phase-locked time steps during a PDE operating cycle. Top row: In-plane velocity vector fields overlaid onto contours of constant vorticity for direct exhaust from the PDE. Bottom row: In-plane velocity vector fields overlaid onto contours of constant vorticity for detonation-driven ejector exhaust.*

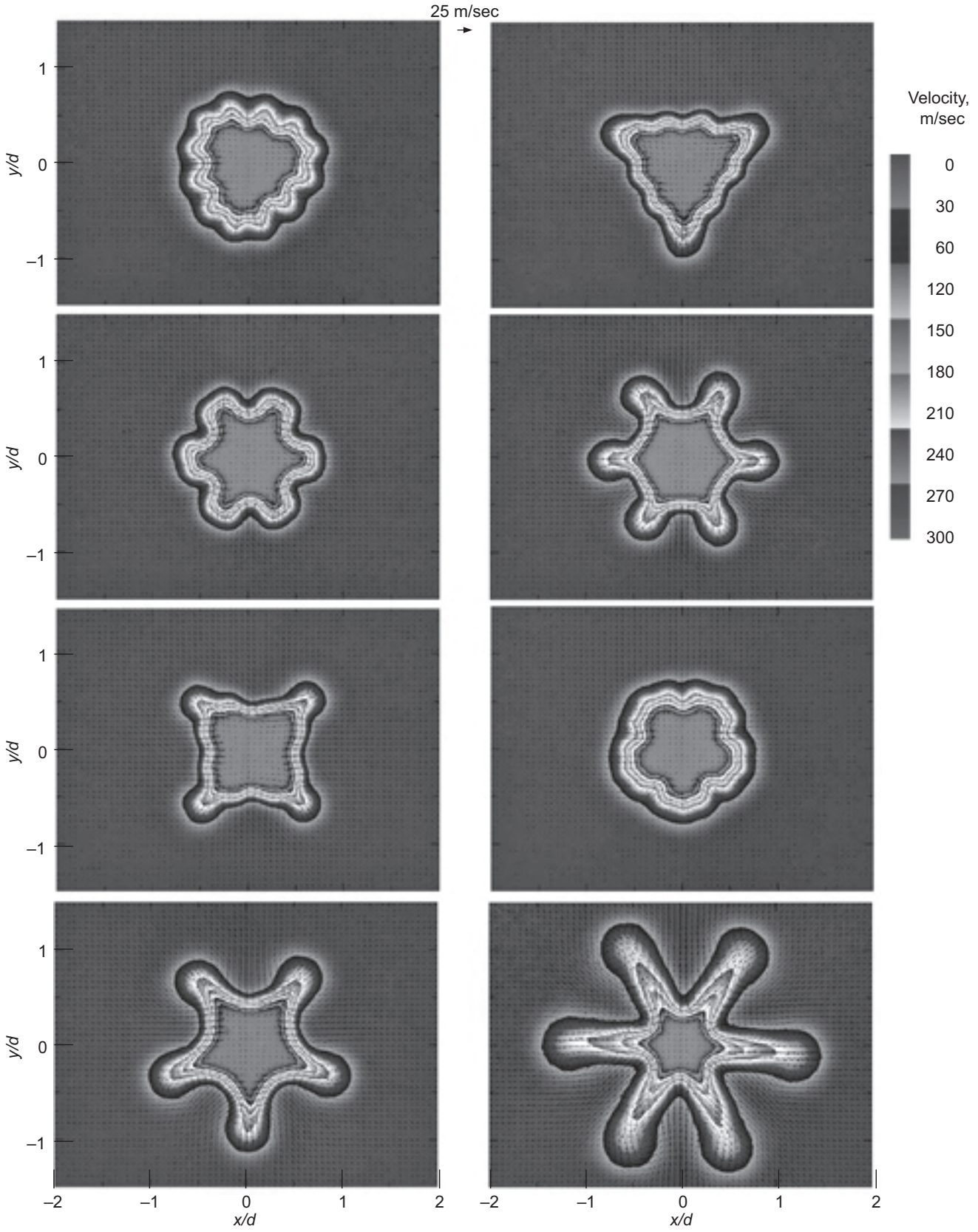


*Sample ensemble-averaged exhaust flow fields measured two jet diameters, d, downstream of exit plane of several chevron nozzles (with different chevron configurations). In-plane velocities are shown as vectors, with the out-of-plane velocity component shown as contours of constant color.*

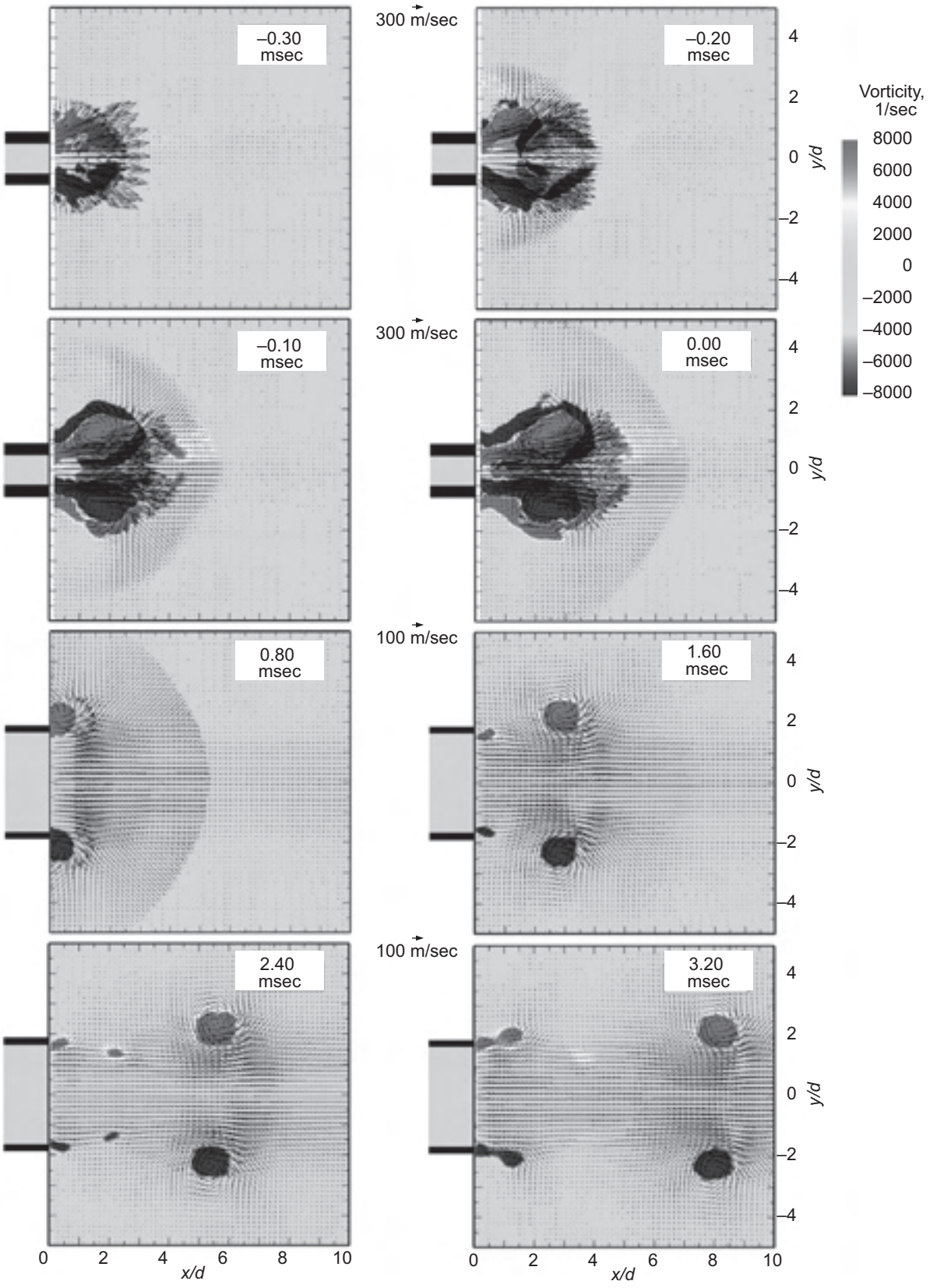


*Experimental arrangement and measurement regions of interest for planar PIV exhaust flow measurements along the centerline axial exhaust from the PDE and the detonation-driven ejector. Shown are velocity vector maps overlaid onto contours of constant velocity at several phase steps during engine operation. The flow is from left to right.*

engine (PDE) and an ejector coupled downstream of a PDE, being investigated as a noise-reduction and thrust-augmentation device for hybrid propulsion applications, were examined to evaluate their phase-averaged cyclic operating behavior. PIV is uniquely advantageous in these situations because of its ability to produce detailed and highly accurate complete flow-field exhaust velocity vector maps. In addition, the use of PIV significantly reduces facility test times over conventional measurement techniques incorporating intrusive diagnostic probes.

Stereoscopic PIV, having become a well-established technique for the measurement of the three components of velocity within a fluid plane, was successfully used to characterize the exhaust flow fields from a parametric test matrix of 16 chevron and 2 baseline circular 50.8-mm-diameter nozzles. During nozzle jet operation, acoustic mach numbers ranged from 0.9 to 1.5 and static temperature ratios ranged from 0.84 to 2.7.Detailed surveys of the single jet flows were performed to capture three-dimensional features of the turbulent exhaust jet evolution. Cross-flow planar measurements were obtained at 12 locations, ranging from 0.1 to 20 nozzle diameters *d* downstream of the nozzle exit planes. Streamwise measurements, along the jet centerlines, were obtained at 10 partially overlapping downstream locations, providing complete axial surveys over a region extending beyond 20 nozzle diameters downstream of the nozzle exit planes. In both optical configurations, the measurement planes were sized to completely capture the fully turbulent jet shear layer growth. The measured three-dimensional mean and turbulent velocity fields, along with computed second-order statistics including axial vorticity and turbulent kinetic energy, were evaluated for all test points. Well-defined streamwise vortex structures in the jet shear layers were measured and documented.

An initial series of planar PIV measurements were successfully performed using the small detonation facility in Glenns' Rocket Lab Test Cell 31 to provide quantitative insight into the mechanisms of thrust augmentation using PDE-coupled ejectors. The data are believed to be the first quantitative PIV measurements made on the exhaust flow field of an operational PDE and include the measurement of the driven exhaust flow out of an ejector placed downstream of the PDE. An examination of the planar PIV velocity data revealed the presence of a highly repeatable, strong emitted vortex with each firing (pulse) of the engine. The peak diameter of the vortex leaving the PDE is very nearly the same as the diameter of the ejector used in this study, which yielded the highest thrust augmentation measured in previous testing. This result is consistent with other unsteady thrust augmentation studies and confirms that the emitted vortex associated with all unsteady thrust augmentation devices plays a central role in the high levels of thrust augmentation observed. Continued analysis of the PIV data is in progress and is expected to provide a validation benchmark for computational solutions of PDE, PDE-driven ejector, and exhaust flow fields, as well as providing insights into determining optimal ejector configurations.

**Bibliography**

Opalski, A.; Wernet, M.; and Bridges, J.: Chevron Nozzle Performance Characterization Using Stereoscopic DPIV. AIAA–2005–0444, 2005.

Opalski, A.; Paxson, D.; and Wernet, M.: Detonation Driven Ejector Exhaust Flow Characterization Using Planar DPIV. AIAA–2005–4379, 2005.

**Find out more about the research of Glenn's Optical Instrumentation Technology Branch:**
http://www.grc.nasa.gov/WWW/OptInstr/

**QSS Group, Inc., contact:**
Dr. Anthony B. Opalski, 216–433–3908, Anthony.B.Opalski@nasa.gov

**Glenn contact:**
Dr. Mark P. Wernet, 216–433–3752, Mark.P.Wernet@nasa.gov

**Authors:**
Dr. Anthony B. Opalski, Dr. Mark P. Wernet, Dr. Daniel E. Paxson, and Dr. James E. Bridges

**Headquarters program office:**
Aeronautics Research

**Programs/Projects:**
QAT, CVCCE

# Approaches Demonstrated for Flaw-Detection Enhancement for Liquid-Crystal-Display-Based Ultrasonic Imaging

Acoustography is a full-field ultrasonic imaging process where a high-resolution two-dimensional acousto-optic (AO) sensor based on liquid-crystal technology is employed to directly convert the ultrasound into a visual image in near real time. Unprocessed acoustography images typically suffer from nonuniformity and a resulting lack of defect sharpness because of spatial variations in the optical brightness response of the acousto-optic sensor field to ultrasonic intensity. These limitations can make acoustography image interpretation difficult, large field applications impractical, and use on samples with a wide range of attenuation difficult. In 2005, a new software methodology was developed and demonstrated to address these limitations.

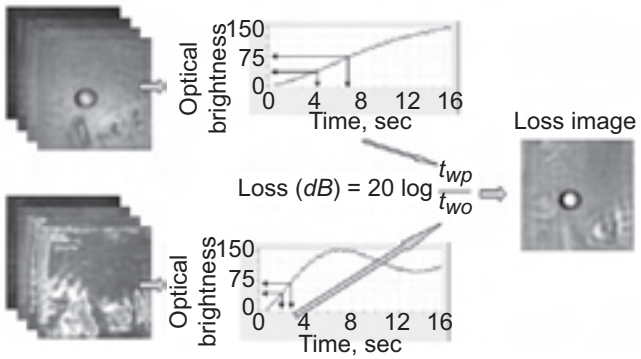


*Nonuniformity and flaw-detection enhancement approach in brief. Black arrows demarcate the two threshold optical brightness levels. The image on the right shows results for a plexiglass sample with a seeded defect. $T_{wp}$, time with part present; $T_{wo}$, time without part present.*

Prior to developing methodologies, a custom acoustography system was developed jointly by the NASA Glenn Research Center and Santec Systems, Inc. The conventional acoustography system was modified from its original implementation to include a National Instruments Signal Generator card to generate the swept sinusoid function, a National Instruments multifunction (NI PCI–6014) card having analog outputs to generate sine waves for AO sensor erasure, and an 8-bit monochrome digital camera capable of 60 frames/sec video capture. The original frame grabber and charge-coupled device (CCD) analog camera were no longer needed and were removed. A radiofrequency amplifier amplifies the swept sinusoid wave from the signal generator card by approximately 30 dB before it reaches the transducer. An entirely new acoustography operating system was developed using LabVIEW 7.1 both to conduct these experiments and to operate the system for general inspection. This operating system allows control of swept sinusoid voltage amplitude and sweep parameters, AO sensor erasure, camera frame captures per second, and camera gain. Data analysis, image analysis, and image processing software code was developed in LabVIEW 7.1 and the associated IMAQ Vision toolkit to implement the methodologies discussed in this study.

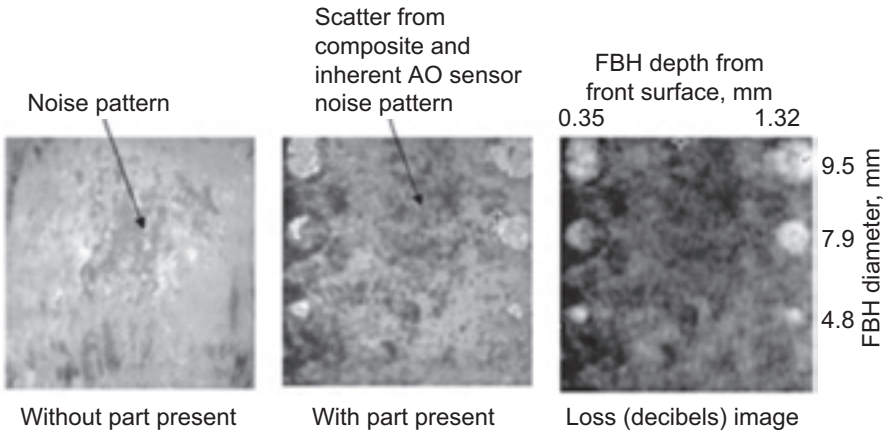


*Acoustography images for the ceramic matrix composite sample with flat bottom holes. Left: Conventional acoustography image without the sample. Center: Conventional acoustography image with the sample. Left: Average loss (decibels) image.*

After system development, a custom algorithm was developed and tested at Glenn that shows promise for nonuniformity correction and flaw detection enhancement in acoustography images. It is based on the principles shown in the preceding figure. Note that a series of images develops as a function of time in the acoustography process. The algorithm developed is based on a time ratio in which, for each pixel level, times are extracted for a specific brightness level with and without the part present, divided together, and converted to decibels so that each pixel can be assigned a "loss" value. Essentially, normalization is occurring with respect to the underlying AO sensor portion at each pixel. This method is novel in that most ultrasonic (and nondestructive evaluation results in general) use voltage or intensity ratios for decibel

assignment (which also was considered in this study). Overall, the custom algorithm is speedier than working with voltage ratios. The right side of the top figure on the preceding page shows the results of experiments performed using a plexiglass sample with seeded defect. The loss image shows the seeded defect extremely clearly and appears to have been successful at removing some of the noise pattern at the bottom center of the original brightness-versus-time images.

Next, the same approach was applied for a ceramic matrix composite sample with seeded defects and the final result is shown as the average loss (decibels) in the bottom left image on the preceding page. In comparison to the center image (unprocessed acoustography image), the defects are somewhat enhanced.

**Bibliography**
Roth, Don J.; et al.: Approaches for Non-Uniformity Correction and Dynamic Range Extension for Acoustography. SPIE Int. Soc. Opt. Eng., vol. 5770, 2005, pp. 124–134.

**Glenn contact:**
Dr. Don J. Roth, 216–433–6017, Donald.J.Roth@nasa.gov

**Author:**
Dr. Don J. Roth

**Headquarters program office:**
Aeronautics Research

**Programs/Projects:**
UEET

## False Alarms Reduced With New Fire Detection System

The NASA Aviation Safety and Security Program has identified false fire alarms as one of the national problems hindering safe expansion of the U.S. air transportation system. Federal Aviation Administration (FAA) surveys of air carriers found that, for fire-detection systems in remote cargo compartments, there were 100 to 200 false alarms for every warning of an actual fire. False alarms negatively impact safety by causing aircrews and air traffic controllers to needlessly employ emergency fire-mitigation procedures and priority landings on the nearest suitable airfield. Unnecessary emergency procedures compromise the air traffic management system. Flight safety is also affected because aircrews subjected to repeated false alarms may be less likely to quickly and aggressively respond to a warning of an actual fire. To address this problem, a team led by the NASA Glenn Research Center developed microelectromechanical systems- (MEMS-) based sensor technology for aircraft cargo compartment fire detection. This task produced a new commercial product, the Multi-Parameter, MicroSensor-Based Low False Alarm Fire Detection System (MMFDS), which was given a 2005 R&D 100 Award as one of the 100 most significant inventions of the year.

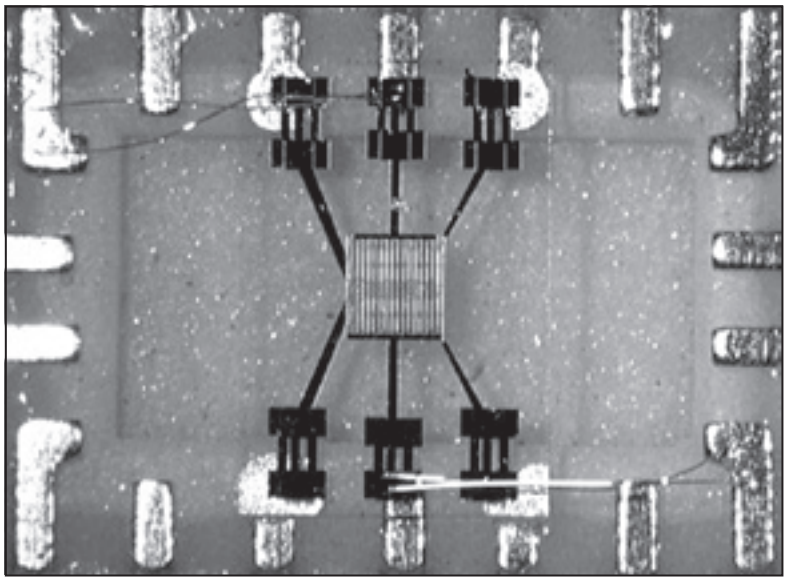

*Tin oxide microsensor used for fire detection.*

The Glenn-led team, which included Makel Engineering, Case Western Reserve University, and The Ohio State University, departed from the standard fire-detection approach of sensing only for the presence of smoke particulates. With these particulate detection approaches, the presence of dust or condensation aerosols can give a false indication of a fire. Instead, the team developed micromultisensor suites to detect the increase in multiple types of

gas species that are emitted by fire at its onset, such as carbon monoxide and carbon dioxide. The fundamental detection approach is to use "orthogonal" sensor technology: different types of sensor systems, which provide different information on the environment, combine so that crew and controllers can better understand the overall condition. This task involves

(1) Measuring multiple parameters associated with a fire, such as smoke in combination with multiple chemical species
(2) Developing fire product sensors (chemical and particulate) that are predominately micro- or nano-based to allow multiple sensors to be integrated into a compact array of reduced size, weight, and power consumption
(3) Advanced processing and control software, forming a "smart" detection system with corresponding fire event modeling

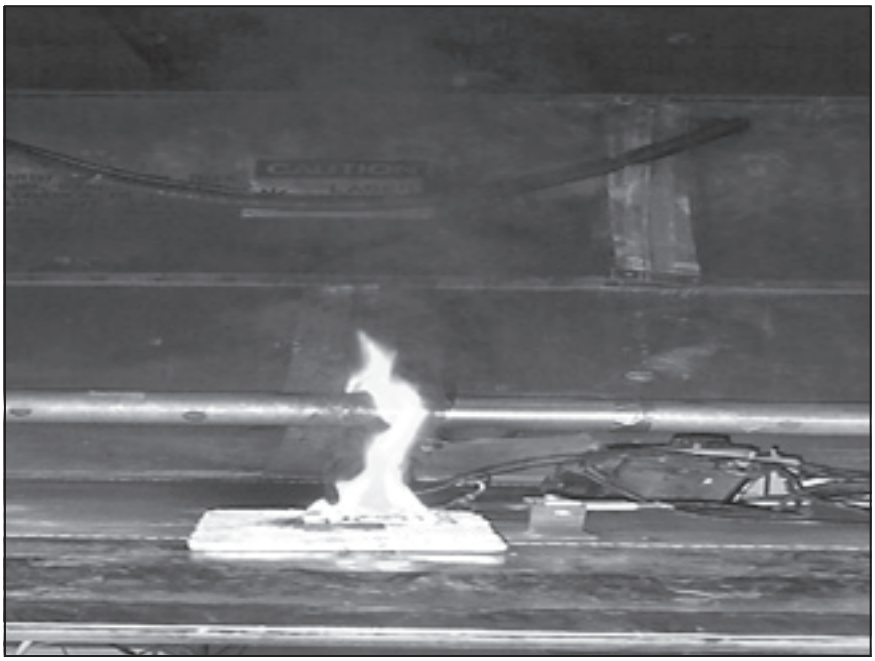

*Fire testing In cargo bay of FAA Boeing 707.*

Complete system tests conducted at the FAA's Testing Facility successfully demonstrated this approach. Fires were set in the cargo bay of a ground-based, instrumented Boeing 707; the MMFDS was mounted alongside of a standard commercial system, and the responses of both systems were monitored. The FAA chose this test procedure to check both false alarm vulnerability and fire-detection capability. The results were significant. Over a series of exposures to dust and humidity, the MMFDS had a zero false alarm rate, whereas the commercial system had a 100-percent false alarm rate. Over the entire fire test series, the MMFDS sensed the onset of an actual fire as well as the conventional detector, if not better, and within the standard FAA requirement of fire detection within 1 min. The test demonstrated the complete elimination of false alarms with the newly developed hardware and software system. The new commercial product is now available for fire detection with low false detection.

**Find out more about chemical species gas sensors at Glenn:**
http://www.grc.nasa.gov/WWW/chemsensors/

**Glenn contacts:**
Dr. Gary W. Hunter, 216–433–6459, Gary.W.Hunter@nasa.gov;
Dr. Jennifer C. Xu, 216–433–6669, Jennifer.C.Xu@nasa.gov; and
Robert C. McKnight, 216–433–2034, Robert.C.McKnight@nasa.gov

**Authors:**
Dr. Gary W. Hunter, Dr. Jennifer C. Xu, and Robert C. McKnight

**Headquarters program office:**
Aeronautics Research

**Programs/Projects:**
Aviation Safety, CEV,
Life Support & Habitation

**Special recognition:**
2005 R&D 100 Award, Associate Administrators Choice Award (Turning Goals into Reality)

# Nanometer Step Height Standard Chip Developed for Calibration of Scanning Probe Microscopy Instruments

NASA Glenn Research Center engineers, in collaboration with Sest, Inc., and the Ohio Aerospace Institute (OAI), have developed a greatly improved diagnostic tool to evaluate and verify the operation and calibration of scanning probe microscopy (SPM) instruments used for measuring nanoscale objects, meeting a vitally important need for the nanotechnology field that is expected to grow dramatically over the next decade. The Nanometer Step Height Standard is a calibration standard chip made of single-crystal silicon carbide (SiC). The small SiC chip (seen on the fingertip in the photograph) contains an array of over 100 step pyramids like those shown in the highly magnified atomic force microscope image of the photograph inset. Each side of the nanoscale step pyramid features regularly spaced steps nearly 1-μm apart, with atomically flat terraces between step risers of either 0.5 or 1.0 nm in height, as chosen during fabrication. These step heights are around 10 times smaller than those of previous standards for SPM instrument calibration. The height of the steps is directly linked to the atomic spacing of the atoms in the SiC crystal structure, which is a well-known physical constant. Therefore, unlike previous standards, the SiC Nanometer Step Height Standards do not have the expensive and time-consuming requirement to be individually calibrated and certified by the National Institute of Standards and Technology (NIST).

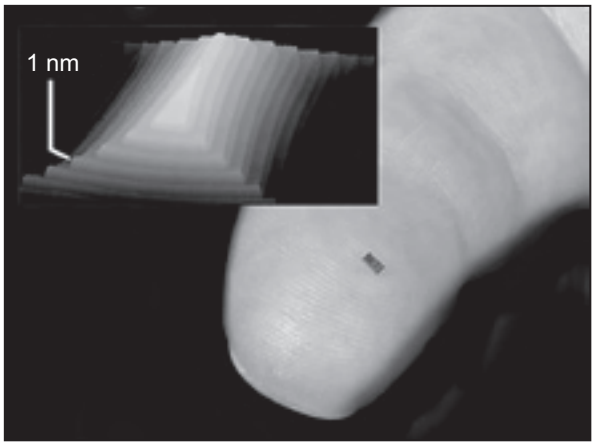


*Nanometer Step Height Standard artifact chip developed to enable greatly improved calibration of scanning probe microscopy instruments. The small SiC chip (seen on the fingertip) contains an array of over 100 step pyramids (like those shown in the highly magnified atomic force microscope image inset) with highly repeatable 1.0-nm height steps produced by high-temperature growth and etching of SiC mesas.*

The nanoscale step structures are produced on the top surfaces of commercial SiC wafers using conventional microelectronics photolithographic patterning and reactive ion etching processes, followed by high-temperature (>1000 °C) SiC epitaxial growth and etching pioneered by the Glenn research team. This process enables hundreds of calibration step structures to be mass-produced on a single SiC wafer, which should greatly increase the availability and affordability of precision SPM calibration for microtechnologies and nanotechnologies worldwide.

**Find out more about silicon carbide electronics at Glenn:**
http://www.grc.nasa.gov/WWW/SiC

**Glenn contacts:**
Dr. Philip G. Neudeck, 216–433–8902, Philip.G.Neudeck@nasa.gov; and
Dr. Phillip B. Abel, 216–433–6063, Phillip.B.Abel@nasa.gov

**Sest, Inc., contact:**
J. Anthony Powell, 216–433–3652,
J.A.Powell@nasa.gov

**Ohio Aerospace Institute (OAI) contact:**
Andrew J. Trunek, 216–433–6736,
Andrew.J.Trunek@nasa.gov

**Authors:**
Dr. Philip G. Neudeck, Dr. Phillip B. Abel,
J. Anthony Powell, and Andrew J. Trunek

**Headquarters program office:**
Aeronautics Research

**Programs/Projects:**
TTPO

**Special recognition:**
2004 R&D 100 Award Winner,
U.S. Patent 6,869,480

# Packaged SiC Transistor Operated at 500 °C for 2000 hr in Oxidizing Air Ambient

A high-temperature silicon carbide (SiC) semiconductor transistor was fabricated, packaged, and electrically operated continuously at 500 °C for over 2000 hr in an air ambient. For the first 500 hr of electrical operation, less than 10-percent change in operational transistor parameters was observed. This is the first semiconductor transistor to demonstrate continuous electrical operation in such a harsh high-temperature oxidizing air environment with excellent stability over such an extended period of time. This demonstration of 500 °C transistor durability represents an important step toward significantly expanding the operational envelope of sensor signal processing electronics for harsh environments such as the high-temperature regions of combustion engines and the surface of Venus.

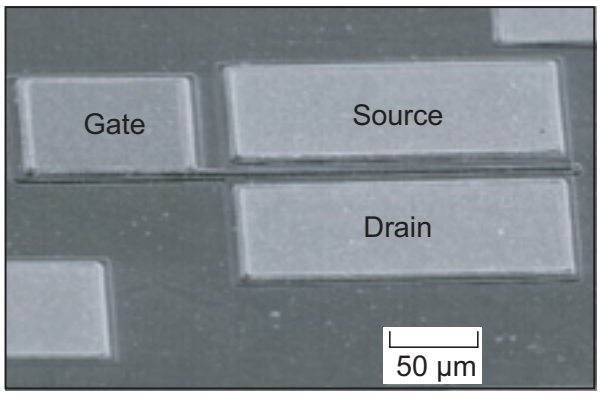


*Scanning electron micrograph of SiC metal-semiconductor field effect transistor structure. The large lighter regions are the metal contacts.*

The emergence of wide bandgap semiconductors, including SiC, diamond, and gallium nitride (GaN), has enabled short-term electrical device demonstrations at ambient temperatures from 500 to 650 °C, well beyond the reach of the silicon semiconductor material that is used to manufacture today's computer and communication electronics. However, wide bandgap transistors had not previously demonstrated sufficient long-term durability when electronically operated at these high temperatures to be considered viable for most envisioned applications. This was especially true when the transistors were tested in air ambient, which chemically attacks, oxidizes, and degrades the electrical ability of metal-semiconductor contacts to carry electrical signals in and out of the semiconductor. Therefore, this new SiC transistor fabrication process, which enabled durability in air, featured multiple levels of high-temperature metal and dielectric passivation to prevent contamination (particularly oxygen) from reaching electrically sensitive interfaces.

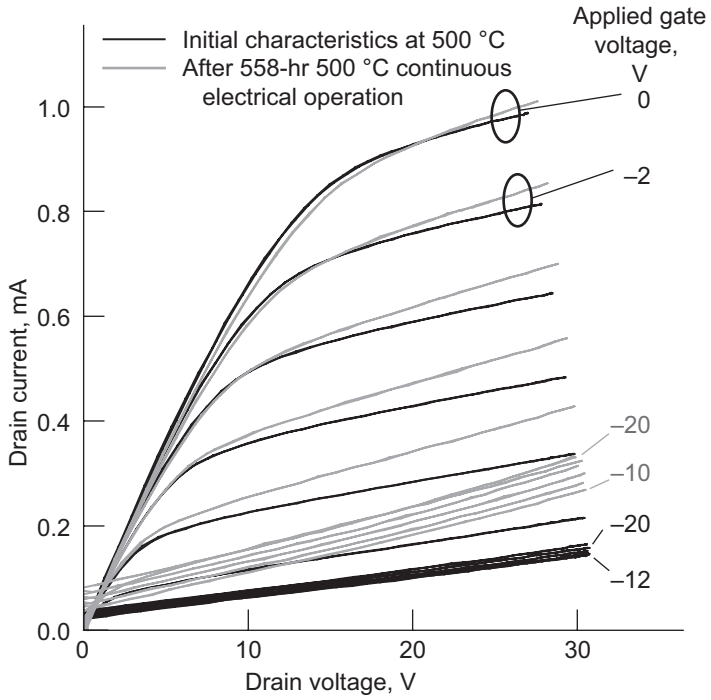


*Operational transistor drain current versus drain voltage characteristics of SiC field effect at 500 °C. Applied gate voltage is indicated in –2-V steps. Substrate bias voltage, $V_{sub}$, –20 V.*

The transistor was a metal-semiconductor field effect transistor (MESFET) fabricated on a 6H-SiC wafer, identical to the device shown in the photomicrograph. A thick-film metallization-based ceramic package with conductive die-attach material and gold wire bonds facilitated long-term testing under electrical bias at 500 °C. The graph shows the transistor current-voltage characteristics at the start of the test and after 558 hr of continuous electrical operation in air at 500 °C. The small change observed in the transistor characteristics is due to increasing leakage current from the metal-semiconductor gate terminal as anneal time increased. This gradual degradation mechanism could be eliminated by a modification to the design of the gate to

the SiC transistor. The remaining electrical contacts and packaging continued to operate successfully without observable electrical degradation for the full duration of the 500 °C test, which exceeded 2000 hr.

**Bibliography**

Okojie, Robert S.: Thermally Stable Ohmic Contacts on Silicon Carbide Developed for High-Temperature Sensors and Electronics. Research & Technology 2000. NASA/TM—2001-210605, 2001, pp. 59–60. http://www.grc.nasa.gov/WWW/RT2000/5000/5510okojie.html

Chen, Liang-Yu: Packaging Technology Designed, Fabricated, and Assembled for High-Temperature SiC Microsystems. Research & Technology 2002. NASA/TM—2003-211990, 2003, pp. 69–70. http://www.grc.nasa.gov/WWW/RT2002/5000/5510chen.html

**Find out more about SiC electronics at Glenn:**
http://www.grc.nasa.gov/WWW/SiC/

**Glenn contacts:**
Dr. Philip G. Neudeck, 216–433–8902, Philip.G.Neudeck@nasa.gov;
Dr. Robert S. Okojie, 216–433–6522, Robert.S.Okojie@nasa.gov; and
Dr. Glenn M. Beheim, 216–433–3847, Glenn.M.Beheim@nasa.gov

**Ohio Aerospace Institute (OAI) contacts:**
David J. Spry, 216–433–3361, David.J.Spry@nasa.gov; and
Dr. Liang-Yu Chen, 216–433–6458, Liangyu.Chen-1@nasa.gov

**Author:**
Dr. Philip G. Neudeck

**Headquarters program office:**
Aeronautics Research

**Programs/Projects:**
GMI, UEET

## First-Principles-Based Battery Model Investigated for the *International Space Station*

The International Space Station (ISS) Program depends on models to predict battery performance. It is critical that predictions are accurate because only simulations can determine if planned operations will maintain sufficient energy in the batteries. Extensive ground-based testing has provided a database of battery pack performance as a function of temperature, depth of discharge, and charge-control methodology. Battery voltage is then calculated from current, temperature, age, and depth of discharge. This model has been continuously improved, making use of additional battery data and modeling of cycle life versus depth of discharge. This technique has proven capable of predicting performance, but it does not allow for insight into electrochemical processes. For this reason, Glenn researchers, along with a University of Akron team, investigated a first-principles model: one based on the fundamental laws of physics that govern the behavior of electrochemical batteries.

A NASA grant was awarded to a University of Akron team, led by Dr. Tom T. Hartley, to develop a fractional calculus approach to dynamically model nickel-hydrogen battery cells on the basis of charge-discharge cycle data. The model used a real-time observer structure to determine instantaneous damage from life-cycle data and to establish an optimal charging profile to minimize damage.

A control system with a real-time observer for an electrochemical cell incorporates a hybrid model into a microprocessor-based simulation and is automated to track parameters as a battery changes during its lifetime. In addition, the algorithm can correct the initial parameters provided to the real-time observer, thereby effectively "learning" the battery system. Measured variables from an actual battery are input to the microprocessor simulation to force the dynamic states of the real-time battery observer (simulation) to converge to the corresponding states in the actual battery. The feedback is crucial since the actual system is highly nonlinear and the dynamic states represent a collection of many actual states. The observer can be used as part of the general decision-making process. If the observer predicts

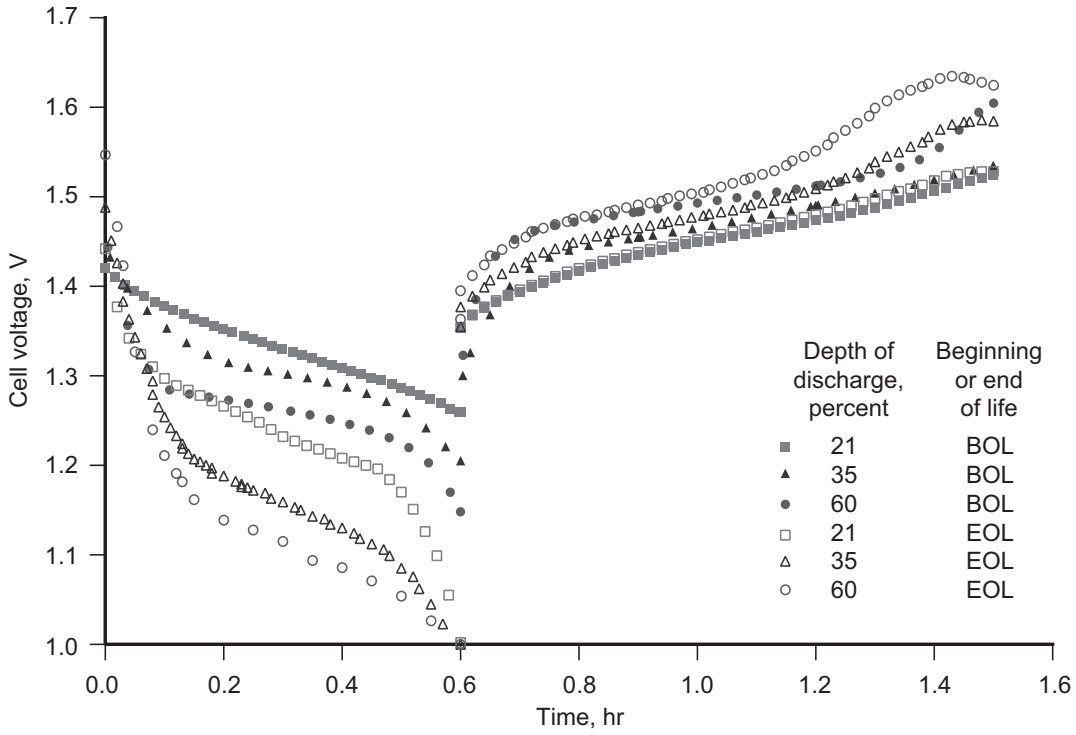


*Advanced control system using an advanced real-time observer.*

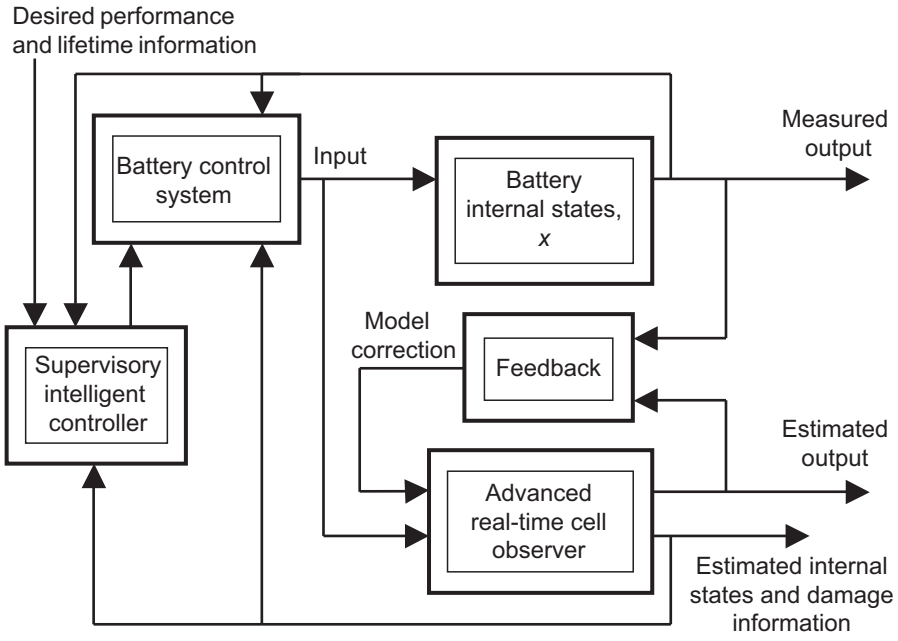


*Model data at 0 °C; cell voltage versus time at beginning and end of life, for three depths of discharge: 20, 35, and 60 percent.*

that certain dynamic states have exceeded the nominal values, the higher level of intelligence can determine if the actual system has become damaged in some way. The advanced controller uses the data provided by the real-time observer to maintain battery performance as the parameters change with time. This requires a continuous change of controller gains as the effects of physical changes in the battery are updated by the advanced real-time observer.

Faraday's Law and variations of the Butler-Volmer equation enabled the modeling of stored charge, diffusing charge, and electrode voltage. The model was enhanced using on-orbit ISS reconditioning data because the battery started out fully discharged, which allowed the model to encompass behavior over the entire operating range. Last, battery current and state-of-charge were used as input to verify the model against normal ISS cycling telemetry (ref. 1). Results showed that this first-principles-based model predicted voltage with an accuracy similar to that of the data-based model in use today.

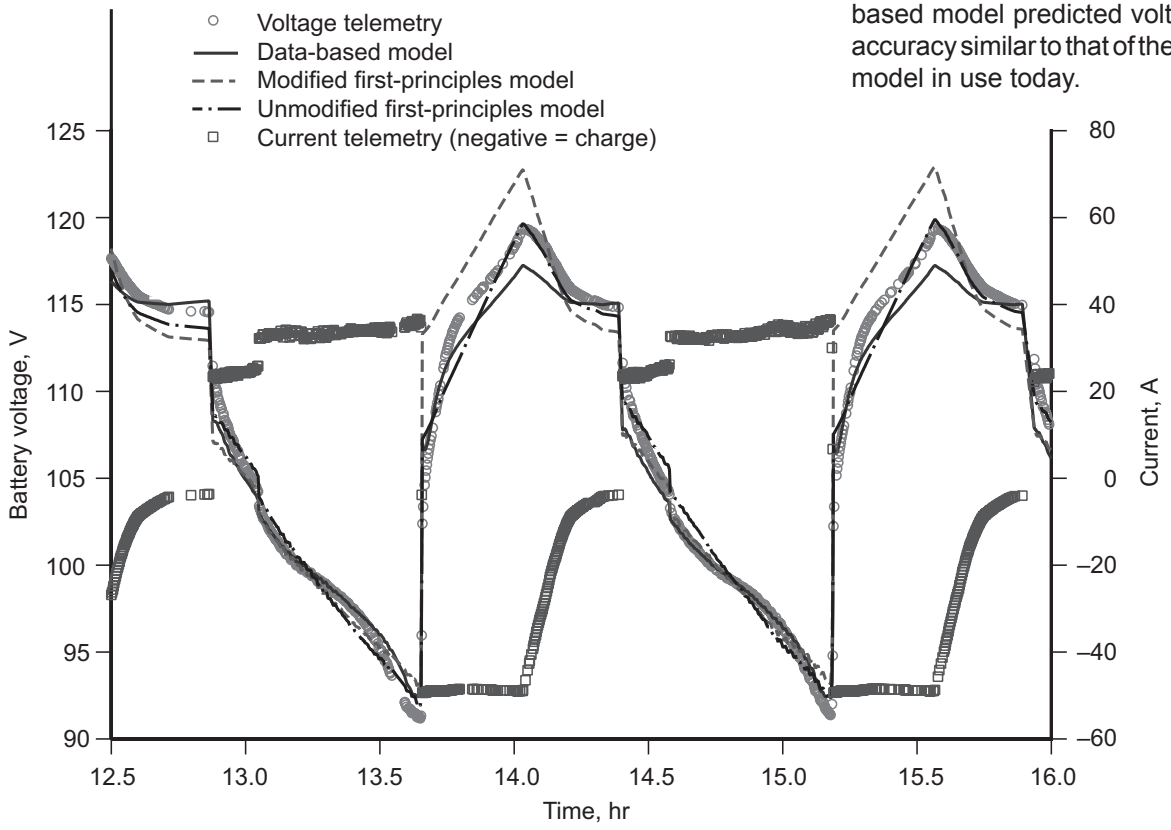


*Data-based and first-principles-based model predictions of battery voltage versus time for ISS cycling on day 90 of 2004.*

In addition, modeling different resistances in charge and discharge improved predictions. However, modeling the batteries at the individual cell level or at the half battery level did not improve voltage predictions markedly in comparison to modeling the ISS battery as a whole. Model accuracy is affected by insight into battery characteristics, such as ampere-hour capacity, which can only be measured by performing reconditioning. This dedicated test requires a battery to be temporarily taken offline and discharged.

Although the nickel-hydrogen battery has been considered to be the industry standard for low-Earth-orbit missions, lithium-ion battery technology with its improved energy density has been baselined on recent missions. Lithium-ion cell testing is being used to evaluate the effects of temperature, end-of-charge voltage, and depth of discharge on the performance of this new battery chemistry. The lithium-ion database will provide input to the advanced control system custom tailored with the lithium-ion model parameters for cell chemistry, cell-to-cell balancing, dynamics, and damage modeling. As test batteries succumb to failures, the control system can be tuned to assist in extending the charge/discharge cycle life. A follow-on program is planned to validate the benefits of this damage-control methodology on battery performance and life.

**Reference**

1. Hartley, Tom T.; and Jannette, Anthony G.: A First Principles Battery Model for the International Space Station. AIAA–2005–5625, 2005.

**Find out more about Glenn's research:**

**Electrochemistry Branch:**
http://www.grc.nasa.gov/WWW/Electrochemistry/

**Power and Propulsion Office:**
http://space-power.grc.nasa.gov/ppo/

**Glenn contacts:**
Anthony G. Jannette, 216–433–2818, Anthony.G.Jannette@nasa.gov; and Thomas B. Miller, 216–433–6300, Thomas.B.Miller@nasa.gov

**Authors:**
Anthony G. Jannette, Michelle A. Manzo, and Thomas B. Miller

**Headquarters program office:**
Exploration Systems

**Programs/Projects:**
Power Systems R&T, ISS, CEV

## Glenn's Fuel Cell Test Laboratory Became Operational

A new, state-of-the-art fuel cell test and evaluation facility came online in 2005 (see the photograph). This unique NASA facility was designed from its inception to safely and efficiently evaluate fuel cells, electrolyzers, ancillary components, fuel cell subsystems, and powerplants. The facility can enable long-term, uninterrupted testing of components and systems under a variety of test conditions and mission power profiles. Robustness of system design, component degradation modes, failure characteristics, operational sensitivity, and life can be evaluated.

*Fuel Cell Test Laboratory at Glenn.*

The facility comprises three separate test cells. Each test cell is currently configured to evaluate hydrogen/air or hydrogen/oxygen fuel cell systems up to a power rating of 25 kW and has been designed to safely operate entirely independent of the others. Higher power levels and alternate fuels can easily be accommodated via facility modifications.

Inside the Fuel Cell Test Laboratory, two control rooms are used for reactant control, product water handling, system purging, powerplant operation, and data acquisition. The three test cells can be controlled and configured from either control room, enabling the isolation of

sensitive or proprietary testing. Functions pertaining to safe reactant handling are controlled through the use of hardwired programmable logic controllers. This control architecture was chosen to avoid failures as a result of software or computer failures. Each test cell is equipped with hydrogen, high oxygen, low oxygen, and thermal sensors to monitor potential safety hazards. Data from these sensors are sent to the facility programmable logic controller for automated cell shutdown in the event that hazardous levels are detected. The sensor output is also connected to a Lab-wide monitoring system to allow for quick response during unattended operation. Video cameras are used to record routine testing as well as to capture any anomalous events. Programmable electronic loads are used to evaluate the power-producing capabilities of the stack, subsystem, or powerplant under test. These loads can be programmed to apply simulated mission power profiles in controlled current, voltage, or resistance modes.

The Fuel Cell Test Laboratory has the infrastructure to monitor individual cell voltages, stack voltages, currents, power, reactant pressures, reactant flow rates, and temperatures to enable total characterization of the test article. There are two facility data-acquisition systems, both of which are connected to the facility Ethernet backbone. The primary data-acquisition system is based on the National Instruments FieldPoint input-output system. The FieldPoint system is a modular, distributed system that easily enables configuration changes to match the data-acquisition requirements of the research articles under test without extensive rewiring. The facility also contains an eight-channel, high-speed data-acquisition system that can collect data at a rate of 200 kHz. This system enables the evaluation of powerplant performance, design, and response with respect to transient events such as rapid changes in power demand.

The extensive current and future capabilities of Glenn's Fuel Cell Test Laboratory enable efficient development and evaluation of fuel-cell-based powerplants for NASA's current and future exploration and aeronautics missions.

**Find out more about Glenn's Electrochemistry Branch:**
http://www.grc.nasa.gov/WWW/Electrochemistry/

**Glenn contact:**
Dr. Patricia L. Loyselle, 216–433–2180, Patricia.L.Loyselle@nasa.gov

**Analex Corporation contact:**
Kevin P. Prokopius, 216–433–6137, Kevin.P.Prokopius@nasa.gov

**Authors:**
Dr. Patricia L. Loyselle and Kevin P. Prokopius

**Headquarters program office:**
Aeronautics Research, Exploration Systems

**Programs/Projects:**
Constellation Systems, VSP

## Life-Cycle Testing of Mars Surveyor Program Lander Lithium-Ion Battery Achieved Over 10,000 Low-Earth-Orbit Cycles

A 28-V, 25-A-hr lithium-ion (Li-ion) battery that was designed, built, and flight-qualified for the 2001 Mars Surveyor Program Lander is being tested at the NASA Glenn Research Center at 0 °C in a low-Earth-orbit cycle (LEO) regime. In 2005, a milestone was achieved when the battery passed 10,000 cycles. This testing is part of a coordinated test program among several organizations to evaluate the performance of Li-ion batteries under a variety of aerospace mission profiles. Five flight-qualified batteries became available for evaluation upon the cancellation of the 2001 Mars Surveyor Program mission. Since then, the batteries have undergone testing in various LEO, geosynchronous orbit, and planetary mission profile regimes. Organizations participating in the evaluations include the NASA Jet Propulsion Laboratory, the Naval Research Laboratory, the Air Force Research Laboratory, and Glenn.

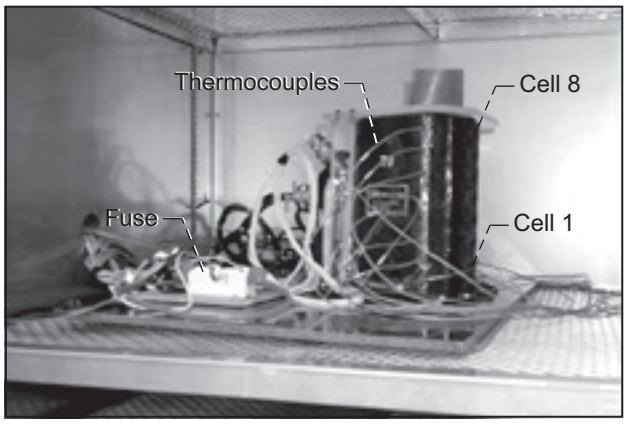


*Mars Surveyor Program Lander Battery in the test chamber.*

The battery contains eight prismatic Li-ion cells connected in series (see the photograph). The cells contain a liquid organic electrolyte,

a mesocarbon microbead anode, and a lithium nickel cobalt oxide ($LiNiCoO_2$) cathode. The battery does not contain charge-balancing electronics.

Glenn's test program began with characterization of the battery to measure baseline performance followed by LEO life-cycle testing at 0 °C, which is ongoing. The LEO test profile consists of a 90-min orbit with a 55-min charge period and a 35-min discharge period during which the battery is discharged to 40-percent depth-of-discharge (DOD). Characterization tests are conducted at 1000-cycle intervals. Thus far, cell balancing, which is performed when the individual cell voltages diverge beyond a predetermined value, has been required only once during the life test, after 7000 cycles.

The battery continues to display excellent performance during its cycling. Some performance metrics are given here, including capacity, end-of-discharge voltage (EODV), efficiency, and specific energy.

Baseline capacity at 100-percent DOD was 25.7 A-hr. At 10,000 cycles, the 100-percent DOD capacity measured 24.2 A-hr, which represents 94 percent of the baseline. The EODV has decreased from an initial 27.95 V at the beginning of LEO cycling to 27.28 V after 10,000 LEO cycles (see the graph). A linear trend projection of the performance would predict a battery EODV of approximately 26.3 V at the 5-yr, 30,000-cycle point, which is well above the 24-V minimum battery-voltage level. However, the electrochemical processes that contribute to battery aging have not been accurately modeled in this simple projection.

Li-ion battery chemistries typically display excellent efficiencies. For this battery, coulombic efficiency is consistently 100 percent throughout LEO cycling. Energy efficiency is between 90 and 93 percent during LEO cycling.

The battery can deliver an average specific energy of 76 W-hr/kg at 100-percent DOD and 32 W-hr/kg during LEO cycling. The specific energy for the battery was calculated using the mass of the entire flight battery assembly, including the cell stack, battery wiring, deck plate, and connectors. In order to meet mission requirements, the Mars lander battery was fortified with robust construction designed to tolerate the impact it would sustain during its landing on the surface of Mars.

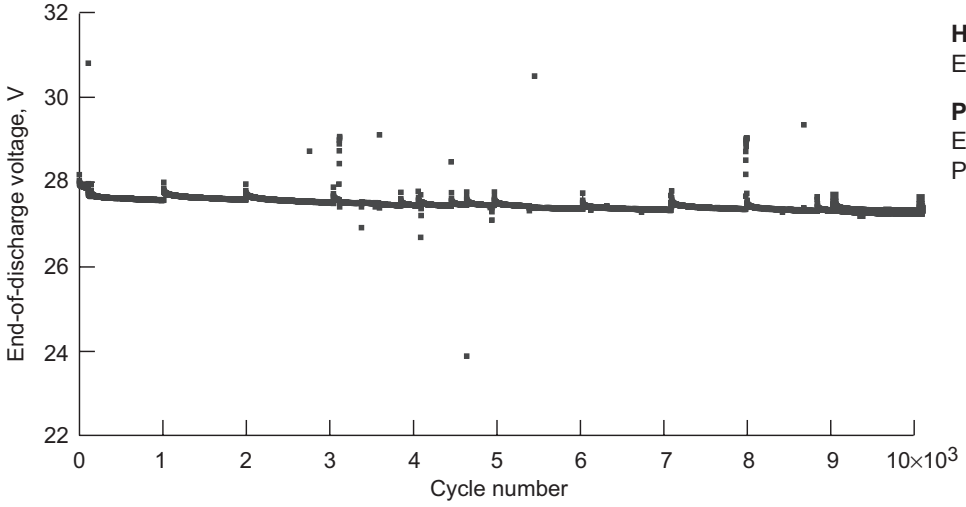


*EODV versus cycle number.*

Li-ion batteries are excellent candidates to provide power and energy storage for satellites in LEO due to their high specific energy, high energy density, and high efficiency. Although Li-ion batteries are increasingly being used for aerospace missions in geosynchronous orbit, some challenges still remain before they can be deemed a suitable replacement for their secondary alkaline battery counterparts in long-cycle-life LEO applications. Life-cycle test data of Li-ion batteries are critical to establishing confidence in Li-ion battery technology for widespread use in manned and unmanned missions.

**Bibliography**

Reid, Concha: Low Temperature Low-Earth-Orbit Testing of Mars Surveyor Program Lander Lithium-Ion Battery. AIAA–2005–5562, 2005.

Reid, C.: Low Temperature Life-Cycle Testing of a Lithium-Ion Battery for Low-Earth-Orbiting Spacecraft. Presented at the NASA Aerospace Battery Workshop, Huntsville, AL, 2004.

**Find out more about Glenn's Electrochemistry Branch:**
http://www.grc.nasa.gov/WWW/Electrochemistry/

**Glenn contacts:**
Concha M. Reid, 216–433–8943, Concha.M.Reid@nasa.gov; and Michelle A. Manzo, 216–433–5261, Michelle.A.Manzo@nasa.gov

**Author:**
Concha M. Reid

**Headquarters program office:**
Exploration Systems

**Programs/Projects:**
Exploration Technology Development Program, Energy Storage Project

# Flywheel Integrated Power and Attitude Control System Demonstrated

This year, NASA Glenn Research Center's Flywheel Development Team experimentally demonstrated the Integrated Power and Attitude Control System, a full-power, high-speed, two-flywheel system, simultaneously regulating a power bus and providing a commanded output torque. Operation- and power-mode transitions were demonstrated up to 2000 W in charge and 1100 W in discharge, while the output torque was simultaneously regulated between $\pm$0.8 N-m.

The G2 and D1 flywheels—magnetically levitated carbon-fiber wheels with permanent magnet motors—were used for the experiment. The units were mounted on an air-bearing table in Glenn's High Energy Flywheel Facility, and the operational speed range was between 20,000 and 60,000 rpm. The bus voltage was regulated at 125 V during charge and discharge, and charge-discharge and discharge-charge transitions were demonstrated by changing the amount of power that the power supply provided between 300 and 0 watts. In a satellite system, this would be the equivalent of changing the amount of energy that the solar array provides to the spacecraft. In addition to regulating the bus voltage, we simultaneously controlled the net torque produced by the two flywheel modules. Both modules were mounted on an air table that was restrained by a load cell. The load cell measured the force on the table, and the torque produced by the two flywheels on the table could be calculated from that measurement, yielding net torques from –0.8 to 0.8 N-m. This was the first Glenn demonstration of the Integrated Power and Attitude Control System at high power levels and speeds.

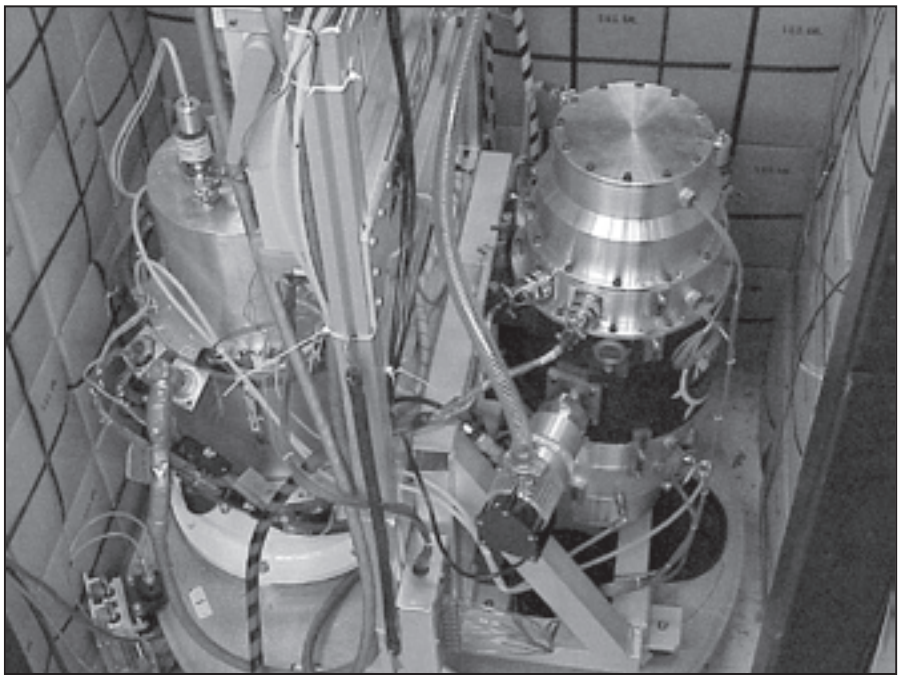

*D1 and G2 flywheel module in High Energy Flywheel Facility.*

Flywheels have advantages over other energy storage systems for missions that require high power, long life, or broad operating temperature range. System studies have quantified the benefits of flywheels for applications like the *International Space Station*, the Momentum Exchange Tether Program, and lunar deployment.

**Find out more about Glenn's research:**

**Aerospace flywheel development:**
http://space-power.grc.nasa.gov/ppo/projects/flywheel/

**Structural Mechanics and Dynamics Branch:**
http://structures.grc.nasa.gov/5930/

**Glenn contacts:**
Raymond F. Beach, 216–433–5320, Raymond.F.Beach@nasa.gov; and James F. Soeder, 216–433–5328, James.F.Soeder@nasa.gov

**University of Toledo contact:**
Ralph H. Jansen, 216–433–6038, Ralph.H.Jansen@nasa.gov

**Author:**
Ralph H. Jansen

**Headquarters program office:**
Exploration Systems

**Programs/Projects:**
Energetics

# High-Power Hall Thruster Designed for Exploration Applications

Hall thruster propulsion systems are a classification of electric propulsion devices that have historically been used to perform stationkeeping functions on communication satellites (ref. 1). A 4.5 kW propulsion system that can efficiently perform orbit insertion in addition to stationkeeping is currently being developed in the commercial sector (ref. 2), and NASA is developing relatively low-power Hall thruster technology that is optimized for space science missions (refs. 3 and 4). In addition, the NASA Glenn Research Center was selected by the Exploration Systems Mission Directorate to design and experimentally demonstrate Hall thruster technology at power levels up to 150 kW. Solar electric transfer vehicles utilizing high-power Hall thruster technology can be used to deliver cargo for lunar missions (ref. 5) and human Mars missions (ref. 6).

During fiscal year 2005, Glenn completed an in-house design of a 150-kW Hall thruster, designated the NASA–1000M. The NASA–1000M was designed to operate at a discharge voltage of 600 V and a discharge current of 250 A. At this nominal operating point, the thruster is expected to produce 6.0 N of thrust and to operate with 2800-sec specific impulse. A solid model rendering of the thruster design is depicted in the figure. A lower power NASA Hall thruster nominally designed to operate at 5 kW is also shown for scale. A design for a laboratory model hollow cathode assembly also was completed.

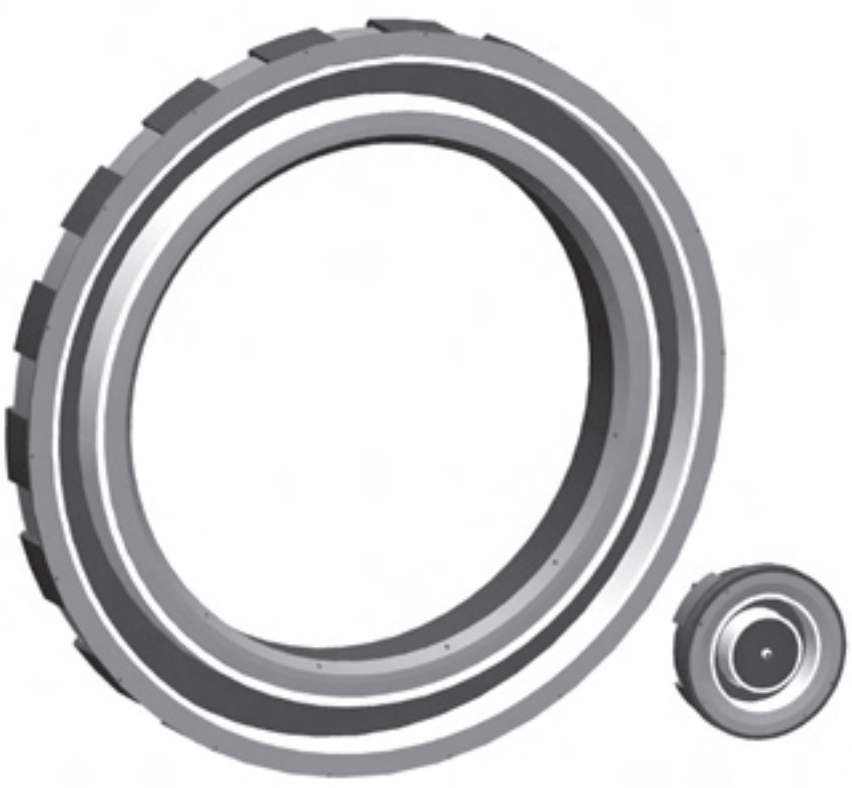

*Solid models. Left: 150-kW NASA–1000M Hall thruster. Right: 5-kW NASA–173M Hall thruster.*


**References**

1. Randoph, T., et al.: Integrated Test of an SPT–100 Subsystem. AIAA–1997–2915, 1997.
2. de Grys, K., et al.: BPT–4000 Multi-Mode 4.5 kW Hall Thruster Qualification Status. AIAA–2003–4552, 2003.
3. Oh, D.: Evaluation of Solar Electric Propulsion Technologies for Discovery Class Missions. AIAA–2005–4270, 2005.
4. Witzberger, K., et al.: NASA's 2004 In-Space Propulsion Refocus Studies for New Frontiers Class Missions. AIAA–2005–4271, 2005.
5. Sarver-Verhey, T., et al.: Solar Electric Propulsion Vehicle Design Study for Cargo Transfer to Earth-Moon L1. AIAA–2002–3971, 2002.
6. Gefert, Leon P.; Hack, Kurt J.; and Kerslake, Thomas W.: Options for the Human Exploration of Mars Using Solar Electric Propulsion. AIP Conference Proceedings, no. 458, 1999, pp. 1275–1280. Available from the NASA Center for Aerospace Information.


**Find out more about Glenn's Hall thruster research:**
http://www.grc.nasa.gov/WWW/hall/


**Glenn contacts:**
David T. Jacobson, 216–433–3691, David.T.Jacobson@nasa.gov; and
Dr. David H. Manzella, 216–977–7432, David.H.Manzella@nasa.gov

**Author:**
David T. Jacobson


**Headquarters program office:**
Exploration Systems

**Programs/Projects:**
Exploration Systems, R&T

# Piezoelectric Ignition Systems Demonstrated for Spacecraft Propulsion Applications

To address the future needs and requirements of NASA's Pulsed Plasma Thruster (PPT) research and development program and of Small Business Innovation Research phase I and II contracts, Face Electronics, LC (Norfolk, VA) is addressing the miniaturization and life extension of current PPT circuits by developing a new discharge initiation module in which the heavy, bulky, and electromagnetic-interference-noisy step-up magnetic transformer is replaced by a lower profile, smaller footprint, higher power density piezoelectric transformer.

Taking as a reference the design specifications of the recent PPT developments for the Earth Observing-1 experimental satellite (EO–1) launched in November 2000, Face implemented a novel ultracompact discharge initiation (DI) circuit that reduces the volume of the reference DI circuit used in the EO–1 satellite to one-third. The complete prototype of the system (called IGNIT–SONER) was tested in May 2005 at NASA Glenn Research Center's facilities. IGNIT–SONER accumulated over 50,000 cycles under full-vacuum conditions ($10^{-6}$ to $10^{-7}$ torr) while operating a PPT model, and it accumulated over 500,000 accumulated cycles under atmospheric lab conditions under maximum firing rates of 5 Hz.

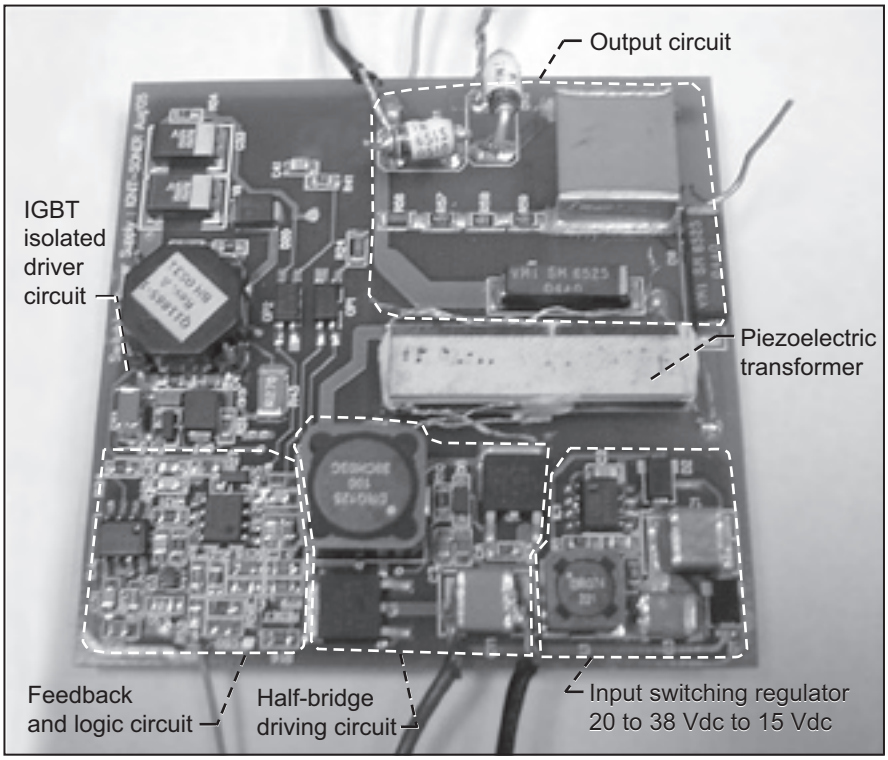


*Latest version of the discharge initiation circuit, the IGNIT–SONER, which uses a piezoelectric transformer to generate high voltage. The prototype measures 2.6 by 2.6 by 0.55 in. (3.70 in.$^3$). IGBT, insulated gate bipolar transistor.*

The research program included different levels of technology innovation and technology integration from the development of a novel piezoelectric transformer design to meet the project specifications to the integration of all the associated electronics to completely operate the discharge initiation systems within a PPT unit. Face readapted its basic patented Transoner technology to provide a transformer able to meet the project requirements. The developed transformer is an isolated PPT having over 3-kV input-to-output isolation and able to step up the input voltage to over 2.5 kV. A major feature of the piezoelectric transformer design is the 5-mm profile, which in combination with surface-mounted components, allows a very compact DI circuitry.

During phase II project development, Face Electronics successfully addressed several design challenges encountered when operating semiconductor spark plugs. The much lower impedance when using these spark plugs under vacuum conditions in comparison to using air-gap spark plugs demanded the modification of the piezoelectric transformer design and the operation strategy. Face overcame these problems by implementing a novel piezoelectric-to-capacitive-discharge circuit.

In an advanced design being implemented, Face intends to provide a self-adjusted mechanism so that the breakdown voltage of the spark plug can be tuned according to the real requirements of the spark plug. Face expects that this mechanism will extend the life operation of PPT systems by gradually increasing the driving voltage to the spark plug as soon as wear and ignition failure are detected. Currently, PPT life is limited mainly by the spark-plug degradation and the incapability of DI circuits to provide the required increase in voltage to continue the operation.

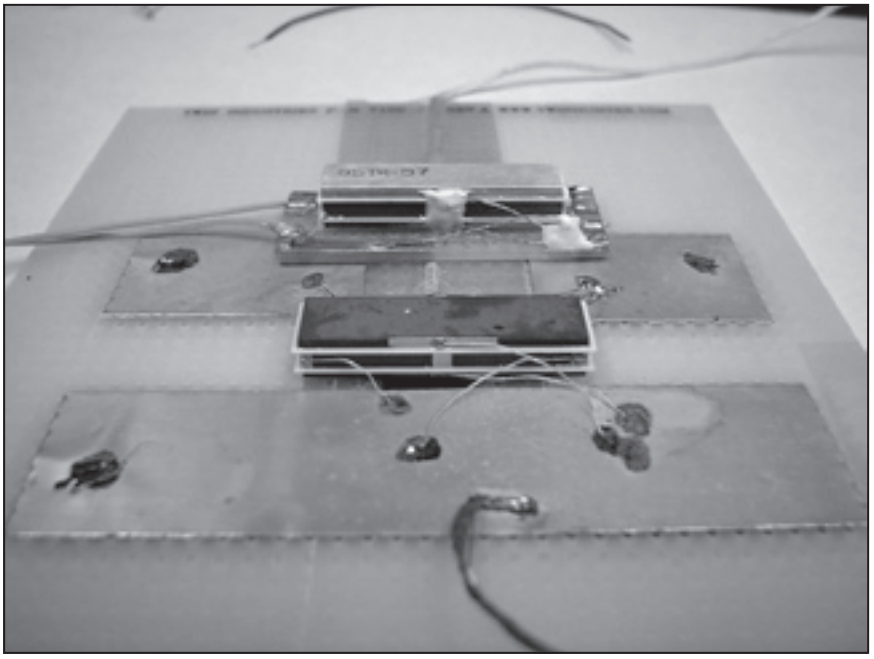

*Different versions of the Transoner piezoelectric transformers developed for this project by Face.*

**Find out more about this research at Face Electronics LC:**
http://www.transoner.com

**Glenn contact:**
Dr. Hani Kamhawi, 216–977–7435,
Hani.Kamhawi-1@nasa.gov

**Face Electronics contact:**
Dr. Alfredo V. Carazo, 757–624–2121,
alfredo@faceco.com

**Authors:**
Dr. Hani Kamhawi and
Dr. Alfredo V. Carazo

**Headquarters program office:**
Aeronautics Research

**Programs/Projects:**
Electric Propulsion

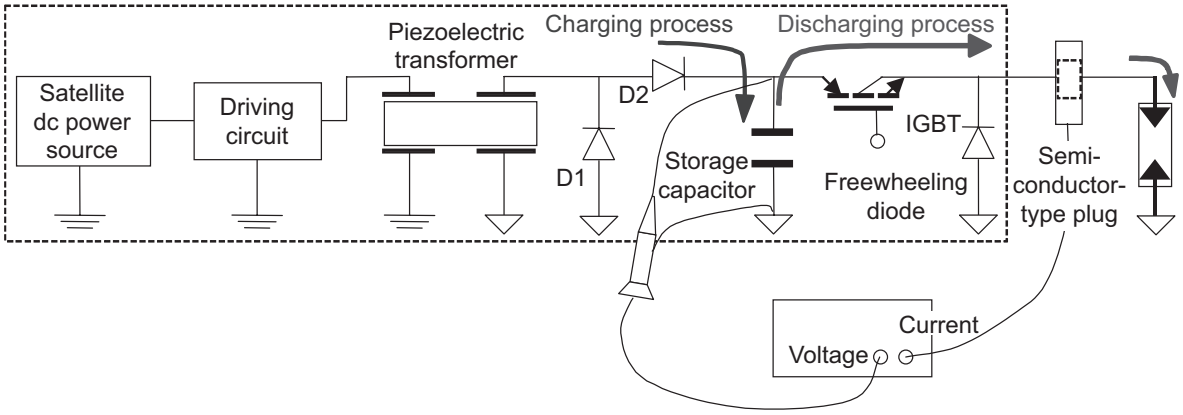


*Piezoelectric-capacitive discharge concept with a storage capacitor connected across the input voltage source. D1 and D2, discharge initiation circuits; IGBT, insulated gate bipolar transistor.*

This promising technology will be useful in a variety of spacecraft applications. The performance achieved promotes consideration of piezoelectric technology not only for piezoelectric igniter applications but also as a replacement for the main transformer in a PPT system. In addition, the technology may be adaptable for other onboard propulsion applications requiring high-voltage generation. Piezoelectric devices are receiving growing interest as replacements for magnetic transformers in a wide range of consumer electronics applications.

# Microwave Discharge and Neutralization Plasma Production Developed as an Alternative to Direct-Current Hollow Cathode Plasmas for Ion Propulsion

Gridded ion propulsion technology holds great promise for enabling future robotic exploration missions with large delta-v requirements. Such missions are made possible by the high-specific-impulse capability of gridded ion thrusters. However, such missions will require that the engines operate continuously for up to 10 years! Thruster lifetime definition, improvement, and validation are, therefore, very important. Microwave plasma production, in contrast to conventional hollow-cathode-based ion-thruster-discharge plasma production, can literally eliminate the discharge cathode failure mechanism. Because microwave electron cyclotron resonance (ECR) plasma production is electrodeless, there is nothing to wear out. In addition, the microwave power source itself has a lifetime measured in hundreds of thousands of hours.

High-power ECR plasma production research conducted at the NASA Glenn Research Center has culminated in the design and testing of a large-area (90- by 40-cm) plasma source. The source has been operated up to 2000 W at a frequency of 2.45 GHz and 2500 W at a microwave frequency of 5.85 GHz. Beam extraction at 2.45 GHz at powers up to 16 kW also has been demonstrated with this flexible device.

Recently, a series of plasma measurements were conducted on the ECR plasma source. Plasma uniformity at the exit plane of the source along the thruster center was measured to be greater than 90 percent. Transverse uniformity was also greater than 90 percent. Current densities measured at the exit plane suggest that the source can satisfy the beam current requirements originally laid out in the 2002 NASA announcement calling for the development of a high-power, high-specific-impulse electric propulsion system. Low measured plasma potentials and the absence of doubly charged xenon, as indicated by emission spectra, suggest a long-life plasma source. The ECR plasma source effort establishes a credible path for the resolution of a key ion thruster failure mode, cathode life. The effort, therefore, establishes a firm base for continued growth and technology readiness level advancement.

In addition, Glenn won a NASA Research Announcement award to develop an electrodeless cathode for charge neutralization under the support of the Advanced Systems and Technology Program of the Prometheus Nuclear Systems and Technologies project. In an ECR cathode, whenever the microwave frequency is tuned to the electron-cyclotron-frequency (by applying suitable magnetic field strength), electrons can be resonantly excited and, thereby, given sufficient energy to cause ionization within a low-pressure gas. During phase I of the three-phase effort, a number of ECR cathode configurations were designed and fabricated and their performance was evaluated. Tests were performed using different microwave-injection schemes (i.e., different antenna types), different ECR cathode chamber configurations, various magnetic field circuits, and various propellants.

At the conclusion of the phase I effort, two competing ECR cathode configurations were successfully operated. An ECR cathode with a longitudinal antenna was operated at 2.45 GHz and generated an electron current of 2.6 A with a xenon flow rate of 3 standard cubic centimeters per minute (SCCM) while consuming only 100 W of microwave power. In addition, a multislot ECR cathode operated at 5.85 GHz generated an electron current of 1.8 A with a xenon flow rate of 4 SCCM while consuming only 100 W of microwave power.

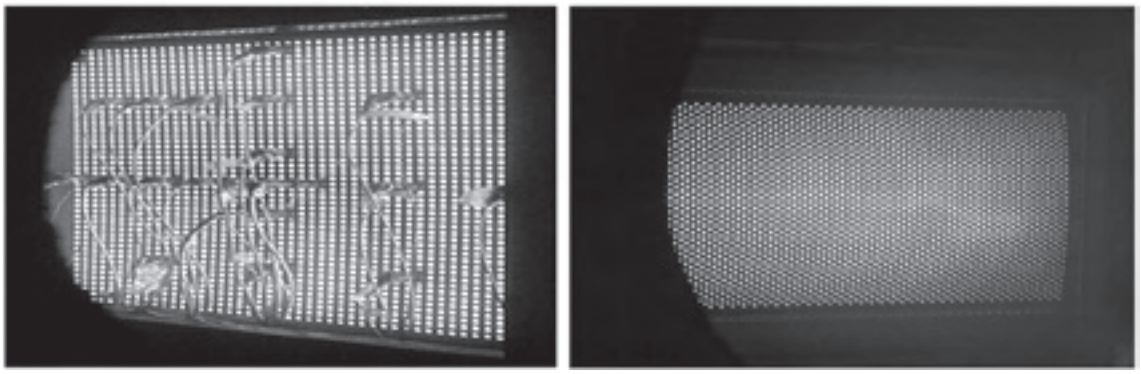

*Microwave ECR ion thruster microwave thruster. Left: Discharge-only testing. Right: Beam-extraction testing.*

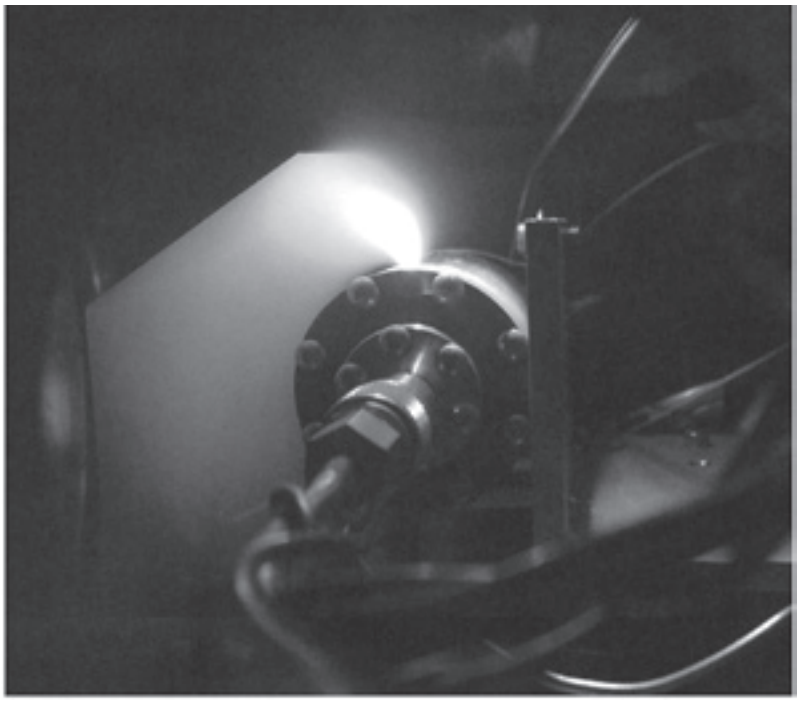

*ECR cathode operating at 100 W.*

**Glenn contacts:**
Dr. Hani Kamhawi, 216–977–7435, Hani.Kamhawi-1@nasa.gov; and
Dr. John E. Foster, 216–433–6131, John.E.Foster@nasa.gov

**Authors:**
Dr. Hani Kamhawi and Dr. John E. Foster

**Headquarters program office:**
Explorations Systems

**Programs/Projects:**
Advanced Systems and Technology Program of the Prometheus Nuclear Systems and Technologies project, Energetics Legacy Program

## Hall Thruster Developed for Robotic Science Missions

During 2005, researchers at the NASA Glenn Research Center successfully developed a new Hall thruster that could make it easier and more cost effective to explore our solar system. The test involved a Hall thruster built under the High Voltage Hall Accelerator (HIVHAC) project. The HIVHAC thruster was designed and fabricated over the last year by a team from Glenn and the Aerojet Corporation (Redmond, WA) to operate efficiently over a wide range of input power levels.

The HIVHAC thruster was demonstrated in a vacuum chamber at Glenn that simulates the environment of space. The thruster operated successfully with input powers between 200 and 2900 W at specific impulses (a measure of propellant fuel economy) between 1000 and 2800 sec. Operation over this wide range of input powers will allow spacecraft to continue thrusting in space far from the Sun, where there is little solar power available to be absorbed by a spacecraft's solar arrays. Operation over this range of specific impulse will allow spacecraft to reach distant destinations utilizing much less propellant than required by chemical propulsion alternatives.

The advantage of Hall thruster propulsion for future solar system exploration over other types of advanced electric propulsion is the potential for much lower cost. Reducing the cost of using electric

*Prototype high-voltage Hall accelerator developed by Glenn and Aerojet.*

propulsion improves its applicability to cost-capped solar system exploration missions such as those conducted through the Discovery, New Frontiers, and Mars Scout programs. Successful development of the Hall thruster required for these missions through the HIVHAC project will lead to the development of a full-scale propulsion system based on this technology.

**Glenn contacts:**
Dr. David H. Manzella, 216–977–7432, David.H.Manzella@nasa.gov; and
David T. Jacobson, 216–433–3691, David.T.Jacobson@nasa.gov

**Author:**
Dr. David H. Manzella

**Headquarters program office:**
In-Space Propulsion, Science Mission

**Programs/Projects:**
Deep space robotic science exploration missions (Discovery, New Frontiers)

## Electric Propulsion Technology Developed for Prometheus 1

In 2005, NASA's Project Prometheus continued comprehensive efforts to develop advanced technologies for space use. One key to these efforts was the development of electric propulsion technologies that would enable new missions, particularly when combined with power generated by a space nuclear reactor (ref. 1). This year, spacecraft requirements were finalized, ion thrusters were tested, and power-processing and control units were chosen for the 200-kW design.

The mission attributes that would be enabled by these technologies include more sophisticated active/passive remote sensing, greater launch window flexibility, spacecraft maneuverability at the destination planet or moon, and greatly increased science data rates. The first proposed mission application, the Jupiter Icy Moons Orbiter mission, focused on a 200-kW Prometheus 1 Spaceship utilizing electric propulsion, as shown in the illustration.

The proposed mission had two principle objectives:
(1) Tour and characterize three icy moons of Jupiter: Callisto, Ganymede, and Europa.
(2) Demonstrate nuclear electric propulsion flight system technologies that would enable a range of revolutionary planetary and solar system missions.

Specific requirements for the Prometheus 1 Spaceship were finalized in July 2005. The requirements were based on Prometheus 1 design team tradeoff analyses, including mission studies to optimize the propulsion parameters. The key driving requirements resulted in the following implementation: six 30-kW ion thrusters (2000-kg xenon throughput), each with a nominal thrust of 0.65 N at 7000-sec specific impulse; six 20-kW Hall thrusters, each with a nominal thrust of 1.0 N (in combination with two ion thrusters, each with a nominal thrust of 0.65 N); a power processor that is more than 96.5-percent efficient and that can operate in radiation levels greater than 5 Mrad; and a single 12,000-kg-capacity, carbon-overwrapped supercritical xenon tank.

The main challenge for the ion thrusters was the qualification of the engine and components in the electric propulsion system for the >2000-kg xenon throughput requirements of the mission (~10 times the state of the art). The basic wear test methodology was to perform component and full-scale tests followed by post-test evaluation. Resulting data were to be used to develop and refine analytical models that could more accurately project for the Prometheus 1 lifetime. Two of these early wear tests were completed this year: precursor ion thruster 2000-hr

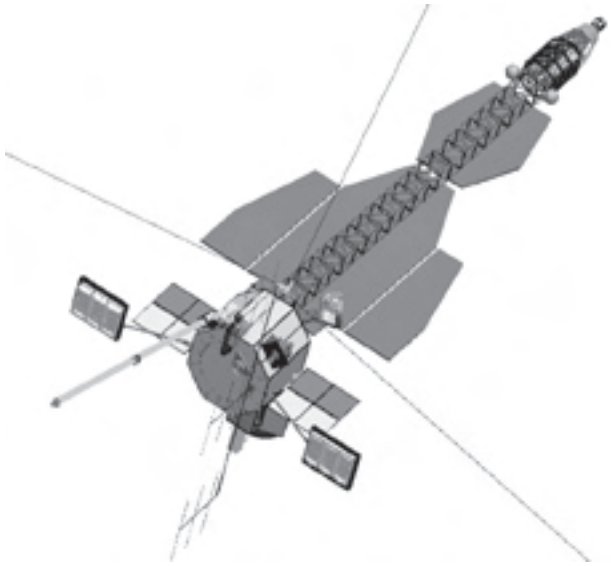

*Spacecraft concept proposed for the Jupiter Icy Moons Orbiter.*

wear tests using the High Power Electric Propulsion (HiPEP) and Nuclear Electric Xenon Ion System (NEXIS) thrusters (refs. 2 to 8).

Work began on designing direct-drive power processing and control (PP&C) units that would provide the required conditioned power to the thrusters for the 200-kW-class nuclear electric propulsion system. These units would operate from a three-phase ac[1] power bus operating at 400 V and would process 30 kW each at 5000 Vdc to operate the ion thruster. Tradeoff studies demonstrated that this was a viable approach that had several advantages over state-of-the-art dc-to-dc[2] converter technology, including simplicity, higher efficiency, and inherent radiation resistance. The beam and accelerator supplies were to be integrated with the discharge, neutralizer, and heater supplies to complete the breadboard PP&C unit (ref. 9).

On the basis of these recent efforts, Hall thruster technology for both the large and small Hall thruster elements was deemed sufficiently mature to proceed directly to the preliminary design phase as soon as a small radiation compatibility effort was completed (ref. 10). Although the Prometheus 1 program has since been cancelled, the technology advances made in this work will be of great benefit to NASA in future exploration missions using electric propulsion.

**References**


1. Oleson, S., et al.: The Electric Propulsion Segment of Prometheus 1. AIAA–2005–3888, 2005.
2. Williams, G.: Wear-Testing of a 21-kW, 7500 s Ion Thruster. AIAA–2005–4396, 2005.
3. Polk, J., et al.: Performance and Wear Test Results for a 20 kW-Class Ion Engine With Carbon-Carbon Grids. AIAA–2005–4393, 2005.
4. Patterson, M., et al.: Herakles Thruster Development for the Prometheus JIMO Mission. AIAA–2005–3890, 2005.
5. Polaha, J., et al.: Random and Sine-Spectrum Vibration Testing of Pyrolytic Graphite Ion Optics. AIAA–2005–4395, 2005.
6. Snyder, J., et al.: Vibration Test and Analysis of a 20-kW-Class Ion Engine. AIAA–2005–4412, 2005.
7. Haag, T.: Mechanical Design of Carbon Ion Optics. AIAA–2005–4408, 2005.
8. Williams, G., et al.: Performance Characterization of a 25-kW High-Specific Impulse Ion Thruster. AIAA–2005–4248, 2005.
9. Pinero, L., et al.: Status of a Power Processor for the Prometheus-1 Electric Propulsion System. AIAA–2005–3895, 2005.
10. Jacobson, D., et al.: An Overview of Hall Thruster Development at NASA's John H. Glenn Research Center. AIAA–2005–4242, 2005.


[1] Alternating current.

[2] Direct-current to direct-current.


**Glenn contact:**
Steven R. Oleson, 216–977–7426, Steven.R.Oleson@nasa.gov

**Authors:**
Steven R. Oleson and Frederick W. Elliott


**Headquarters program office:**
Exploration Systems

**Programs/Projects:**
Project Prometheus

# Brayton-Cycle Power-Conversion Unit Tested for Operational Vibration Levels

Vibration testing was conducted on an operating closed-cycle Brayton power-conversion unit (BPCU) located at the NASA Glenn Research Center. Results from this test were compared with those from a mechanical dynamics computer model of the same unit. This work showed that dynamic forces developed by the BPCU were small and that the model could accurately predict torque and vibration levels. Accurate predictions of BPCU characteristics are essential for spacecraft control/structure interaction analyses and for understanding the operational capabilities of scientific instrumentation onboard.

The BPCU is a fully integrated power-conversion system including a turbo-alternator, recuperator, and gas cooler with helium-xenon working fluid designed for operation up to 2 kWe. The heat source used in the test was a series of silicon-carbide electrical resistance heaters contained in a shell and tube heat exchanger that heated the helium-xenon gas to over 1000 K, simulating a fission reactor source. A commercial chiller with a pumped ethylene glycol cooling loop provided waste-heat rejection. The BPCU utilizes multifoil insulation, which requires a vacuum environment.

The test approach for the 2-kWe Brayton engine required careful planning of measurement sensor types and locations. Test-stand modifications necessary to minimize environmental noise and to ensure accurate dynamic measurements were identified and implemented. Because the analytical model predicted that the 2-kWe BPCU would be a very quiet machine, the Microgravity Emissions Laboratory (MEL) at Glenn was given the test-instrumentation and data-acquisition task. The MEL team utilized a highly sensitive acceleration measurement system at Glenn's Vacuum Facility 6 to record the mechanical dynamics signature. Facility background vibration (due mostly to vacuum pump systems) was measured and found to be too high to discern the very low-level vibration of the BPCU. Consequently, an isolation test stand was designed and built to utilize existing mounting pads within the vacuum tank, and a two-cable suspension system was used to isolate the BPCU from facility vibration. Pretest background noise checks confirmed the effectiveness of the isolation stand's ability to attenuate environmental vibration.

Testing showed minimal excitation ($10^{-15}$ to $10^{-10}$ $g^2$/Hz) in the frequency band of interest (0 to 600 Hz). This is important input to the understanding of on-orbit spacecraft control/structure interactions for a large, flexible spacecraft. With such low disturbances coming from the operating 2-kWe BPCU, issues with spacecraft control/structure interactions are not expected. In addition, on the basis of the experimental data, an operating BPCU would not impact scientific measurement onboard the notional spacecraft application.

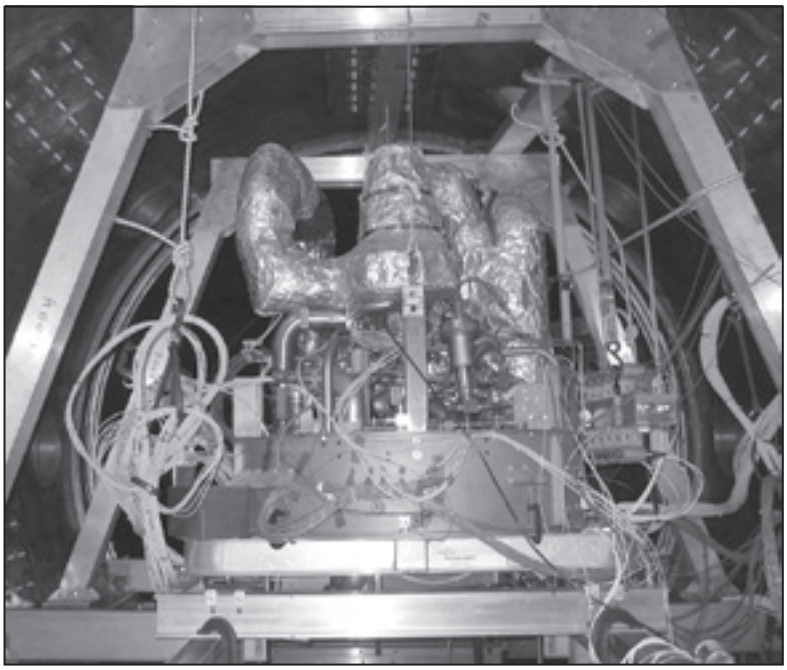

*BPCU installed in vibration isolation stand.*

**Find out more about the research of Glenn's Thermo-Mechanical Systems Branch:**

http://www.grc.nasa.gov/WWW/tmsb/

**Glenn contact:**
Dr. Michael J. Barrett, 216–433–5424,
Michael.J.Barrett@nasa.gov

**Analex Corporation contact:**
David S. Hervol, 216–433–9624,
David.S.Hervol@nasa.gov

**Authors:**
David S. Hervol, Damian R. Ludwiczak,
Dr. Dzu K. Le, Anne M. McNelis,
Albert Y. Yu, and Sergey Samorezov

**Headquarters program office:**
Exploration Systems

**Programs/Projects:**
Project Prometheus

# Novel Analysis Tools Created to Enable Stirling Radioisotope Space Power Systems

NASA and the Department of Energy are developing a high-efficiency Stirling radioisotope power system for future NASA space science missions, including such potential uses as powering rovers on planetary surfaces, lunar communication stations, and spacecraft power for deep-space missions. Stirling analysis tools are key elements in the ability to design, analyze, diagnose, test, and subsequently, improve these Stirling power systems. The NASA Glenn Research Center has created a suite of industry-leading tools for dynamic system analysis and multidimensional thermodynamic and electromagnetic analyses. These provide a complete picture of both overall system and detailed component behavior. In addition, Glenn research on understanding losses in Stirling systems has led to improved one-dimensional Stirling design codes.

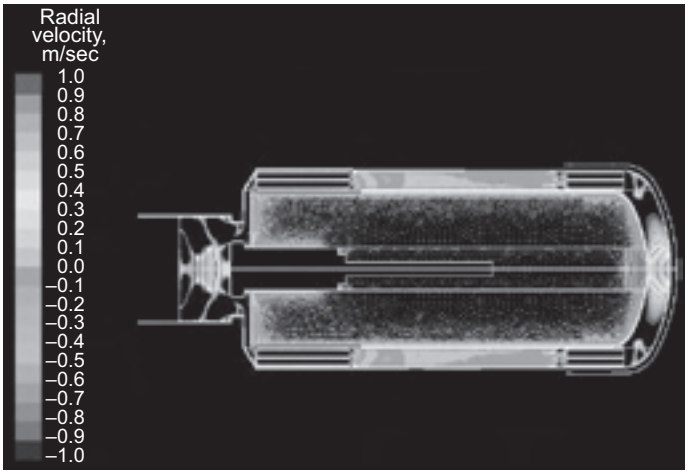


*Radial velocity distribution inside a Stirling engine. Time, 5.1547 sec.*

Lockheed Martin (Valley Forge, PA) is the system integrator for the 110-W, first-generation Stirling radioisotope power system, known as the Stirling Radioisotope Generator (SRG110). Infinia Corporation (Kennewick, WA) is providing the Stirling convertor (integrated Stirling engine and linear alternator). The SRG110 is being developed under contract to the Department of Energy, with Glenn providing key supporting technology developments and advanced technology efforts. The projected SRG110 system efficiency of 23 percent will reduce the required amount of radioisotope by a factor of 4 or more in comparison to currently used radioisotope thermoelectric generators. A next-generation Stirling system is expected to exceed 30-percent efficiency and to double the power output per unit mass for a radioisotope power system.

The Stirling System Dynamic Model (SDM), based on Ansoft Simplorer, is a nonlinear, time-domain model that simulates Stirling cycle thermodynamics; heat flow; gas, mechanical, and mounting dynamics; the linear alternator; and the controller. It allows complex interactions among the various Stirling subsystems to be studied and can model transient and dynamic phenomena from startup to full-power conditions. In 2005, SDM's thermodynamic modeling was improved by coupling the SDM to Sage, an industry-standard Stirling design code. In addition, linear modeling techniques were developed that can produce models to be used with classical controls and stability analysis techniques.

*Parallel computer cluster for high-speed processing of complex-geometry Stirling simulations.*

The first U.S. multidimensional computational fluid dynamics (CFD) model for a complete Stirling engine was developed in 2005. The preceding figure shows the radial velocity distribution for an axisymmetric simulation of the Stirling engine being developed for the SRG110, and the photograph shows the Microway 32-processor parallel computer cluster that was set up to run the multidimensional models. More recently, a complete three-dimensional simulation was achieved for this same engine. The commercial CFD code FLUENT is used for the simulation platform.

These analysis tools have affected the SRG110 design as well as advanced technology efforts. The SDM has been used to provide key input for the SRG110 controller development and to study system integration issues and off-nominal behavior. The SDM is also being used in the design of advanced controllers and linear alternators. The three-dimensional

electromagnetic model, based on Ansoft Maxwell, was used to estimate the linear alternator's margin to demagnetization, which impacted SRG110 magnet selection. This demagnetization margin was verified with test data in 2005.

The multidimensional CFD models will soon be used to evaluate effects that could not previously be studied with simpler models and cannot be determined from testing. These include the effects of uneven circumferential heating and the effect of possible regenerator bypass flow that may be caused by small dimensional changes due to heater head creep over very long operating times. The CFD models have also already been used to provide estimations of operating temperatures that cannot otherwise be determined for parts undergoing reliability studies. Perhaps most importantly, this set of tools can enable detailed investigation of a design and its modifications before expensive hardware is fabricated.

**Bibliography**

Dyson, R.W., et al.: Fast Whole-Engine Stirling Analysis. AIAA–2005–5558, 2005.

Regan, Timothy F.; and Lewandowski, Edward J.: Development of a Stirling System Dynamic Model With Enhanced Thermodynamics. AIP Conference Proceedings, vol. 746, no. 1, 2005, pp. 658–665.

Geng, Steven M.; Niedra, Janis M.; and Schwarze, Gene E.: Overview of NASA Magnet and Linear Alternator Research Efforts. AIP Conference Proceedings, vol. 746, no. 1, 2005, pp. 666–673.

**Find out more about the research of Glenn's Thermo-Mechanical Systems Branch:**
http://www.grc.nasa.gov/WWW/tmsb/

**Glenn contacts:**
Dr. Rodger W. Dyson, 216–433–9083, Rodger.W.Dyson@nasa.gov;
Dr. Roy C. Tew, 216–433–8471, Roy.C.Tew@nasa.gov; and
Steve M. Geng, 216–433–6145, Steven.M.Geng@nasa.gov

**SEST contacts:**
Tim F. Regan, 216–433–2086, Timothy.F.Regan@nasa.gov; and
Ed J. Lewandowski, 216–433–5525, Edward.J.Lewandowski@nasa.gov

**Authors:**
Dr. Rodger W. Dyson and
Lanny G. Thieme

**Headquarters program office:**
Science Mission

**Programs/Projects:**
Nuclear Radioisotope Power System Development

## Brayton Power-Conversion Modeling Enhanced With Closed-Cycle System Simulation

One form of power conversion under investigation in NASA Glenn Research Center's Thermal Energy Conversion Branch is the closed-Brayton-cycle engine. Producing power from tens-of-kilowatts to multimegawatts, the Brayton engine lends itself to potential space nuclear power applications such as electric propulsion or surface power. The Thermal Energy Conversion Branch recently enhanced its closed-Brayton-cycle design and analysis capabilities by transporting its legacy code, the Closed Cycle Engine Program (CCEP), from Fortran to a more suitable modeling environment known as the Numerical Propulsion System Simulation (NPSS). The updated engine program, called the Closed Cycle System Simulation (CCSS), has been used so far to create models with multiple engines, higher-fidelity components, and thermal transients to match data from test hardware.

The NPSS modeling environment was created at Glenn as a joint effort with industry and the Department of Energy and is maintained by Glenn. It offers improved features such as an unlimited number of input, output, and solver variables, a powerful differential equations solver, the option of either a text or graphical user interface, and the ability to couple with external programs to increase the fidelity of individual components.

An unlimited number of variables allow a user to build models that converge to more elaborate design specifications and operate in a more flexible fashion during off-design analysis. A CCSS model was constructed of two closed-Brayton-cycle engines that shared a common gas inventory and were plumbed together at the heat-source heat exchanger. Although the engines were designed under identical specifications, they could be operated individually at different power levels. The CCSS solver was employed to appropriately balance the gas inventory shared between the two engines.

In a combined effort with Glenn's Turbomachinery and Heat Transfer Branch and Thermal Energy Conversion Branch,

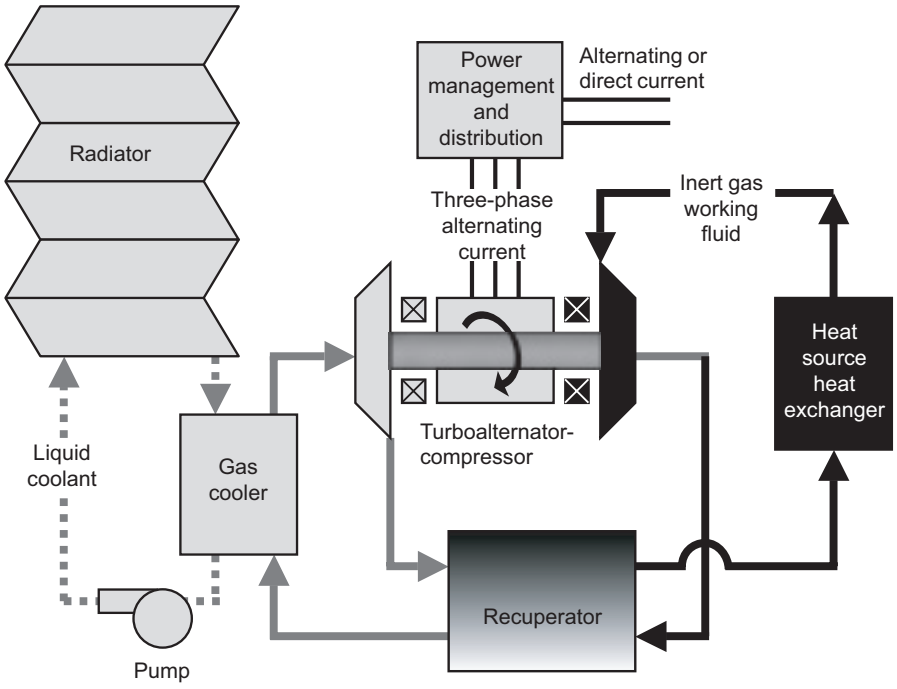


*Recuperated closed-Brayton-cycle power-conversion system with heat rejection.*

CCSS was coupled to the mean-line compressor and turbine codes Quick and Radial Turbine Design, increasing turbomachinery fidelity over CCSS's generic performance tables. Fidelity could be increased even further by coupling CCSS to computational fluid dynamics programs. The ability to couple CCSS to external codes could facilitate collaboration with codes developed by other Government agencies or by industry.

A CCSS model of Glenn's 2-kWe closed-Brayton-cycle engine (MiniBRU) was constructed, and results were compared with transient test data. Attention was given particularly to the model's recuperator and electric heater components because their large masses contribute most to the engine's thermal transients. The CCSS model was able to reproduce the thermal transient timescales exhibited by the MiniBRU for operational step changes in shaft rotational speed and electric heater power input.

CCSS combines the legacy source code of CCEP with the power and extensibility of the NPSS modeling environment. More elaborate design and off-design studies can be conducted than were possible with CCEP. Efforts over the past year have enabled CCSS to replace CCEP as the Thermal Energy Conversion Branch's closed-Brayton-cycle design and analysis tool.

**Bibliography**

Johnson, Paul K.: Closed-Cycle Engine Program Used To Study Brayton Power Conversion. Research & Technology 2004, NASA/TM—2005-213419, 2005, pp. 101–102. http://www.grc.nasa.gov/WWW/RT/2004/RP/RPT-johnson.html

Lavelle, Thomas; Khandelwal, Suresh; and Owen, Albert: Intermediate Fidelity Closed Brayton Cycle Power Conversion Model. NASA/TM—2006-213993, 2006. http://gltrs.grc.nasa.gov/cgi-bin/GLTRS/browse.pl?2006/TM-2006-213993.html

**Find out more about the research of Glenn's Thermo-Mechanical Systems Branch:**
http://www.grc.nasa.gov/WWW/tmsb/

**Analex Corporation contact:**
Paul K. Johnson, 216–433–3814, Paul.K.Johnson@nasa.gov

**Glenn contacts:**
Dr. Michael J. Barrett, 216–433–5424, Michael.J.Barrett@nasa.gov; and Thomas M. Lavelle, 216–977–7042, Thomas.M.Lavelle@nasa.gov

**Author:**
Paul K. Johnson

**Headquarters program office:**
Exploration Systems

**Programs/Projects:**
Project Prometheus, nuclear power systems for electric propulsion or surface power

# Stirling Power Convertors Demonstrated in Extended Operation

A Stirling Radioisotope Generator supplying over 100 W of electric power (SRG110) is being developed by Lockheed Martin Astronautics (Valley Forge, PA). This development effort is under contract to the Department of Energy (Germantown, MD). The generator will be a high-efficiency electric power source for NASA space science missions with the capability to operate in the vacuum of deep space or in a gaseous atmosphere like that found on the surface of Mars. The generator converts heat into electric power as the heat is supplied by a plutonium heat source.

The NASA Glenn Research Center is supporting Lockheed Martin Astronautics and the SRG110 project by providing key data to enhance performance and mitigate risk for what will be the first dynamic power system used in space. High system efficiency was achieved through the use of free-piston Stirling power-conversion technology. Long life has been achieved through the use of noncontacting moving components: there are no wear mechanisms. The Glenn tasks include in-house testing of Stirling convertors and advanced controllers, materials evaluation and heater head life assessment, structural dynamics testing and analysis, assessment of organics, and reliability analysis. A parallel effort to develop an advanced technology Stirling convertor with reduced mass and increased efficiency complements the SRG110 project.

To demonstrate the capability for long life, Glenn is conducting extended-operation tests of flight-prototype Stirling power convertors known as Technology Demonstration Convertors (TDC's) that were developed by Infinia Corporation (formerly known as the Stirling Technology Company, Kennewick, WA). TDC's #13 and #14 recently passed 2 years of operation and now have over 18,400 hr of extended operation. The power output and efficiency have remained nearly constant throughout this test. TDC's #15 and #16 began testing at Glenn earlier this year and have accumulated over 4200 hr of extended operation. TDC's #5 and #6 have been operating in a thermal vacuum environment intended to simulate operation in deep space and have accumulated over 4600 hr. The total operating time of all the convertors at Glenn has surpassed 58,000 hr with no failures to report. Operation is continuing in support of Lockheed Martin Astronautics and the SRG110 project. This effort is supported by NASA's Science Mission Directorate, Radioisotope Power Systems.

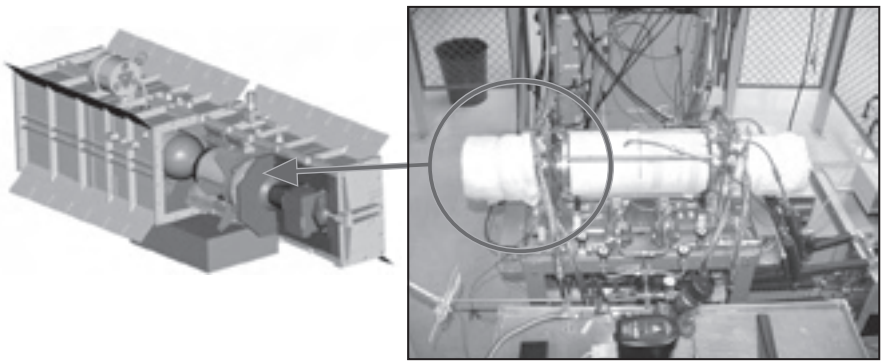

*Left: SRG110. Right: TDC's #13 and #14 on extended operation test at Glenn. (Photograph courtesy of Lockheed Martin Astronautics; used with permission.)*

**Bibliography**

Thieme, Lanny G.; and Schreiber, Jeffrey G.: Advanced Technology Development for Stirling Convertors. Proceedings of the Space Technology and Applications International Forum, Albuquerque, NM, 2004.

Schreiber, Jeffrey G.; and Thieme, Lanny T.: Accomplishments of the NASA GRC Stirling Technology Development Project. AIAA–2004–5517, 2004.

**Find out more about the research of Glenn's Thermo-Mechanical Systems Branch:**
http://www.grc.nasa.gov/WWW/tmsb/

**Glenn contact:**
Jeffrey G. Schreiber, 216–433–6144, Jeffrey.G.Schreiber@nasa.gov

**Author:**
Jeffrey G. Schreiber

**Headquarters program office:**
Science Mission

**Programs/Projects:**
RPS

# Alpha-Voltaic Power Source Designs Investigated

In an alpha-voltaic power source, a radioactive substance that emits energetic alpha particles is coupled to a semiconductor p/n junction diode or solar cell. An alpha-emitting radioistope is used instead of a beta-emitting one to ensure a simple design that needs minimum shielding to contain the radiation. Americium-241 ($Am^{241}$), with a half-life of 432.7 years and an activity of 3.5 curies per gram (Ci/g), emits a 5.5-MeV alpha particle. As the alpha particles penetrate into the p/n junction, they decelerate and give up their energy by creating electron-hole pairs in the semiconductor. These electron-hole pairs are collected by the p/n junction and are converted into useful electricity much like a solar cell. The primary reason alpha voltaics have not been technologically successful to date is that the alpha particles damage the semiconductor material so as to degrade the electrical output of the solar cell in just a matter of hours. At the NASA Glenn Research Center, several alpha-voltaic particle source designs were investigated that address this problem.

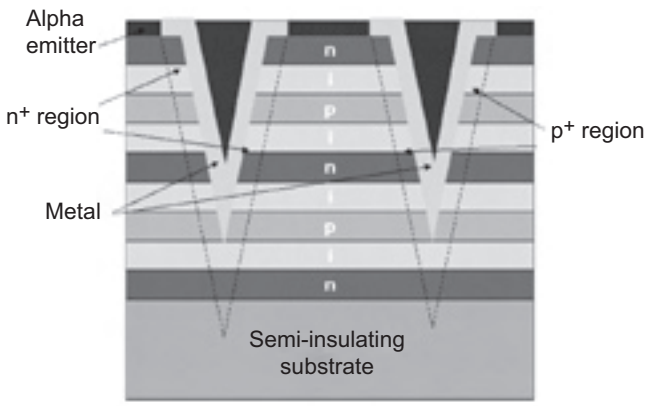


*"Nipi' structured alpha-voltaic battery.*

They key to future development resides in the ability to limit the radiation degradation in the photovoltaic portion of these devices. One approach to solving this problem is to use semiconductor materials that are more radiation tolerant. An indium gallium phosphide (InGaP) cell was fabricated and tested under alpha emission. The device degraded substantially but was found to recover significantly with an anneal at 200 °C for 1 hr.

A second approach involves the use of nonconventional device designs such as a lateral junction "nipi" device. This design spatially separates the n and p layers of a cell, which permits charge separation and transport to occur within two separate orthogonal planes, thus ensuring a higher radiation tolerance (see the schematic to the top right).

The third approach uses an intermediate material to absorb the incident alpha energy and reemit it as light, without undergoing significant radiation damage. This material could be incorporated in a device structure to convert the alpha radiation indirectly. A possible candidate for this application would be a semiconducting quantum dot. In this design, seen in the following diagram, you would choose a phosphor material whose emissions were tailored to the bandgap of the photovoltaic device to ensure a high conversion efficiency while the phosphor protects the p/n junction of the device.

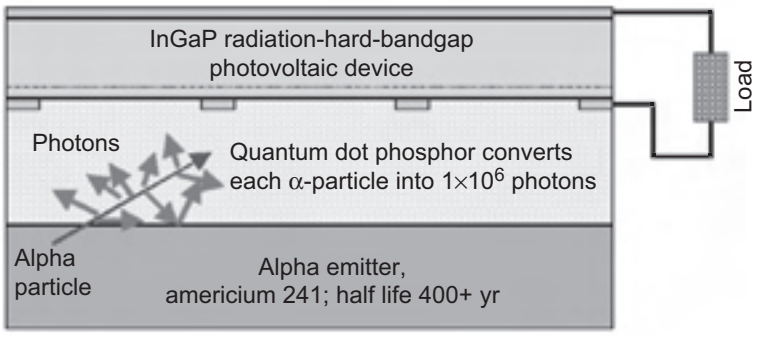


*Alpha-voltaic battery using an intermediate quantum dot absorber layer.*

The graph on the following page shows the current-versus-voltage output of an alpha-voltaic battery that used an InGaP cell coated with zinc sulfide:gold (ZnS:Ag) intermediate absorber quantum dots after it was placed in contact with $Am^{241}$.

A single alpha-voltaic stack would consist of an electrochemically deposited $Am^{241}$ film on a thin metal foil alpha-particle source sandwiched between layers of quantum dots, with the quantum dots sandwiched between the bifacial p/n junction photovoltaic devices seen in the final figure.

Such a device, whose area would be less than 1 $cm^2$ and whose weight would be approximately 3 g, could generate up to 5 mW, if 2.5 Ci of $Am^{241}$ was used (i.e., 2 mW/mCi).

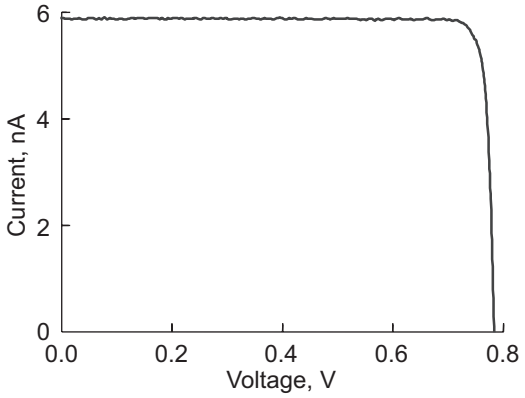


*Current-versus-voltage output of an alpha-voltaic battery. Operating temperature, –135 °C.*

The quantum-dot alpha-voltaic devices could operate at low temperatures at which current battery systems would be rendered useless. In addition, they could be easily fabricated in microscale sizes, which is extremely difficult with conventional battery chemistries. This attribute makes them extremely attractive for microsystem applications such as biomedical or microelectromechanical systems (MEMS) sensors. These small devices could provide low levels of power for an extremely long period of time (i.e., >100 years) and could operate over a wide range of environments with little, if any, loss of performance, most notably at extremely low temperatures (i.e., < 100 K) but also in harsh biological environments.

**Find out more about the research of Glenn's Photovoltaic and Space Environments Branch:**
http://www.grc.nasa.gov/WWW/5000/pep/photo-space/

**Glenn contact:**
Dr. Sheila G. Bailey, 216–433–2228, Sheila.G.Bailey@nasa.gov

**Rochester Institute of Technology contact:**
Dr. Ryne P. Raffaelle, 585–475–5149, rprsps@rit.edu

**Authors:**
Dr. Sheila G. Bailey, David M. Wilt, Dr. Ryne P. Raffaelle, and Dr. Stephanie L. Castro

**Programs/Projects:**
Glenn's IR&D

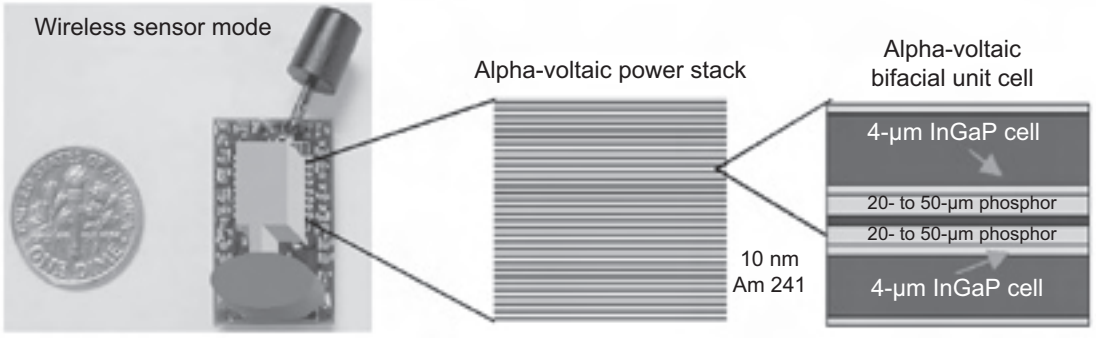


*Alpha-voltaic power stack.*

# Carbon Nanotubes Synthesized and Assessed for Space Photovoltaics

The enhancement of polymeric solar cells through the addition of nanostructured material complexes has been investigated to facilitate exciton dissociation and carrier transport through a polymer matrix. The dispersion of single-wall carbon nanotubes (SWNTs) into poly-3-octylthiophene (P3OT) has been shown to dramatically improve both the electrical conductivity and optical absorption of the polymer in comparison to the pure polymer. The photoresponse of solar cells using P3OT doped with SWNTs is significantly improved over the undoped version under simulated air mass zero (AM0) illumination. In addition, cadmium selenide (CdSe) quantum dots (QDs) have been used by several groups to facilitate exciton dissociation and improve the efficiency of P3OT-based solar cells. Through the synthesis of QD–SWNT complexes, researchers at the NASA Glenn Research Center produced a nanostructured additive for polymeric solar cells that exhibits both a high electron affinity and high electrical conductivity. This year, researchers from Glenn and the Rochester Institute of Technology (RIT) synthesized copper-indium-sulfide- (CIS-) QD/SWNT complexes and assessed their viability as an additive in polymeric solar cells.

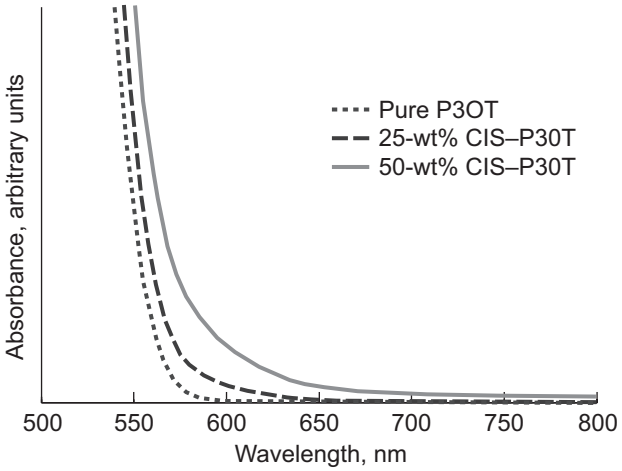


*Optical absorbance versus wavelength for P3OT doped with CIS QDs.*

There are four main problems to address in improving polymeric solar cells:

(1) Photon absorption—The polymer and additives must have a suitable bandgap to capture a significant portion of the solar spectrum.

(2) Exciton diffusion—The limited diffusion lengths (~10 nm) of polymeric excitons necessitate a novel device structure or appropriate volume fractions of nanomaterial additives.

(3) Exciton dissociation—There must be a sufficient difference in potential energy levels to overcome the exciton binding energy for electron-hole dissociation.

(4) Carrier transport—High hole conductivity is needed in the polymer, and high electron conductivity is needed in the material additives.

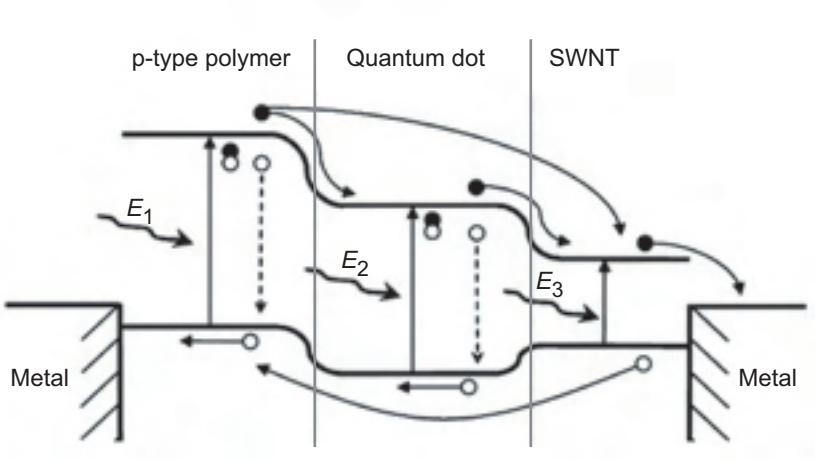


*Energy-level (E) diagrams adjusted in relation to the vacuum level and equilibrated at the Fermi energy for a QD–SWNT-polymer solar cell showing the electronic transitions from optical absorption, exciton dissociation, and resulting carrier transport of the components (ref. 1); $E_1 > E_2 > E_3$.*

An ideal nanomaterial additive for a polymeric solar cell would have a high electron affinity, low percolation threshold, high electrical conductivity, and a suitable bandgap. Although this may be achieved by a single material, another approach would be to combine nanomaterials with complementary characteristics: for example, combining appropriate covalently or noncovalently semiconducting QDs to an SWNT (ref. 1).

A possible idealized energy band diagram for a polymeric solar cell with QD–SWNT complexes is shown in the diagram to the left. The relative levels have been adjusted to illustrate a favorable relationship between the materials. Such a combination is possible for bandgaps and electron affinities that have been reported in the literature for the various constituents.

SWNTs were synthesized using an alexandrite laser vaporization process (ref. 2). Raw soot was purified using conventional nitric acid and thermal oxidation steps to achieve SWNT mass fractions of >95 wt% in the overall sample; then, CIS QDs were prepared by conventional colloidal organometallic chemical bath syntheses (ref. 3). QD–SWNT complexes

were formed through covalent and noncovalent attachment schemes involving carboxylic acid-functionalized SWNTs with CIS-mercaptoacetic acid QDs.

The addition of lower bandgap QDs and SWNTS can enhance the absorption spectrum of an ordinary polymeric solar cell. The graph at the top of the preceding page shows how the addition of CIS QDs changes the optical absorbance of P3OT. The graph to the right shows that absorbance improves dramatically when nanotubes are combined with CIS.

Photovoltaic devices of the nanomaterial-P3OT composites were made by spin coating the materials onto commercially obtained indium-tin-oxide- (ITO-) coated polyethylene terapthalate (PET) substrates that were pretreated with a thin film of polyethylenedioxythiophene (PEDOT). Thermally evaporating aluminum grid contacts were used. The bottom right graph shows the AM0 photoresponse of a P3OT solar cell with a 50-wt% doping of CIS QDs.

Covalent and noncovalent attachment schemes to SWNTS were attempted to address the deficiencies associated with using QDs alone. A dramatic improvement in the cell characteristics with the addition of SWNTs is shown in the bottom left graph.

QD–SWNT complexes, which combine a high electron affinity and low percolation threshold, provide an attractive nanomaterial additive for polymeric solar cells. By using a simple covalent coupling reaction, researchers from Glenn and RIT demonstrated that such complexes are possible. Initial prototype cells using these complexes in a P3OT-based device showed enhanced photoconversion in comparison to undoped cells. The quantum confinement found in the nanomaterials described should allow for the optimization of absorption to the solar spectrum and efficient device designs that will increase performance in polymeric solar cells.

The authors acknowledge the support of NASA through grants NCC3–956 and NAG3–2484, the National Science Foundation through grant ECS–0233776, and BP Solar.

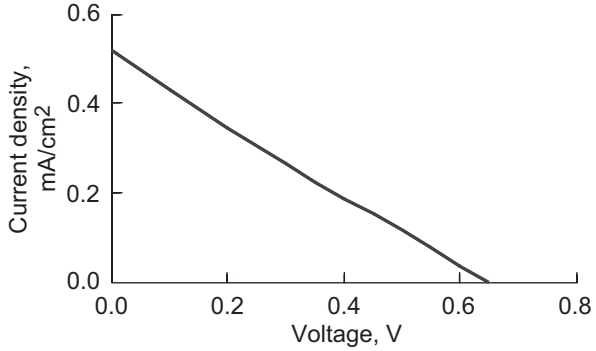


*Current-versus-voltage photoresponse of a nanomaterial-P3OT solar cell under 1-sun AM0 illumination.*

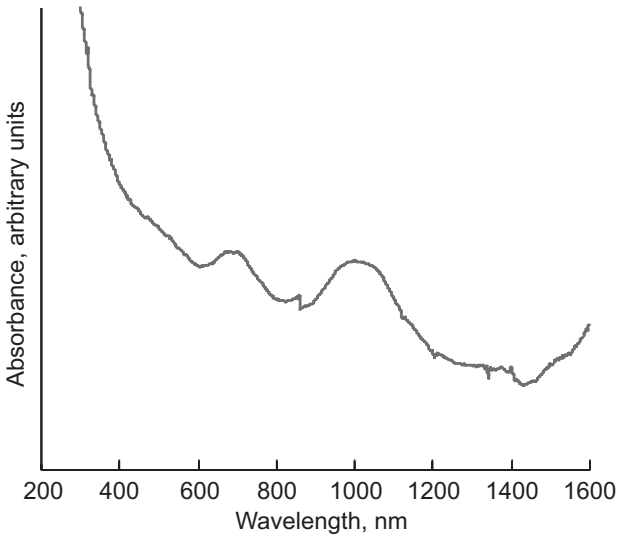


*Optical absorbance of CIS–SWNT complexes.*

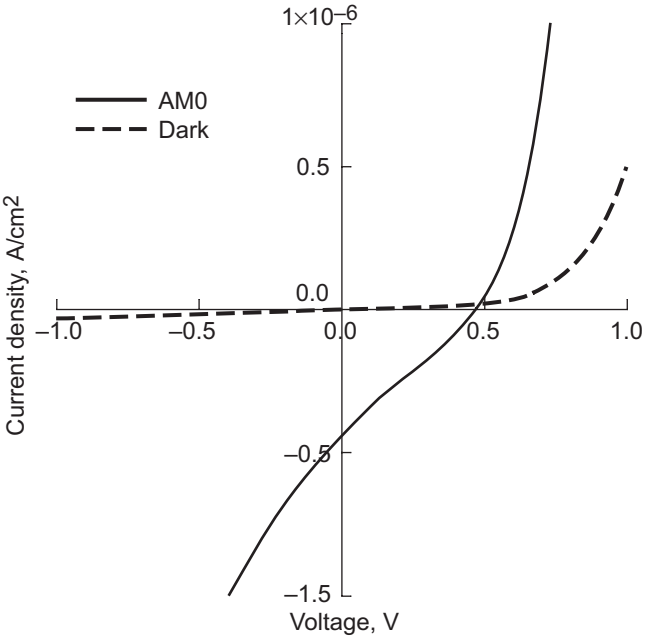


*Current-versus-voltage photoresponse of a 50-wt% CIS–P3OT composite solar cell under 1-sun AM0 illumination.*

**References**

1. Landi, B.J., et al.: Single-Wall Carbon Nanotube-Polymer Solar Cells. Progress in Photovoltaics, vol. 13, no. 2, 2005, pp. 165–172.
2. Landi, B.J., et al.: CdSe Quantum Dot-Single Wall Carbon Nanotube Complexes for Polymeric Solar Cells. Solar Energy Materials and Solar Cells, vol. 87, nos. 1–4, 2005, pp. 733–746.
3. Landi, B.J., et al.: Effects of Alkyl Amide Solvents on the Dispersion of Single-Wall Carbon Nanotubes. J. Phys. Chem. B, vol. 108, no. 44, 2004, pp. 17089–17095.

**Find out more about the research of Glenn's Photovoltaics and Space Environments Branch:**
http://www.grc.nasa.gov/WWW/5000/pep/photo-space/

**Glenn contact:**
Dr. Sheila G. Bailey, 216–433–2228, Sheila.G.Bailey@nasa.gov

**Rochester Institute of Technology contact:**
Dr. Ryne P. Raffaelle, 585–475–5149, rprsps@rit.edu

**Authors:**
Brian J. Landi, Dr. Ryne P. Raffaelle, and Dr. Sheila G. Bailey

**Headquarters program office:**
Exploration Systems

**Programs/Projects:**
ESR&T ICP

# Indium Arsenide (InAs) Quantum Dots Grown for Space Solar Cells

A nanostructured approach to semiconductor device development is based on the fact that the electrical, optical, mechanical, and even thermal properties of these materials can be controlled by changing the particle size (ref. 1). When carriers are confined in dimensions comparable to the Bohr exciton radius of the bulk semiconductor, their energy states become quantized. These nanoscale pieces of semiconductor are called quantum dots (QDs) or "artificial atoms" because of their discrete-like energy states. In the same way that bringing a number of atoms together in a solid results in "energy bands," bringing a number of QDs together in an array also results in bands.

A groundbreaking theoretical study by Luque and Marti (refs. 2 and 3) predicted that a single intermediate electronic band created by QDs would offer a conversion efficiency of 63.2 percent when it was inserted into an ordinary solar cell. This greatly exceeds the maximum conversion efficiency (i.e., 31 percent) for a single-junction device (refs. 4 and 5), and it is

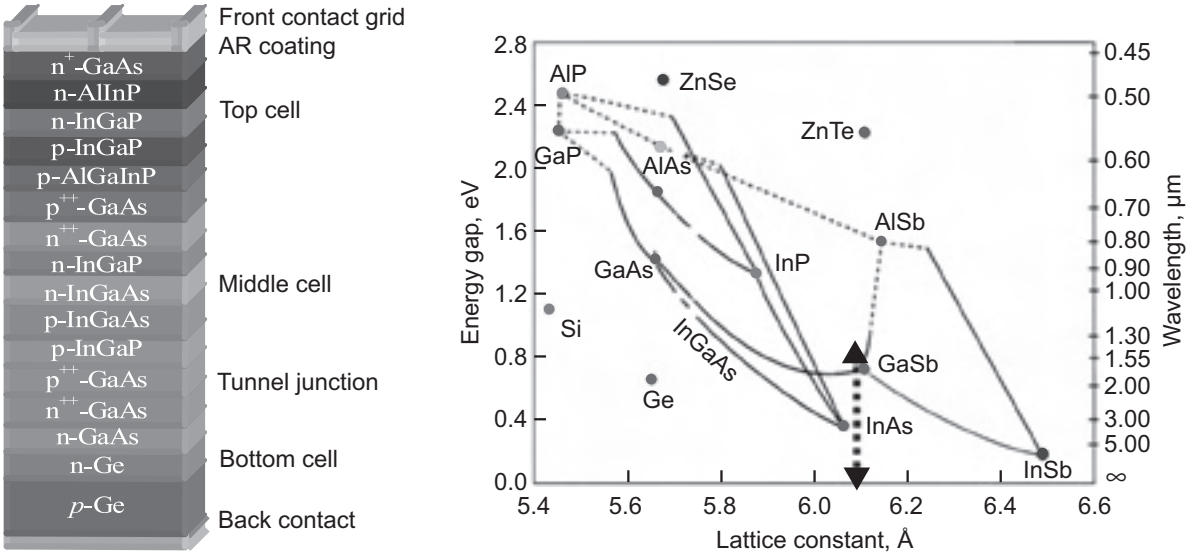


*Left: Lattice-matched triple-junction solar cell; AR, antireflective. Right: Crystal growers' chart with a dashed arrow indicating a lattice-matched triple-junction cell on germanium.*

approximately a factor of 2 better than current state-of-the-art space solar cells. In addition to efficiency enhancement, QD cells hold the promise of improved radiation tolerance and temperature coefficients (refs. 5 to 7).

QD structures can be fabricated using a self-assembly technique called the Stranski-Krastanov growth mode. This technique takes advantage of the strain energy generated from the lattice mismatch between the host material and the QD material to transition from two-dimensional layer-by-layer growth to three-dimensional "island" growth. A series of QD layers with intermediate cladding layers can be grown to produce self-organized three-dimensional arrays.

The current state of the art in space photovoltaics is the lattice-matched, triple-junction solar cell. It is essentially three different cells grown epitaxially with connecting tunnel junctions between. The illustration on the preceding page shows the basic device structure layer compositions and doping for a lattice-matched, triple-junction solar cell. The lattice-matched approach puts a constraint on the available bandgaps (see the graph on the preceding page) and, therefore, how the solar spectrum is divided between the junctions. The cell is optimized through current-matching of the individual junctions. In this particular design, the middle indium gallium arsenide (InGaAs) junction is the current-limiting and, therefore, the efficiency-limiting junction. Incorporating an InAs quantum dot array can lower the effective bandgap of the middle cell, providing subgap absorption and improving the cell's short-circuit current.

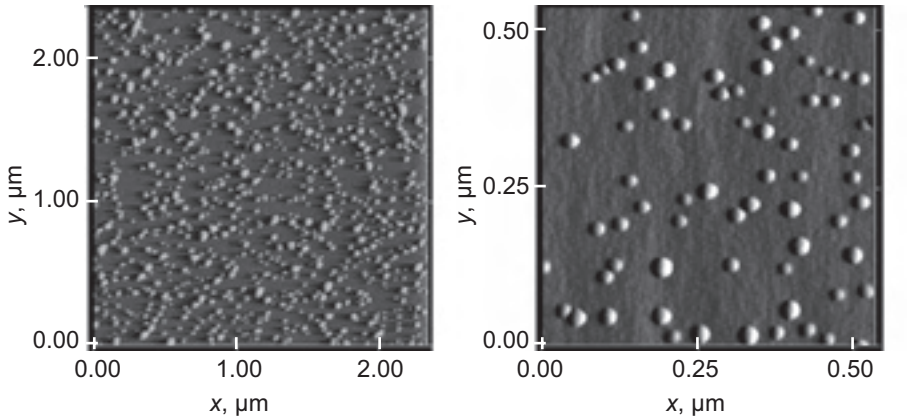


*Atomic force micrographs of InAs QDs. Left: Grown at 450 °C at 1.0 Å/sec on GaAs. Right: Grown at 480 °C at 0.34 Å/sec on 1.2-eV metamorphic In0.13Ga0.87As grown at 675 °C on GaAs.*

An alternative to the ordinary lattice-matched approach to multijunction solar cells is the metamorphic, or lattice-mismatched, approach. This approach also can benefit from the introduction of QD arrays. In a metamorphic triple-junction cell, the InGaAs junction (bottom cell) of the three-cell stack is the current-limiting junction. This situation is further exacerbated when these devices are used in space, because the bottom junction is the one most affected by radiation degradation.

This year, Glenn researchers demonstrated the ability to grow both the lattice-matched and mismatched InAs on InGaAs using Stranski-Krastonow growth (see the photomicrographs). Cross-sectional analysis of the atomic force micrograph structures yielded an average diameter of $20 \pm 5$ nm and height of $5 \pm 1$ nm (see the graph on the left), yielding an effective bandgap of 1.04 eV for a bulk bandgap of InAs of 0.38 eV and an electron effective mass of 0.023. The graph on the right shows the spectral response of a nonoptimized InGaAs device in which InAs dots were added to the depletion region. The small peak beyond 1.2 eV confirms some subgap conversion that which was not seen in the non-QD-containing control cell.

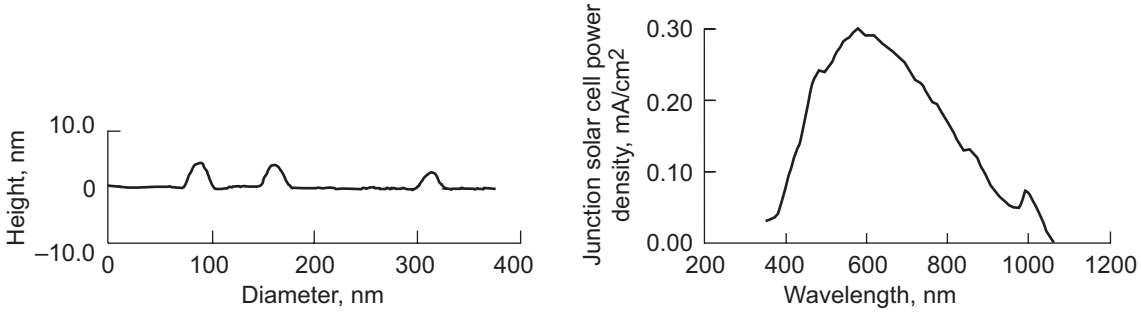


*Left: Cross section of the atomic force micrograph shown in the preceding figure yielding an approximate InAs QD height of 5.0 nm. Right: Spectral response of an InGaAs solar cell with a 10-layer InAs QD array.*

**References**

1. Williams, F.; and Nozik, A.J.: Irreversibilities in Mechanism of Photoelectrolysis. Nature, vol. 271, no. 5641, 1978, pp. 137–139.
2. Luque, A.; and Marti, A.: Increasing the Efficiency of Ideal Solar Cells by Photon Induced Transitions at Intermediate Levels. Phys. Rev. Lett., vol. 78, no. 26, 1997, pp. 5014–5017.
3. Marti, A.; Cuadra, L.; and Luque, A.: Quantum Dot Intermediate Band Solar Cell. Conference Record of the Twenty-eighth IEEE Photovoltaic Specialists Conference, Anchorage, AK, 2000, pp. 940–943.
4. Shockley W.; and Queisser, H.J.: Detailed Balance Limit of Efficiency of P–N Junction Solar Cells. J. Appl. Phys., vol. 32, no. 3, 1961, p. 510.
5. Marcinkevicius, S., et al.: Changes in Carrier Dynamics Induced by Proton Irradiation in Quantum Dots. Physica B, vol. 314, nos. 1–4, 2002, pp. 203–206.
6. Walters, R.J., et al.: Radiation Hard Multi-Quantum Well InP/InAsP Solar Cells for Space Applications. Progress in Photovoltaics, vol. 8, no. 3, 2000, pp. 349–354.
7. Sobolev, N.A., et al.: Enhanced Radiation Hardness of InAs/GaAs Quantum Dot Structures. Phys. Stat. Sol. B, vol. 224, no. 1, 2001, pp. 93–96.

**Find out more about Glenn's Photovoltaics and Space Environments Branch:**
http://www.grc.nasa.gov/WWW/5000/pep/photo-space/

**Glenn contact:**
Dr. Sheila G. Bailey, 216–433–2228, Sheila.G.Bailey@nasa.gov

**Rochester Institute of Technology contact:**
Dr. Ryne P. Raffaelle, 585–475–5149, rprsps@rit.edu

**Authors:**
Dr. Sheila G. Bailey, David M. Wilt, Dr. Ryne P. Raffaelle, and Dr. Samar Sinharoy

**Programs/Projects:**
Glenn's IR&D and SBIR, ESR&T ICP

## Integrated Photovoltaic and Communications Technology Demonstrated

Several advancements were made in integrated photovoltaic and communications technology this year. In the first, NASA Glenn Research Center's Photovoltaic Branch, in collaboration with Glenn's Antenna, Microwave and Optical Systems Branch and personnel from the Naval Research Laboratory demonstrated photovoltaic (PV, or solar cell) technologies integrated with radio-frequency (RF) and optical communication technologies. The PV-RF-optical communications demonstration (see the following photograph) consists of a high-efficiency monolithic multijunction solar array (indium-galium-phosphide/gallium arsenide, InGaP/GaAs) integrated with X-band RF patch antennas. The electrically insulating semiconductor substrate used to fabricate the solar array structure also serves as the dielectric spacer between the coplanar RF waveguide feed network, which is deposited on the rear surface, and the patch antenna elements located on the front surface. By altering the geometry of the feed network on the rear surface, one can alter the radiating pattern to radiate in any direction needed. Thus, a large solar array could be composed of various patch antenna sections, each designed to radiate in a particular direction. A simple RF switching network would be all that was required to effectively steer the beam. Another application of this integrated technology is in miniaturized antennas for surface-to-surface or distributed systems technologies, whereby a miniature package could contain power generation and RF communications, as well as a variety of sensor or functional capabilities.

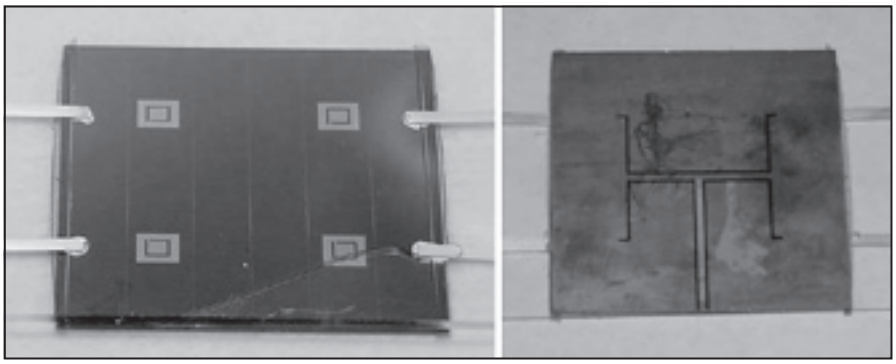

*Integrated solar array and X-band RF communications system. The device is approximately 9 cm$^2$ (3 cm by 3 cm) and consists of six photovoltaic cells connected in series and four X-band patch antennas.*

The second advancement, a partnership of researchers from Glenn and the Naval Research Laboratory, demonstrated a matchbook-sized system consisting of a solar array and a modulating retroreflector (MRR) optical communication system (see the left photograph on the next page). The MRR technology (developed at the Naval Research Laboratory) operates by modulating a reflected laser beam, thereby encoding data. Thus, to communicate via the MRR, an interrogator directs

a laser beam (1550 nm in this example) onto the MRR. An optical corner cube reflects the incident beam back to the interrogator. A semiconductor modulator in front of the corner cube alternately transmits or absorbs the reflected beam. The demonstration device transmitted a digital identification code at a 100-kHz data rate while consuming 3.5 mW of power. With the addition of a supercapacitor for energy storage, the system was capable of extended operation in the absence of sunlight. The battery shown in this photograph is included only as a size reference.

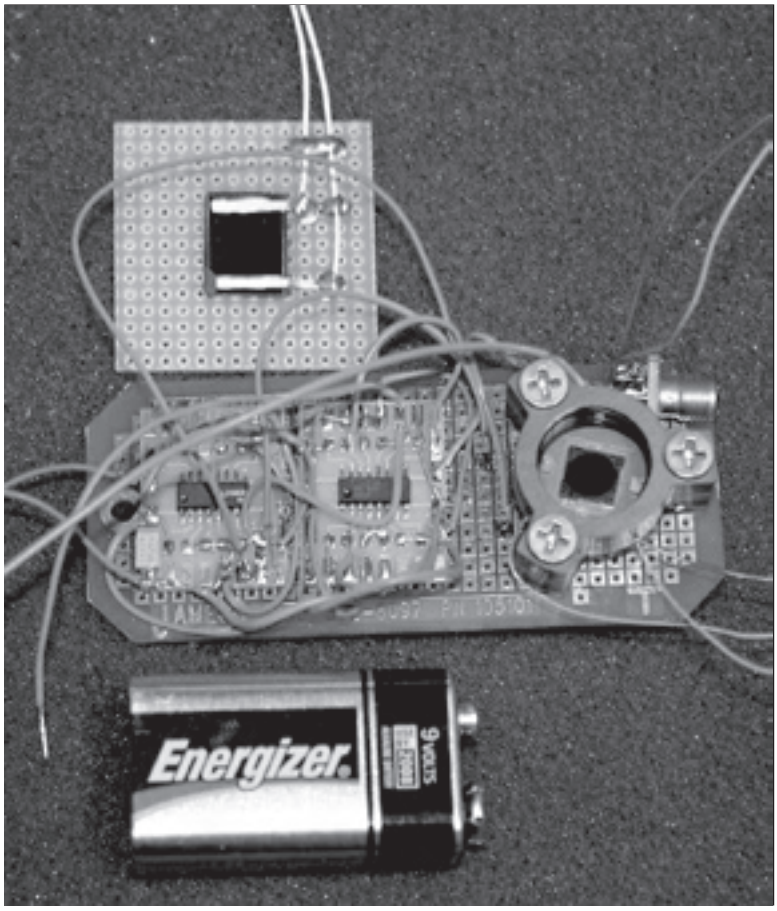


*Matchbook-sized solar-powered MRR demonstration. The battery was added for scale purposes only.*

For the third advancement, Glenn developed a PV device capable of generating the required electrical power from the probe laser beam used to interrogate the MRR. The device (see the top right photograph) consists of four PV arrays connected in parallel, with each array tuned to efficiently convert 1550-nm laser illumination into electrical energy. The MRR resides beneath a 1-cm-diameter aperture in the center of the wafer.

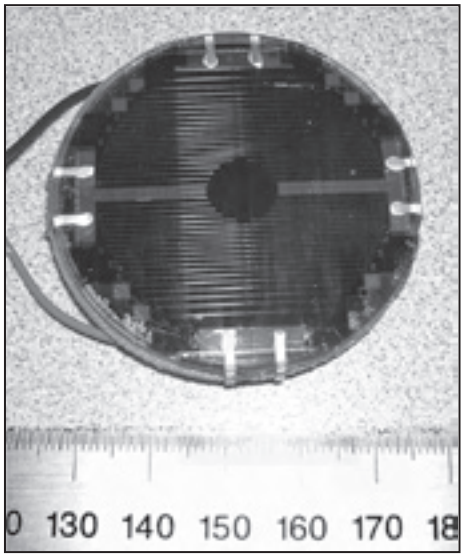


*1550-nm-laser-power converter.*

**Glenn contacts:**
David M. Wilt (integrated PV–RF-optical communications technology), 216–433–6293, David.M.Wilt@nasa.gov;
Eric B. Clark (integrated PV–RF communications technology), 216–433–3926, Eric.B.Clark@nasa.gov;
Dr. Félix A. Miranda, 216–433–6589, Felix.A.Miranda@nasa.gov; and
Dr. Richard Q. Lee, 216–433–3498, Richard.Q.Lee@nasa.gov

**Author:**
David M. Wilt

**Headquarters program office:**
Exploration Systems

**Programs/Projects:**
Exploration Systems, Science Mission

# Contamination Flakes in the Discharge Chamber of a NASA Solar Electric Propulsion Technology Readiness (NSTAR) Ion Engine Found To Be Test-Cell Generated

Contamination flakes in the propulsion discharge chamber of a NASA Solar Electric Propulsion Technology Readiness (NSTAR) xenon-ion engine were evaluated at the NASA Glenn Research Center. NASA's Deep Space 1 spacecraft, launched in October 1998, was a technology-validation mission that flew a single 30-cm-diameter NSTAR xenon-ion engine as its primary propulsion system, providing the first successful flight of an ion propulsion system. The NSTAR ion engine successfully completed the mission in December 2001 after 16,265 hr of operation in space. The success of the mission stimulated interest in future NASA science missions utilizing solar electric propulsion for required lifetimes in excess of 20,000 hr. As a result, assessing the ultimate service life capability of ion thrusters is vital, requiring extensive ground testing and data analysis.

To determine this capability, researchers conducted a long-duration test, called the Extended Life Test (ELT) of the Deep Space 1 spare flight ion thruster at the Jet Propulsion Laboratory (JPL) in collaboration with Glenn. The test was started in October 1998 and concluded on June 26, 2003, after 30,352 hr of operation. The ELT was terminated prior to its end of life so that the engine components could be analyzed to provide critical information to ion propulsion system designers. The primary purpose of the ELT was to determine the ultimate service life capability of the NASA 30-cm ion thruster technology. The left photograph shows the Deep Space 1 spare flight ion thruster taken shortly after completion of the ELT. Extensive post-test analyses were conducted at JPL and Glenn, with collaborative efforts from other groups.

Post-test inspection of the ELT engine revealed numerous small contaminant flakes uniformly distributed over the bottom of the discharge chamber. Some of these flakes are shown in the optical photograph on the right. Internally generated flakes are a major threat to thruster reliability and durability because they can short the ion optics or the cathode. However, if the flakes were generated externally (from the facility), they would not be a threat to in-space reliability and durability. Therefore, determining the origin of the flakes was critical to the understanding of the degradation mechanisms of long-life ion thruster operation.

Extensive analyses were conducted at Glenn on the NSTAR ELT discharge chamber contaminant flakes to determine the source of the particles (e.g., from within the thruster, from the screen or accelerator grids, or from outside the thruster). Analyses included optical microscopy and particle length histograms, field-emission scanning electron microscopy combined with energy-dispersive spectroscopy, and atomic-oxygen-plasma exposure tests. The results indicate that the majority of discharge chamber flakes consist of a layered structure, typically with either two or three layers. Flakes comprising two layers were typically found to have a molybdenum- (Mo-) rich layer on one side and a carbon- (C-) rich layer on the other side (see the top figure on the next page). Flakes comprising three layers were found to be sandwichlike structures with Mo-rich exterior layers and a C-rich interior layer. The presence of the C-rich layers indicates that these particles were produced by sputter deposition buildup

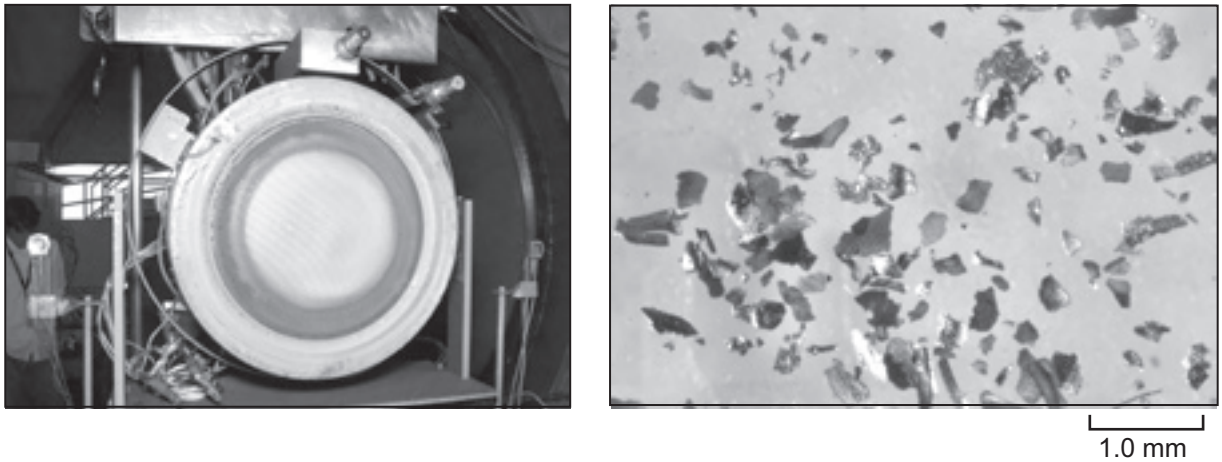


*Left: NSTAR ELT ion thruster after 30,352 hr of operation. Right: Optical micrograph of discharge chamber flakes.*

on a surface external to the discharge chamber from ion sputter erosion of the graphite target in the test chamber. This contaminant layer became thick enough that particles spalled off and then were electrostatically attracted into the ion thruster interior, where they were coated with Mo from internal sputter erosion of the screen grid and cathode components.

A particle-size histogram based on measurements of approximately 1500 flakes (shown in the bar chart) further indicated that the source of the particles was the spalling of carbon flakes from downstream surfaces. Analyses of flakes taken from the downstream surface of the accelerator grid supported this theory. The production of the downstream carbon flakes, and hence the potential problems associated with the flake particles in the ELT ion thruster engine, was determined by Glenn to be a facility-induced effect that would not occur in space.

**Glenn contacts:**
Kim K. de Groh, 216–433–2297, Kim.K.deGroh@nasa.gov; and Bruce A. Banks, 216–433–2308, Bruce.A.Banks@nasa.gov

**Authors:**
Kim K. de Groh, Bruce A. Banks, and Christina A. Karniotis

**Headquarters program office:**
Exploration Systems

**Programs/Projects:**
Project Prometheus, ion propulsion

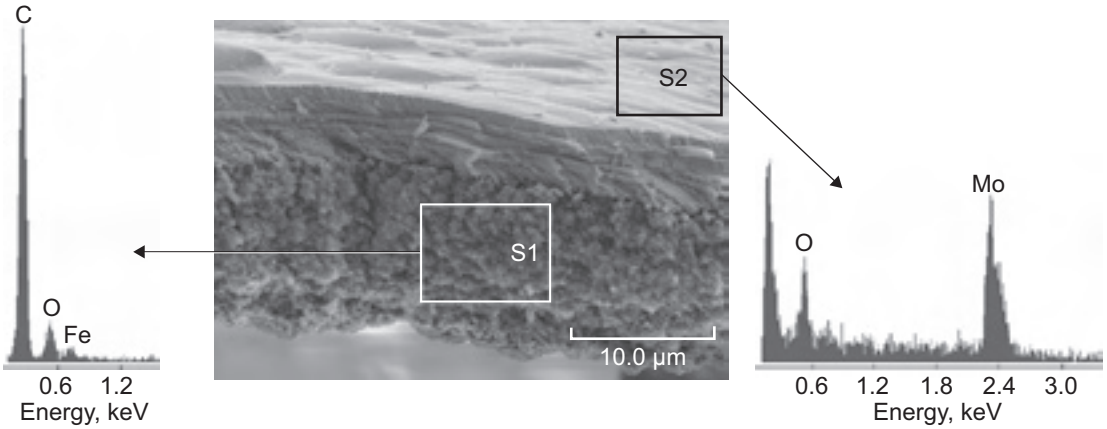


*Electron micrograph of the edge of a two-layered flake showing two distinct layers with corresponding chemistries (S1 is a C-rich layer, and S2 is a Mo-rich layer).*

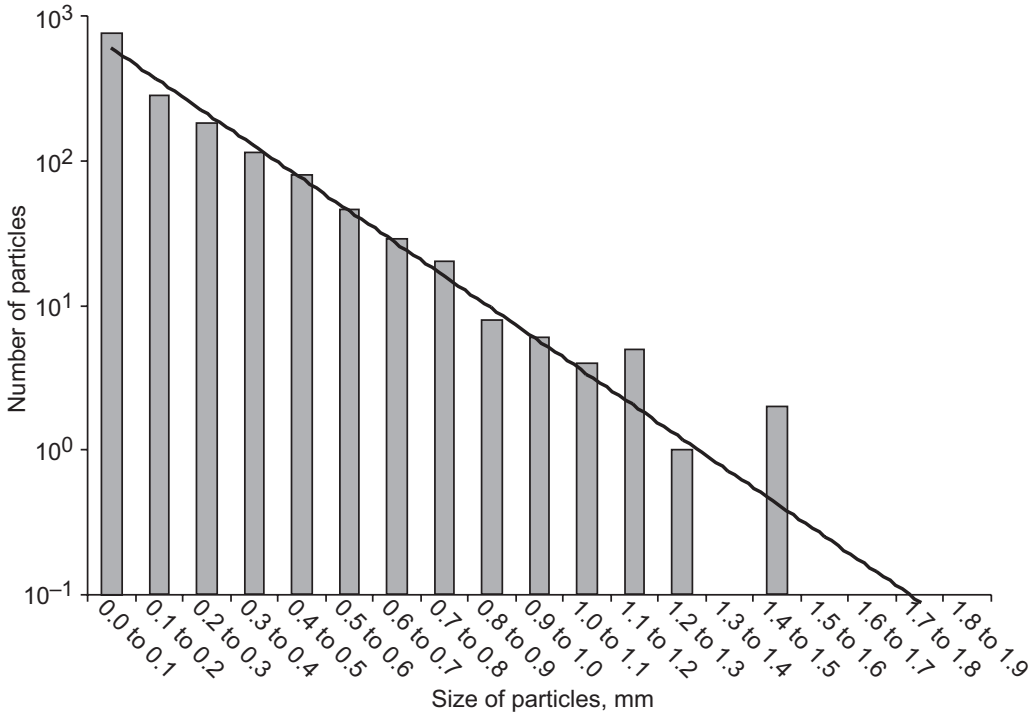


*Particle-size histogram based on the longest dimension of 1538 flakes.*

# Conductive Thermoplastic Composites Fabricated

This year, electrically conducting polymer matrix composites were successfully fabricated at the NASA Glenn Research Center from bromine-intercalated graphite fibers and three different thermoplastic resins. All demonstrated relatively low electrical resistivities, comparable to those of composites made with thermosetting resins.

Increasing the electrical conductivity of graphite fibers through intercalation, the insertion of guest atoms or molecules between the graphene planes, is a technology that has been investigated since pitch-based graphite fibers first became available 25 years ago. Applications include electrically conductive composite structures for electrostatic dissipation, electromagnetic interference shielding, and ground return planes that could save between 30 and 90 percent of the mass of the structure, in comparison to aluminum (ref. 1). Composites made from intercalated graphite fibers have been fabricated since the late 1980s, but they have always been made with thermosetting resins. This is partially due to the fact that most applications for these materials were in the aerospace industry, where epoxies, polyimides, and polyisocyanates are the standard resins used with graphite fibers. In addition, most intercalation compounds are not very stable at high temperatures, so limited exposure to curing cycles is important.

However, with the advent of higher temperature stable intercalation compounds, like those intercalated with bromine, these considerations become irrelevant because these compounds are stable even at cure temperatures as high as 3000 °C (ref. 2). This technology is also becoming more attractive in applications outside of the aerospace industry in commodity products. Thermoplastic resins, which can be reheated and molded several times, have definite advantages over thermosetting resins for manufacturability. In addition, radiation shields made by combining materials with some high-atomic-mass atoms (which are most efficient at stopping x-rays and $\gamma$-rays) with materials containing a lot of hydrogen (which is most efficient at stopping high-energy protons), are being considered for spacecraft that require extended human stays in space. Intercalated graphite fibers contain high-atomic-mass atoms, such as bromine; and thermoplastic polymers, such as polyethylene, contain a large fraction of hydrogen.

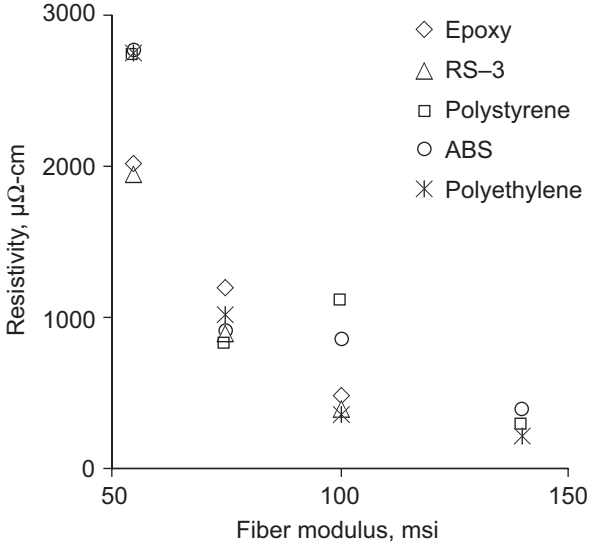


*Resistivity of composites made from varying resins as a function of the elastic modulus of the fiber in the composite; msi, millions of pounds per square inch.*

Glenn researchers made composites by combining bromine-intercalated graphite fibers with a variety of thermoplastics—including polyethylene, polystyrene, and acrylonitrile butadiene styrene copolymer (ABS)—and compared their electrical properties with those of composites made from the thermosetting resins epoxy and RS–3 (a polyisocyanate). As is illustrated in the graph, the results indicate that the electrical conductivity of thermoplastics is comparable to that of composites made with thermosetting resins. Thus, applications in which composites made with intercalated graphite fibers and thermosetting resin have been well suited should also work well with composites made with thermoplastic resins, but with lower cost and improved manufacturability.

**References**

1. Gaier, J.R.: Intercalated Graphite Fiber Composites as EMI Shields in Aerospace Structures. IEEE Trans. Electromagn. Compat., vol. 34, issue 3, 1992, pp. 351–356.
2. Gaier, James R., et al.: The Resistivity of Intercalated Graphite-Carbon Composite Preforms. ICCE–10, Tenth International Conference on Composites/Nano Engineering, International Community for Composites Engineering and College of Engineering, University of New Orleans, New Orleans, LA, 2003, p. 195.

**Glenn contact:**
Dr. James R. Gaier, 216–433–6686, James.R.Gaier@nasa.gov

**Author:**
Dr. James R. Gaier

**Headquarters program office:**
Aeronautics Research, TTPO

**Programs/Projects:**
High-conductivity, low-weight applications such as electromagnetic shielding enclosures and ground planes, Exploration Systems

# Honeycomb Target Evaluated for Reducing Backsputter From Chamber Walls During Long-Life Tests of Ion Thrusters

Ion thrusters used for electric propulsion in space need to be operated for long durations in vacuum chambers on Earth in order to verify and test their operation and durability. Thrust is produced by the ejection of high-energy ions. In ground-laboratory testing, the high-speed ions ultimately impact the end wall of the vacuum chamber and some of the chamber wall (typically a metal) is sputtered, causing the ejection of material that can travel back and deposit on the ion thruster. This is called backsputter. Backsputter rates for metals are high enough that even during a short test a coating can develop on the downstream surface of the ion thruster. This coating can short the ion-acceleration optics and insulators, leading to early atypical breakdown and failure of the ion thruster. To reduce the chance of this atypical type of breakdown, carbon targets are installed for the ions to impact. Carbon has one of the lowest sputter yields of any material and can greatly reduce the amount of backsputter on the ion thruster, but for life testing of thrusters, which involves months of operation, even this low rate of backsputter can cause problems. Several configurations of a honeycomb target were evaluated at the NASA Glenn Research Center to determine if changing the geometry of the target could reduce the backsputter rate by changing the line-of-sight arrival of the backsputtered material and trapping some of the sputter ejecta.

A test was conducted in a small vacuum chamber at Glenn to compare backsputter ejecta from a standard Grafoil target to that from a high-aspect-ratio aluminum honeycomb backed with Grafoil. Two configurations were tested. The first (top part of the figure) simulated magnetic bending of the beam into the honeycomb and measured the sputter ejecta deposited at the source location. The second (bottom part of the figure) involved placing the honeycomb at various angles with respect to the beam and measured the ejecta deposited near the source. Fused-silica substrates partially covered with Kapton tape were used to measure the thickness of sputter-deposited material arriving at that location.

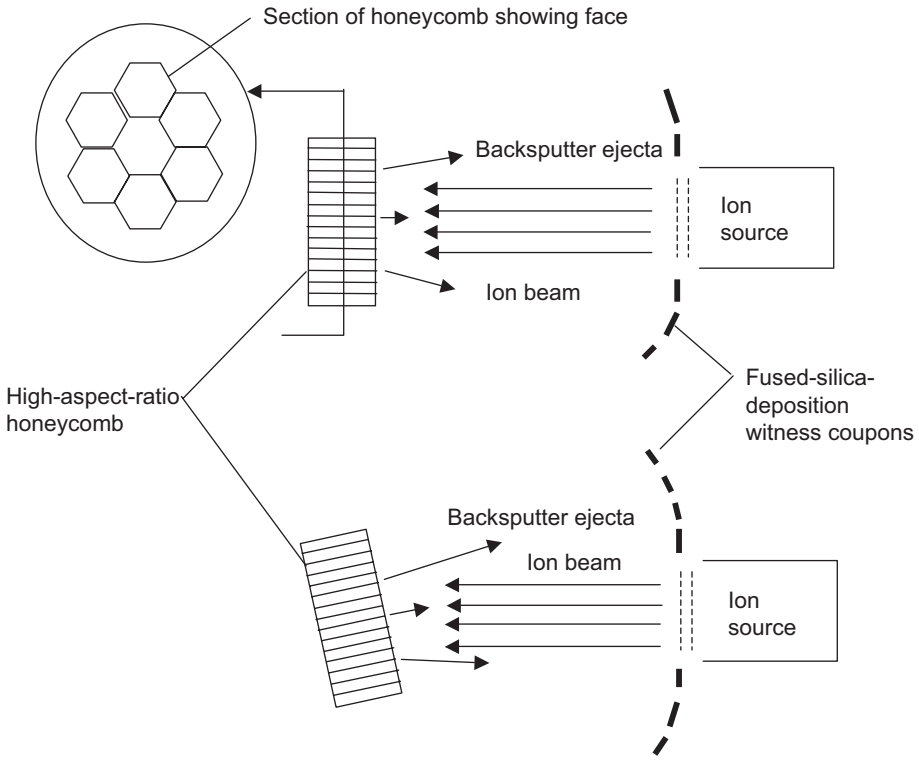


*Configuration of honeycomb tests in relation to an ion source.*

The results of the inclined honeycomb testing indicated that angling the axis of the honeycomb cells at or less than 5° with respect to the ion source did not attenuate the sputter ejecta. In fact, for higher angles, there was actually greater backsputter than that observed for normal incidence on Grafoil at the same location.

However, simulating the arrival of a magnetically bent beam of ions provided substantial reductions in backsputtered ejecta in comparison to Grafoil. The backsputter rate with respect to Grafoil was reduced to 18 percent for a bend of approximately 15° and to 3 percent at a bend of 75°. Thus bending the beam into the honeycomb so that the thruster does not have a view of the surfaces where ions are impinging enables the honeycomb to trap most of the sputter ejecta and to reduce the backsputter rate in comparison to when the target is bombarded head on. The low-backsputter technique does rely upon the use of magnetic bending of the broad ion beam with sufficient angle to cause trapping. Although the magnetic bending requirement adds complexity to the vacuum facility in the region of the downstream ion beam, the technique does demonstrate that there are low-backsputter options to conventional planar targets. This encouraging result may enable greater accuracy in ion-thruster life prediction based on long-life ground testing.

**Find out more about the research of Glenn's Electro-Physics Branch:**
http://www.grc.nasa.gov/WWW/epbranch/ephome.htm

**Glenn contacts:**
Sharon K. Miller, 216–433–2219, Sharon.K.Miller@nasa.gov;
Donald A. Jaworske, 216–433–2312, Donald.A.Jaworske@nasa.gov; and
Bruce A. Banks, 216–433–2308, Bruce.A.Banks@nasa.gov

**Authors:**
Sharon K. Miller and Elisa M. Vogel

**Headquarters program office:**
Exploration Systems

**Programs/Projects:**
Project Prometheus, or other applications where electric propulsion is used

## Silicon Germanium Power Transistors Developed for Cryogenic Space Missions

The Low Temperature Electronics Program at the NASA Glenn Research Center emphasizes development of electronics for low-temperature space missions. In this program, silicon-germanium-based transistors and diodes were developed to obtain efficient and reliable operation under cryogenic temperatures. The illustration shows a significant gain increase at cryogenic temperatures of a silicon germanium power transistor that was developed for Glenn by GPD Optoelectronics, Inc., under a Small Business Innovation Research contract. This increase in gain at low temperatures is a desirable feature because typical silicon transistors do not operate well at lower temperatures and lose the ability to amplify signals.

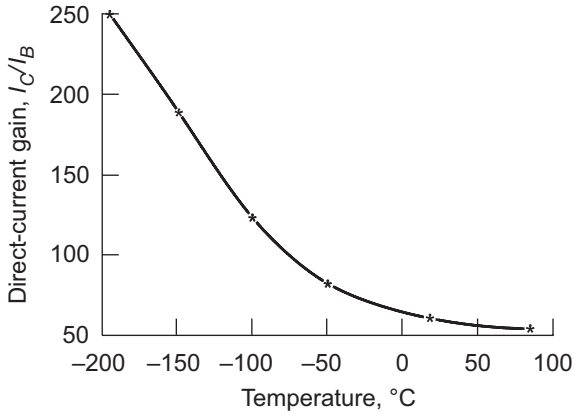


*Direct-current gain of a new silicon germanium transistor as a function of temperature. SiGe HBT (serial number HBT–16–25); collector emitter voltage, 8 V; base current, $I_B$, 50 mA.*

The environmental temperature in many of NASA space-exploration missions, such as deep-space probes and outer planetary exploration, is significantly below the range for which conventional commercial-off-the-shelf electronics are designed. Presently, spacecraft in a low-temperature environment carry radioisotopes or other heating elements to maintain the onboard electronics at approximately 20 °C. Cryogenic electronics not only tolerate the harsh environment of deep space but reduce system size and weight by eliminating the heating units, thereby reducing system development and launch costs. Cryogenic electronics also have potential uses in terrestrial applications, including magnetic-levitation transportation systems, medical diagnostics, cryogenic instrumentation, and superconducting magnetic energy-storage systems.

These research efforts are being conducted with the support of the NASA Electronic Parts and Packaging (NEPP) Program, and through collaboration with other Government agencies, industrial and aerospace companies, and academia. The NEPP supports missions as well as technology development efforts at the NASA Goddard Space Flight Center, the NASA Langley Research Center, and the Jet Propulsion Laboratory.

**Glenn contact:**
Richard L. Patterson, 216–433–8166,
Richard.Patterson@nasa.gov

**QSS Group, Inc., contact:**
Dr. Ahmad Hammoud, 216–433–8511,
Ahmad.Hammoud@nasa.gov

**Authors:**
Richard L. Patterson and
Dr. Ahmad Hammoud

**Headquarters program office:**
Exploration Systems, Office of Safety and Mission Assurance

**Programs/Projects:**
Lunar landers, Mars orbiters and landers, JWST, Shuttle Orbiter GPS, NEPP, NEPAG, and Europa Lander

**Find out more about the research of Glenn's Electro-Physics Branch:**
http://www.grc.nasa.gov/WWW/epbranch/ephome.htm

# PROPULSION SYSTEMS

## Concepts Explored for Atmospheric Mining in the Outer Solar System

A preliminary study and review of methods of creating fuels in the outer solar system was conducted at the NASA Glenn Research Center in support of NASA's exploration mission. Mining in the outer solar system is an important option for exploration because launching and bringing all the materials for exploration from Earth is expensive and may make the idea of long-term exploration untenable. The large reserves of atmospheric gases in the outer planets are an excellent resource for fuels and other life-sustaining or colony-building gases.

The highly energetic gases available in the outer planet atmospheres are excellent fuels for chemical and nuclear propulsion systems. Hydrogen and methane are excellent fuels for chemical rockets that can be used to ascend from and descend to the surfaces of moons. Hydrogen can also be the fuel of choice for nuclear fission and fusion rockets. Helium 3 (3He) is another future fusion reactor fuel that can be found in outer planet atmospheres (ref. 1). In addition, hydrogen, helium, and other ices found deep below the surface of Uranus and Neptune may be crucial to exploration beyond the solar system.

Atmospheric mining may be easier than mining on the surfaces of outer-planet moons, and the planets with abundant gases are in good locations for way stations for exploring beyond the edges of our solar system. On the other hand, the delta-V (change in velocity) required to repeatedly access the atmosphere of Jupiter or another outer planet and then return to orbit can be quite high. In addition, because the planets typically have powerful magnetic fields, vehicles will need to have good resistance to radiation to operate reliably.

One of the attractive materials that can be extracted from the solar system is 3He. It is deposited in lunar regolith (moon dust) and exists in the outer planet atmospheres. This material can be an excellent nuclear fusion fuel and can reduce the neutron radiation created during the fusion process, extending the life of future power reactors. However, the fraction of 3He in the lunar regolith is quite small: perhaps less than 5 to 100 parts per billion.

The predicted concentration of 3He in the helium portion of the atmosphere of Uranus is also quite small: approximately 1 part in 10,000. Despite the small levels, the argument has been made that it would be easier to extract 3He from gaseous helium in the outer planet atmosphere than from lunar regolith. Factories stationed in the atmosphere could mine the gas robotically and await orbital vehicles to gather the 3He and deliver it to other parts of the solar system.

If atmospheric mining of 3He could be made highly efficient, it could be much more attractive than lunar regolith mining, especially after a pipeline of deliveries was established. The figure illustrates one of three atmospheric mining options discussed in reference 1. Aerostats, or balloon-borne factories, are used to process and separate the atmosphere into the materials needed for propulsion.

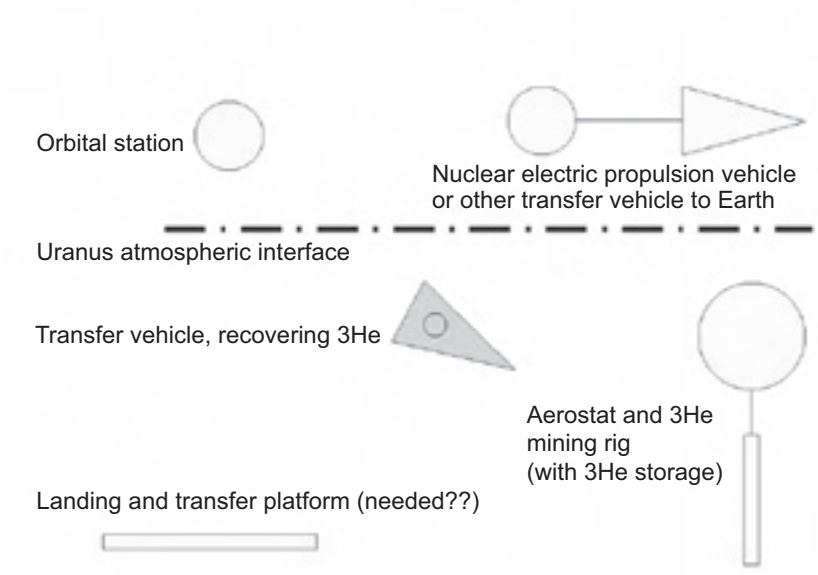


*Atmospheric mining of Uranus with aerostats.*

**Reference**

1. Palaszewski, B.: Atmospheric Mining in the Outer Solar System. AIAA–2005–4319, 2005.

**Find out more about fuels and space propellants for reusable launch vehicles:**
http://sbir.grc.nasa.gov/launch/foctopsb.htm

**Glenn contact:**
Bryan A. Palaszewski,
216–977–7493, 216–433–5802 (fax),
Bryan.A.Palaszewski@nasa.gov

**Author:**
Bryan A. Palaszewski

**Headquarters program office:**
Exploration Systems

**Programs/Projects:**
CEV, Vehicle Systems, RAC

# Combustion Experiments Performed With Metallized Gelled Propellants in a Pulse Detonation Engine

A series of combustion tests were performed at the NASA Glenn Research Center with metallized gelled JP-8/aluminum fuels in a pulse detonation engine (PDE). Nanoparticles of aluminum with diameters of 60 to 100 nm were used. Gellants were nanoparticles composed of hydrocarbon alkoxide materials. Using simulated air (a nitrogen-oxygen mixture), researchers investigated the ignition potential of metallized gelled fuels with nanoparticle aluminum. Ignition of the JP-8/aluminum was possible with 23-wt% or less oxygen loading in the simulated air. JP-8 fuel alone was unable to ignite with less than 30-wt% oxygen loading in the simulated air. Single-shot tests of the metallized gelled fuel were used to demonstrate the capability of the fuel to improve fuel detonability. The tests were conducted at ambient temperatures and with maximal detonation pressures of 1340 psia.

During testing, only single-shot firings of the PDE were conducted with the metallized gelled fuel. Multiple shots were not planned as we wished to see if any improvements were possible with the gelled fuel. In many cases, improvements in the detonation velocity were observed. Further testing and analyses will be required to optimize the configuration of the PDE.

Metallized gelled fuels have many applications in aeronautics and space flight. Although the applications of PDEs are in the future, testing should continue to reveal the best operating points for these engines. Increased metal loading testing would allow better packaging of the fuel in the missile or other aerospace vehicle. The combustion efficiency for the higher metal loadings, which has not yet been investigated, is a good area for continued research. The use of a compressor section to improve the PDE seems warranted.

A metallized gelled JP-8/aluminum fuel was created to be combusted in a PDE. The fuel was formulated successfully with JP-8, nanometer-sized aluminum particles, and nanoengineered gellants. A sonicator was used to assure complete mixing of the fuel components for the testing, and the fuel remained stable for the 1- to 2-week time from formulation to engine firing. Metal loadings in the JP-8/aluminum ranged from 4.85 to 25 wt%, and gellant amounts ranged from 1 to 1.2 wt%

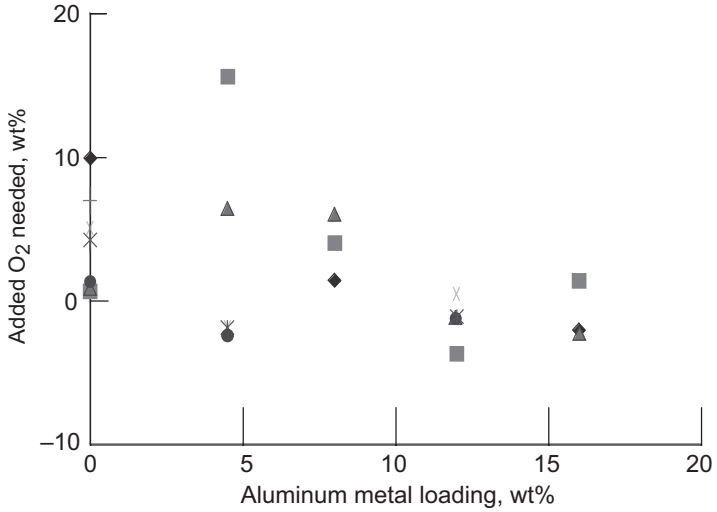


*Added oxygen ($O_2$) required for a PDE with metallized gelled JP-8/aluminum fuel; 23-wt% $O_2$ baseline.*

A minimum aluminum loading of 12- to 18-wt% nanometer-sized particles allowed JP-8/aluminum combustion in the PDE without oxygen addition. A PDE with metallized gelled fuels might reduce dependence on added oxygen for ignition and might simplify engine design. Also, by increasing the fuel density, the metallized gelled fuel can make the vehicle more compact. Metallized gelled propellants and propulsion could offer many vehicle advantages and create a bright future for many high-energy aerospace visions.

**Bibliography**
Palaszewski, B., et al.: Metallized Gelled Propellants Combustion Experiments in a Pulse Detonation Engine. AIAA–2004–4191, 2004.

**Find out more about fuels and space propellants for reusable launch vehicles:**
http://sbir.grc.nasa.gov/launch/foctopsb.htm

**Glenn contacts:**
Bryan A. Palaszewski,
216–977–7493, 216–433–5802 (fax),
Bryan.A.Palaszewski@nasa.gov; and
Kevin J. Breisacher, 216–977–7475,
Kevin.J.Breisacher@nasa.gov

**Authors:**
Bryan A. Palaszewski, Kevin J. Breisacher, John M. Jurns, and Kimberly A. Kearns

**Headquarters program office:**
Aeronautics Research

**Programs/Projects:**
Vehicle Systems, RAC

# Miniature Pump for Spacecraft Designed and Tested

Spacecraft propulsion systems commonly use pressure-fed, 100-lbf class engines for the apogee insertion of geostationary satellites and for axial maneuvers of unmanned planetary spacecraft. Performance increases in these propulsion systems can be obtained by operation at higher chamber pressures. High-chamber-pressure operation, however, is not practical with pressure-fed systems, since the increases in propellant and in pressurant tank masses offset the engine performance gains. Pumped systems are required to derive a performance benefit from high-pressure operation. The use of pump technology has the potential to increase a satellite's payload by 35 to 40 percent, but the feasibility of making a high-efficiency centrifugal pump small enough (0.5-in.-diameter impeller tip) for a 100-lbf class rocket engine has never been demonstrated.

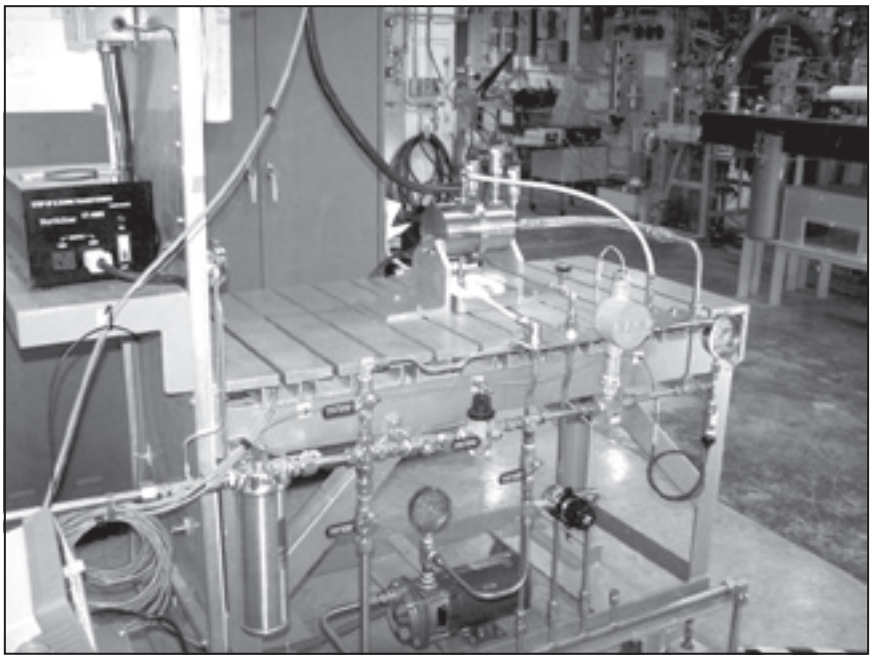

*Two-stage centrifugal pump installed in Glenn's Research Combustion Laboratory.*

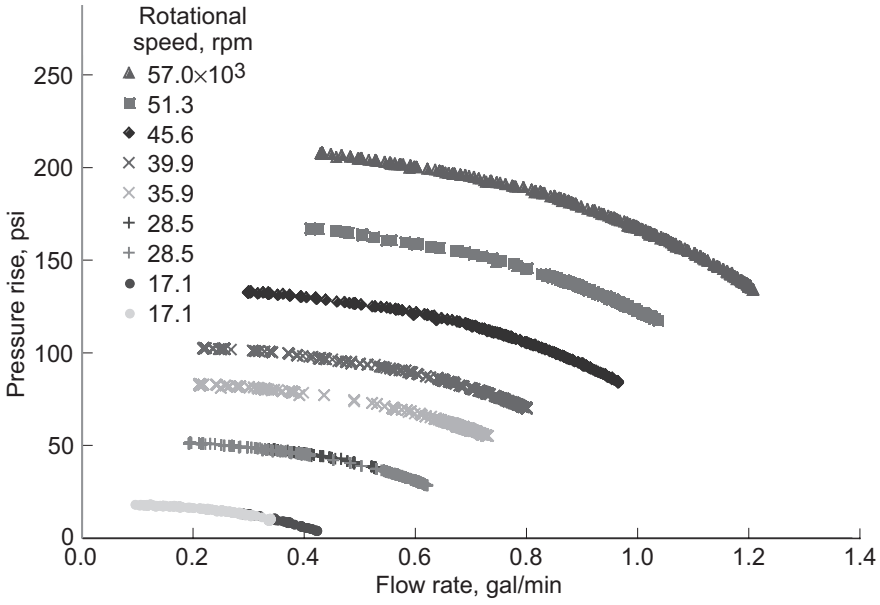


*Pump performance map as a function of rotational speed.*

Modern machine tool capabilities have made the design of such a pump possible. A two-stage pump with an overall pressure rise of 250 psia was designed and fabricated. The design includes crossover deswirl vanes between the stages and an exit volute. The mechanical layout of the pump is an overhung two-stage configuration with interstage seals and bearings exterior to the pump. Design criteria included compatibility with a hydrazine propellant. Supporting stress and dynamic analyses of the design were performed; then, the anticipated design performance was predicted with a steady, three-dimensional viscous flow calculation.

The two-stage centrifugal pump was tested in NASA Glenn Research Center's Research Combustion Laboratory using water as a surrogate fluid for hydrazine. The pump ran at speeds up to 57,000 rpm and flow rates up to 1.2 gal/min. In general, pressure rises of about 75 percent of the predicted values were observed for the various flow rates and speeds. The pump delivered a pressure rise of 190 psi at 0.8 gal/min with an efficiency in the 45- to 50-percent range. Several branches from Glenn contributed to this effort. The Engine Systems Branch and Electric Propulsion Branch conducted thermodynamic and mission analyses of the pumped spacecraft systems. The Compressor Branch designed the hydraulics for the pump impellers and diffusion systems.

The Mechanical and Rotating Systems Branch was responsible for the mechanical design and fabrication of the pump, and the Thermal and Fluid Systems Branch, the Avionics, Power, and Communications Branch, and the Mechanical and Rotating Systems Branch designed the pump stand and its data-acquisition system.

This successful effort, started in fiscal year 2004, was funded by NASA's Energetics Legacy Program. It showed that the fabrication technologies exist to build high-efficiency pumps. These pumps have flow rates relevant to spacecraft propulsion and pressure increases that can significantly benefit mission payloads.

**Find out more about Glenn's research:**

**Engine Systems Technology Branch:**
http://www.grc.nasa.gov/WWW/enginesys/

**Compressor Branch:**
http://www.grc.nasa.gov/WWW/5810/

**Power and On-Board Propulsion Technology Division:**
http://powerweb.grc.nasa.gov/branches/5430.html

**Mechanical and Rotating Systems Branch:**
http://www.grc.nasa.gov/WWW/7725/

**Thermal and Fluid Systems Branch:**
http://www.grc.nasa.gov/WWW/7730/

**Electrical and Avionics Systems Branch:**
http://www.grc.nasa.gov/WWW/7720/7720.htm

**Glenn contacts:**
Dr. Steven J. Schneider, 216–977–7484, Steven.J.Schneider@nasa.gov; and Joseph P. Veres, 216–433–2436, Joseph.P.Veres@nasa.gov

**Authors:**
Dr. Steven J. Schneider, Joseph P. Veres, Brian D. Reed, Dr. Chunill Hah, Anthony L. Nerone, Cameron C. Cunningham, Thomas G. Kraft, Paul F. Tavernelli, and Bryan Fraser

**Headquarters program office:**
Exploration Systems

**Programs/Projects:**
Advanced Space Technology; Power, Propellants, and Chemical Systems; Energetics Legacy Program; Spacecraft Propulsion

# MATERIALS AND STRUCTURES

## Critical Contributions to the Space Shuttle Return-to-Flight Effort Made by Glenn's Ballistic Impact Team

Following the *Space Shuttle Columbia* accident investigation, NASA initiated the Return to Flight program, which established numerous technical issues requiring resolution prior to the launch of STS–114. NASA Glenn Research Center's Ballistic Impact Team was given the task of conducting numerous critical ballistic impact testing and analysis programs to investigate and quantify the physics of debris impact on the reinforced carbon/carbon wing leading edges, nose caps, orbiter windows, and external tank structures. The test programs ranged from fundamental material characterization tests to full-scale tests of the orbiter wing leading edge and nose cap, which identified critical impact damage threats to various shuttle components. Glenn researchers examined damage threats from potential impactors, including shuttle thermal-protection foams and ablators as well as ice formed on the shuttle's external tank. The analysis effort at Glenn encompassed the development of high-fidelity material models for implementation into the explicit finite-element impact-analysis code LS DYNA. The analysis method is now being used to analyze impact events on the shuttle system.

Glenn's Ballistic Impact Team addressed six elements that were critical to the success of the Return to Flight program:

(1) Extensive impact testing and characterization of six shuttle thermal-protection debris materials as well as ice (Glenn's fatigue laboratory provided static materials testing for this effort as needed.)
(2) External tank foam and booster separation motor aluminum-oxide particle debris impact testing on full-scale orbiter windows
(3) Ice and foam impact testing on the external tank structure to assess resulting secondary debris threats and potential degradation of the external tank thermal-protection system
(4) Over 100 impact tests on flat reinforced carbon/carbon panels to establish critical impact damage thresholds for the material as well as to validate material models developed for LS DYNA

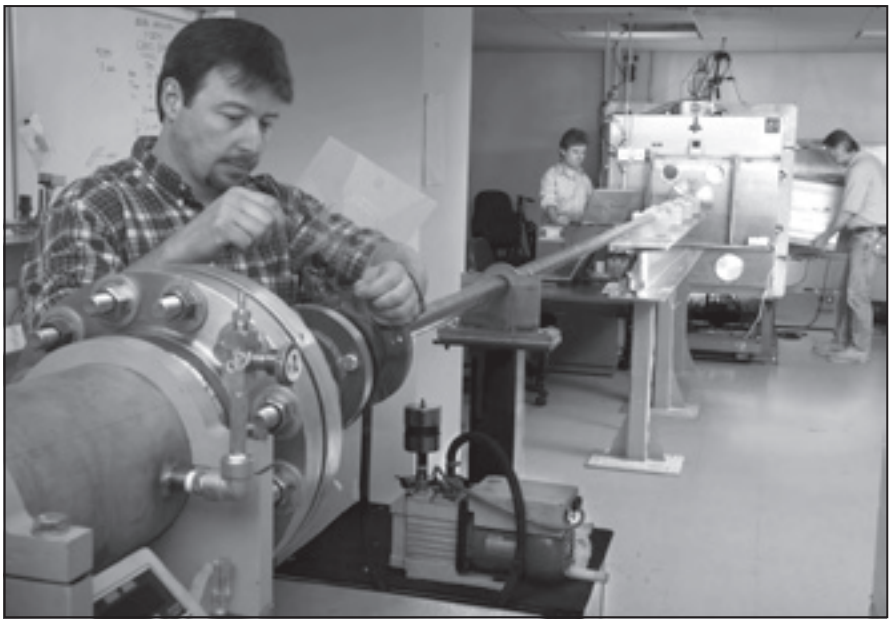

*External tank structural impact tests being conducted in the Ballistic Impact Laboratory.*

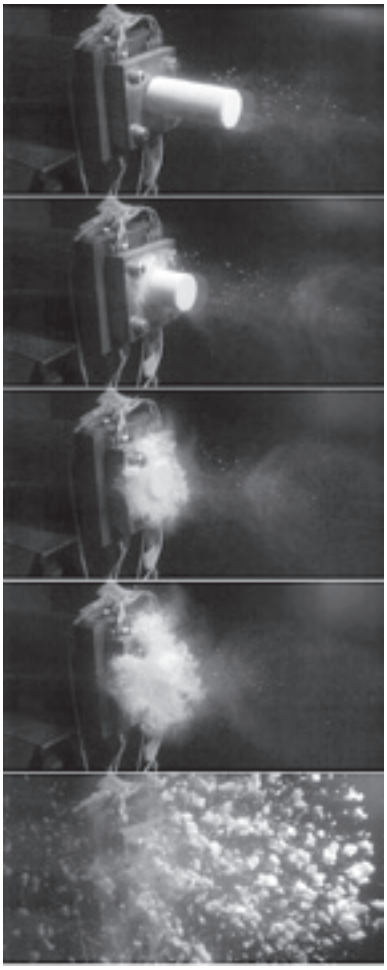

*High-speed digital photography captures the behavior of external tank foam undergoing an impact event.*

(5) Material model development and support of production analysis runs for the Shuttle Program Impact Analysis Team
(6) Analysis and testing support at Southwest Research Institute for full-scale tests of the wing leading edge and nose cap

Each element was successfully completed on time, leading to the successful launch of STS–114 in July 2005. As a result of Glenn's testing, the design of the orbiter windows was changed, the external tank was cleared as safe to fly, and a previously unavailable physics-based impact analysis capability was established for the shuttle program. As a consequence of Glenn Ballistic Impact Team contributions, mission safety for future shuttle operations increased dramatically.

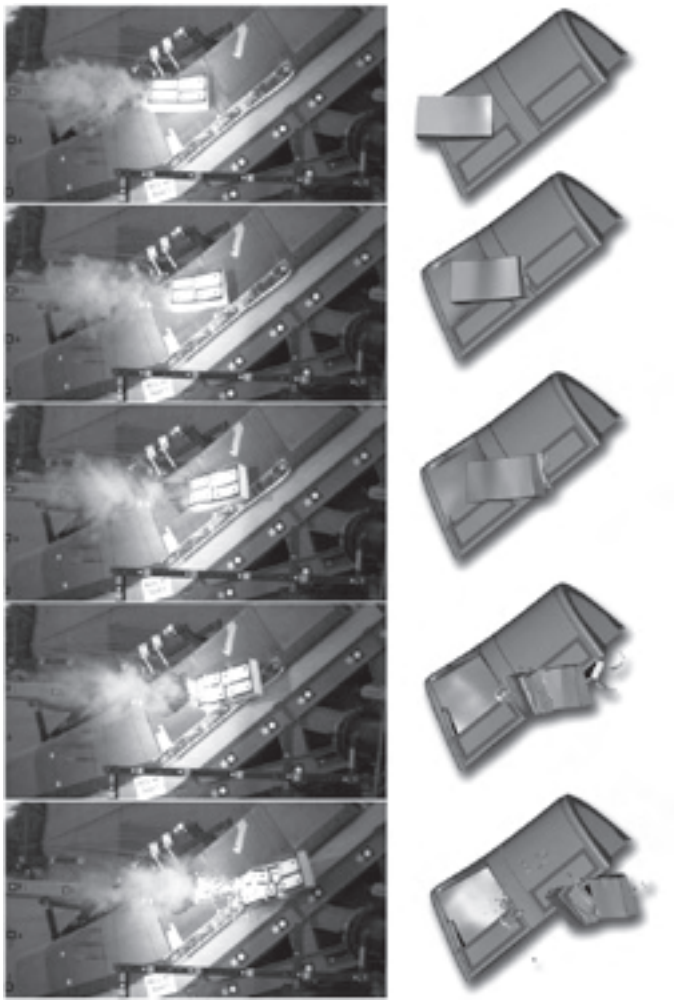

*Material models developed by Glenn's Ballistic Impact Team were implemented into the LS DYNA impact analysis code and used to predict impact damage for future shuttle missions.*

**Bibliography**

Melis, Matthew, et al.: A Summary of the Space Shuttle Columbia Tragedy and the Use of LS–DYNA in the Accident Investigation and Return to Flight Efforts. Prepared for the 8th International LS–DYNA Users Conference, Dearborn, MI, 2004.

Melis, M.E., et al.: A Summary of the NASA Glenn Ballistic Impact Lab Contributions to the Columbia Accident Investigation. 2005 Proceedings of the Annual Reliability and Maintainability Symposium, Alexandria, VA, 2005, pp. 284–290.

**Glenn contacts:**

Matthew E. Melis, 216–433–3322, Matthew.E.Melis@nasa.gov; and Dr. Michael Pereira, 216–433–6738, J.M.Pereira@nasa.gov

**Authors:**

Matthew E. Melis, Dr. J. Michael Pereira, Dr. Kelly S. Carney, Dr. Robert K. Goldberg, Dr. Santo A. Padula II, and Duane M. Revilock, Jr.

**Headquarters program office:**

Space Shuttle

**Programs/Projects:**

RTF, Aviation Safety, CEV, NGLT, Columbia Accident Investigation

**Special recognition:**

One NASA Peer Team Award

# Analysis and Modeling Methods Being Developed for Evaluating External Tank Foam

The Columbia Accident Investigation Board's conclusion that the tragic loss of the *Space Shuttle Columbia* was caused principally by the liberation of insulating foam from the bipod ramp of the external tank (ref. 1) launched an extensive series of studies to identify the cause of and the factors influencing foam shedding. Through various laboratory experiments, it became apparent that defects in the foam resulting from the spraying process have a significant influence on foam-shedding phenomena (ref. 2).

Although more stringent foam spraying and processing specifications have been established to limit both the size and number of defects, it is improbable that these defects will be completely eliminated. Vehicle safety, therefore, relies on developing an ability to assess the potential for a foam-shedding event with critical significance. To accomplish this, researchers need to accurately quantify the foam stress states during ascent and to understand how defects interact with the surrounding stresses to produce a fracture event.

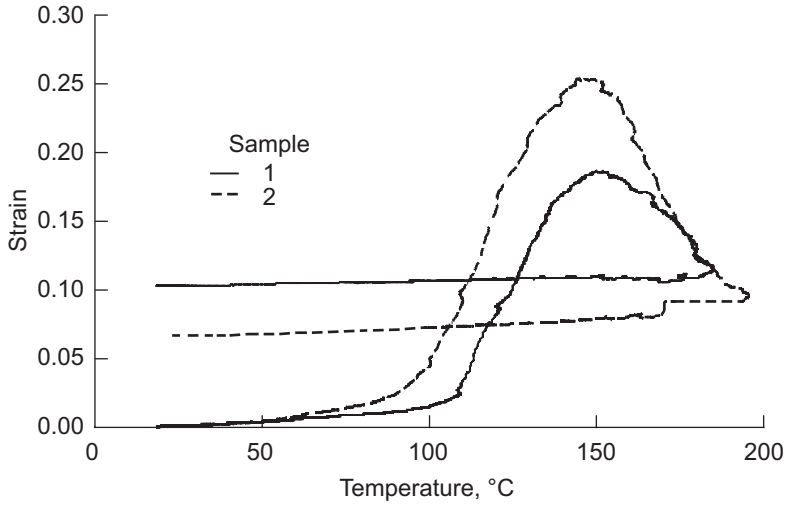


*Thermal expansion behavior of BX–265 foam normal-to-rise.*

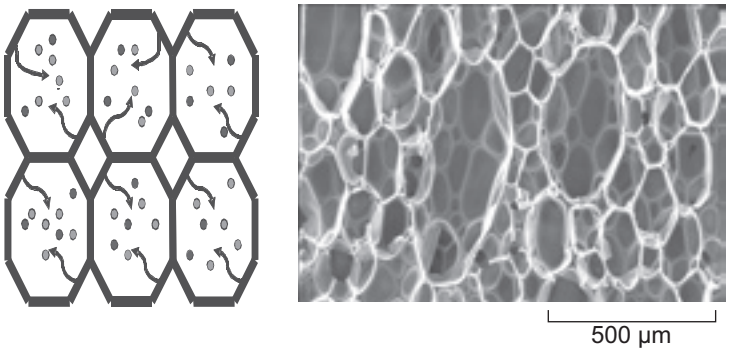


*Factors influencing the complex thermomechanical behavior of polymer foams. Left: Accumulation of volatiles inside cells. Right: Foam microstructure.*

The stress analysis of foam is challenging by itself. For the shuttle application, it is further complicated by severe temperature gradients across the foam layer during shuttle ascent. Because the foam cell walls are a polymer, the glass transition, the release of volatiles, and the thermal decomposition of the material contribute to the complex thermal expansion and thermomechanical behavior (see the graph). The foam cell structure shown in the bottom figure also plays a significant role because it introduces anisotropy in the mechanical and physical properties.

Researchers in the Materials and Structures Division at the NASA Glenn Research Center are conducting a series of research studies to develop improved analysis methods for simulating the complex thermostructural behavior of the rigid closed-cell polymeric foams used to insulate the shuttle's external tank. The goal is to develop accurate analysis tools to identify the mechanisms responsible for foam failure and debris liberation (see the final figure). These tools will also help to assess the criticality of specific foam defects on the basis of measurable defect characteristics, such as size, shape, depth, and location.

Both macromechanics and micromechanics models are being developed to account for the physical and chemical changes that occur in the material as well as the influence of the foam microstructure on the thermostructural behavior. Experimental studies are being conducted to (1) determine critical material property values for input to analysis models, (2) study the fracture behavior of rigid, closed-cell polymeric foams, and (3) study the significant physical and chemical processes that occur in the material to help guide the development of the physics-based models. So

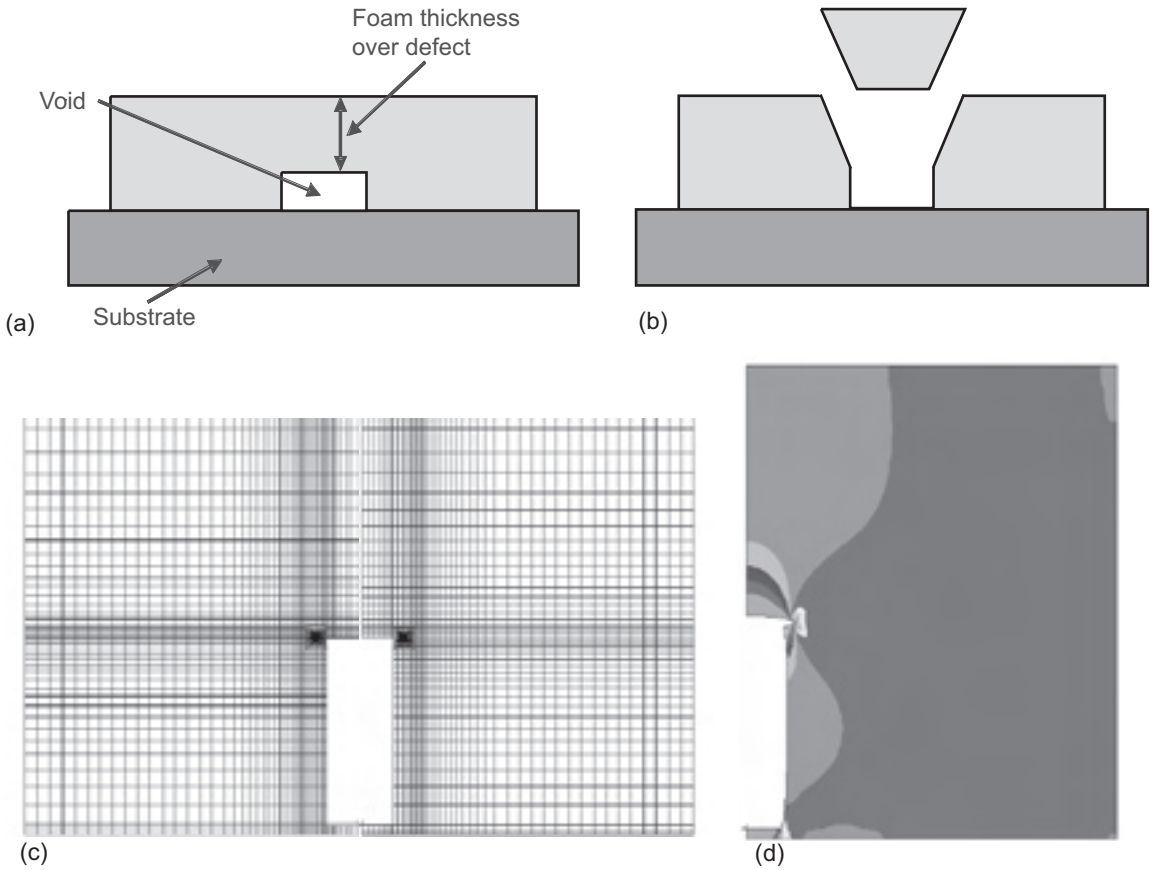


*Illustration of the divot test setup. (a) Foam divot test setup. (b) Formation of a divot. (c) Finite-element model of divot test. (d) Stress contours in foam.*

far, a formulation has been derived to account for the increase in the cell gas pressure due to thermal decomposition of the polymer (see the left side of the bottom figure on the preceding page). Also a finite element model has been established to describe the divot tests (see the figure on this page).

**References**

1. Columbia Accident Investigation Board Report, Vol. 1, NASA, Washington, DC, 2003. http://caib.nasa.gov/news/report/default.html
2. Dornheim, Michael A.: External Tank Makeover. Aviat. Week Space Technol., vol.161, no.13, 2004, pp. 57–61.

**Find out more about the research of Glenn's Life Prediction Branch:**
http://www.grc.nasa.gov/WWW/LPB/

**Glenn contacts:**
Dr. Roy M. Sullivan, 216–433–3249, Roy.M.Sullivan@nasa.gov; and
Dr. Bradley A. Lerch, 216–433–5522, Bradley.A.Lerch@nasa.gov

**Author:**
Dr. Roy M. Sullivan

**Headquarters program office:**
NESC

**Programs/Projects:**
Space Shuttle

# High-Temperature Chemical Reactions in Reinforced Carbon/Carbon Studied

Reinforced carbon/carbon (RCC) has been used successfully as thermal protection on the space shuttle orbiter nose cap and wing leading edge for many missions. During reentry, this material is exposed to the harsh environment of high temperatures, rapid velocities, and reactive gases. RCC consists of a two-dimensional layup of carbon fiber fabric together with several layers of oxidation protection. The oxidation protection can be summarized as follows. A conversion coating of silicon carbide (SiC) is followed by infiltration of tetra-ethyl orthosilicate (TEOS), which decomposes to silicon dioxide ($SiO_2$) on heating. Then, two outer coats of a sodium-silicate-based glass sealant are applied. In this study at the NASA Glenn Research Center, a series of controlled laboratory experiments was used in conjunction with observations of mission-exposed RCC to reveal the three major routes to degradation: oxidation of the carbon through cracks and fissures, sealant loss via vaporization, and silica/carbon reactions.

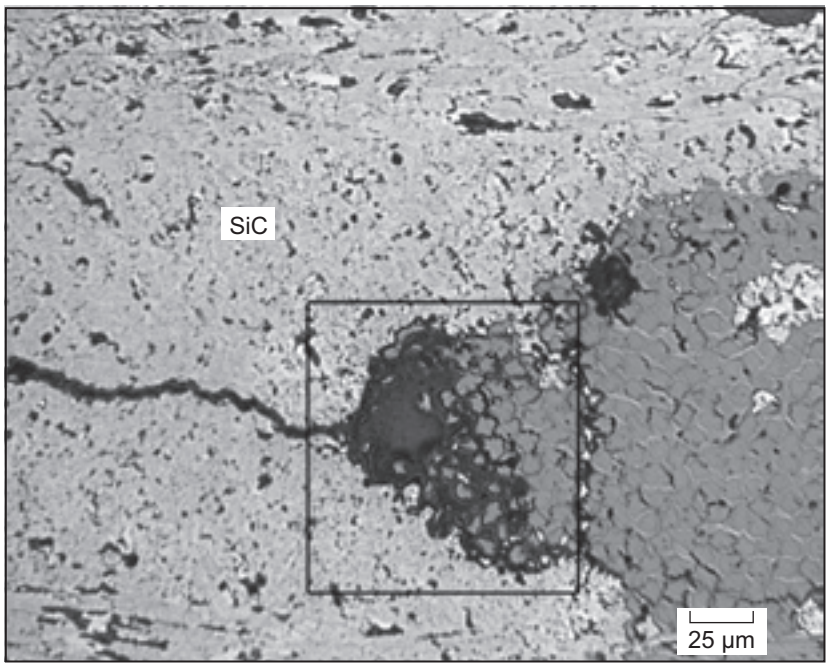


*RCC oxidized in a furnace for 1 hr at 1100 °C.*

Oxidation through cracks and fissures in RCC is a well-known issue. Despite the protection system, some oxidation is known to occur, particularly when the sodium silicate layer is depleted. The preceding image shows a typical cavity formed by the oxidation of RCC that has a SiC conversion coating with no glass sealants. The important features are (1) a clear path from the atmosphere to the carbon, which is the crack in this case, and (2) fibers exhibiting preferential attack along the edges. These features allow a pore created in oxidation to be distinguished from a pore created during processing. It is essential to make this distinction to assess any oxidation damage.

A two-stage diffusion model has been adapted to describe the oxidation of carbon through the cracks (ref. 1). Because of the thermodynamic incompatibility of carbon, gaseous carbon monoxide (CO(g)), and gaseous carbon dioxide ($CO_2$(g)), the oxidation of carbon is treated is two steps:

$$C + CO_2 = 2\ CO$$
$$½\ O_2 + CO = CO_2$$

The illustration below shows this schematically for a straight pore. Diffusive fluxes are derived for each region of the pore, and the consumption of carbon is calculated. Agreement between the observed values and the calculated values is within an order of magnitude. The disparity is likely due to the complex geometry of a crack in comparison to that of a straight pore.

A second important reaction is the vaporization loss of the sodium-silicate-based sealant. Sealant depletion is a well-known problem for mission-exposed RCC. Laboratory studies have provided data to establish an Arrhenius curve for sodium silicate vaporization in a boundary-layer-limited flux situation, illustrated in the graph on the next page. Extension of these data to sealant loss for stagnation flow arcjet tests looks promising.

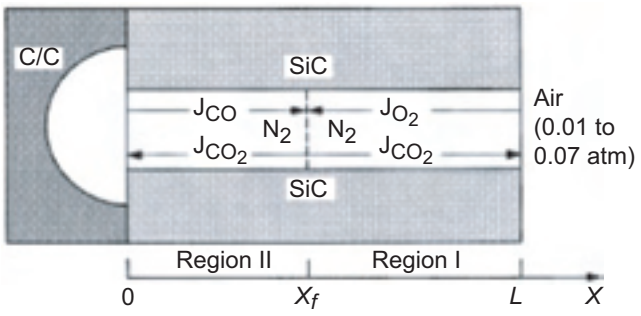


*Two-step diffusion-oxidation process for the oxidation of RCC through cracks. $J_i$ is the flux (grams or moles per unit area minus unit time) of species i; $X_f$, boundary of $CO/CO_2$ and $CO_2/O_2$ region; L, length of pore; X, diffusion direction.*

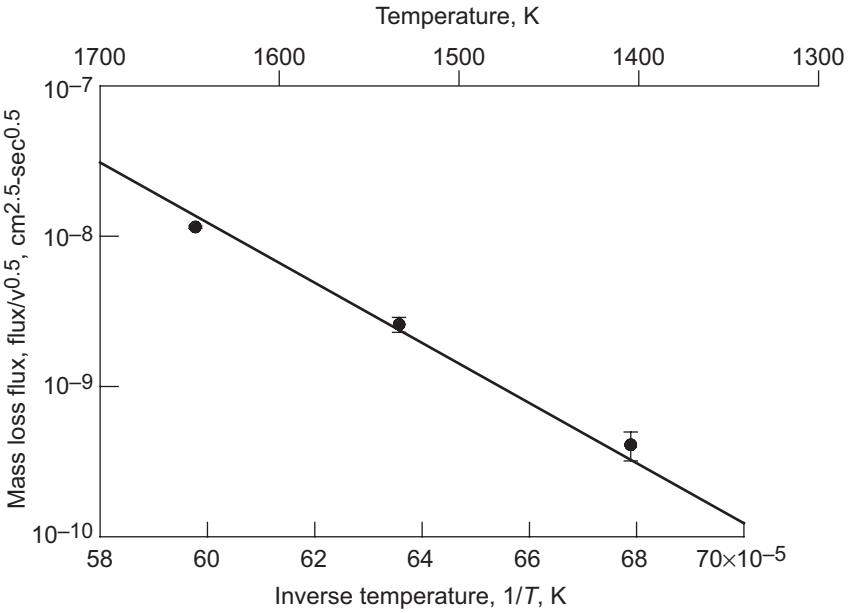


*Arrhenius plot for the mass loss flux of silica-saturated sodium silicate normalized to velocity.*

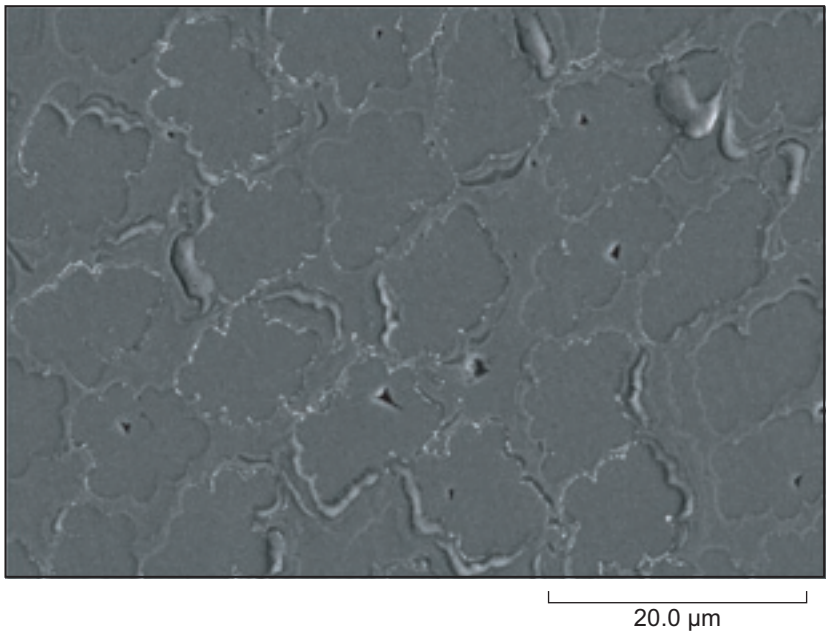


*RCC with TEOS-derived silica treated in argon for 15 min at 1600 °C. The small bright regions around the fibers are SiC.*

A third type of reaction is the interaction of TEOS-derived $SiO_2$ with the carbon/carbon substrate. Processing involves infiltration of RCC with TEOS, using a vacuum to draw the TEOS through the thickness of the RCC. Necessarily, a small amount of TEOS remains in the carbon/carbon and is converted to $SiO_2$. It is well-known that carbon reacts with $SiO_2$ to form SiC (ref. 2). Laboratory experiments on carbon/carbon with TEOS-derived $SiO_2$ show small regions of SiC developing in both vacuum and argon atmospheres. This is shown in the photomicrograph. These three types of reactions are critical in understanding and assessing the long-term performance of RCC in reentry environments.

**References**

1. Jacobson, Nathan S., et al.: Oxidative Attack of Carbon/Carbon Substrates Through Coating Pinholes. Carbon, vol. 37, 1999, pp. 411–419.
2. Jacobson, Nathan S.; Lee, Kang N.; and Fox, Dennis S.: Reactions of Silicon Carbide and Silicon(IV) Oxide at Elevated Temperatures. J. Am. Ceram. Soc., vol. 75, issue 6, 1992, pp. 1603–1611.

**Find out more about the research of Glenn's Durability and Protective Coatings Branch:**
http://www.grc.nasa.gov/WWW/EDB/

**Glenn contact:**
Dr. Nathan S. Jacobson, 216–433–5498, Nathan.S.Jacobson@nasa.gov

**Authors:**
Dr. Nathan S. Jacobson, Dr. Donald Curry, and Neal Webster

**Headquarters program office:**
Orbiter Project Office

**Programs/Projects:**
Space Shuttle Orbiter, RTF

# Glenn Refractory Adhesive for Bonding and Exterior Repair (GRABER) Technology Given 2005 R&D 100 Award

Robust in-space repair technologies are critically needed for the safe operation of the space shuttle as well as the repair and refurbishment of the thermal protection system structures of Crew Exploration Vehicles (CEV). Glenn Refractory Adhesive for Bonding and Exterior Repair (GRABER) was developed at the NASA Glenn Research Center for the repair of reinforced carbon/carbon (RCC) composite thermal protection system structures. The GRABER material has shown multiuse capability for the in-space repair of small cracks and as an adhesive and sealant for RCC leading-edge material. It is a refractory adhesive paste with desired ceramic fillers in a polymer/phenolic resin matrix with appropriate additives such as surfactants. The paste, which is applied to the damaged or cracked area of the RCC composite components with a caulking gun, cures at 100 to 120 °C and transforms into a high-temperature ceramic during reentry conditions.

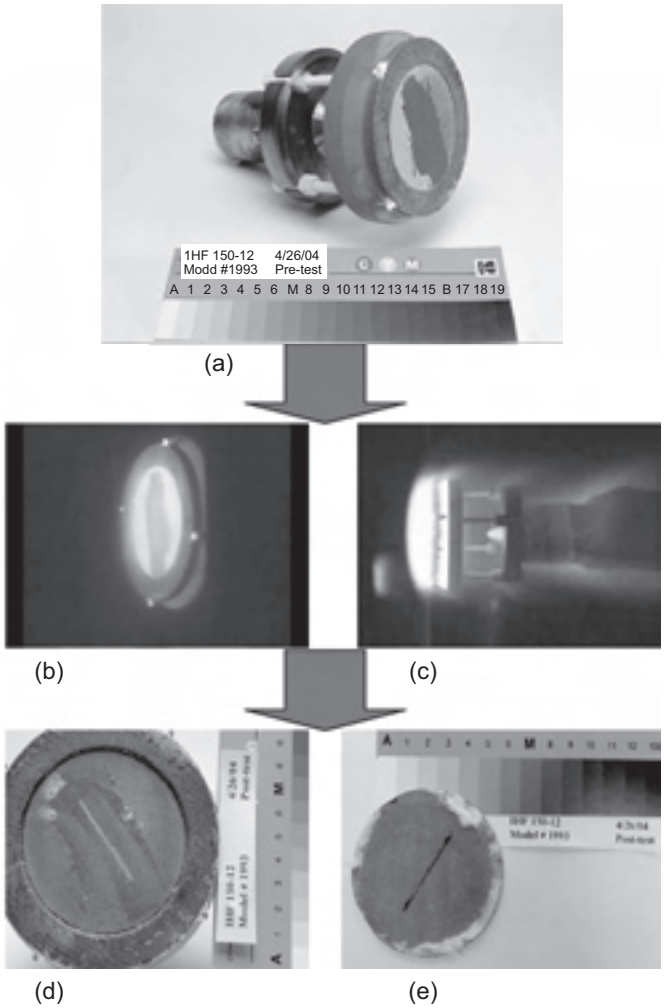


*RCC specimens. (a) Pretest crack-repaired RCC specimen. (b) Arcjet testing, front view. (c) Arcjet testing, side view. (d) Post-test, front-side macrograph. (e) Post-test, back-side macrograph.*

GRABER-based materials have multifunctionality and versatility for a wide variety of repair applications. This material was developed primarily to repair small cracks and coating delaminations. For the evaluation of the plasma resistance of this material system, cracks were introduced in RCC specimens by machining slots. These slots (0.035-in. and 1/16-in. wide and 1.5-in. long) were filled with GRABER-based repair compounds and tested in arcjet facilities at the NASA Johnson Space Center and the NASA Ames Research Center for approximately 15 min. All six samples survived the tests without any burn through. The photographs to the left show the pretest crack-repaired RCC specimen, views during arcjet testing, and post-test front-side and back-side macrographs. The GRABER-based repair materials stop the plasma flow through the specimen and prevent any damage. It is important to point out that unrepaired RCC specimens with similar damage had significant burn through because of the plasma oxidation of the RCC, and the small-crack region became a large hole, leading to catastrophic damage.

As an adhesive and sealant in the patch/plug concept, GRABER has performed exceptionally well in plasma torch and arcjet testing in simulated atmospheric reentry environments. The photograph on the next page shows a plug-repaired article where GRABER was used as the sealant. This specimen survived arcjet testing under simulated reentry conditions. GRABER materials also are being used to prepare adhesive patches and flexible ceramic prepregs that use different types of fabrics to repair large areas of damage. The fabric prepregs based on this material system have been used to make ceramic matrix composites and functional coatings and to repair carbon/carbon composites for a wide variety of ground-based applications. Further development and testing efforts are underway to optimize GRABER's properties and extend the application temperature.

The GRABER technology was given a 2005 R&D 100 Award. This technology also received honorable mention in Northern Ohio Live Magazine's 25th Awards of Achievement in the Science and Technology Category.

**Find out more about this research:**

**Glenn innovations receive R&D 100 Awards:**
http://www.nasa.gov/centers/glenn/news/2005/05-036_R&D_100_Awards.html

**Great Lakes Industrial Technology Center (GLITeC) article about GRABER:**
http://www.glitec.org/OhioLab/techSept05.htm

**STSliftoff.com article about GRABER:**
http://www.stsliftoff.com/rtf/glenn/pdffiles/90860main_M_1518_graber.pdf

**Glenn contact:**
Dr. Andrew J. Eckel, 216–433–8185, Andrew.J.Eckel@nasa.gov

**QSS Group, Inc., contact:**
Dr. Mrityunjay Singh, 216–433–8883, Mrityunjay.Singh@nasa.gov

**Authors:**
Dr. Mrityunjay Singh and Tarah P. Shpargel

**Headquarters program office:**
Space Operations

**Programs/Projects:**
RTF

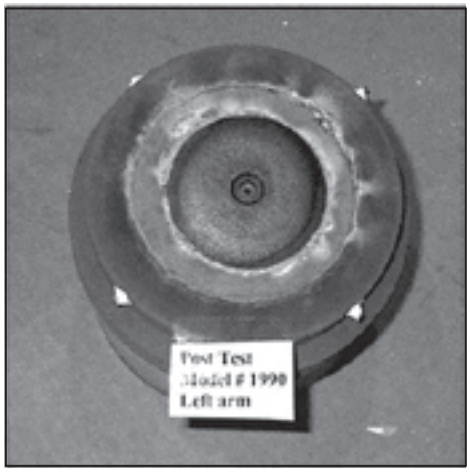


*RCC specimen plug-repaired using GRABER 5A as the sealant, shown after arcjet testing.*

**Special recognition:**
2005 R&D 100 Award; Honorable mention in the Science and Technology Category for Northern Ohio Live Magazine's 25th Awards of Achievement

## Flexible Metallic Overwrap Concept Evaluated for Potential On-Orbit Repair of Space Shuttle Leading Edges

On-orbit repair concepts for the space shuttle orbiter wing leading edges have been actively pursued since the *Space Shuttle Columbia* accident. Several teams have collaborated to design "kits" to repair damage to the reinforced carbon/carbon (RCC) leading edges, which can range from scratches to holes 16 in. in diameter. Atmospheric reentry of the orbiter imposes extreme requirements on the RCC as well as on any repair concepts. These requirements include temperatures up to 3000 °F for over 15 min in the presence of an extremely oxidizing plasma environment.

One proposal for on-orbit repair of large damage areas along RCC leading edges is an overwrap concept utilizing a thin (0.010- to 0.015-in.) rhenium (Re) sheet measuring 24 in. wide by 24 in. long (see the photograph on the right). Re possesses excellent high-temperature strength, good low-temperature ductility, and good fabricability. A commercial R512E coating (made of silicon, iron, and chromium: 60Si-20Fe-20Cr) was chosen to protect the Re substrate from the harsh oxidizing environment of atmospheric reentry since coatings that form silicides with the refractory metal base material are particularly effective against catastrophic oxidation. The top figure on the next page shows that the application of the R512E on Re produces three distinct silicide layers in the coating. The innermost layer is $(Re,Cr,Fe)_2Si$, the next columnar layer is $(Re,Cr,Fe)Si_{1.8}$, and the outermost layer is a silicide with Cr and Fe as the major constituents.

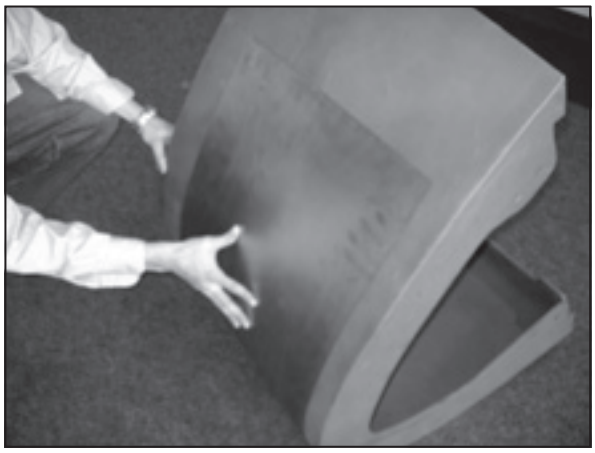

*Overwrap concept.*

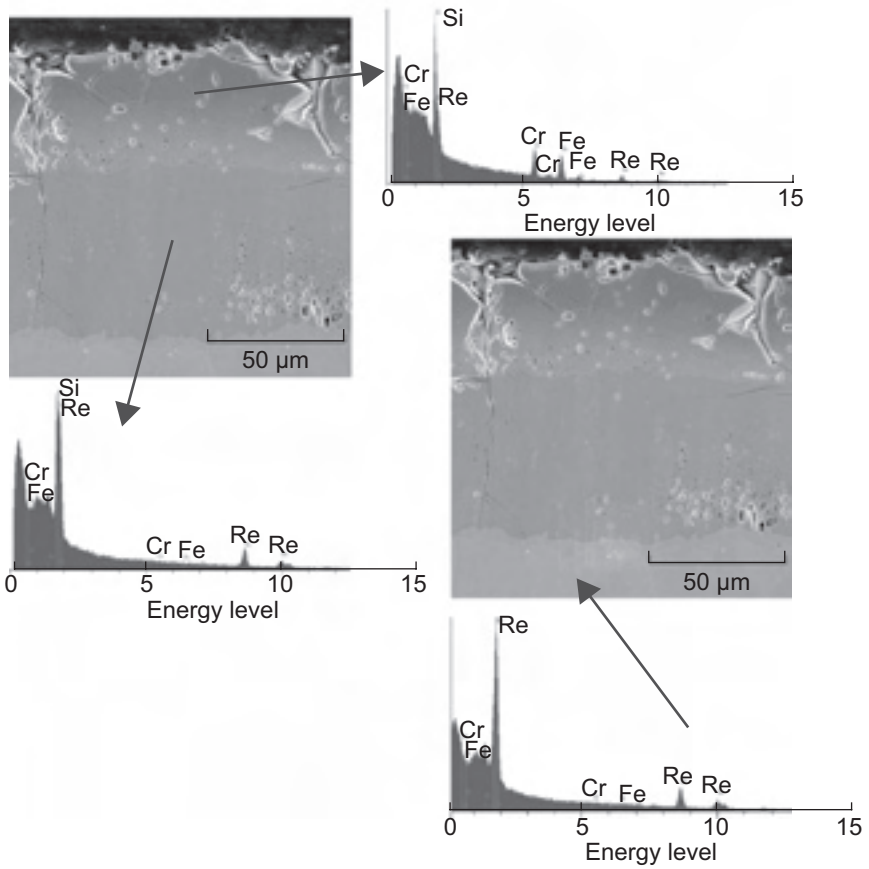


*Re+R512E forms three distinct layers.*

One poor characteristic of the R512E coating is that it is inherently brittle and could crack when the thin-gauge metallic overwrap is bent to follow the curvature of the orbiter leading edges. In anticipation of this situation, a "Type A" sodium silicate coating is applied over the R512E; this coating effectively flows into the cracks at the reentry temperatures, providing additional protection for the refractory metal substrate. This coating performs the same function on the current RCC material.

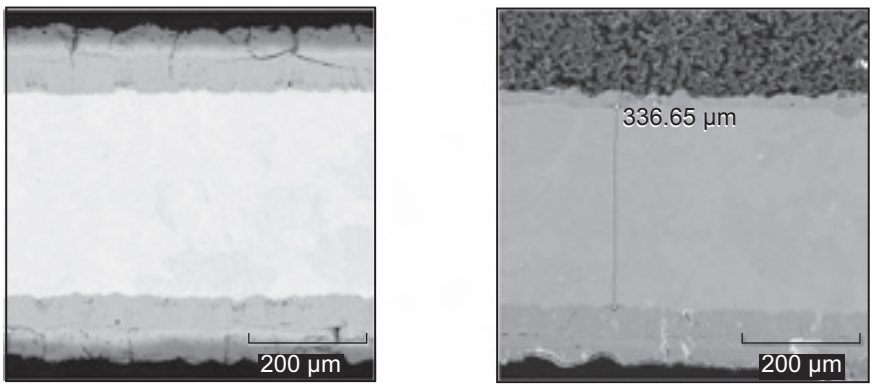


*Cross section of Re+R512E. Left: As-coated. Right: Postarcjet test.*

Arcjet testing of 2.8-in.-diameter coated Re disks simulated the high-temperature oxidizing conditions experienced by the leading edge during reentry (greater than 3000 °F over the 15-min test duration). Both coated Re concepts (Re+R512E+Type A and Re+Ir+R512E+Type A) passed this arcjet testing. The photomicrographs at the bottom of this page show cross sections of the test article in both the as-processed and postarcjet conditions. The coating effectively protected the substrate, and a heavy oxidation layer exists on the post-test surface. However, the other silicide layers are intact, and the Re substrate is essentially untouched.

The photographs on the next page show both pretest and post-test conditions for the Re+R512E+Type A. Although the front side of the specimen shows evidence of attack, no penetration or failure occurred. That photograph also shows that 93 percent of the original Re substrate survived the exposure, a substantial safety margin. The degree of attack on the backside of the specimen was negligible. This is significant because the backside is adjacent to damage that is targeted for repair. Results for the Re+Ir+R512E+Type A concept were similar to those for Re+R512E+Type A.

Given the successful arcjet test results, the Re-based concept was selected by the development team of the NASA Langley Research Center and the NASA Glenn Research Center for additional testing and scale up. Scale-up activities underway to evaluate the Re+R512E+Type A concept include larger panel fabrication, more arcjet testing, and attachment concepts.

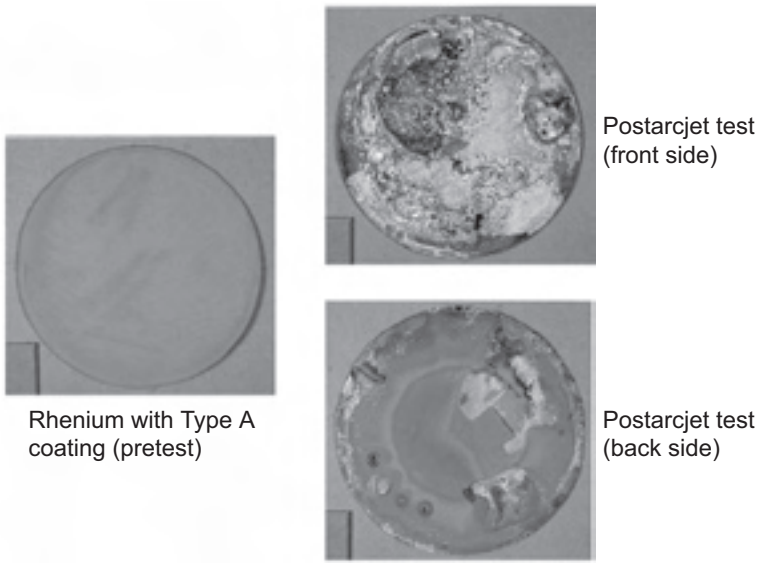


*The Re/R512E concept passed arcjet testing, with no sample burn through after 1000 sec.*

**Glenn contacts:**
Frank J. Ritzert, 216–433–8199,
Frank.Ritzert@nasa.gov; and
Dr. James A. Nesbitt, 216–433–3275,
James.A.Nesbitt@nasa.gov

**Author:**
Frank J. Ritzert

**Headquarters program office:**
Vehicle Systems

**Programs/Projects:**
RTF

## Root Cause Determined for Cracking in the Niobium Reaction Control System Thrusters for the Space Shuttle Orbiter

There are 38 primary reaction control system (RCS) thrusters on each space shuttle orbiter that are used to provide attitude (pitch, yaw, and roll) maneuvers, as well as translation maneuvers along the orbiter axis. Cracking was discovered in an RCS thruster in April 2004 after a chamber repair and rejuvenation was performed. Relief radius cracking had been observed in seven thrusters in the 1970s and 1980s prior to flight. Because of the concern that hot combustion gases could leak through the cracks and damage the space shuttle orbiter, RCS thruster cracking was considered a "critical 1/1 failure," meaning loss of vehicle with no redundancies. This concern was compounded by the fact that the extent of cracking damage in the thruster fleet was unknown, since no reliable nondestructive evaluation methods were available to detect cracks in thrusters installed on the vehicle.

The NASA Engineering and Safety Center (NESC) requested that a materials consultation on the thruster cracking problem occur in parallel with the efforts of the Space Shuttle Orbiter Program Office's Materials and Processing Division. The NESC team, which was led by the NASA Glenn Research Center, was composed of Glenn, NASA Langley Research Center, and NASA Marshall Space Flight Center scientists and engineers who conducted a detailed review of the relevant literature and of the documentation from the previous RCS thruster failure analyses from the 1970s and 1980s. The NESC team concluded from the review that the prior failure analyses lacked sufficient documentation to support the conclusions that stress

*RCS thruster being examined optically for cracking in the relief radius.*

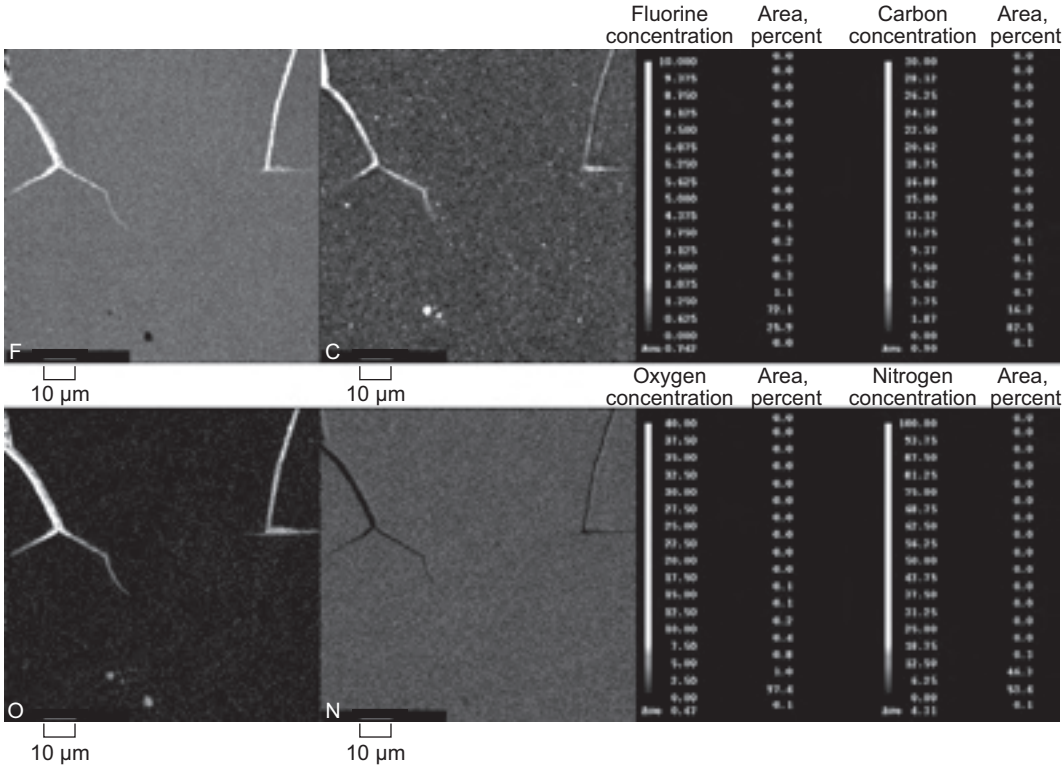


*Electron microprobe dot maps showing the crack tip of the relief radius crack. Levels of fluorine (F), carbon (C), oxygen (O), and nitrogen (N) are shown within the crack, with brighter areas indicating higher concentrations of each element. Qualitative levels (in weight percent) are shown in the keys. This figure is shown in color in the online version of this article (http://www.grc.nasa.gov/WWW/RT/2005/RX/RX06-mackay.html).*

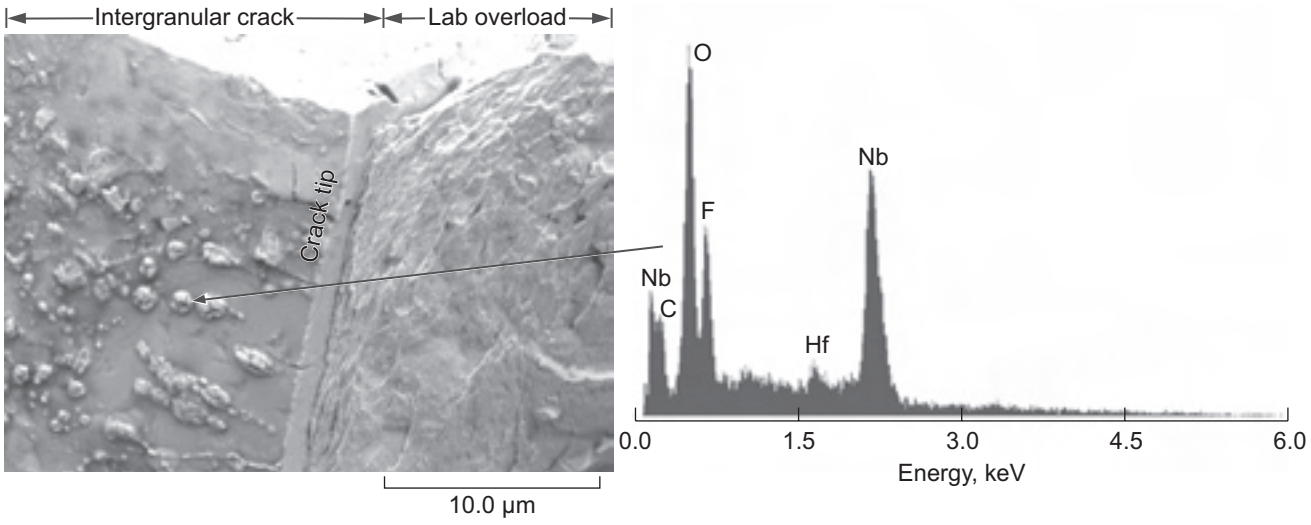


*reaction products that were chemically analyzed. The lab overload region denotes the region of the fracture that was opened in the lab to more clearly observe key features on the crack surface. Right: Energy-dispersive spectrosocopy scan showing elevated levels of C, O, and F associated with the oxide nodule on the intergranular crack.*

corrosion cracking or hot-salt cracking was the root cause of the thruster cracking. Subsequently, the NESC team identified and conducted new materials characterization and mechanical tests focused on (1) substantiating the root cause of the cracking in the RCS thrusters and (2) determining if the cracks were likely to grow in service. Electron microprobe analyses and field emission scanning electron microscopy performed on thruster hardware (serial number 120) and on niobium test specimens demonstrated that the thruster material was not susceptible to the root cause proposed in the earlier failure analyses. These in-depth analyses coupled with mechanical test results supported the conclusion that hydrogen embrittlement was the likely cause of cracking.

In the second phase of the NESC consultation, an independent failure analysis of another thruster (serial number 132) was conducted. Examination of the thruster crack surfaces confirmed that the oxide features on the intergranular crack surfaces were similar from the crack mouth to the crack tip and that no changes in crack mode were observed across the fracture surfaces. This work contributed to the conclusions that the thruster cracking was produced during original manufacturing as a result of processing with fluoride-containing acids and that no appreciable crack growth was observed for the thrusters after manufacturing. This extensive examination enabled the most comprehensive data to be obtained on crack-depth profiles for any RCS thruster hardware to date and will aid in the development of both stress analyses and nondestructive evaluation methods for in situ crack examinations. More detailed information on the NESC materials consultation of the thruster cracking issue can be found in reference 1.

**Reference**

1. MacKay, Rebecca A., et al.: Reaction Control System Thruster Cracking Consultation: NASA Engineering and Safety Center (NESC) Materials Super Problem Resolution Team (SPRT) Findings. NASA/TP—2005-214053, 2005. http://gltrs.grc.nasa.gov/cgi-bin/GLTRS/browse.pl?2005/TP-2005-214053.html

**Glenn contacts:**
Dr. Rebecca A. MacKay, 216–433–3269, Rebecca.A.MacKay@nasa.gov; and
David R. Hull, 216–433–3281
David.R.Hull@nasa.gov

**Authors:**
Dr. Rebecca A. MacKay, David R. Hull, Terry R. McCue, James W. Smith, Stephen W. Smith, and Sandeep R. Shah

**Programs/Projects:**
NESC (NASA Langley)

## Epoxy and Layered Silicate Nanocomposite Tanks Produced and Tested for Cryogen Storage Applications

It is envisioned that next-generation space exploration vehicles will have integral liquid hydrogen and liquid oxygen cryogenic fuel tanks that not only contain fuel, but function as load-carrying structures during launch and flight operations. Traditionally, metallic tanks have been used for housing cryogenic fluids. The advantages of such tanks include high strength, high stiffness, and low permeability. Presently, it appears that the replacement of traditional metallic cryogenic fuel tanks with polymer matrix composite tanks may decrease weight significantly, and hence, increase load-carrying capabilities (ref. 1).

However, the tanks must be able to withstand flight loads and temperatures ranging from –250 to 120 °C, without loss of cryogenic fuel due to microcracking or delamination. Research of the NASA Glenn Research Center has led to the development of epoxy-clay nanocomposites with up to 70-percent lower hydrogen permeability than that of the base epoxy resin. Filament-wound carbon-fiber-reinforced tanks made with this nanocomposite had a fivefold lower helium leak rate than the corresponding tanks made without clay. Use of these advanced composites would eliminate the need for a liner in composite cryotanks, thereby simplifying construction and reducing propellant leakage.

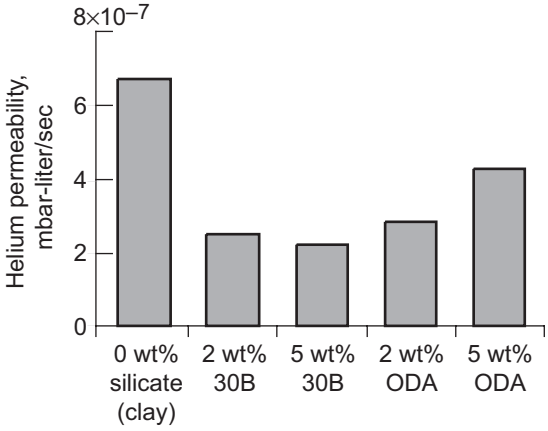


*Helium permeability of Epon 826 with various amounts of layered silicate in comparison to the base resin (clay). ODA, organically modified clay from Michigan State University (East Lansing, MI); 30B, Closite 30B—organically treated clay from Southern Clay Products (Gonzales, TX).*

The significant enhancements in barrier performance that are typically reported for clay nanocomposites depend on the level of separation of the silicate. A high level of dispersion creates a maximum path length for the permeating gas, thereby slowing the leak rate. As shown in the bar chart on the preceding page, addition of layered silicate into Epon 826 decreased permeability by 30- to 70-percent in comparison to the base resin. This reduction is common when the clay is simply added to the matrix because the resulting morphology is a combination of intercalated and exfoliated silicate layers, randomly arranged throughout the sample. It has been assumed that orienting the clay layers within the sample would produce the lowest permeability.

Test tanks (see the photograph) were prepared, and the helium permeability was measured at room temperature and 25 psi. The nanocomposite matrix tanks showed a fivefold decrease in the helium leakage rate in comparison to the tank composed of a neat resin matrix.

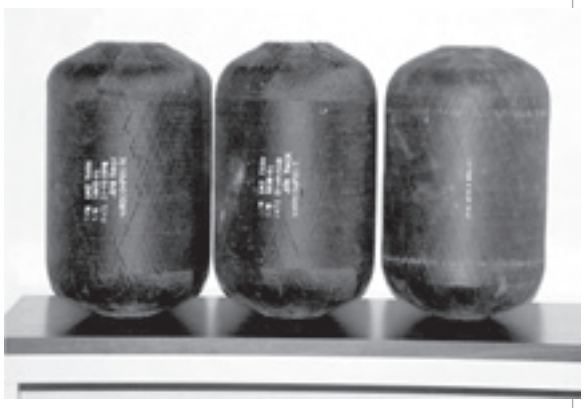

*Nanocomposite matrix (left and center) and neat resin (right) test tanks.*

The coefficient of thermal expansion is an important parameter to consider when developing materials for composite cryogenic tanks. The primary cause of microcracking is the difference in the coefficient of thermal expansion (CTE) of the matrix and that of the reinforcing carbon fibers. The results (shown in the top bar chart) indicate up to a 25-percent decrease in the CTE for the nanocomposite samples. A decrease in the CTE of the nanocomposite can be attributed to the fine dispersion and rigidity of the clay platelets in the epoxy matrix, which can inhibit the expansion of polymer chains as the temperature increases (ref. 2).

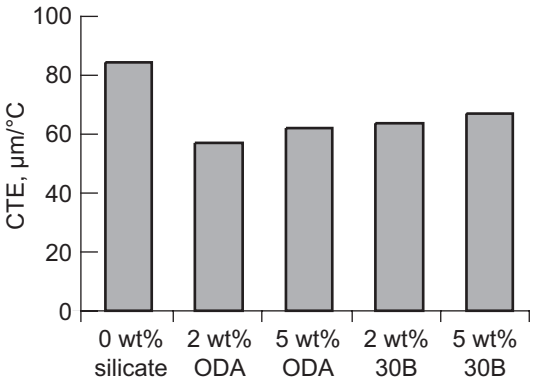


*CTE of nanocomposite samples on Epon 826 compared with that of the base resin (clay).*

Impact testing has shown that the nanocomposites have a decreased toughness in comparison to the base resin. This is commonly observed when a rigid filler is added. In this case, however, the decrease is minimal. The final bar chart shows the notched impact results for the neat resin and nanocomposites.

In summary, dispersion of layered silicate clays in two separate epoxy matrices reduced both the resin permeability and the CTE. The resin toughness varied. However, these results, as well as preliminary data from the composite tank, suggest that nanocomposite materials may be well suited for linerless composite tanks.

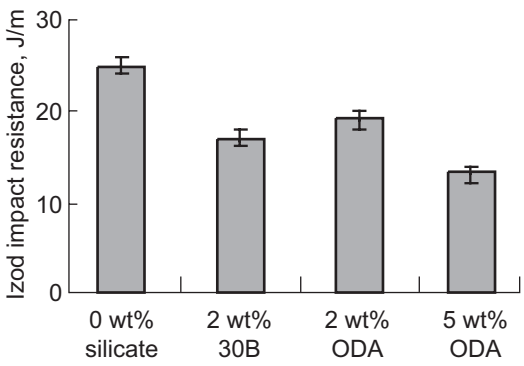


*Izod impact resistance of notched nanocomposite samples of Epon 826 with D230 curing agent compared with the base resin (clay).*

**References**

1. Gates, T., et al.: Thermal/Mechanical Durability of Polymer-Matrix Composites in Cryogenic Environments. AIAA–2003–1600, 2003.
2. Robinson, M.; Eichinger, J.; and Johnson, S.: Hydrogen Permeability Requirements and Testing for Reusable Launch Vehicle Tanks. AIAA–2002–1418, 2002.

**Glenn contact:**
Sandi G. Miller, 216–433–8489, Sandi.G.Miller@nasa.gov

**Author:**
Sandi G. Miller

**Headquarters program office:**
Aeronautics Research

**Programs/Projects:**
LEAP

# Crack-Growth Properties of Specialty Windows for the *International Space Station* Fluids and Combustion Facility Evaluated

The *International Space Station* Flow Enclosure Accommodating Novel Investigations in Combustion of Solids (FEANICS) module is designed to perform various combustion experiments in zero gravity. The module fits into a chamber known as the Combustion Integrated Rack and is observed via eight pressurized sapphire windows as shown in the following figure. The FEANICS project intends to replace one of the sapphire windows with a 63-mm-diameter zinc selenide (ZnSe) window that will allow a laser beam of 10.6-μm wavelength to pass. The laser will be used to ignite materials in a zero-gravity environment and thereby study combustion and improve safety in space vehicles.

ZnSe is a soft, weak ceramic that exhibits crack growth in the presence of water. Furthermore, it has a large average grain size. This results in single grains dominating behavior by fracturing at energies lower than expected from data generated with macrocracks. Thus, the design of hardware, such as a window fabricated from polycrystalline ZnSe, requires not only the usual life analysis performed for fracture-critical components on the *International Space Station*, but consideration of the potential for failure from single grains. Unfortunately, much of the data available on ZnSe were generated by using large cracks spanning many grains.

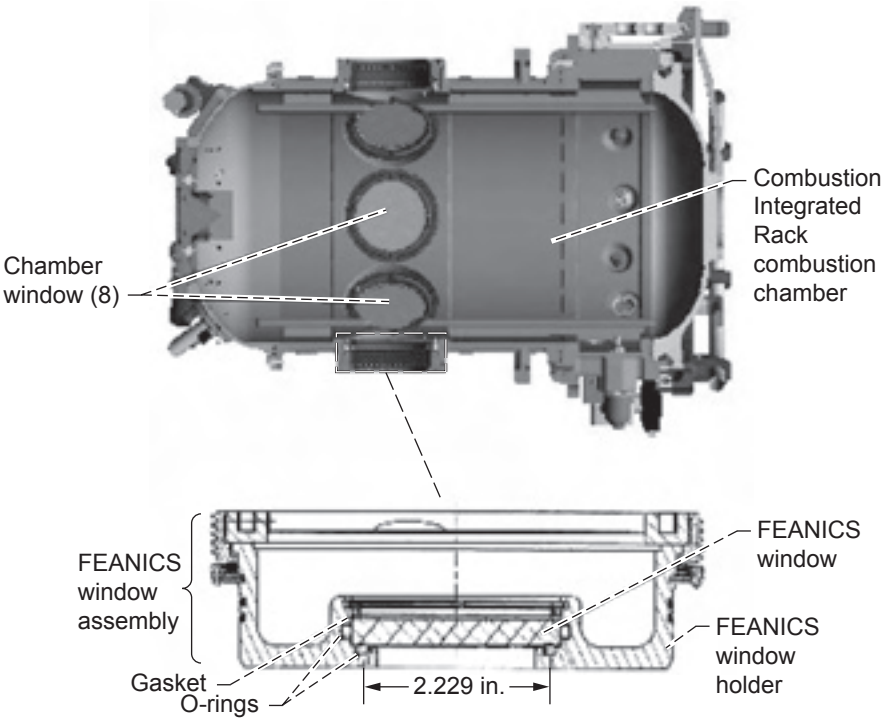


*Combustion Integrated Rack and ZnSe window assembly for use with the FEANICS module.*

In order to design a window sufficient to sustain the required mission pressure cycle and humidity, researchers at the NASA Glenn Research Center reviewed the literature on chemically-vapor-deposited ZnSe (ref. 1) and reinterpreted it for failure from small, realistic flaws. The reinterpretation of the existing data resulted in a substantial change in the crack-growth parameters and the predicted component life. For ceramics and glasses, slow-crack-growth can be described by the equation

$$\nu = AK_I^n \qquad (1)$$

where $A$ and $n$ are slow-crack-growth parameters and $K_I$ is the mode I applied stress intensity. For 100-percent humidity, the slow-crack-growth parameters were estimated as $n \approx 40$ and $A_{macro} \approx 1000$ m/sec $(MPa\sqrt{m})^{-n}$ for macrocrack failure as shown on the right side of the graph on the following page.

Two approaches were used to determine parameters for small-crack failure: (1) strength-based data were analyzed using small-crack-fracture energies, and (2) macrocrack curves were shifted to the small-crack region by

$$A_{single} = A_{macro}\left(\frac{K_{ICmacro}}{K_{ICsingle}}\right)^n \qquad (2)$$

where $A_{macro}$ and $K_{ICmacro}$ are the macroscopic slow-crack-growth coefficient and fracture toughness, respectively, and $A_{single}$ and $K_{ICsingle}$ are the corresponding single-crystal values.

For 100-percent humidity, the slow-crack-growth parameters for small-crack or single-crystal failure were estimated to be $n \leq 40$ and $A_{single} = 10^{20}$ m/sec $(MPa\sqrt{m})^{-n}$ as shown on the left side of the graph on the following page.

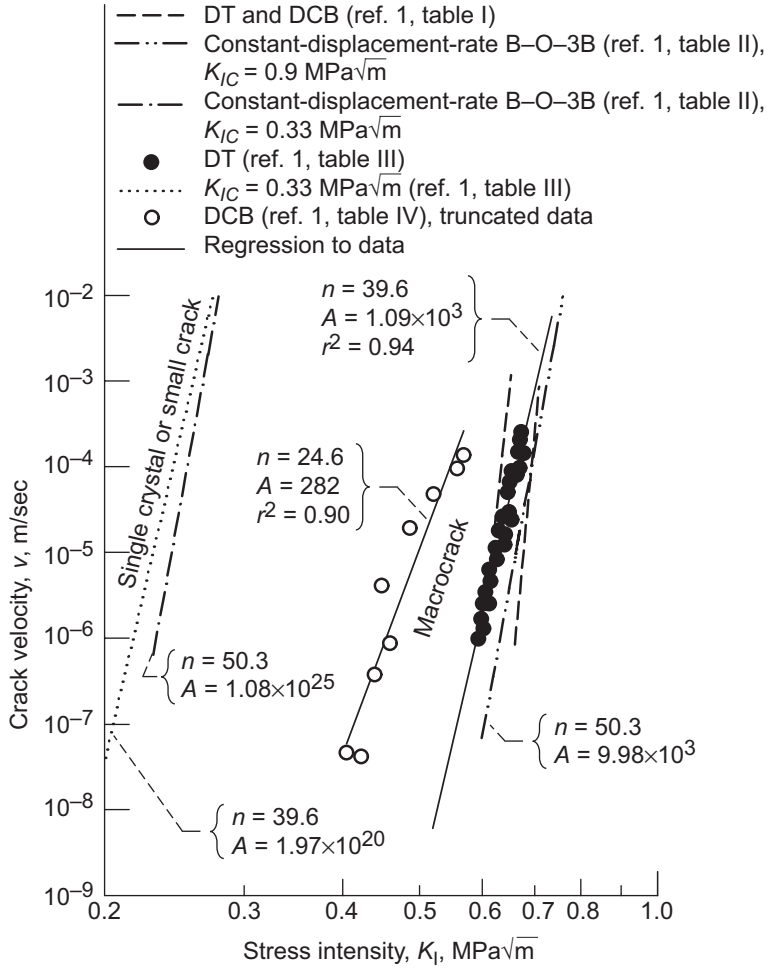


*Crack-growth velocity v as a function of stress intensity factor $K_I$ for ZnSe in water. Two types of crack growth are shown: that within a single grain and that from a large crack encompassing many grains. DCB, double-cantilever beam; DT, double torsion; B–O–3B, point loading of circular plates supported by three balls; $K_{IC}$, fracture toughness; A and n, slow-crack-growth parameters; r, Pearson coefficient.*

Reasonable agreement between the strength-based data and the shifted macrocrack data was exhibited for both 45-percent relative humidity air and water, implying that equation (2) gives a reasonable estimate of crack-growth parameters for small cracks.

In addition to reinterpreting the available literature, Glenn researchers measured properties such as strength, hardness, and grain size for currently available ZnSe by testing windows similar to the actual hardware. The measured properties were found to be in good agreement with literature on well-polished test specimens. Fracture toughness was noted to vary by a factor of 3: the measurements ranged from 0.33 to 0.9 MPa√m, with the lower values representing failure from small flaws within grains and the larger values representing macroscopic cracks in dry environments. Future work may include testing of witness coupons manufactured concurrently with the flight window.

**Reference**

1. Salem, Jonathan A.: Estimation of ZnSe Slow-Crack-Growth Properties for Design of the Flow Enclosure Accommodating Novel Investigations in Combustion of Solids (FEANICS) Windows. NASA/TM—2005-213359, 2005. http://gltrs.grc.nasa.gov/cgi-bin/GLTRS/browse.pl?2005/TM-2005-213359.html

**Find out more about the research of Glenn's Life Prediction Branch:**
http://www.grc.nasa.gov/WWW/LPB/research/acl/

**Glenn contacts:**
Dr. Jonathan A. Salem, 216–433–3313, Jonathan.A.Salem@grc.nasa.gov; and Charles L. Denniston, 216–433–8534, Charles.L.Denniston@nasa.gov.

**Author:**
Dr. Jonathan A. Salem

**Headquarters program office:**
HSRT

**Programs/Projects:**
Life Support & Habitation, Microgravity Science

# Active Clearance Control System Concept Performance Tests Successfully Completed at NASA Glenn

A state-of-the-art active clearance control (ACC) test rig has been fabricated and installed at the NASA Glenn Research Center (see the photograph). This rig is designed to evaluate the feasibility of implementing a fast-acting mechanical actuation system in the high-pressure turbine section of a modern jet engine to precisely adjust the clearance between the tips of rotating turbine blades and the sealing shroud that encases the rotor. Minimizing this clearance can reduce the spill of combustion gases over the ends of the turbine blades, thus enhancing both the efficiency and overall performance of the engine. Current engines cool the outer engine case flanges to decrease the clearance between the blade tips and the shroud. This system, however, is limited by slow response times and does not monitor the dynamic, asymmetric blade-tip-to-shroud clearance. For this reason, clearances must be set conservatively during engine buildup to avoid blade-tip to seal-shroud collisions during extreme engine condition transients (e.g., takeoff and reacceleration), thus foregoing the benefits of tighter tip clearances during cruise.

Reducing engine tip clearances by 0.010 in. would decrease specific fuel consumption by approximately 0.8 to 1 percent, significantly decrease nitrogen oxides ($NO_x$), carbon monoxide, and carbon dioxide emissions, and lower exhaust gas temperature by approximately 10 °C. Additional benefits of tighter tip clearances include increased engine time-on-wing, decreased operating and maintenance costs, and increased mission range and payload capabilities.

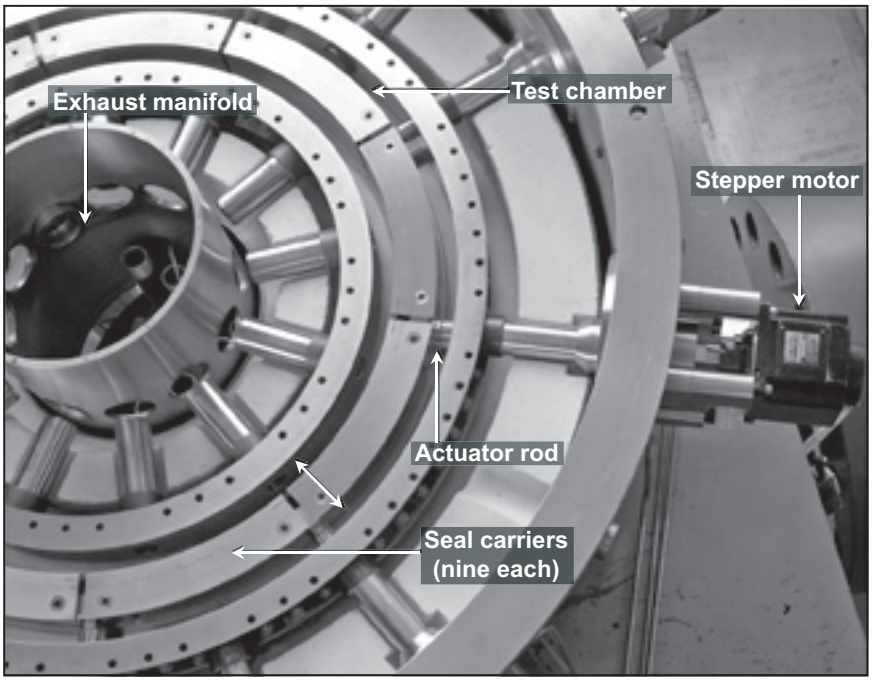


*Closeup of ACC rig showing internal components.*

The new test rig installed at Glenn employs a fast-acting mechanical actuation system designed to improve on existing clearance-control methods (see the photograph). Simulated tip clearances in the test rig are tracked using capacitance-based proximity probes coupled with nine independent mechanical actuators through a closed-loop control scheme. The actuators position the segmented seal carriers to achieve the desired clearance levels on the basis of positional feedback from the proximity probes. The test rig simulates the geometry, temperature, and pressure differentials found in a high-pressure turbine section, allowing investigation of the candidate kinematic systems, seal concepts, and controls needed to implement the ACC system in an engine.

Room-temperature testing of the ACC rig showed that the kinematic system allowed seal carrier motion over a 0.080-in. range, which easily encompasses the range needed for future turbine engine applications. The system leakage was tested at pressures up to 120 psig—comparable to pressure differentials anticipated in future engines. Seal effective leakage flow area was comparable to an engine industry reference level. Cyclic open-loop actuation of the seal carriers over a $\pm$0.035-in. range (radially inward and outward) at 20 psig (the load limit of current stepper actuators) was used to examine system repeatability. This test showed that the carriers returned to their original locations after 20 cycles to within the 0.001-in. resolution of the gauge pin measurement technique used. Closed-loop actuation of the seal carriers using proximity probe feedback showed that the system could track a simulated engine flight clearance profile with better than 0.001-in. accuracy while satisfying required clearance change rates (see the graphs on the following page).

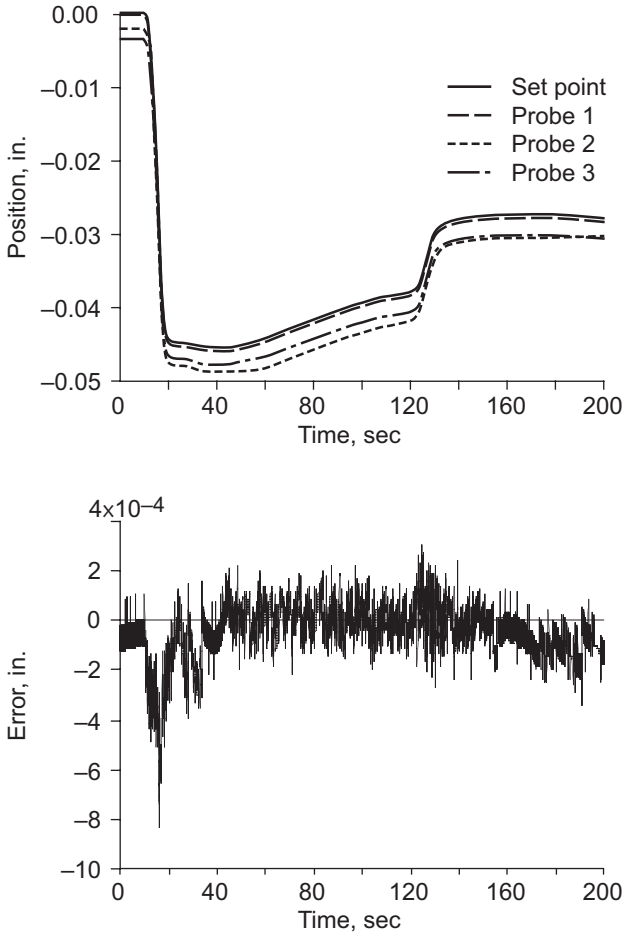


*ACC test rig tracking of a simulated flight clearance profile at 20 psig from flight idle (time zero). Data include the commanded clearance set point, three proximity probe readings measuring actual clearances, and a corresponding plot of error versus time (<0.001-in. error). The test was conducted at ambient temperature, and control was based on the minimum of the three probe readings. The negative position indicates radially outward movement.*

**Bibliography**
Steinetz, Bruce M., et al.: Evaluation of an Active Clearance Control System Concept. NASA/TM—2005-213856 (AIAA–2005–3989), 2005.http://gltrs.grc.nasa.gov/cgi-bin/GLTRS/browse.pl?2005/TM-2005-213856.html

**Find out more about this research at Glenn:**

**Turbine seals:**
http://www.grc.nasa.gov/WWW/TurbineSeal/

**Structural seals and thermal barriers:**
http://www.grc.nasa.gov/WWW/structuralseal/

**Mechanical Components Branch:**
http://www.grc.nasa.gov/WWW/5900/5950/

**Glenn contact:**
Dr. Bruce M. Steinetz, 216–433–3302, Bruce.M.Steinetz@nasa.gov

**Authors:**
Dr. Bruce M. Steinetz, Dr. Scott B. Lattime, Shawn C. Taylor, Jonathan A. DeCastro, Jay J. Oswald, and Kevin J. Melcher

**Headquarters program office:**
Aeronautics Research

**Programs/Projects:**
UEET, Propulsion 21

## Laser Rig High-Heat-Flux Testing of Thermal Barrier Coatings at NASA Glenn Proved To Be Especially Valuable for Testing Combustor Section Coatings

The laser rigs at the NASA Glenn Research Center provide a relatively simple, affordable, and versatile approach to high-heat-flux testing. The laboratory consists of three lasers—two different 3.5-kW lasers and a 1.5-kW laser that has a 7.5-kW enhanced pulse capability—as well as a variety of test stations. These industrial carbon dioxide lasers deliver energy at 10.6 μm, an ideal wavelength for testing zirconia-based or other oxide ceramics because these ceramics tend to be opaque to that wavelength.

The laser rigs can achieve engine-level transient and steady-state temperature and thermal gradients. A wide variety of test configurations have been employed, with the most important configuration to date involving the high-heat-flux testing of 1-in.-diameter buttons of the type typically used for furnace testing. A

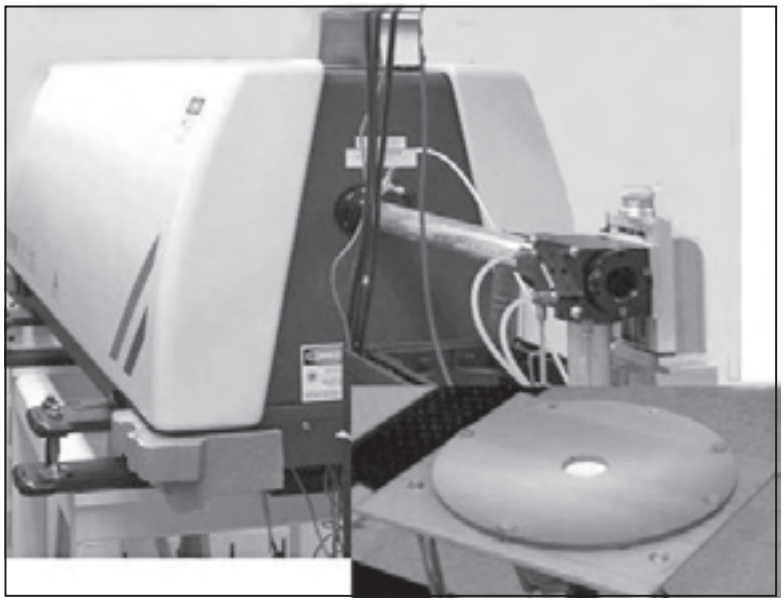

*One of the 3.5-kW laser rigs at Glenn. The inset shows the stainless steel specimen holder that sandwiches a 1-in.-diameter test coupon that is held by loops of platinum wire.*

variety of laser beam heating patterns have been employed, including uniform, trapezoidal, and gaussian—with the latter pattern being similar to the heating pattern from a torch test.

The term “trapezoidal” refers to the cross section of a heating pattern that is uniform over a central region (for example, 0.75 in.) and that tapers to low power toward the edge of the specimen. If considered in three dimensions, this geometry can also be referred to as a “truncated cone.” The uniform and trapezoidal heating patterns employ a faceted integrating lens combined with specimen or lens rotation to even out irregularities in the beam pattern that are caused by diffraction. The maximum heat flux that can be delivered to

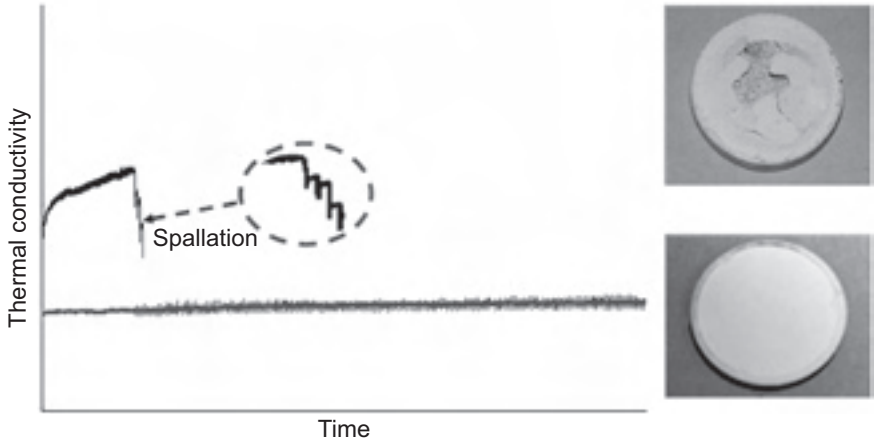


*Example of thermal conductivity—measured in the laser rig—of two specimens, one that held up very well to the high-temperature exposure and another that failed during testing.*

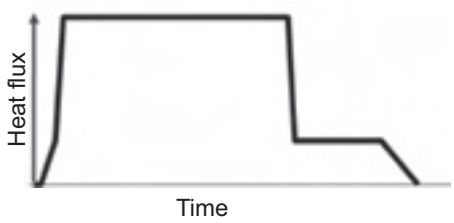


*Example of a controlled heating rate approximating the heating profiles in a gas turbine engine.*

the specimen generally increases as the heating pattern is changed from uniform to trapezoidal to gaussian. As a point of reference, the trapezoidal beam configuration can routinely pass a heat flux of about $0.7\times10^6$ Btu/hr-ft$^2$ (220 W/cm$^2$) through the specimen, and this could be increased to approximately $1.0\times10^6$ Btu/hr-ft$^2$ (315 W/cm$^2$) with modification to the beam delivery and backside cooling systems. Also, thinner substrates and substrate roughness facilitate the removal of the higher heat fluxes from the backsides of the specimens.

In addition to durability testing, the rigs are usually used to measure thermal conductivity. The uniform beam configuration provides the most straightforward measurement of conductivity. However, other beam geometries can also be used for conductivity measurement of calibration to correct for the loss of one-dimensional heat-transfer conditions. One benefit from recording conductivity is that the plot of conductivity versus time is an excellent way to monitor specimen health. An increasing plot of conductivity versus time generally indicates sintering, whereas a decreasing plot generally indicates delamination cracking.

The rigs have proven to be especially useful for qualifying combustor-section thermal barrier coatings for engine tests. They can readily achieve and accurately monitor the required combustor-level heat fluxes and the thermal conditions of coatings and substrates in an engine. Also, one of the rigs can be configured to allow ramped heating to represent the heating rates that the coating would

experience in the engine, and an intermediate-level heat flux that represents idle conditions can be programmed. As a result, a heating profile can mimic the actual exposure of coatings in a gas turbine engine. This year, the rigs helped engine designers to qualify coating vendors, to demonstrate coating system durability, and to determine appropriate coating thicknesses. They also provided thermal conductivity versus time-at-temperature design data.

**Find out more about the research of Glenn's Durability and Protective Coatings Branch:**
http://www.grc.nasa.gov/WWW/EDB/

**Glenn contacts:**
Dr. Robert A. Miller, 216–433–3298, Robert.A.Miller@nasa.gov; and
Dr. Dongming Zhu, 216–433–5422, Dongming.Zhu@nasa.gov

**Authors:**
Dr. Robert A. Miller and Dr. Dongming Zhu

**Headquarters program office:**
Aeronautics Research

**Programs/Projects:**
VSP, UEET

## Delamination-Indicating Thermal Barrier Coatings Using a Luminescent Sublayer Implemented Successfully

Although thermal barrier coatings (TBCs), most commonly composed of yttria-stabilized zirconia (YSZ), provide beneficial thermal protection for turbine engine components, the risk of premature failure compromises the reliability of TBCs. Nondestructive diagnostic tools that could reliably assess the damage state of TBCs would alleviate the risk of premature TBC failure by indicating when the TBC needed to be replaced before the level of TBC damage threatened engine performance or safety. To meet this need, researchers at the NASA Glenn Research Center in collaboration with Penn State University successfully implemented a new TBC coating design that is self-indicating for delamination.

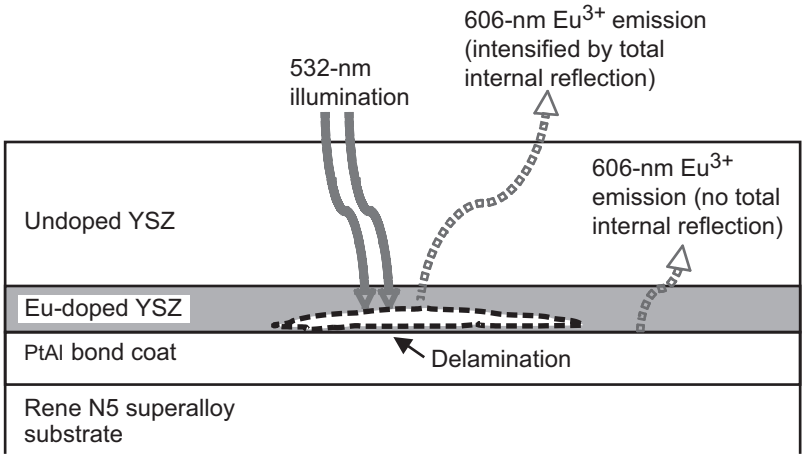


*Concept for a TBC that is self-indicating for delamination. This TBC is translucent to 532-nm excitation, which excites europium ion ($Eu^{3+}$) emission at 606 nm from a buried Eu-doped layer. Emissions of 606-nm $Eu^{3+}$ through the overlying undoped YSZ are enhanced by delamination-crack-induced total internal reflection. PtAl, platinum aluminide.*

The figure on this page illustrates the concept of using luminescence sensing to detect TBC delamination. The YSZ TBC incorporates an initial sublayer that is doped with europium (Eu) below the overlying undoped YSZ. Strong luminescence at a wavelength of 606 nm (red) from the buried Eu-doped layer can be excited by a 532-nm (green) wavelength excitation that travels through the overlying undoped YSZ. Luminescence enhancement occurs when delamination cracks occur within or below the Eu-doped layer (see the figure). The enhanced luminescence arises because of the total internal reflection of a large fraction of both the excitation and emission radiation at the interface between the Eu-doped layer and the delamination crack.

TBCs with a 7-μm-thick Eu-doped YSZ sublayer beneath a 125-μm undoped YSZ overlayer were deposited by multiple-ingot electron-beam physical-vapor deposition without disrupting TBC growth. To demonstrate delamination indication, researchers induced a localized TBC delamination by scratching the coating with a stylus. The delaminated region can be faintly discriminated in

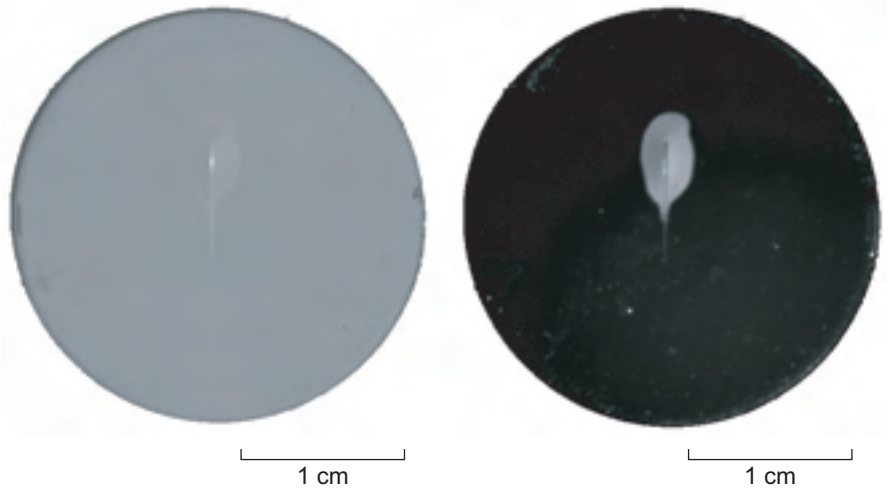


*Delamination-indicating thermal barrier coating. Enhanced $Eu^{3+}$ 606-nm luminescence detected from scratch-induced delaminated region. The TBC consists of a 7-μm-thick Eu-doped YSZ sublayer beneath a 125-μm undoped YSZ overlayer. Left: White light image. Right: $Eu^{3+}$ luminescence image.*

a standard white light image (see the left image), but it stands out strongly in a luminescence image because of the greatly enhanced red emission originating from that area (see the right image). Luminescence imaging was very simple to implement and can be achieved by using only a light-emitting diode (LED) illumination source and a camera with a bandpass filter. High-resolution luminescence images were obtained within a few seconds that immediately identified regions of TBC delamination that would otherwise be difficult to detect, thereby showing great promise for the routine inspection of TBCs. Funding for this work was provided by the Propulsion 21 Thermal Management and Advanced Cooling Task.

**Find out more about the research of Glenn's Durability and Protective Coatings Branch:**
http://www.grc.nasa.gov/WWW/EDB/

**Glenn contacts:**
Dr. Jeffrey I. Eldridge, 216–433–6074, Jeffrey.I.Eldridge@nasa.gov; and Timothy J. Bencic, 216–433–5690, Timothy.J.Bencic@nasa.gov

**Authors:**
Dr. Jeffrey I. Eldridge and Timothy J. Bencic

**Headquarters program office:**
Aeronautics Research

**Programs/Projects:**
Propulsion 21, UEET

## NiCrAlY and CuCr Protective Coatings Tested for Copper-Based Thrust Chambers

Copper-chromium (CuCr) and nickel-chromium-aluminum-yttrium (NiCrAlY) coatings were applied by kinetic metallization to GrCop-84 substrates (an advanced copper-based alloy developed at the NASA Glenn Research Center specifically for rocket thrust chambers, ref. 1). The coatings showed excellent cyclic oxidation behavior at 600 °C. In addition, the CuCr coatings showed excellent compatibility with the GrCop-84 substrates during thermal exposures. Similarly, when a CuCrAl bond coat was used with the NiCrAlY coating, the two-layer coating also showed excellent compatibility with the GrCop-84 substrate. Both coatings show outstanding potential to provide oxidation protection for copper-based rocket thrust chambers.

Advanced rocket thrust chambers, such as those on the Space Shuttle Main Engines, are made of copper-based alloys possessing both high strength and high thermal conductivity. Although the high thermal conductivity allows the cryogenic fuel to cool the copper alloy, a thin oxide scale forms on the surface exposed to the hot gas. Because the gases flowing in the combustion chamber are extremely turbulent, this thin oxide scale can be repeatedly reduced to metallic copper and reoxidized in a process known as "blanching," which can weaken the chamber lining. Consequently, coatings were explored to provide oxidation protection for higher temperature use and to eliminate this blanching effect.

CuCr coatings form a protective oxide scale based on chromium oxide ($Cr_2O_3$) that is extremely stable and able to protect thrust chambers from blanching attack (ref. 2). NiCrAlY coatings, used routinely to provide oxidation protection in aeroengines, form protective alumina scales with even greater stability than $Cr_2O_3$ and, consequently, are not

susceptible to blanching. Various coating techniques have been explored to deposit NiCrAlY and CuCr coatings on copper-based thrust chambers. One technique is kinetic metallization—an impact consolidation process in which solid-state metallic powders are deposited without melting to produce a coating (ref. 3). An inert carrier gas, commonly helium, is used to accelerate the powder particles through a specially designed sonic nozzle to velocities just below the sonic speed of the gas. Since the powder particles are deposited at low temperatures and in an inert gas, there is almost no oxidation of the powder or substrate during deposition, an important consideration for coating copper-based components.

For any coating, a prime concern is adherence of the coating to the substrate. The best adherence results when strong metallurgical bonds form. Short diffusion anneals can allow interdiffusion between the coating and substrate strengthening this bond. However, for certain materials, interdiffusion can result in the formation of porosity, known as Kirkendall porosity, at or near the interface, which can degrade coating adherence. In addition to thermal exposure during operation, thrust chambers often undergo a higher temperature thermal exposure during fabrication associated with the brazing operation that attaches the liner to an outer jacket. This brazing operation, although short, is typically several hundred degrees higher than the normal chamber operating temperature and results in the greatest amount of interdiffusion.

Kinetic metallization coatings were deposited on coupons of GrCop-84 by Innovative Technologies, Inc. (Inovati), of Goleta, California. NiCrAlY coatings, with and without a bond coat, as well as three CuCr coatings were deposited and evaluated. Both NiCrAlY and the CuCr coatings showed excellent oxidation behavior during thermal cycling at 600 °C (see the graph). In agreement with earlier results for similar CuCr coatings (ref. 4), none of the coated samples showed any weight loss, in contrast to results for the uncoated copper alloy. After a simulated braze anneal (950 °C for 30 min), significant porosity developed when the NiCrAlY was deposited directly on the substrate (see the left image below). However, when a CuCrAl bond coat was deposited prior to the NiCrAlY coating, no porosity developed after annealing (see the center image). Similarly, the CuCr coatings showed excellent compatibility with the GrCop-84 substrates during thermal exposures, with no porosity observed after annealing (see the right image). Consequently, both coating systems, NiCrAlY with a CuCrAl

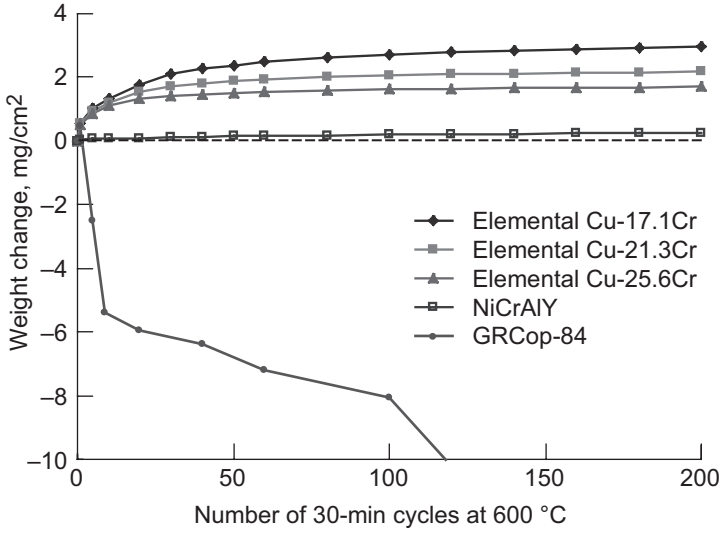


*Weight change during thermal cycling at 600 °C for NiCrAlY and three blended elemental CuCr coatings compared with that of uncoated GrCop-84.*

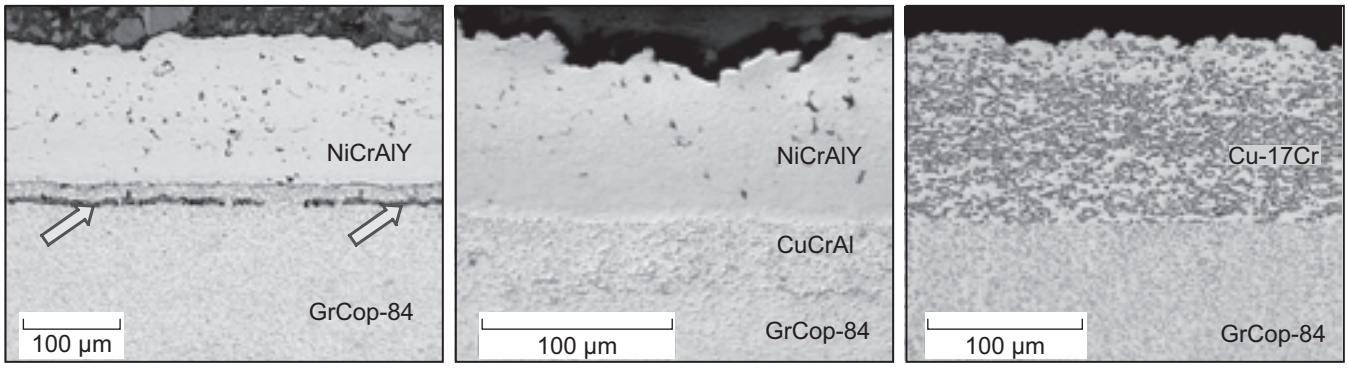


*Microstructure of the coated GrCop-84 substrate after a simulated braze anneal of 950 °C for 30 min. Left: NiCrAlY applied directly on GrCop-84. Porosity indicated by arrows. Center: NiCrAlY with CuCrAl bond coat. Right: CuCr applied directly on GrCop-84.*

bond coat, and CuCr coatings demonstrate excellent potential for protecting copper-based rocket thrust chambers from oxidation.

**References**


1. Veazey, Matthew V.: A Paradigm Shift for Process Control? Mater. Perf., vol. 43, no. 12, 2004, pp. 16–19.
2. Chiang, K.T.; Krotz, P.D.; and Yuen, J.L.: Blanching Resistant Cu-Cr Coating by Vacuum Plasma Spray. Surf. Coat. Technol., vol. 76–77, 1995, pp. 14–19.
3. Robinson, T.: Coatings: Kinetic Metallization. 2004 MDA Technology Applications Report, Missile Defense Agency, Advanced Applications Program, 2004, pp. 36–37. http://www.inovati.com/pages/tech/pubs/publications.html#Papers
4. Ogbuji, Linus U.: Oxidation Behavior of Cu-Cr Environmental Barrier Coatings on Cu-8Cr-4Nb. Surf. Coat. Technol., vol. 197, nos. 2–3, 2005, pp. 327–335.


**Find out more about the research of Glenn's Durability and Protective Coatings Branch:**
http://www.grc.nasa.gov/WWW/EDB/


**Glenn contact:**
Dr. James A. Nesbitt, 216–433–3275, James.A.Nesbitt@nasa.gov

**Author:**
Dr. James A. Nesbitt


**Headquarters program office:**
Space Exploration

**Programs/Projects:**
Constellation Systems

## Probabilistic Fracture Strength of High-Aspect-Ratio Silicon Carbide Microspecimens Predicted

Single-crystal silicon carbide (SiC) microsized tensile specimens were fabricated with deep reactive ion etching (DRIE) in order to investigate the effect of stress concentration on the room-temperature fracture strength. This was of interest because microsized turbomachinery that are being developed for power and propulsion applications rotate at very high revolutions per minute and, hence, operate with very high stresses. SiC is an excellent material choice for these harsh environment applications because of its ability to maintain strength, resist creep, and resist oxidation at gas turbine operating temperatures. At the NASA Glenn Research Center, researchers developed SiC microfabrication technology as well as characterization and life-prediction design methodology.

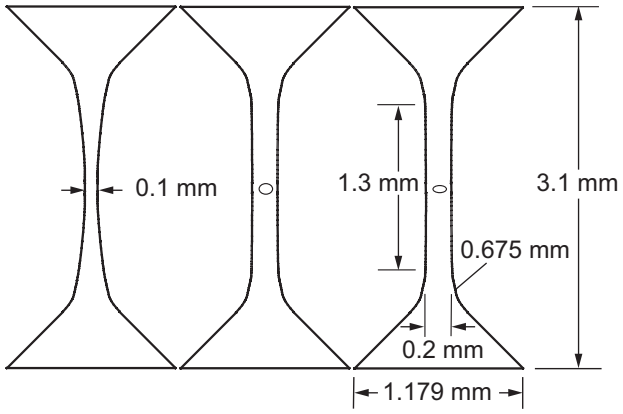


*Basic schematic of the dogbone microtensile specimens (not to scale). The gauge section is 1.3 mm long. Left: Curved, without a central hole feature. Center: Circular hole. Right: Elliptical hole.*

Our testing program had three purposes:

(1) Demonstrate the fabrication of simple structures—microtensile specimens in this case—that have high aspect ratios (vertical dimension or etch depth divided by lateral feature size) with sufficient strength, surface finish, and dimensional tolerance suitable for PowerMEMS (microelectromechanical systems for electrical power generation). A highly directional DRIE process was used to fabricate the specimens.

(2) Correlate process improvements with fracture strength response, where the fracture strength is defined as the level of stress at the highest stressed location in the structure at the instant of specimen rupture.

(3) Test how well the Weibull probabilistic distribution predicts the strength of miniature SiC components. This was done with specimen geometries with various levels of stress concentration and tested a fundamental premise of Weibull theory—that strength increases as the area (or volume) under the highest stress decreases.

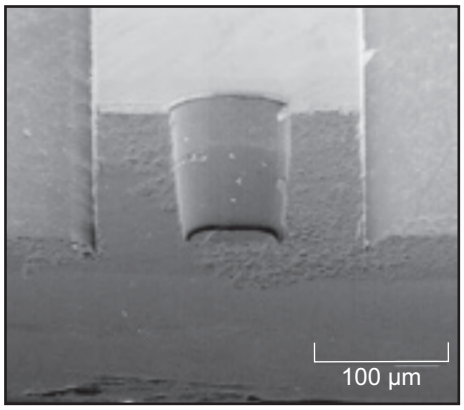


*Cross section of a single-crystal SiC test specimen with a circular hole etched to a depth of 140 μm, as observed using a scanning electron microscope. The nickel mask is at the top. Notice the through-the-thickness variation in width of the circular hole.*

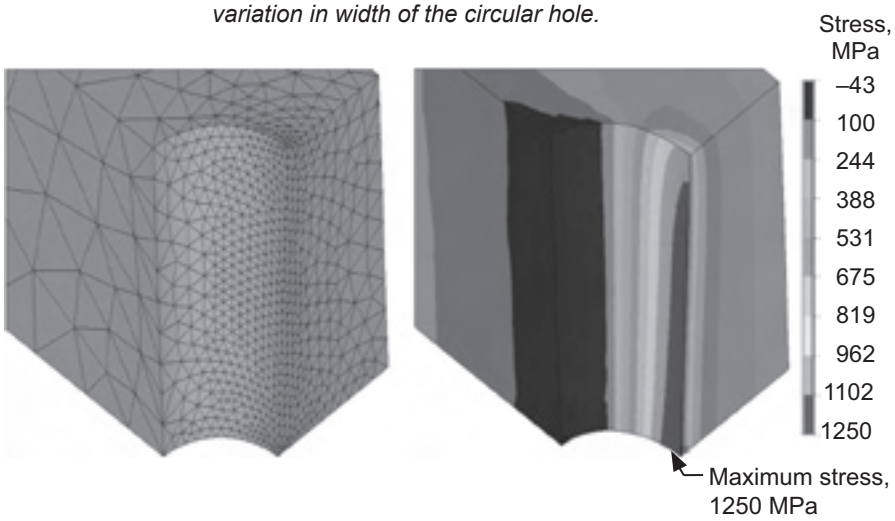


*Left: Example quarter-symmetry mesh. Right: Principal stress solution for the circular-hole specimen. Minimum stress, –43 MPa; maximum stress, 1250 MPa. This figure is shown in color in the online version of this article (http://www.grc.nasa.gov/WWW/RT/2005/RX/RX13L-nemeth.html).*

Specimens without a hole (and hence, with no stress concentration), with a circular hole, and with an elliptical hole were fabricated (see the drawing on the preceding page). The microtensile specimens had significant specimen-to-specimen variations and through-the-thickness variations in dimensions because of the fabrication process (see the photograph above). To account for the specimen-to-specimen variation in strength due to the variable severity of flaws from the etching process and for specimen-to-specimen through-the-thickness variations in dimensions (each specimen had different dimensions, and the dimensions changed from the top to the bottom of each specimen), researchers used the Glenn-developed Ceramics Analysis and Reliability Evaluation of Structures—Life (CARES/*Life*) code with the ANSYS Probabilistic Design System (PDS) to predict the strength response of the specimens with stress concentration. Several hundred trials were run with ANSYS PDS with varying specimen dimensions (see the grid and plot, bottom figure, for an example of a finite element mesh and stress solution of a specimen from ANSYS PDS), and CARES/*Life* was used to predict fracture strength from each trial.

The graph on the next page shows the results from the CARES/*Life* and ANSYS PDS simulations. Simulation results that used the curved specimen geometry strength response as a baseline to predict the strength of the specimens with stress concentration showed good correlation for the circular-hole specimen geometry and some overprediction of the strength of the elliptical-hole specimens. The overprediction of strength for the elliptical hole specimens was likely due to inaccuracies of the stress solution for the highly localized stresses near irregular surfaces. Overall, these results tend to support using the Weibull distribution for the design and analysis of SiC microelectromechanical systems (MEMS) if an accurate stress solution can be obtained. Furthermore, the use of CARES/*Life* with ANSYS PDS demonstrated that component-level life prediction can be performed in a fully probabilistic design space.

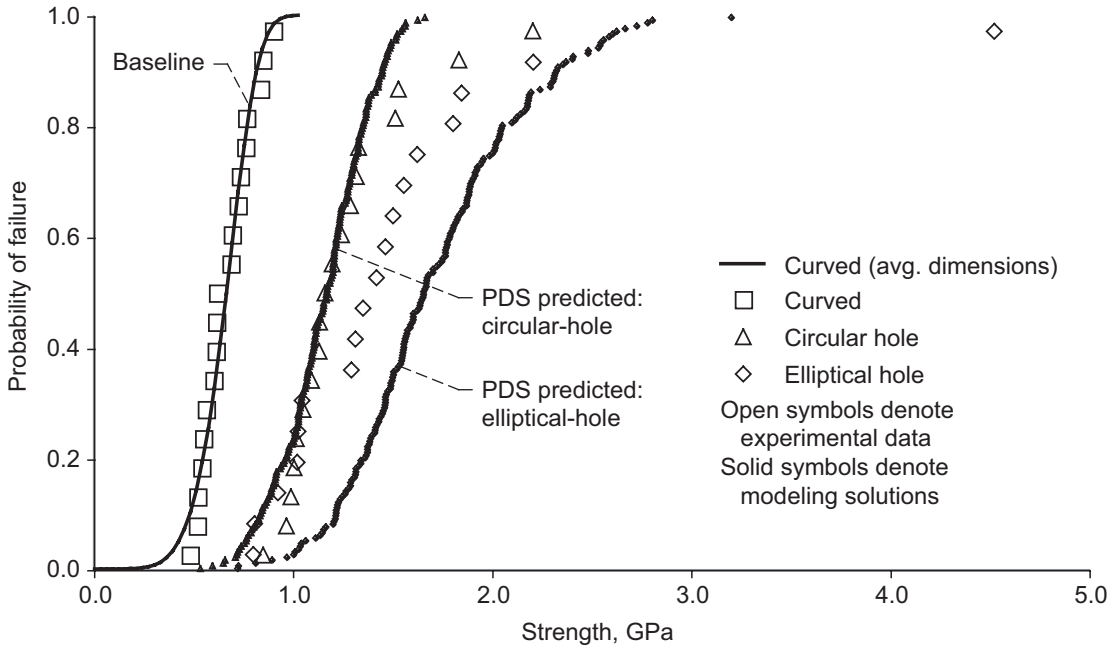


*Cumulative distribution plot of CARES/Life and ANSYS PDS Monte-Carlo simulation results for the circular-hole and elliptical-hole specimens compared with experimental data. The Weibull parameters estimated from the curved specimen data were used as a baseline to predict the strength response of the other specimen geometries.*

**Glenn contacts:**
Noel N. Nemeth, 216–433–3215, Noel.N.Nemeth@nasa.gov; and
Dr. Glenn M. Beheim, 216–433–3847, Glenn.M.Beheim@nasa.gov

**Authors:**
Noel N. Nemeth, Laura J. Evans, Prof. Osama M. Jadaan, Prof. William N. Sharpe, Dr. Glenn M. Beheim, and Mark A. Trapp

**Headquarters program office:**
Aeronautics Research

**Programs/Projects:**
AEFT, UEET

## Numerical Analysis Methods Developed for Predicting the Oxidation Behavior in Carbon Silicon-Carbide Composite Structures

Carbon silicon-carbide composites (C/SiC) have been proposed for a variety of future spacecraft applications such as liquid engine combustion chambers, control surfaces, and thermal protection for reentry vehicles. The ability of C/SiC to maintain its strength and stiffness at high temperatures as well as its low density make it an attractive candidate material for these high-temperature applications. One shortcoming of C/SiC is that, in the presence of oxygen, the carbon fibers and pyrocarbon fiber coating will oxidize at elevated temperatures, limiting the durability and useful life of the C/SiC component. The susceptibility of C/SiC to oxidation degradation does not forbid its use in future launch vehicle applications, as long as it can be verified through testing and analysis that the component will maintain its strength and stiffness throughout its service life, with the demonstration of sufficient safety factors.

The physics of carbon oxidation is well understood, and equations to define the dependence of the rate of oxidation with temperature and oxygen partial pressure have been long established (refs. 1 and 2). However, since the temperature and stress state vary within the C/SiC component and since the local oxygen vapor pressure is tied to the stress state through the process of diffusion, the temperature and local oxygen partial pressure, and thus the oxidation rates,

will vary within a C/SiC component. For designers to use C/SiC components in future spacecraft applications, they need a design analysis tool that can determine the spatial distribution of the extent of oxidation and the resulting residual strength and stiffness in the C/SiC component as a function of the time, temperature, and environmental oxygen concentrations to which the C/SiC structure is exposed.

A numerical method to predict the oxidation behavior and oxidation patterns in C/SiC composite structures was developed at the NASA Glenn Research Center from the mechanics of the flow of ideal gases through a porous solid (ref. 3). The application of flow-through-porous-media theory to the C/SiC oxidation problem results in a set of two coupled nonlinear differential equations written in terms of the partial pressures of the oxidant and oxide. The differential equations are solved simultaneously at discrete time steps, and utilizing a suitable time-marching scheme, the partial vapor pressures of the oxidant and oxides are obtained as a function of the spatial location and time. The local rate of carbon oxidation is determined using the map of the local oxidant partial vapor pressure along with the Arrhenius rate equation. The nonlinear differential equations are cast into matrix equations by applying the Bubnov-Galerkin weighted residual method, allowing for the solution of the differential equations numerically.

Thus far, the numerical method has been utilized to model the carbon oxidation and weight loss behavior of C/SiC specimens during thermogravimetric experiments. It successfully reproduced the influence of temperature on the rate of carbon oxidation (see the top figure). In addition, it replicated the profound influence of temperature on the oxidation pattern (see the bottom figure), which has been observed in other experimental studies.

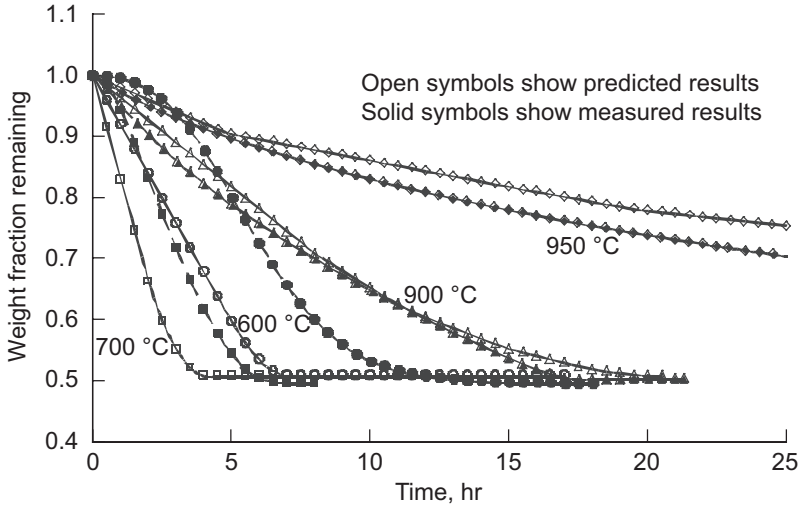


*Comparison of predicted and measured carbon weight fraction versus time for thermogravimetric analysis specimens at various temperatures.*

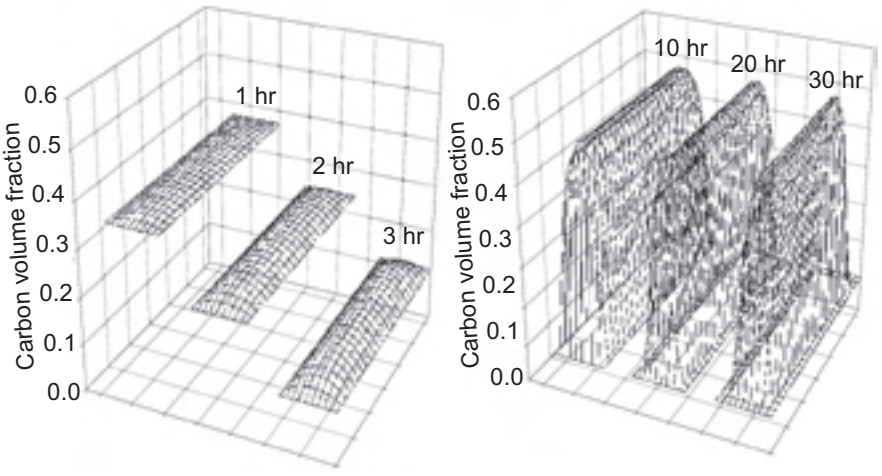


*Spatial distribution of carbon volume fraction at various times within an interior section of a prismatic C/SiC specimen of rectangular cross section. Results show the effect of temperature on the carbon fiber volume distributions. Left: Test conducted at 700 °C. Right: Test conducted at 950 °C.*

**References**

1. Gulbransen, E.A.; Andrew, K.F.; and Brassart, F.A.: The Oxidation of Graphite at Temperatures of 600 °C to 1500 °C and at Pressures of 2 to 76 Torr of Oxygen. J. Electrochem. Soc., vol. 110, no. 6, 1963, pp. 476–483.
2. Ismail, I.M.K.: On the Reactivity, Structure, and Porosity of Carbon-Fibers and Fabrics. Carbon, vol. 29, 1991, pp. 777–792.
3. Sullivan, Roy M.: A Model for the Oxidation of Carbon Silicon Carbide Composite Structures. Carbon, vol. 43, no. 2, 2005, pp. 275–285.

**Glenn contact:**
Dr. Roy M. Sullivan, 216–433–3249, Roy.M.Sullivan@nasa.gov

**Author:**
Dr. Roy M. Sullivan

**Headquarters program office:**
Aeronautics Research

**Programs/Projects:**
NGLT

**Special recognition:**
Best Paper Award 2005 for Glenn's Materials and Structures Division

# Design Analysis Methods Developed for Carbon-Fiber-Reinforced Silicon-Carbide Composite Structures

Carbon-fiber-reinforced silicon-carbide (C/SiC) composite technologies are being developed and advanced with the notion that they will find widespread use in the aerospace industry in the near future. Potential applications include turbine blades, combustion chambers, control surfaces, and thermal protection systems. Indeed, C/SiC composites are an attractive option for designers of advanced spacecraft and advanced space propulsion systems, since C/SiC composites are lightweight and maintain their strength and stiffness at high temperatures.

However, many challenges must be overcome to advance C/SiC composite technologies. These composites are vulnerable to carbon fiber oxidation from environmental oxygen attack. Matrix microcracks formed during the fabrication process and a significant pore volume due to insufficient infiltration provide a free path for oxygen to attack the carbon fibers, resulting in the loss of carbon fibers and thus a reduction in composite strength and stiffness. Other obstacles are that the material's stress-strain response is nonlinear even at low stress levels and that the material responds to stress differently in tension than compression. These problems are not unrelated to the carbon oxidation problem. They all arise from the fact that the SiC matrix in C/SiC composites is usually severely cracked in the as-processed state. The nonlinear stress-strain response, the temperature-dependent properties, and the dissimilar response to tension and compression loading all complicate the structural analysis of components made of C/SiC composites.

The objective of this work was to develop analysis methods that incorporate analytical material models into a structural solution routine. In this way, the complex material behavior that is inherent to C/SiC composite materials is accounted for in the structural analysis solution. Micromechanics-based material models were developed at the NASA Glenn Research Center for predicting the response properties of two C/SiC composites: a two-dimensional plain weave and a three-dimensional woven angle interlock architecture. The micromechanics-based material models were calibrated by correlating the predicted material response properties with the measured properties.

Four-point beam-bending subelement specimens were fabricated with these two fiber architectures, and four-point bending tests were performed at room temperature and at 2000 °F. Displacements and strains were measured at various locations along the beam and recorded as a function of load magnitude. The calibrated material models were used in concert with a nonlinear finite-element solution using the ABAQUS (ABAQUS, Inc., Providence, RI) finite-element code to simulate the structural response of these two materials in the four-point beam-bending tests. The structural response predicted by the nonlinear analysis method, limited to an inert environment in this work, compared favorably with the measured response for both materials and for both test temperatures. Results showed that the material models scale up fairly well from the coupon to the subcomponent level. This approach presents an integrated analysis, material model development, and test approach that is providing the basic understanding necessary to characterize and utilize these materials in various aerospace applications.

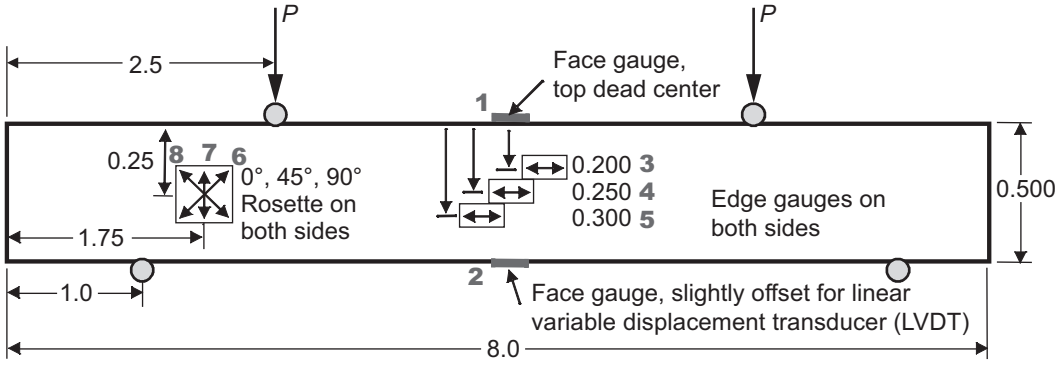


*Four-point flexure subelement showing loading and strain gauge locations. All dimensions given in inches unless indicated otherwise.*

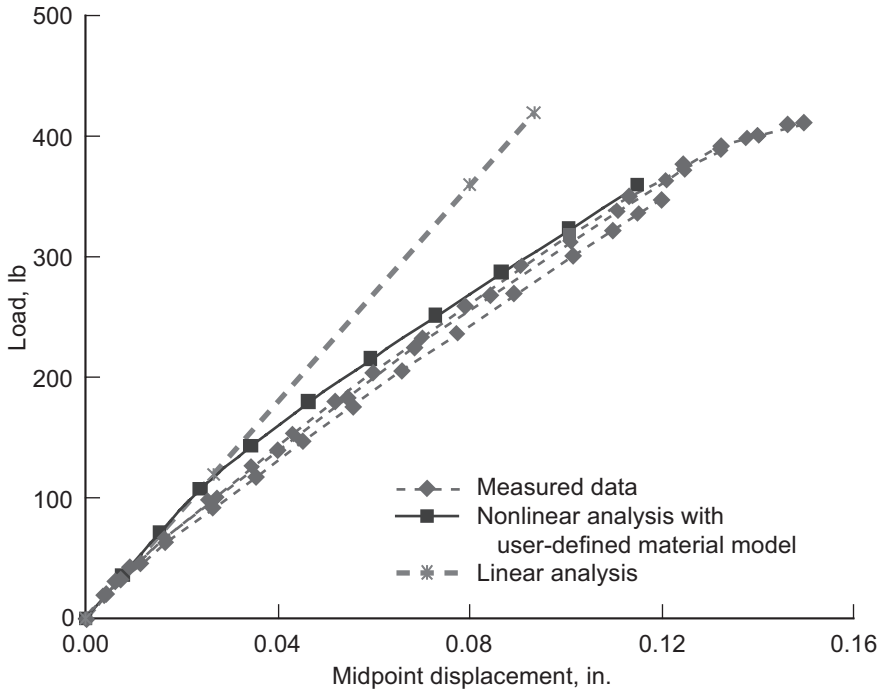


*Load versus midpoint displacement of a two-dimensional, quasi-isotropic, four-point flexure specimen at room temperature.*

**Glenn contact:**
Dr. Roy M. Sullivan, 216–433–3249,
Roy.M.Sullivan@nasa.gov

**Authors:**
Dr. Subodh K. Mital and
Dr. Roy M. Sullivan

**Headquarters program office:**
Aeronautics Research

**Programs/Projects:**
NGLT

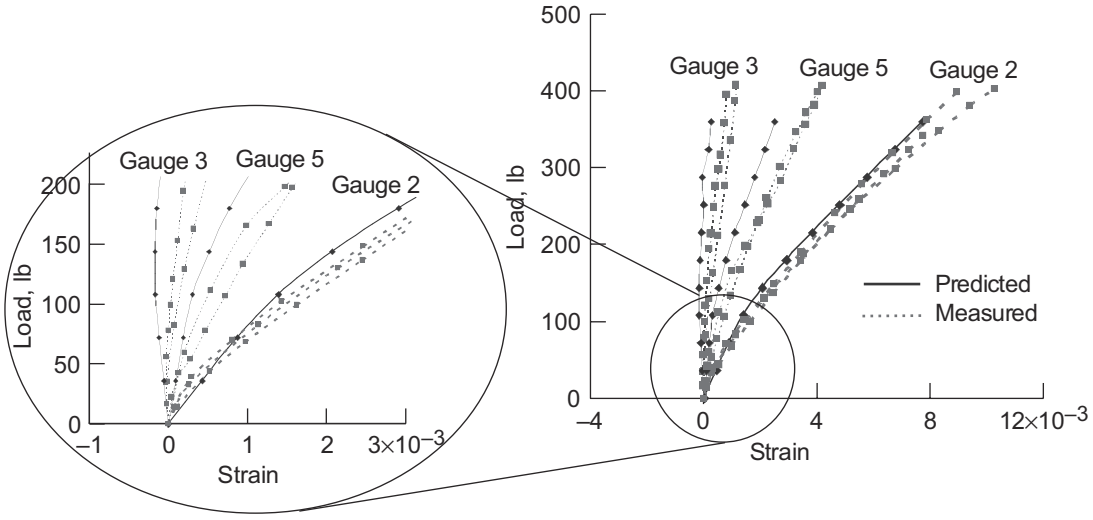


*Load versus strain at gauges 2, 3, and 5 for a two-dimensional, quasi-isotropic, four-point flexure specimen at room temperature.*

# Advanced SiC/SiC Ceramic Composite Systems Developed for High-Temperature Structural Applications

The NASA Glenn Research Center has developed advanced silicon carbide (SiC) fiber-reinforced SiC-matrix composite systems that can operate for hundreds of hours under stress at temperatures to 1450 °C (2640 °F) and above. These SiC/SiC systems are designed to be lightweight (~30 percent of metal density) and, in contrast to monolithic ceramics and carbon-fiber-reinforced ceramic composites, to reliably retain their structural properties for long times under aggressive high-temperature environments. The key to developing these systems was to first understand the process-structure-property relationships for their potential commercial constituents: fiber, fiber architecture, fiber interphase coating, and matrix, and then to use this understanding to develop advanced processes that significantly improve the thermostructural performance of the constituents.

These advancements were achieved in a series of steps. First, Glenn researchers gained an understanding of the materials and process relationships for available SiC fibers. Then, they developed processes that convert commercial Sylramic fibers into Sylramic-iBN SiC fibers that display thermal stability to over 1700 °C, high tensile strength, high creep-rupture resistance, and high thermal conductivity, and that possess a thin in situ grown boron nitride (BN) surface layer for added environmental durability (ref. 1). Further capability was derived by understanding how the Sylramic-iBN fibers can be arranged in certain fiber architectures to provide thin-walled backside-cooled SiC/SiC components with desirable in-plane and through-the-thickness thermostructural properties (ref. 2).

Next, the interphase coatings for the Sylramic-iBN fibers were addressed. Because commercial chemical vapor infiltration (CVI) for conventional BN coatings is done at relatively low temperatures, Glenn needed to develop advanced processes that produce BN-based coatings that are more thermally, dimensionally, and environmentally stable, but still retain the prime interphase requirement of weak bonding with the Sylramic-iBN fiber (ref. 2).

Finally, although SiC matrices produced by CVI can provide SiC/SiC composites with good thermal conductivity and creep-rupture resistance, these properties are not optimum because current commercial CVI processes are typically performed near 1000 °C, resulting in nonstoichiometric matrix microstructures containing free silicon and high porosity. These problems were minimized through the development of (1) annealing treatments that effectively eliminate the free silicon, and (2) polymer-infiltration and pyrolysis (PIP) processes that fill the pore content with stoichiometric SiC, thereby allowing temperatures above silicon's melting point (1410 °C) (refs. 2 and 3).

The table lists some key thermostructural properties for two advanced SiC/SiC systems fabricated into thin-walled panels using Glenn's constituent technologies. System A was produced by the more conventional two-dimensional approach of fabric layup, whereas System B uses a 2.5-dimensional architecture with a low content of Sylramic-iBN fibers running through the panel thickness. Both systems display excellent in-plane strength and creep-rupture properties up to 1450 °C, but System B shows much

TYPICAL PROPERTIES FOR ADVANCED SiC/SiC COMPOSITE PANELS FABRICATED USING GLENN-DEVELOPED CONSTITUENT MATERIALS AND PROCESSES

| Property | System A | System B |
|---|---|---|
| Upper-use temperature, °C | 1450 | 1450 |
| Architecture | 2-dimensional, 0°/90° layup | 2.5-dimensional, woven |
| Matrix | CVI+PIP SiC | CVI+PIP SiC |
| Elastic modulus at room temperature, GPa | 190 | 190 |
| Proportional limit strength at room temperature, MPa | 150 | 150 |
| Ultimate strength at room temperature, MPa | 380 | 360 |
| Through-the-thickness strength at room temperature, MPa | 10 | 25 |
| Through-the-thickness conductivity, W/m-K | | |
| Room temperature | 28 | 55 |
| 600 °C | 23 | 36 |
| 1200 °C | 12 | 26 |
| Creep strain at 69 MPa for 300 hr at 1450 °C, percent | ~0.2 | ~0.2 |
| Rupture life at 69 MPa in air at 1450 °C, hr | >500 | >500 |

higher through-the-thickness strength and thermal conductivity because of the use of state-of-the-art Sylramic-iBN fiber through the panel wall. These Glenn technologies are available for transfer under a NASA Space Act Agreement. Approaches for scale up, and further improvements have been identified.

**References**

1. DiCarlo, James A.; and Yun, Hee Mann: New High-Performance SiC Fiber Developed for Ceramic Composites. Research & Technology 2001, NASA/TM—2002-211333, 2002, pp. 8–9. http://www.grc.nasa.gov/WWW/RT2001/5000/5100dicarlo1.html
2. Yun, Hee Mann; DiCarlo, James A.; and Bhatt, Ramakrishna T.: Advanced SiC/SiC Ceramic Composites for Airbreathing and Rocket Propulsion Engine Components. Proceedings of JANNAF Conference, Charleston, SC, June 2005.
3. Bhatt, Ramakrishna T.; and DiCarlo, James A.: Method Developed for Improving the Thermomechanical Properties of Silicon Carbide Matrix Composites. Research & Technology 2003, NASA/TM—2004-212729, 2004, pp. 20–21. http://www.grc.nasa.gov/WWW/RT/2003/5000/5130bhatt.html

**Glenn contact:**
Dr. James A. DiCarlo, 216–433–5514, James.A.DiCarlo@nasa.gov

**Authors:**
Dr. James A. DiCarlo, Dr. Hee Mann Yun, and Dr. Ramakrishna T. Bhatt

**Headquarters program office:**
Aeronautics Research

**Programs/Projects:**
IR&D

## Cumulative Fatigue Behavior Investigated for a Woven, Melt-Infiltrated SiC/SiC Composite

Advanced gas turbine engines will operate at higher temperatures than current engines to improve engine efficiency. Consequently, the designers of these engines need materials that can withstand elevated temperatures and provide sustained performance. Ceramic matrix composites (CMCs) are the preferred class of materials because of their high-temperature capability and high specific strength. In fact, a woven, melt-infiltrated SiC/SiC composite was identified as a candidate combustor liner material for advanced gas turbine engines (ref. 1). Since gas turbine engine components are subjected routinely to cyclic loads at elevated temperatures, the fatigue durability of the CMC needed to be characterized under different mechanical loading conditions and temperatures.

At the NASA Glenn Research Center, the cumulative fatigue behavior of the candidate material, a woven, melt-infiltrated SiC/SiC composite, was investigated. The influence of R-ratio (minimum load/maximum load in a cycle) on the fatigue life of the woven SiC/SiC composite (manufactured in September 1999 and designated as N22) was initially established by conducting fatigue tests at R-ratios of 0.05 and 0.50. Two test temperatures (1038 and 1204 °C) were used, and five tests were conducted for each temperature and R-ratio combination. Tensile properties of the CMC at these two temperatures are reported in reference 2. For all the fatigue tests, a maximum stress of 179 MPa (which is higher than the proportional limit strength of the CMC at both temperatures) and a frequency of 0.33 Hz were used. At both temperatures, higher R-ratio tests (with larger mean stresses) yielded longer fatigue lives than lower R-ratio tests (see the bar chart). The error bars in the bar chart represent observed scatter in the fatigue life data.

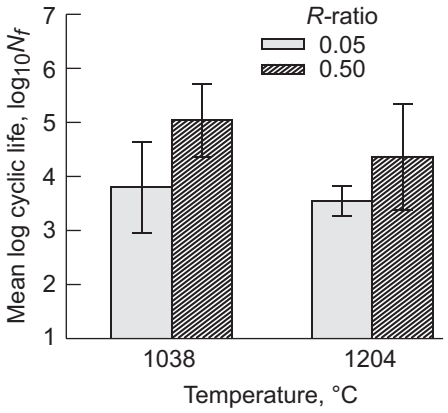


*Mean logarithmic fatigue lives and extreme values for the woven SiC/SiC composite. Maximum stress, 179 MPa; frequency, 0.33 Hz.*

Cumulative fatigue tests, at an R-ratio of 0.05 followed by an R-ratio of 0.50 on the same specimen, were subsequently conducted at the same two temperatures. In these tests, a life fraction $n_1/N_1$ (where $n_1$ is the number of applied cycles and $N_1$ is the previously established average cyclic life) of 0.1, 0.25, and so forth, was

first applied at an R-ratio of 0.05. Each test was then switched to an R-ratio of 0.50 and continued until the specimen failed or accumulated $10^6$ cycles (runout) at the second loading condition. The number of cycles sustained by the specimen at the second loading condition $n_2$ and the corresponding average cyclic life $N_2$ were used to calculate the second life fraction $n_2/N_2$ and to analyze the cumulative fatigue data (see the graph). In this graph, the initial life fraction $n_1/N_1$ is plotted against the sum of life fractions, $(n_1/N_1) + (n_2/N_2)$, from both loading conditions, and the upward arrow indicates a runout. Miner's linear damage rule, developed originally for metallic alloys, dictates that the sum of life fractions should be near unity for cumulative fatigue tests. For the loading conditions investigated, the majority of the cumulative fatigue data (except for two tests) were above unity, indicating that Miner's rule constituted a lower bound for this CMC in most cases.

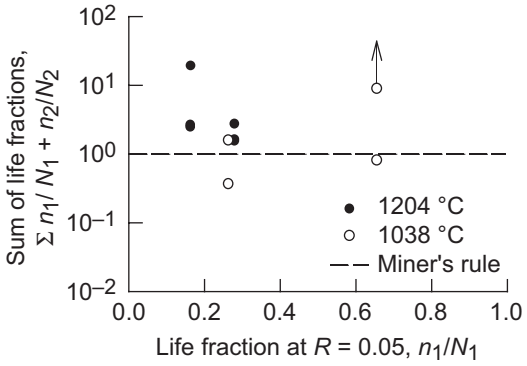


*Evaluation of the applicability of Miner's linear damage rule with cumulative fatigue results from the woven SiC/SiC composite.*


**References**

1. Brewer, David: HSR/EPM Combustor Materials Development Program. Materi. Sci. Eng., vol. A261, 1999, pp. 284–291.
2. Kalluri, Sreeramesh; Calomino, Anthony M.; and Brewer, David N.: Comparison of Elevated Temperature Tensile Properties and Fatigue Behavior of Two Variants of a Woven SiC/SiC Composite. Ceram. Eng. Sci. Proc. vol. 26, no. 2, 2005, pp. 303–310.



**Ohio Aerospace Institute (OAI) contact:**
Dr. Sreeramesh Kalluri, 216–433–6727, Sreeramesh.Kalluri@nasa.gov

**Glenn contact:**
Dr. Anthony M. Calomino, 216–433–3311, Anthony.M.Calomino@nasa.gov

**U.S. Army Research Laboratory at Glenn contact:**
David N. Brewer, 216–433–3304, David.N.Brewer@nasa.gov

**Authors:**
Dr. Sreeramesh Kalluri,
Dr. Anthony M. Calomino, and
David N. Brewer


**Headquarters program office:**
Aeronautics Research

**Programs/Projects:**
VSP

## Multicomponent Hafnia-Based Oxide Systems Developed, Characterized, and Evaluated for Advanced Ceramic-Matrix-Composite Barrier-Coating Applications

Advanced multicomponent thermal and environmental barrier coatings were developed at the NASA Glenn Research Center for low-emission SiC/SiC ceramic matrix composite (CMC) combustor liner and vane applications by extending the component temperature capability to 1650 °C (3000 °F) in oxidizing and water-vapor-containing combustion environments (refs. 1 to 4). The coating systems demonstrated improved phase stability, lower lattice and radiation thermal conductivity, and improved sintering and thermal stress resistance under simulated engine heat-flux and thermal cycling conditions. These improvements were due largely to the defect-clustering structures, which are purposely designed to promote the creation of thermodynamically stable oxide defect clusters and/or nanophases within the coating systems.

The top figure on the next page is a high-resolution transmission-electron-microscopy lattice image that reveals atomic-level defect clusters through moiré patterns in a plasma-sprayed multicomponent $HfO_2$-$(Y,Nd,Yb)_2O_3$ coating. This is the first time that defect clusters have been characterized and demonstrated for advanced $HfO_2$ systems.

As mapped in the left graph on the next page, the thermal conductivity of

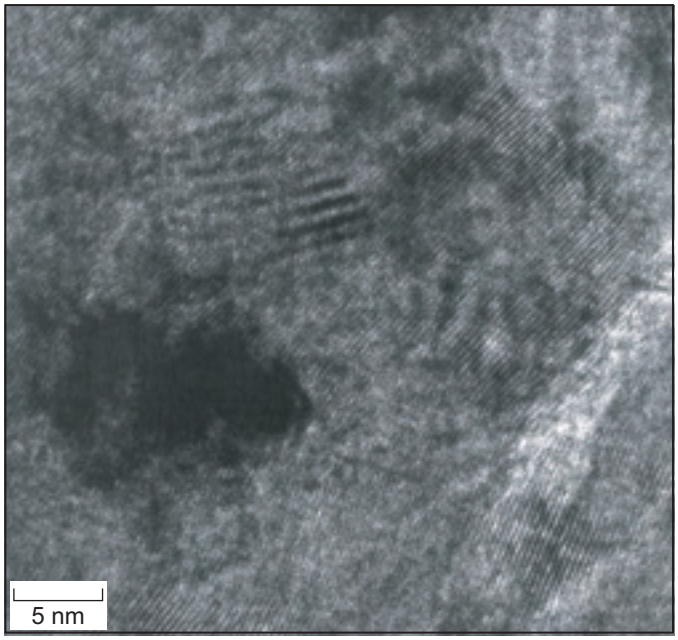


*High-resolution transmission-electron-microscopy lattice image with moiré patterns that indicate defect clusters in a plasma-sprayed $HfO_2$-$(Y,Nd,Yb)_2O_3$ coating.*

plasma-sprayed $HfO_2$-based coatings was determined by a laser heat-flux technique at 1650 °C. The initial thermal conductivity and 20-hr sintering thermal conductivity of the $HfO_2$-$Y_2O_3$ coatings generally decreases as the $Y_2O_3$ concentration increases, indicating that thermal stability increases with $Y_2O_3$ content. However, as shown in this example, the advanced, multicomponent rare-earth-doped $HfO_2$-$(Y,Nd,Yb)_2O_3$ coatings achieved even lower thermal conductivity and greater thermal stability than the $HfO_2$-$Y_2O_3$ pseudobinary oxide systems.

The multicomponent $HfO_2$-based coatings demonstrated long-term cyclic durability and water vapor stability. The graph on the right illustrates the durability exhibited by the multicomponent $HfO_2$-18mol%$(Y,Gd,Yb)_2O_3$ coating on a modified mullite/mullite + 20wt%BSAS/Si environmental barrier coating (EBC) system during 1650 °C thermal cycling testing. The coating system possessed a relatively low and stable thermal conductivity, without visual damage after the testing, demonstrating sintering stability and cyclic durability on SiC/SiC composites under the thermal-gradient cyclic-testing conditions (300 hr at 1650 °C). In addition, 6-atm high-pressure burner rig results (see the figure on the next page) indicated the excellent water vapor stability of the coating system in burner rig combustion environments. Continued coating system development is underway to further improve the coating temperature capability and durability under simulated engine environments while reducing the overall coating thickness and surface roughness.

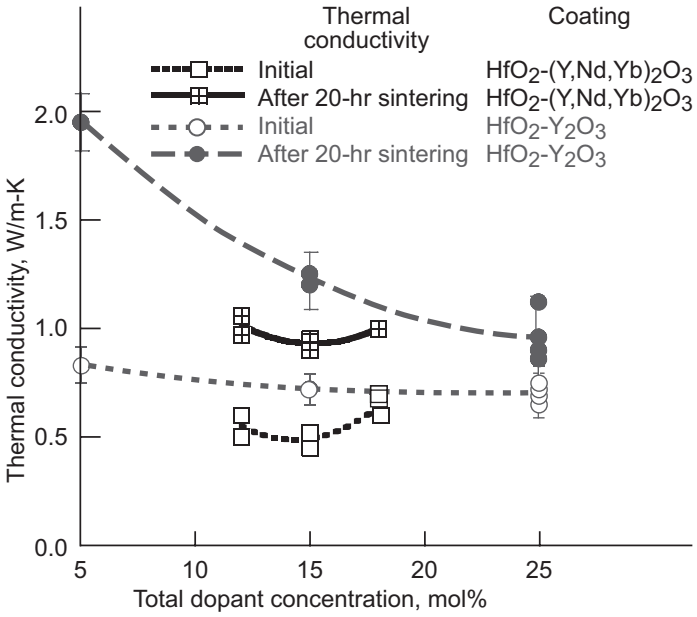


*Thermal conductivity of plasma-sprayed $HfO_2$-based coatings determined by a laser heat-flux technique.*

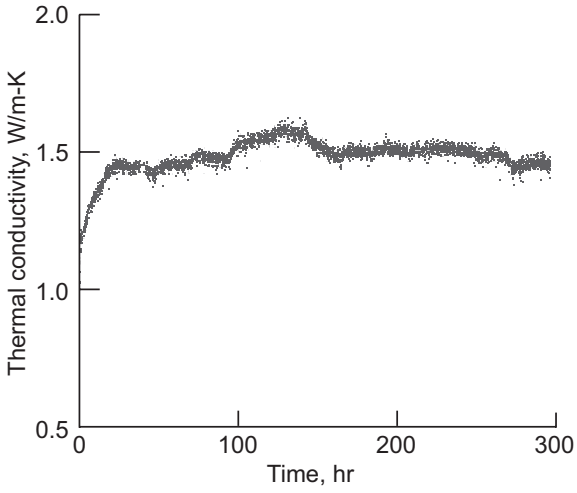


*Multicomponent $HfO_2$-18mol%$(Y,Gd,Yb)_2O_3$/rare-earth-doped mullite/$HfO_2$-based thermal and environmental barrier coating systems demonstrated 300-hr long-term 1650 °C sintering and cyclic durability on a SiC/SiC CMC substrate under thermal gradient cyclic testing. Surface temperature, 1650 °C (3000 °F); interface temperature, 1316 °C (2400 °F).*

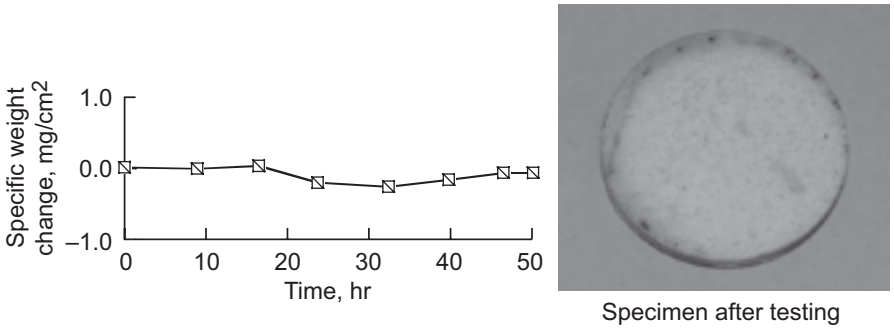


Specimen after testing

*Multicomponent $HfO_2$-$(Y,Gd,Yb)_2O_3$/rare-earth-doped mullite/Si thermal and environmental barrier coating systems demonstrated excellent water vapor stability and durability in high-pressure burner rig testing environments. Gas temperature, 1454 °C (2650 °F) at 6 atm; gas velocity, 25 m/sec. Left: Weight changes versus time. Right: Specimen after testing.*

**References**


1. Zhu, Dongming; and Miller, Robert A.: Thermal and Environmental Barrier Coatings for Advanced Propulsion Engine Systems. NASA/TM—2004-213129 (ARL–TR–3263), 2004. http://gltrs.grc.nasa.gov/cgi-bin/GLTRS/browse.pl?2004/TM-2004-213129.html
2. Zhu, Dongming, et al.: Advanced Oxide Material Systems for 1650 °C Thermal/Environmental Barrier Coating Applications. NASA/TM—2004-213219 (ARL–TR–3298), 2004. http://gltrs.grc.nasa.gov/cgi-bin/GLTRS/browse.pl?2004/TM-2004-213219.html
3. Zhu, Dong-Ming, et al.: Advanced Environmental Barrier Coatings Development for Si-Based Ceramics. NASA/TM—2005-213444, 2005. http://gltrs.grc.nasa.gov/cgi-bin/GLTRS/browse.pl?2005/TM-2005-213444.html
4. Zhu, Dongming; and Miller, Robert A.: Thermal and Environmental Barrier Coatings for Advanced Turbine Engine Applications. NASA/TM—2005-213437, 2005. http://gltrs.grc.nasa.gov/cgi-bin/GLTRS/browse.pl?2005/TM-2005-213437.html


**Find out more about the research of Glenn's Durability and Protective Coatings Branch:**
http://www.grc.nasa.gov/WWW/EDB/


**U.S. Army Research Laboratory at Glenn contact:**
Dr. Dongming Zhu, 216–433–5422, Dongming.Zhu@nasa.gov

**Authors:**
Dr. Dongming Zhu and Dr. Robert A. Miller


**Headquarters program office:**
Aeronautics Research

**Programs/Projects:**
UEET, LEAP

## Crack-Driving Forces Investigated in a Multilayered Coating System for Ceramic Matrix Composite Substrates

Melt-infiltrated SiC/SiC composites are emerging as the leading material for shrouds, vanes, and combustor liners in commercial gas turbines because of their high thermal conductivity and excellent thermal shock resistance, creep resistance, and oxidation resistance in comparison to other ceramic matrix composites and to the nickel- and cobalt-based superalloys used in current engines. One risk that can significantly reduce the lives of the SiC/SiC composites in an engine environment is the lack of environmental durability in the presence of water vapor. Oxide coatings have shown promise in providing environmental protection for these SiC/SiC composites because of their resistance to corrosive environments up to 1250 °C. To further extend the thermal capability of SiC/SiC ceramic composite components to the hot-wall surface temperatures (up to 1650 °C), researchers are developing thermal and environmental barrier coatings (TEBCs) under the NASA Ultra-Efficient Engine Technology (UEET) Project.

At the NASA Glenn Research Center, baseline plasma-sprayed yttria-stabilized zirconia (YSZ: $ZrO_2$-8wt%$Y_2O_3$) thermal barrier coatings (TBCs) and BSAS+mullite/Si layered environmental barrier coatings (EBCs) showed excellent adherence to SiC/SiC ceramic matrix composite substrates under thermal cycling in burner rig tests up to 1250 °C (ref. 1). However, the same coating system tested to higher temperatures (up to 1480 °C), especially under a temperature gradient, resulted in coating-delamination failures (as seen in the following figure) that were attributed to an increase in the

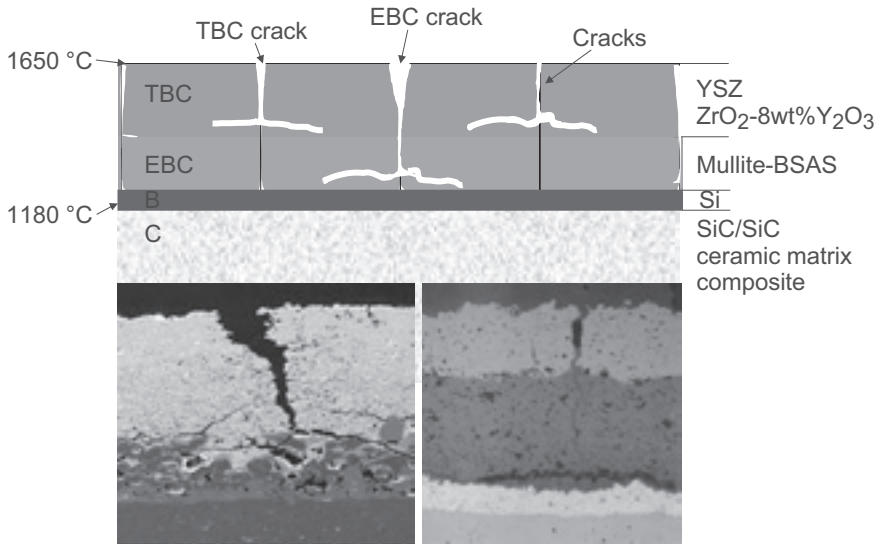


*Typical observed cracking in multilayered coating systems.*

crack-driving forces in the coating. Therefore, research is being performed to develop advanced TEBC coating systems that can last for the tens of thousands hours required for gas turbine applications. The ideal TEBC system should have low thermal conductivity, good high-temperature stability, and resistance to sintering.

The effects of temperature gradients and coating configurations were analyzed using finite-element analysis models based on the observed cracking in a YSZ baseline TEBC system (ref. 2). The crack-driving forces as a function of crack length, coating layer thickness, top coating modulus, and sintering time were synthesized to provide insight into the material properties required in minimizing the cracking and delamination observed in the baseline TEBC protecting system for SiC/SiC composite material. The variation of the effective stress intensity factor (SIF) with sintering time was calculated as a function of the TBC elastic modulus. The analysis assumed a constant crack length of 0.5 mm in the TBC layer for a TEBC geometric construction of a 0.381-mm-thick TBC layer and a 0.254-mm-thick EBC under the thermal gradient condition. The effective SIF increased with increasing TBC modulus starting from 1 MPa-$m^{1/2}$ for a TBC modulus of 5 GPa to well above 10 MPa-$m^{1/2}$ for a TBC modulus of 50 GPa (above any measured fracture toughness $K_{IC}$ of plasma-sprayed YSZ; see the graph). As the TBC layer sintered during exposure, the effective SIF increased with time upon cooldown. The crack-driving forces increased quickly within the first 50 hr of exposure and then increased more gradually with increasing time. The initial rise of the SIF was gentler for a low-modulus TBC material in the range of 5 to 10 GPa and was steeper for the higher modulus TBC (20 to 50 GPa). The results show that highly compliant materials are desirable in a TEBC system to accommodate the coefficient of thermal expansion mismatch and the temperature gradient.

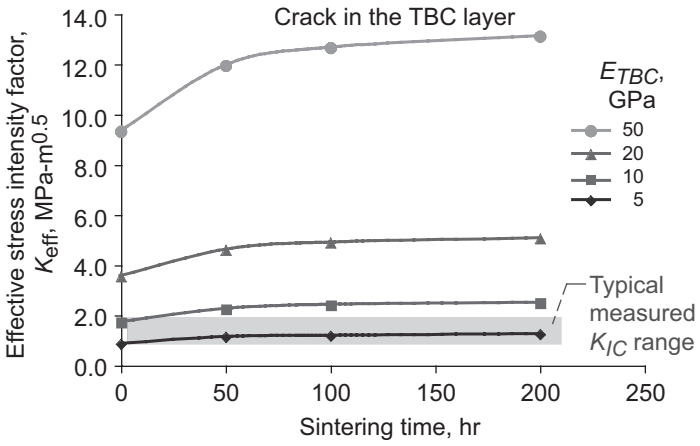


*Variation of the stress intensity factor with time for various TBC elastic moduli ($E_{TBC}$). TBC thickness, 0.381 mm; EBC thickness, 0.254 mm; crack length, 0.5 mm; $K_{IC}$, measured fracture toughness of the TBC.*

**References**

1. Zhu, Dong-Ming, et al.: Advanced Oxide Material Systems for 1650 °C Thermal/Environmental Barrier Coating Applications. NASA/TM—2004-213219 (ARL TR–3298), 2004. http://gltrs.grc.nasa.gov/cgi-bin/GLTRS/browse.pl?2004/TM-2004-213219.html
2. Ghosn, Louis J.; Zhu, Dongming; and Miller, Robert A.: Crack Driving Forces in a Multilayered Coating System for Ceramic Matrix Composite Substrates. NASA/TM—2005-213835, 2005. http://gltrs.grc.nasa.gov/cgi-bin/GLTRS/browse.pl?2005/TM-2005-213835.html

**Find out more about the research of Glenn's Durability and Protective Coatings Branch:**
http://www.grc.nasa.gov/WWW/EDB/

**Ohio Aerospace Institute (OAI) contact:**
Dr. Louis J. Ghosn, 216–433–3822, Louis.J.Ghosn@nasa.gov

**Glenn contact:**
Dr. Robert A. Miller, 216–433–3298, Robert.A.Miller@nasa.gov

**Authors:**
Dr. Louis J. Ghosn, Dr. Dongming Zhu, and Dr. Robert A. Miller

**Headquarters program office:**
Aeronautics Research, VSP

**Programs/Projects:**
UEET, low-emission combustors

# Silicone Elastomers Evaluated for Sealing Applications in Space Environments

An advanced docking and berthing system (ADBS) is being developed by the NASA Johnson Space Center to support future missions in NASA's vision for space exploration. This mechanism would serve as an interface between pressurized manned and autonomous modules to join space vehicles and structures. The ADBS will improve the functionality of mechanisms currently in use for the human exploration of space.

All docking and berthing mechanisms currently in use, including the common berthing mechanism used on the *International Space Station*, are composed of two nonidentical halves, which limit their functionality to mating only with structures having the opposite configuration interface. The ADBS, however, is an androgynous system, such that each system half is an identical replicate of any other, and any two vehicles or modules each having an ADBS can mate with the other without regard to gender. In addition, the ADBS system is designed to perform docking and berthing types of mating, such that both manned and unmanned autonomous vehicles and structures can be joined.

The androgynous nature of the ADBS, however, creates challenges for the sealing interface between the two pressurized modules. Since each system half is an exact replicate of its mating counterpart, the gas seals must seal against each other instead of against a conventional flat surface. The NASA Glenn Research Center is supporting this project by developing the gas seals for the ADBS system.

The environmental operating temperatures to which the ADBS will be exposed are expected to be –50 to 50 °C (–58 to 122 °F). Therefore, the elastomeric compound from which the seal is manufactured must remain compliant at temperatures below the minimum operating temperature of –50 °C (–58 °F). Since silicone rubber is the only class of elastomer that encompasses that temperature range and is commonly molded into seals, this study focused on three elastomers within the silicone class. An additional requirement is that the seal material be classified as a low-outgassing compound, per ASTM E595, having a total mass loss less than 1.0 percent and collected volatile condensable materials less than 0.1 percent.

The unconventional interaction between the gas seals makes the adhesion between two similar elastomers very important. If the adhesion forces between the seals are too great, the seals will not allow the space structures and vehicles to separate from one another without dislodging one of the two systems' seals. The removal of one of the seals would render the attachment point useless and must be avoided, so Glenn researchers used an adhesion test to quantify these adhesion forces (see the top graph).

The ADBS is also designed for a service life of 5 to 10 years. During its lifespan, the system is expected to undergo many mating-demating cycles, while being continuously exposed to the space environment. Since the seals would be compressed during each mating cycle and released during each

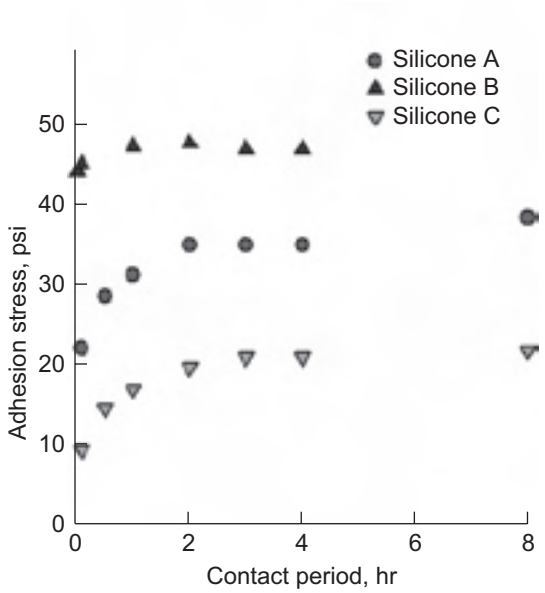


*Effect of contact period on elastomer-to-elastomer adhesion for three silicone elastomers.*

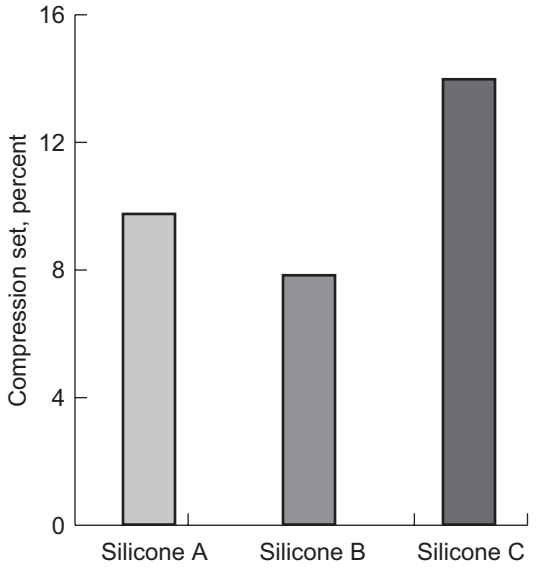


*Compression set results for three silicone elastomers.*

vehicle separation, the ability of the seal's elastomer compound to retain its elastic properties after prolonged compression is important. Glenn researchers used a compression set test to quantify this ability (see the bar chart on the preceding page).

Planned future work includes exposing the silicone elastomers to atomic oxygen and ultraviolet radiation to simulate time on orbit. The samples are then to be subjected to compression set, adhesion, and leakage tests to determine the effects of space environment exposure.

**Find out more about Glenn's structural seal and thermal barriers research:**
http://www.grc.nasa.gov/WWW/structuralseal/

**Glenn contact:**
Dr. Bruce M. Steinetz, 216–433–3302, Bruce.M.Steinetz@nasa.gov

**Authors:**
Dr. Christopher C. Daniels, Patrick H. Dunlap, Jr., Dr. Bruce M. Steinetz, Marta Bastrzyk, and Leigh Duren

**Headquarters program office:**
Exploration Systems

**Programs/Projects:**
CEV

## Densities of Polymer Crosslinked Aerogels Minimized

Because of their low density and insulating properties, silica aerogels are attractive candidates for many thermal, optical, electrical, and chemical applications. However, their inherent fragility has restricted the use of such materials to, for example, insulation in only extreme temperature environments, such as Mars. Future space exploration missions demand lighter-weight, robust, dual-purpose materials for insulation, radiation protection, and structural members of habitats, rovers, astronaut suits, and other items. Previous work at the NASA Glenn Research Center showed that covalently bonding a polymer coating to the surface of a silica framework before supercritical drying occurred would reinforce the aerogels and increase their strength in comparison to uncrosslinked aerogels with a similar silica framework. Previously, polymer crosslinked aerogels had been reported with density ranges of 0.2 to 0.5 g/cm$^3$.

In 2005, Glenn carried out a study to systematically adjust processing variables to control the macroscopic properties of polymer crosslinked aerogels with much lower densities. These materials may not be suitable as structural materials, but they maintain some mechanical integrity over uncrosslinked silica aerogels of similar density and are superior insulating materials.

In the study, researchers varied the concentration of the silanes in the starting gel, the concentration of polymer crosslink (di-isocyanate) that the gels were exposed to, and the reaction temperature. Then, the resulting gels were characterized for a variety of properties. Empirical models were derived from these measurements so that significant effects of the variables on the measured properties could be discerned. The top graphs on the next page show the empirical models for density and stress at break. As evidenced from these graphs, temperature has a pronounced effect on both measured responses. Density and maximum stress were higher for all combinations of both polymer concentration and silane concentration when the materials were cured at the higher temperature. Density and maximum stress at break both increased with increasing silane concentration as well. As is also evident from these graphs, increasing the di-isocyanate concentration had a pronounced effect on stress, strongly increasing the maximum stress at break. Although its effect on density was modest, it was still statistically significant.

Within the bounds of the present study, the highest density crosslinked aerogel produced the highest maximum stress at break. Stress at break for these aerogels was 350 times stronger than for the corresponding uncrosslinked aerogel, whereas density only increased by a factor of 2. The lowest density crosslinked aerogels still exhibited a fortyfold increase in stress at break over the corresponding uncrosslinked aerogels with the same twofold increase in density. These aerogels boasted a nominal density of 0.036 g/cm$^3$ and were flexible.

The models can be used to predict properties of monoliths prepared using other polymer and silane combinations. This is shown in the bottom graphs on the next page. The graphs show slices from the three-dimensional surfaces of monoliths that were density and maximum stress cured at 71 °C and of monoliths that were made using no polymer, 6 wt% polymer, and 13 wt% polymer. For example, it may be desirable for a particular application to make a polymer crosslinked aerogel

with the lowest possible density and a maximum stress at break of at least $1\times10^6$ N/m$^2$. The point at position A shows that this aerogel would have to be made using about 24.5 wt% silane and 13 wt% polymer, and that the density of this aerogel would be a little above 0.4 g/cm$^3$. If a lower strength could be tolerated ($1\times10^6$ N/m$^2$, for example), aerogel B, which can be made from 7.5 wt% silane and 6 wt% polymer is predicted to have a density of a little over 0.1 g/cm$^3$.

This method of picking and choosing the desired aerogel properties for a given application can be expanded upon by quantifying for a broader range of processing conditions (for example, varying the amount of water, catalyst, washings, etc.) and for a host of other properties such as thermal conductivity, compressive strength, density, and modulus and stress at break. This would enable researchers to tailor the materials for a wide variety of applications.

**Find out more about the research of Glenn's Durability and Protective Coatings Branch:**
http://www.grc.nasa.gov/WWW/EDB/

**Glenn contacts:**
Dr. Mary Ann B. Meador, 216–433–3221, Maryann.Meador-1@nasa.gov;
Dr. Nicholas Leventis, 216–433–3202, Nicholas.Leventis-1@nasa.gov; and
Dr. Lynn A. Capadona, 216–433–5013, Lynn.A.Capadona@nasa.gov

**Authors:**
Dr. Mary Ann B. Meador,
Dr. Nicholas Leventis, and
Dr. Lynn A. Capadona

**Headquarters program office:**
Aeronautics Research, Exploration Systems

**Programs/Projects:**
Advanced EVA, Vehicle Systems

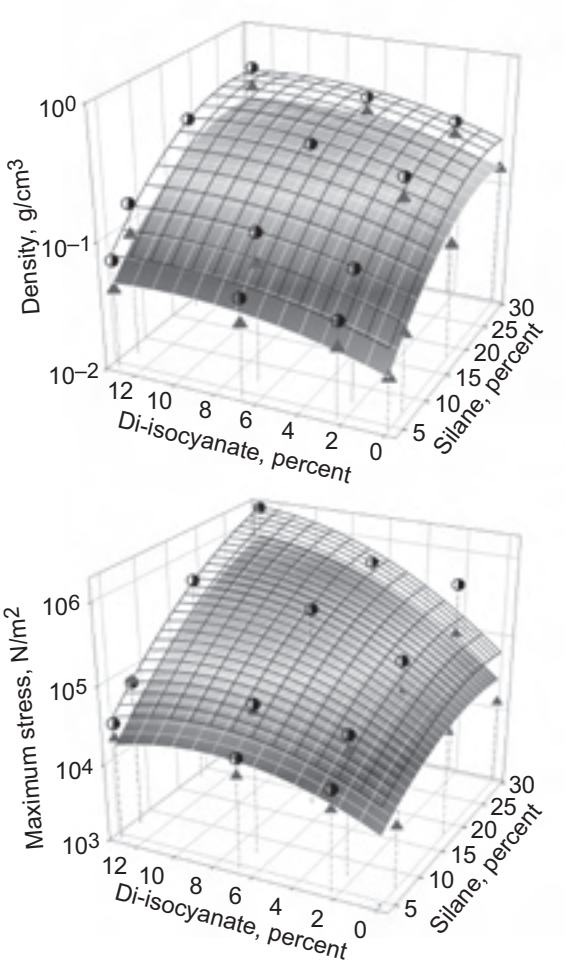


*Top: Response surface models for density plotted versus di-isocyanate and silane concentration. Bottom: Maximum stress at break of polymer crosslinked aerogels plotted versus di-isocyanate and silane concentration. The transparent surface shows predictions for 72 °C-cured aerogels, and the shaded surface shows predictions for room-temperature-cured aerogels. Data points from the study also are shown.*

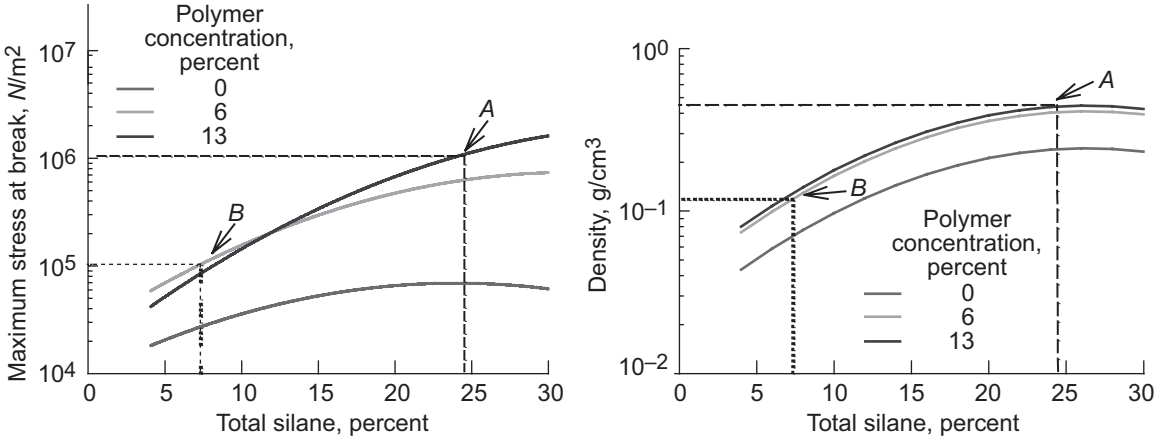


*Slices of the response surface models for maximum stress at break and density plotted versus total silane concentration.*

# New Perylene Dye Prepared

There has been a considerable interest in the development of highly conjugated organic materials for use in molecular sensors and electronics, flat panel displays, solid-state lighting, and lightweight photovoltaics. Perylenes (see the top figure), primarily perylene bisimides, are one class of conjugated organics that has received particular attention for these applications. These compounds absorb and emit in the visible region of the spectrum and have large photoluminescence and electroluminescence efficiencies, making them well suited for many of the applications mentioned. All perylene bisimides reported to date have been linear systems prepared by conventional imidization chemistry.

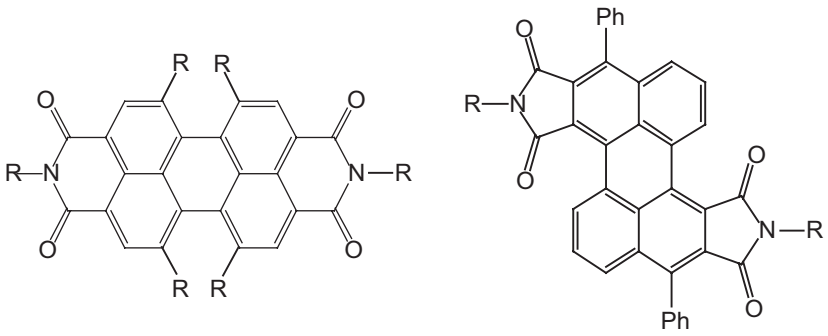


*Comparison of the chemical structure of a conventional "linear" perylene bisimide with that of the new Z-shaped perylene bisimide.*

In fiscal year 2005, researchers from the NASA Glenn Research Center and the Ohio Aerospace Institute (OAI) developed a new synthetic approach that enables the preparation of a novel class of Z-shaped perylene bisimides (see the top figure). This new approach offers greater flexibility in the types of perylene bisimides that can be prepared and enables the "tuning" of the electronic and optical properties of these molecules by the placement of appropriate groups on the sides and ends of the perylene. In addition, these bisimides can be readily incorporated into polymers both at the imide rings and on the pendant groups.

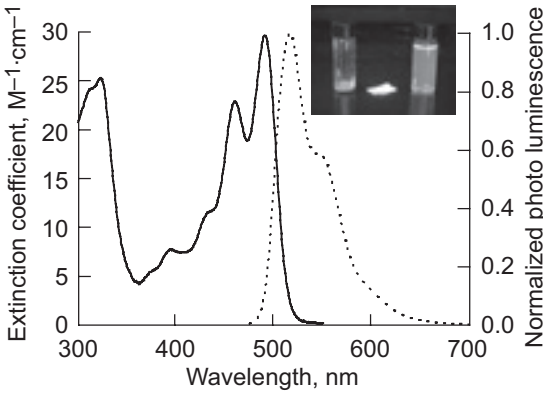


*Absorption and emission spectra of Z-shaped perylene bisimide in dichloromethane. The inset shows fluorescence emission from the bisimide in a pure microcrystalline sample (left), in a polystyrene film (center), and in dichloromethane solution (right) excited with a hand-held, broadband ultraviolet source. This figure is shown in color in the online version of this article (http://www.grc.nasa.gov/RT/2005/RX/RX22P-meador1.html).*

Like conventional linear perylene bisimides, these new Z-shaped systems have absorption in the visible region of the spectrum and exhibit intense fluorescence. An example of the absorption and emission spectra of one of these dyes is shown in the bottom figure. In solution and doped into a polystyrene film, this dye exhibits a bright lime-green fluorescence (see the inset). Unlike conventional perylene bisimides, a pure solid sample of this new bisimide has a reddish-orange fluorescence. This change in color is due to the formation of excited-state complexes in which the perylene molecules stack one on top of the other. It should be possible to exploit this behavior in the development of "molecular strain gauges" by incorporating these perylene stacks into a polymer film that could change color from orange to green when stretched.

These materials are under further development for use in electroluminescent polymers for solid-state lighting and displays for spacecraft and aircraft, fluorescent dyes for chemical sensors, and electrically conductive polymers for use in molecular electronic devices.

**Find out more about the research of Glenn's Polymers Branch:**
http://www.grc.nasa.gov/WWW/5000/materials/polymers/

**Glenn contact:**
Dr. Michael A. Meador, 216–433–9518, Michael.A.Meador@nasa.gov

**Ohio Aerospace Institute (OAI) contacts:**
Dr. Daniel S. Tyson, 216–433–3188, Daniel.S.Tyson@nasa.gov; and
Dr. Faysal Ilhan, 216–433–6094, Ulvi.F.Ilhan@nasa.gov

**Authors:**
Dr. Michael A. Meador, Dr. Daniel S. Tyson, and Dr. Faysal Ilhan

**Headquarters program office:**
Aeronautics Research

**Programs/Projects:**
Vehicle Systems, Exploration Systems

# Polymers Developed That Change Shape When Exposed to Ultraviolet LIght

Adaptive materials are finding considerable interest because of their ability to change shape under an applied stimulus, such as an electric current or heat. These materials have a broad range of aerospace applications ranging from the deployment of large-area solar arrays and antennas for satellites to "morphing" aircraft. A considerable amount of work has focused on the development of piezoelectric polymers that can change shape under an applied electric current. More recently, researchers have demonstrated that liquid crystalline elastomers that are doped with a photochromic dye will also change shape (bend) when exposed to ultraviolet light of a certain wavelength. Upon irradiation, the photochromic dye changes shape, disrupts the packing of the liquid crystalline elastomers, and causes the polymer film to bend. These materials, known as photomechanical polymers, offer some distinct advantages over piezoelectric systems. They have faster response times, are not sensitive to electromagnetic interference, and are more compatible with the advanced fly-by-light (fly-by-fiber) approaches being proposed for future aircraft.

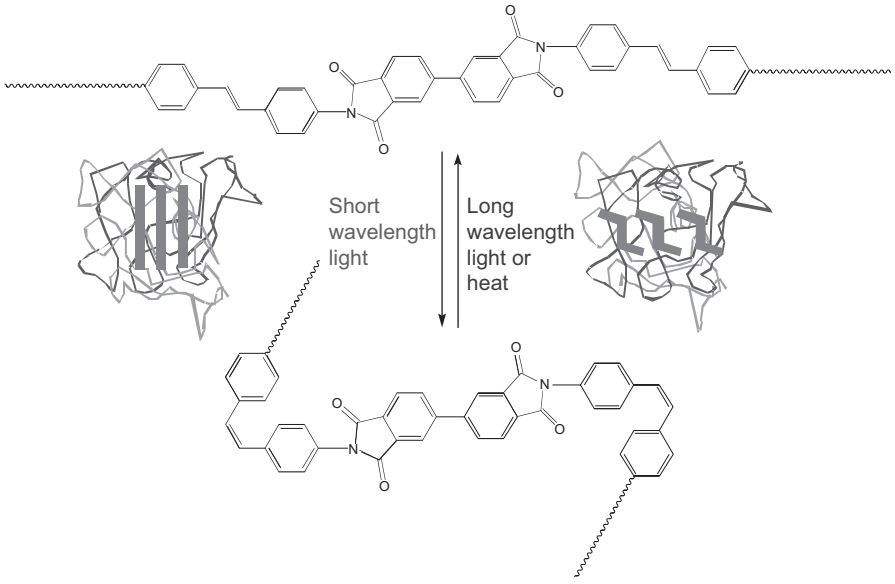


*Schematic representation of photomechanical polymers showing the isomerization of a photochromic additive and its incorporation in a polymer.*

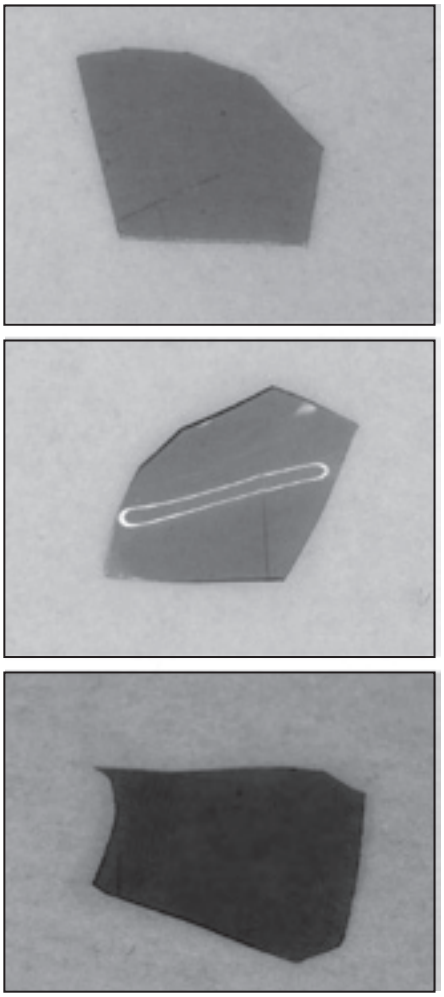

*Top: Polymer film before irradiation. Center: Polymer film after irradiation at 200 to 400 nm. Bottom: Polymer film after irradiation at 400 to 500 nm. Initially, the film is flat and has some surface roughness; upon irradiation, the sample begins to curl; irradiation with longer wavelength light causes the film to flatten out. Surprisingly, the films are now smooth.*

Researchers at the NASA Glenn Research Center have developed a new class of photomechanical polymers that incorporate a photochromic unit into a series of rod-coil block copolymers. These materials are designed to undergo a controlled phase separation leading to regions of highly ordered rods and coils (see the chemical diagram). Incorporation of the photochromic unit as part of the rods leads to an ordered environment similar to that in liquid crystalline materials. The advantage of this approach over previously reported dye-doped systems is that attachment of the dye to the polymer chain enables the control of its placement within the film and ensures that the dye does not leach out or evaporate during use.

The photographs show a film from one of these polymers before irradiation (top) and after 15 min irradiation with short-wavelength (200- to 400-nm) light (center). After just a few minutes of short-wavelength irradiation, the film begins to display signs of curling, and after 15 min it has nearly curled into a cylinder. Irradiation of the curled film with longer wavelength (400- to 500-nm) ultraviolet light causes the film to relax, and it becomes flat again (bottom). Further modifications of these polymers and a more thorough investigation of the photomechanical effects in these materials are underway.

**Find out more about the research of Glenn's Polymers Branch:**
http://www.grc.nasa.gov/WWW/5000/materials/polymers/

**Glenn contact:**
Dr. Michael A. Meador, 216–433–9518, Michael.A.Meador@nasa.gov

**Ohio Aerospace Institute (OAI) contact:**
Dr. Daniel S. Tyson, 216–433–3188, Daniel.S.Tyson@nasa.gov

**Authors:**
Dr. Michael A. Meador, Dr. Daniel S. Tyson, and Pushan Dasgupta (participant in NASA's 2005 Summer High School Apprenticeship Research Program, SHARP)

**Headquarters program office:**
Aeronautics Research

**Programs/Projects:**
Vehicle Systems, Exploration Systems

# Solid-Film Lubricants Tested for Galling and Wear Protection of Ti-6Al-4V Under Fretting Conditions in NASA and Department of Defense Aerospace Applications

Conventional titanium alloys have poor tribological properties because they are chemically active and exhibit strong adhesion when in contact with themselves and other materials (ref. 1). This adhesion causes high friction and ultimately galling, which results in heavy surface damage—such as the Galileo spacecraft's high-gain antenna (which could not deploy because the titanium alloy component on the antenna was stuck to a nickel-base superalloy component) and severe galling and fretting on titanium-based alloy fan blade-disk couples in fan engine aircraft propulsion systems (ref. 2).

The NASA Glenn Research Center and the Air Force Research Laboratory have been working to reduce fretting wear and fatigue damage in titanium alloys, particularly Ti-6Al-4V. The tribological properties of monolithic Ti-6Al-4V alloy can be improved by the application of an advanced solid-film lubricant, such as a multiwalled carbon nanotube (MWNT) coating (see the photomicrographs). Such advanced solid-film lubricants may decrease adhesion and subsequent galling and may increase wear resistance under fretting conditions. This study investigated whether or not solid-film lubricants could decrease the wear and galling of Ti-6Al-4V in cyclic relative motion.

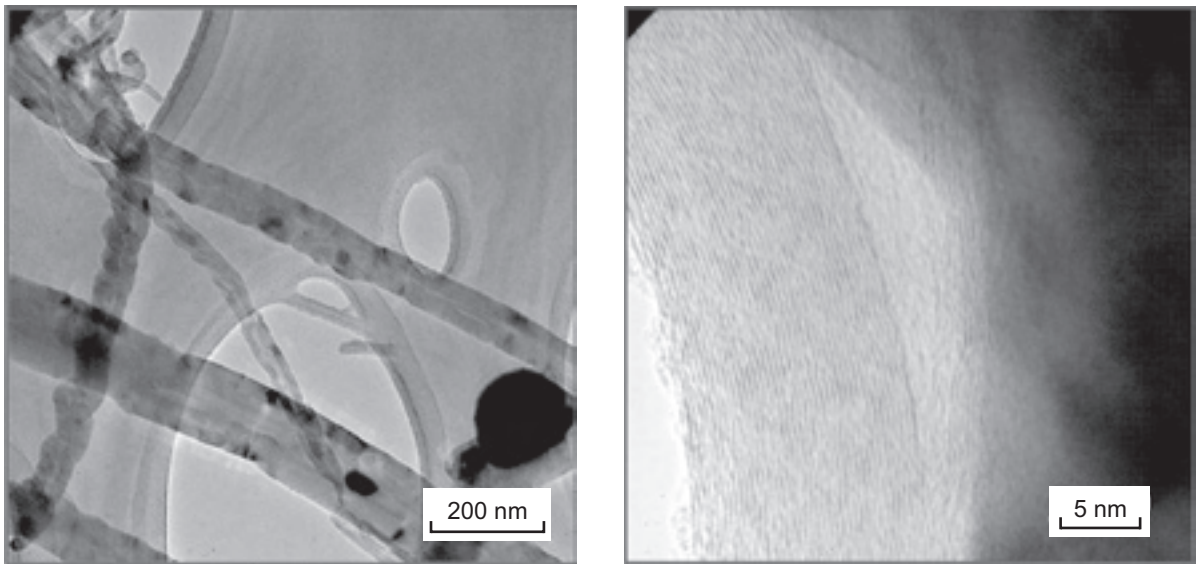


*High-resolution transmission electron micrographs of dispersed MWNTs. Left: Overview. Right: Details.*

Fretting experiments in cyclic relative motion were conducted with 10-wt% TiC/Ti-6Al-4V hemispherical pins in contact with solid-film lubricants—MWNTs, diamondlike carbon (DLC), $MoS_2$, and graphitelike carbon (GLC)—coated on Ti-6Al-4V disks and also in contact with bare alloy disks of Ti-6Al-4V, Ti-48Al-2Cr-2Nb, and nickel-based superalloy 718. All experiments were conducted at a load of 1.0 N, a frequency of 80 Hz, and a slip amplitude of 50 μm for 1 hr at 296, 423, and 523 K in air. The TiC/Ti-6Al-4V composite was used for the counterpart pin specimens because uniformly distributed particle-strengthened titanium matrix composites can now be produced at a cost lower than for many continuous-fiber composites (refs. 3 and 4).

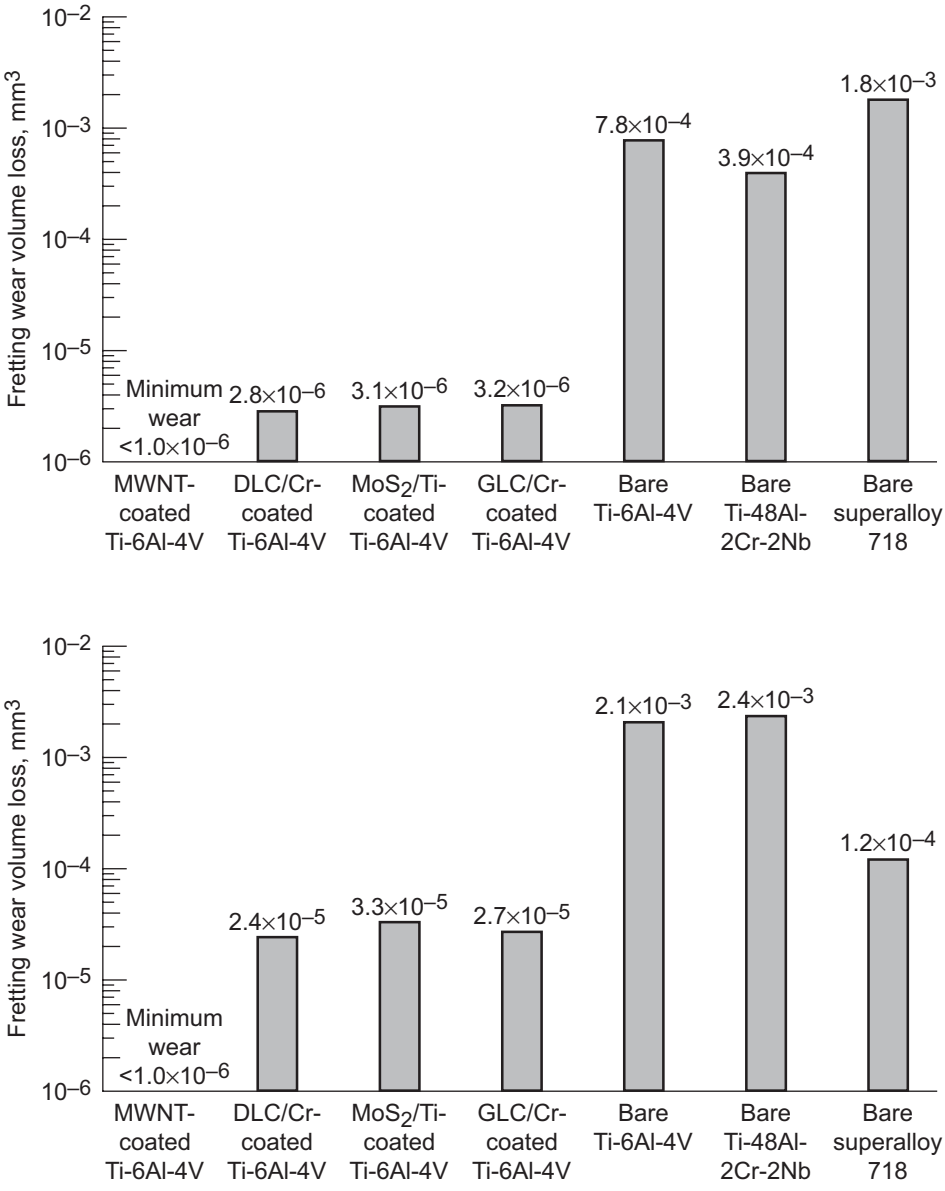


*Fretting wear volume loss at 296 K in air for TiC/Ti-6Al-4V pins in cyclic relative motion contact with different disk materials: Ti-6Al-4V coated with MWNTs, DLC, $MoS_2$, and GLC, and bare Ti-6Al-4V, Ti-48Al-2Cr-2Nb, and nickel-base superalloy 718. Top: Volume loss of pins. Bottom: Volume loss of disks.*

The bar graphs show the pin and disk wear volume losses. All the solid-film lubricant coatings dramatically improved the wear of both the pin and disk. The MWNT coating reduced pin and disk wear so much that they were almost not measurable. When an MWNT-coated Ti-6Al-4V substrate disk was brought into contact with a composite TiC/Ti-6Al-4V pin under fretting, strong bonds were formed between the MWNTs and the composite, protecting both the pin and disk from wear. Scanning electron microscopy indicated that the entire contact area of the pin contained transferred MWNTs, and the contact area of the MWNT-coated Ti-6Al-4V disk contained residual MWNT coating. The wear volume losses for both the pin and disk were much lower than $10^{-6}$ $mm^3$.

The wear volume loss of a composite TiC/Ti-6Al-4V pin fretted against DLC/Cr-, $MoS_2$/Ti-, and GLC/Cr-coated Ti6Al-4V disks was 1/274th, 1/251st, and 1/247th, respectively, of that fretted against bare Ti-6Al-4V. The wear volume loss of the pin fretted against DLC-coated Ti-6Al-4V was $2.8\times10^{-6}$ $mm^3$, whereas that of the pin slid against bare Ti-6Al-4V was $7.8\times10^{-4}$ $mm^3$. The wear volume loss of DLC/Cr-, $MoS_2$/Ti-, and GLC/Cr-coated Ti-6Al-4V disks was 1/88th, 1/64th, and 1/10th, respectively, of that of bare Ti-6Al-4V.

When solid-film lubricants were applied to Ti-6Al-4V, alloy-to-alloy contact was avoided, and no galling occurred in the contacts during fretting. When bare alloy disks were brought into contact with TiC/Ti-6Al-4V, however, strong adhesion, galling, and severe fretting damage occurred in the contacts. This investigation indicates that solid-film lubricants may be suitable antigalling and antiwear films for aerospace applications under fretting conditions.

**References**

1. Miyoshi, Kazuhisa: Solid Lubrication Fundamentals and Applications. Marcel Dekker, New York, NY, 2001.
2. Chakravarty, S., et al.: Effect of Surface Modification on Fretting Fatigue in Ti Alloy Turbine Components. JOM, vol. 47, no. 4, 1995, pp. 31–35.
3. Abkowitz, Stanley, et al.: Commercial Application of Low-Cost Titanium Composites. JOM, vol. 47, no. 8, 1995, pp. 40–41.
4. Thesken, John C., et al.: Particulate Titanium Matrix Composites Tested—Show Promise for Space Propulsion Applications. Research & Technology 2003, NASA/TM—2004-212729, 2004, pp. 156–157. http://www.grc.nasa.gov/WWW/RT/2003/5000/5920thesken.html

**Glenn contacts:**
Dr. Kazuhisa Miyoshi, 216–433–6078, Kazuhisa.Miyoshi@nasa.gov; and
Dr. Kenneth W. Street, Jr., 216–433–5032, Kenneth.W.Street@nasa.gov

**Air Force Research Laboratory contact:**
Dr. Jeffrey H. Sanders, 973–724–3368, Jeffrey.sanders@wpafb.af.mil

**National Center for Microgravity Research contact:**
Dr. Randy L. Vander Wal, 216–433–9065, Randy.L.VanderWal@nasa.gov

**University of Kentucky contact:**
Dr. Rodney Andrews, 859–257–0265, Andrews@caer.uky.edu

**Authors:**
Dr. Kazuhisa Miyoshi,
Dr. Jeffrey H. Sanders,
Dr. Kenneth W. Street, Jr.,
Dr. Randall L. Vander Wal, and
Dr. Rodney Andrews

**Headquarters program office:**
Aeronautics Research

**Programs/Projects:**
MTLAMPS, AFFT, ESR&T (ASTP)

**Space Act Agreements:**
SAA3–307–18 and SAA3–307–28

## Forces Generated by the Ballistic Impact of Ice Evaluated

Impact damage from ice is a potential problem in many aerospace and industrial applications, including jet engines and airframes, ground-based turbomachinery, and spacecraft launch systems. In particular, ice impact damage is considered a serious threat to the space shuttles because of the potential damage that can result when ice formed on the external fuel tank sheds during launch. As part of NASA's return-to-flight effort, a test program was conducted at NASA Glenn Research Center's Ballistic Impact Facility to study the impact behavior of ice projectiles. The objectives of the study were to measure the forces generated by different types of ice, both to quantify the damage potential and to generate data to aid in developing computational models to simulate ice impact.

Ice, in its solid form, is a crystalline material that can be made up of single or multiple grains. In practical applications, ice can be solid (fully dense) or be partially filled with air in the form of bubbles. The effect of the granular makeup and density on the strength of ice was one of the phenomena to be quantified in this study.

Forces due to ice impact were measured by firing ice projectiles at a single piezoelectric load cell assembly oriented at incidence angles of both 90° and 45°. The ice projectiles were cylinders of various sizes, ranging in diameter from 0.44 (7/16) to 1.25 in. and in length from 1.5 to 3.3 in. These projectiles were accelerated by a 12-ft-long, 2-in.-diameter gas gun using a polycarbonate sabot. Impact velocities were in the range of 300 to 800 ft/sec. All tests were conducted in a vacuum.

Initial tests were conducted to observe the fracture behavior of ice. Using a digital high-speed imaging system, running at 260,010 frames/sec, Glenn researchers studied the impact of ice on a solid aluminum target (see the photographs). We found that, in the range of impact velocities of interest, the speed of a fracture wave is much greater than the impact velocity. The practical implication of this is that the projectile completely fractures as soon as the impact occurs, and in the velocity range of this study, the structural properties of the ice have little effect on the impact force. This was supported by experimental results, which demonstrated that the measured impact forces were quite repeatable from test to test, and that the response was not dependent on the granular makeup (see the graph). The measured force, however, was directly dependent on the density of ice, as was expected.

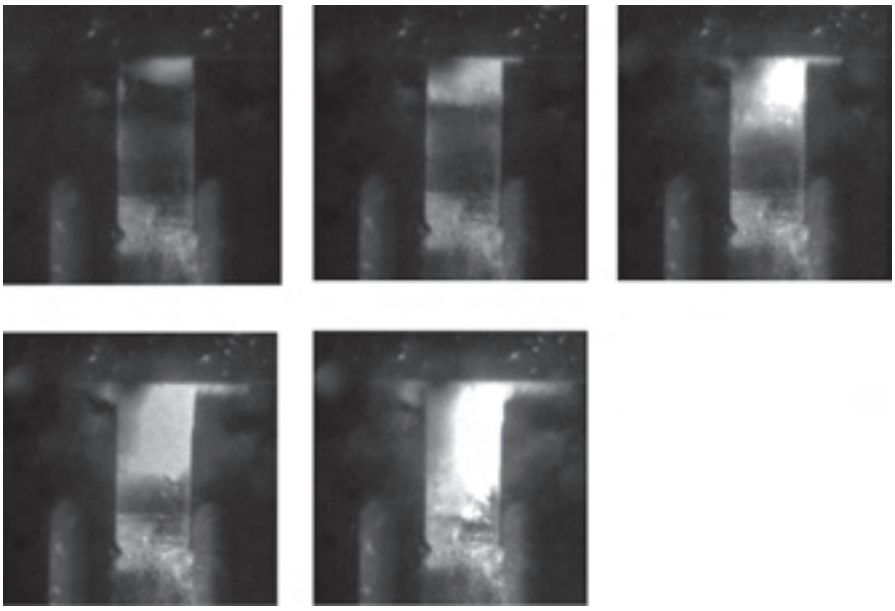

*A series of five images taken at the moment of impact, showing the progression of a fracture wave in ice. The fracture wave traveled approximately 1.92 in. in 15.38 μsec, or 10,400 ft/sec.*

Results of these experiments were used to develop computational models that accurately predict ice impact damage in structures. The techniques developed also were used under a reimbursable space act agreement to successfully evaluate design changes in industrial airfoils that significantly reduce the damage due to ice impact.

**Glenn contacts:**
Dr. J. Michael Pereira, 216–433–6738, J.M.Pereira@nasa.gov;
Dr. Santo A. Padula II, 216–433–9375, Santo.A.Padula@nasa.gov;
Duane M. Revilock Jr., 216–433–3186, Duane.M.Revilock@nasa.gov; and
Matthew E. Melis, 216–433–3322, Matthew.E.Melis@nasa.gov

**Authors:**
Dr. J. Michael Pereira,
Dr. Santo A. Padula II,
Duane M. Revilock, Jr., and
Matthew E. Melis

**Headquarters program office:**
Vehicle Systems

**Programs/Projects:**
Space Shuttle

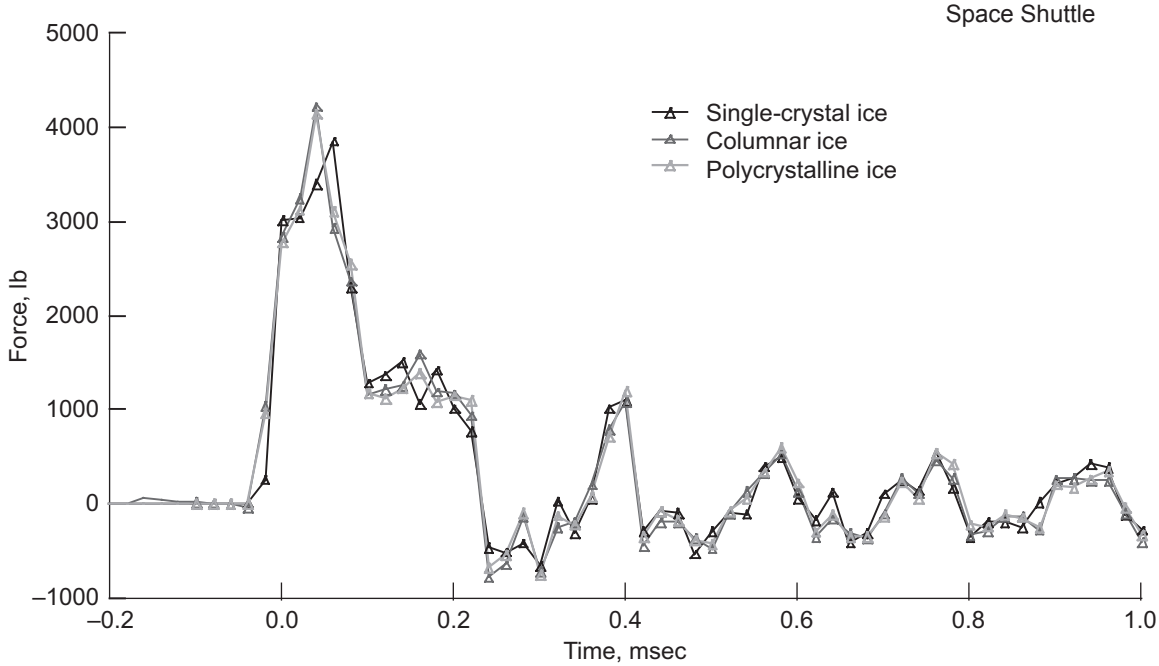


*Forces measured from impacts involving three types of ice: single-crystal (one grain), columnar (multiple grains elongated over the whole length), and polycrystalline (randomly oriented equiaxed grains). Impact velocity was approximately 700 ft/sec. There was no significant difference in the response from the three types of ice.*

# Advanced Heat Treatment Technology for Superalloy Disks Verified

As operating temperatures of gas turbine engines increase, there is a need for superalloy turbine disks that can operate with rim temperatures in excess of 1300 °F. To meet this need, a new generation of nickel-base superalloys, such as ME3, Alloy 10, and LSHR, has been developed. These alloys all contain a high percentage of gamma-prime precipitates, $Ni_3Al$, and refractory element additions to achieve strength at temperature. Although they provide advantages over older alloys, the continuing need for high tensile strength at intermediate temperatures in the bore of a disk, which runs much cooler than the rim, as well as high creep strength in the rim also demands innovative heat treatments that can optimize bore and rim properties.

Traditional heat treatments produce fine-grain disks when the solution temperature is maintained below the gamma-prime solvus and produce coarse-grain disks when the solution temperature is maintained above the gamma-prime solvus. Fine-grain disks yield high strength at intermediate temperatures, whereas coarse-grain disks yield high creep strength at elevated temperatures. Recently, several advanced heat-treatment technologies have been developed that can produce a superalloy disk with a fine-grain bore and a coarse-grain rim. Tradeoff studies by GE Aircraft Engines and Allison Advanced Development Company (AADC) have identified the potential advantages offered by superalloy disks that employ a dual grain structure for advanced gas turbine engine applications. The GE Aircraft Engines report cited reduced fatigue for a disk with a dual grain structure in comparison to a coarse-grain disk, whereas the AADC report cited a creep benefit for a disk with a dual grain structure in comparison to a fine-grain disk.

One of the advanced heat-treatment technologies for producing superalloy disks with a dual grain structure was developed by the NASA Glenn Research Center to minimize cost and production problems. This process, known as dual microstructure heat treatment, or DMHT, has been demonstrated for a variety of disk shapes and sizes at the Ladish Company and Pratt & Whitney's Forging Part Center. The basic concept behind the DMHT process utilizes the thermal gradient between the interior and exterior of the forging during the initial phase of a conventional heat treatment to develop a dual grain structure. By enhancing the thermal gradient with insulated heat sinks placed on the top and bottom surface of the forging, researchers can obtain the desired dual grain structure by using a conventional gas-fired furnace maintained at a temperature above the gamma prime solvus of the alloy. The forging and heat sink package is placed

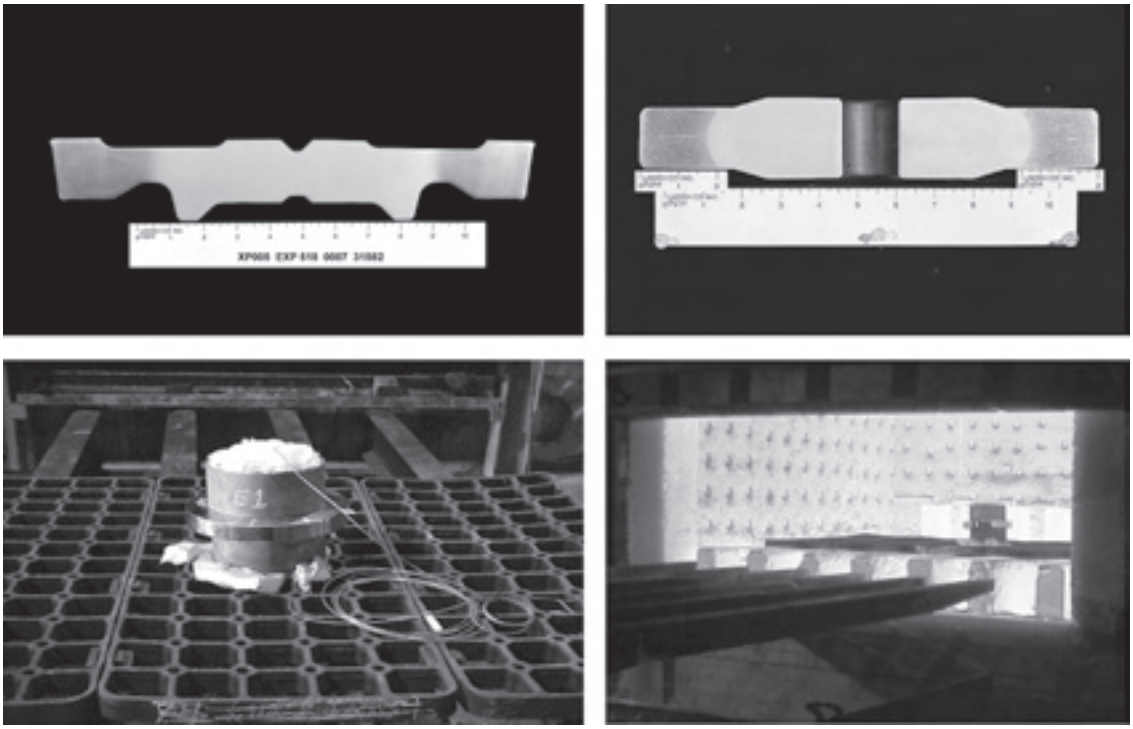

*Top: Etched sections of DMHT forgings showing dual grain structure. Bottom: Hardware and furnace used to produce DMHT disks.*

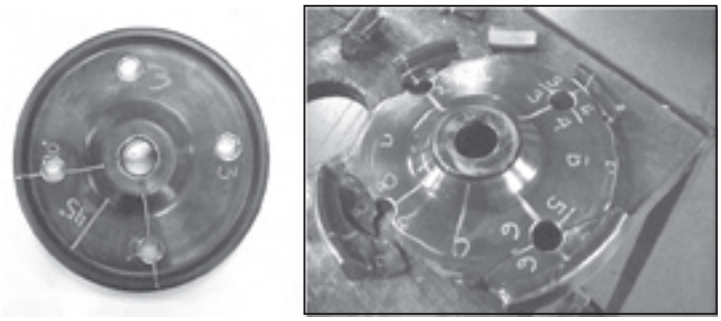

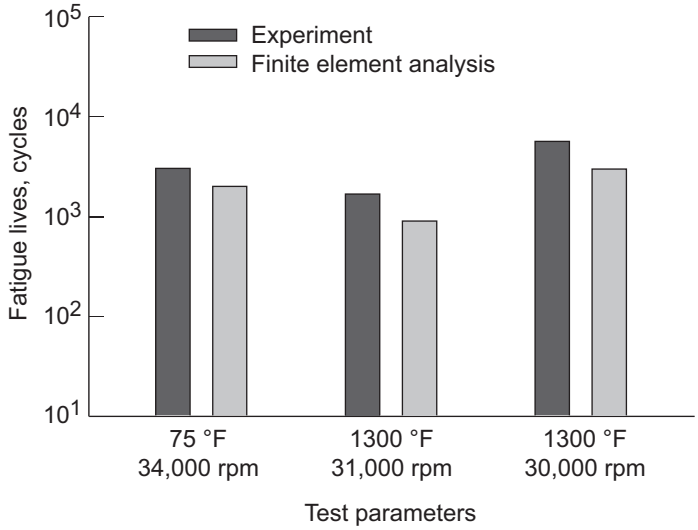


*Top: DMHT disk used in cyclic spin testing to verify the fatigue durability of the grain-size transition zone. Bottom: Experimental and predicted fatigue lives for DMHT disks.*

in the hot furnace; it is removed when the outer periphery of the forging has exceeded the solvus but before the center of the forging reaches the solvus, thereby producing the desired dual grain structure. The effect of DMHT processing on tensile and creep properties has been demonstrated using test coupons machined from disk forgings as well as spin testing of DMHT disks. These tests have confirmed the strength benefits of a fine-grain bore and the enhanced creep resistance of a coarse-grain rim.

More recently, the fatigue performance of DMHT disks was studied using test coupons machined from disk forgings and cyclic spin testing of DMHT disks. The coupon testing confirmed the enhanced fatigue resistance associated with a fine-grain bore. Cyclic spin testing of DMHT disks was performed with two goals in mind. First, the grain-size transition zone was intentionally loaded to high stress levels by employing web holes in the disk that bisected the grain-size transition zone. Second, the fatigue lives of the DMHT disks were estimated using advanced elastic-plastic finite-element techniques. The results of these tests and the analyses showed that the grain-size transition zone of the DMHT disk could withstand significant loads that exceeded the predicted fatigue lives. The next step in the development of this technology calls for demonstrating a DMHT disk in a ground-based engine to assess safety and reliability under realistic operating conditions.

**Find out more about the research of Glenn's Advanced Metallics Branch:**
http://www.grc.nasa.gov/WWW/AdvMet/webpage/

**Glenn contact:**
John Gayda, 216–433–3273,
John.Gayda-1@nasa.gov

**Authors:**
Dr. John Gayda, Dr. Timothy P. Gabb, and Pete T. Kantzos

**Headquarters program office:**
Aeronautics Research

**Programs/Projects:**
Aviation Safety

# Relationship Between Microstructure and Hold-Time Crack-Growth Behavior in Nickel-Based Superalloys Investigated

The increase in the operating temperatures of the new generation of advanced gas turbine engines has focused attention on the time-dependent properties of powder-metallurgy nickel-based superalloys. At these higher temperatures, the ability of the alloys to resist crack growth under extended hold times becomes a design-limiting mechanical property. A considerable amount of research has been performed to explain and model hold-time crack-growth behavior in superalloys. Most of the research has focused on trying to identify the grain-boundary phases that are most susceptible to an environmental attack and that would reduce an alloys' resistance to hold-time crack growth. Over the years, a number of grain-boundary species have been proposed to be susceptible to environmental attack, but none of these hypotheses has withstood the test of time.

A well-controlled study was performed at the NASA Glenn Research Center to determine the variables that influence the hold-time crack-growth resistance of two newly developed powder-metallurgy superalloys, Alloy 10 and ME3. The effects of both compositional changes and variation in heat treatments were investigated. The results indicate that significant changes in the alloy's composition did not have an appreciable effect on hold-time crack-growth resistance, provided that the heat treatment remained constant.

In contrast to the composition study, the heat treatments evaluated produced changes in the crack growth resistance of up to an order of magnitude. Quantitative image analysis was performed to analyze the microstructural features produced by each heat treatment.

We found that the cooling $\gamma'$ precipitate size distribution was the most important variable controlling hold-time crack-growth behavior. The larger the mean size of the cooling precipitates, the better was the resistance to hold-time crack growth. To gain further insight into the role of precipitate size distribution on time-dependent properties, we determined the alloys' stress relaxation behavior as a function of precipitate size and volume fraction. An increase in the precipitate size corresponded directly to an increase in stress relaxation. On the basis of these observations, we proposed that the size and distribution of the precipitates play an important role in determining the extent of the crack-tip stress relaxation that occurs during hold times through creep-type processes. The different crack-tip stress relaxation rates have a significant effect on the crack-driving forces, producing a large variation in the measured hold-time crack-growth resistance. The microstructures that produced larger precipitates showed the most stress relaxation and, thus, the lowest crack-driving force, which in turn produced the slowest crack-growth rates.

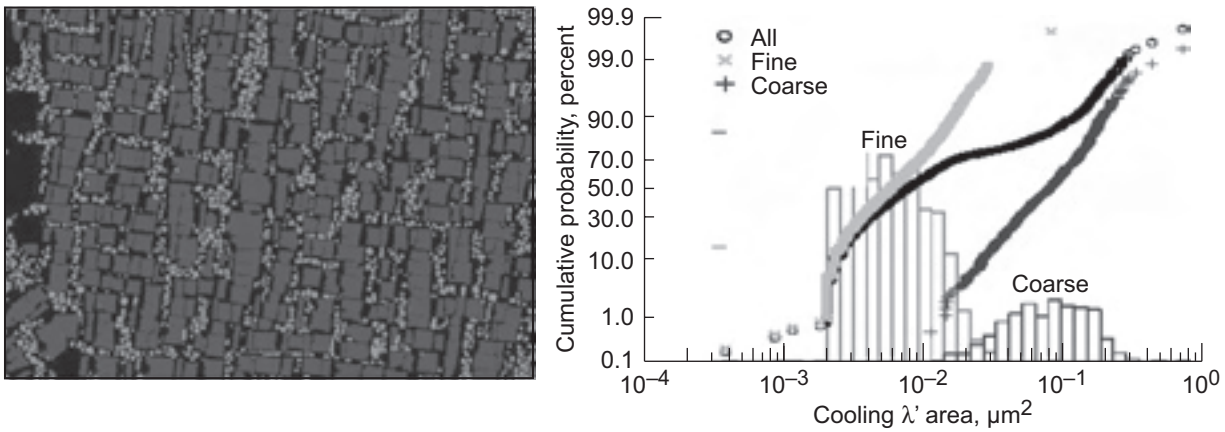


*Quantitative image analysis was performed to determine precipitate size distribution. Air-cooled; 1149 °C re-solution. Light areas indicate fine precipitate. Dark areas indicate coarse precipitate. This figure is shown in color in the online version of this article (http://www.grc.nasa.gov/WWW/RT/2005/RX/RX28L-telesman.html).*

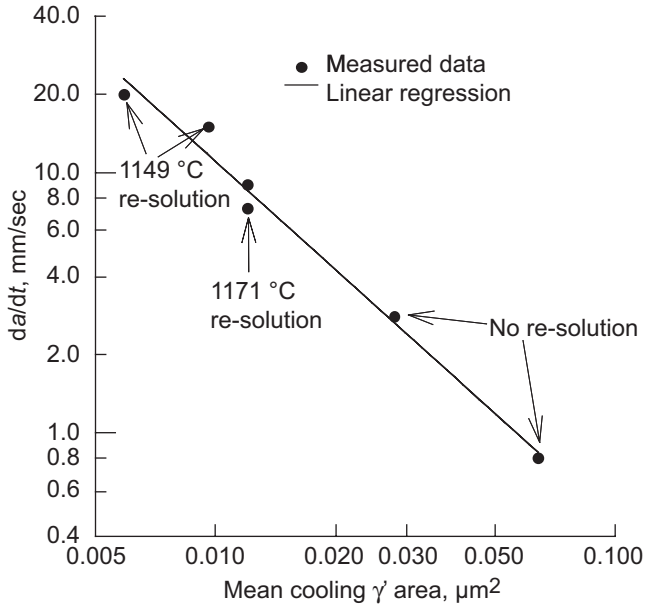


*A close relationship exists between precipitate size and hold-time crack-growth resistance; crack growth per second, da/dt, at 25 MPa-m$^2$ = 1.87×10$^{-7}$ (cooling γ' area)$^{-1.385}$; r$^2$ = 0.98.*

**Glenn contacts:**
Jack Telesman, 216–433–3310, Ignacy.Telesman-1@nasa.gov;
Tim Gabb, 216–433–3272, Timothy.P.Gabb@nasa.gov; and
John Gayda, 216–433–3273, John.Gayda-1@nasa.gov

**U.S. Army Research Laboratory at Glenn contact:**
Pete Bonacuse, 216–433–3309, Peter.J.Bonacuse@nasa.gov

**Ohio Aerospace Institute (OAI) contact:**
Pete Kantzos, 216–433–5202, Pete.T.Kantzos@nasa.gov

**Authors:**
Jack Telesman, Peter J. Bonacuse, Pete T. Kantzos, Dr. Timothy P. Gabb, and Dr. John Gayda

**Headquarters program office:**
Aeronautics Research

**Programs/Projects:**
Aviation Safety, Vehicle Systems

## Wire Drawing and Postprocessing Procedures Developed for a New NiTiPt High-Temperature Shape-Memory Alloy

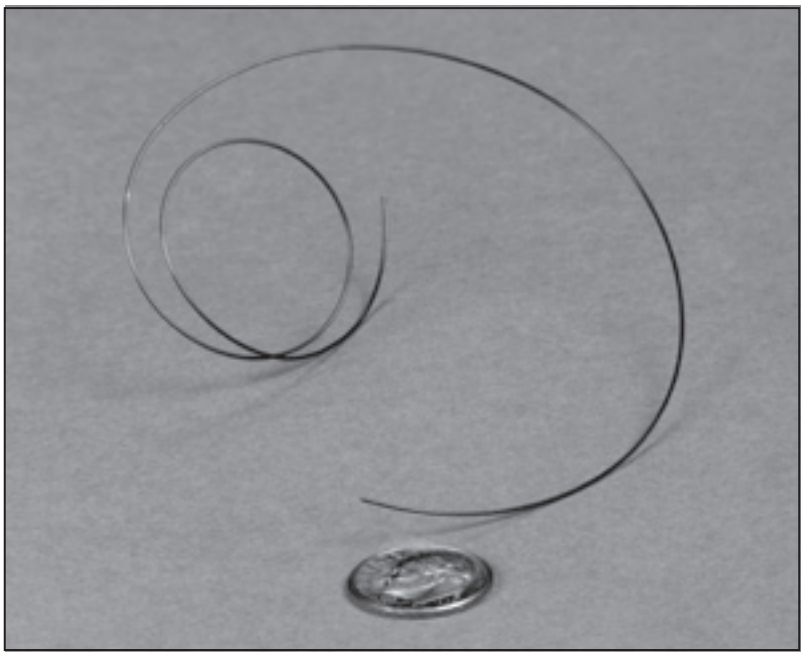

*Example of a piece of experimental NiTiPt 20-mil-diameter wire developed for shape-memory actuator applications requiring a high-temperature alloy.*

The development of shape-memory alloys that could operate at temperatures greater than 400 °F would provide an enabling technology for the development of "smart structures" used to control the noise, emissions, or efficiency of gas turbine engines or for the creation of morphing structures permitting more efficient flight over a large envelope of conditions from subsonic to hypersonic. Interest in high-temperature shape-memory alloys (HTSMA) also has been growing in the automotive, process control, and energy industries. However, as is often the case, materials development has seriously lagged component design, with current commercial alloys severely limited in their temperature capability. The two largest challenges to developing a viable HTSMA for demonstration purposes or for commercial use are (1) identification and development of an alloy with an

acceptable balance of properties including high transformation temperatures, high work output, stability, and good fatigue life and (2) the availability of the material in an appropriate product form such as fine wire. These challenges are being addressed in a recent collaboration between the NASA Glenn Research Center and Dynalloy, Inc. (Costa Mesa, CA).

Processing procedures have been successfully developed for the wire drawing of a promising new nickel-titanium-platinum (NiTiPt) HTSMA along with post-processing procedures, such as annealing and training, to prepare the material for actuator applications. The alloy has been processed into 0.020-in.-diameter wire (see the photograph on the preceding page) but could just as easily be processed into finer diameters. After postdrawing heat treatment and training, the behavior of the new NiTiPt wire is extremely stable. The transformation temperatures for the martensite start and austenite finish temperatures are 545 and 570 °F, respectively, and the transformation temperatures are stable with respect to repeated thermal cycling to as high as 840 °F. The hysteresis is narrow, just 25 °F, making the material ideal for actuator applications requiring active control. The transformation strain at 25 ksi is about 1.5 percent, and the corresponding work output is 375 in.-lb/in.$^3$ This is about half the work output that is possible from commercial NiTi wire. However, the NiTiPt wire is capable of repeated actuation in high-temperature environments (up to about 500 °F), whereas commercial "high-temperature" NiTi alloys are limited to about 100 to 200 °F.

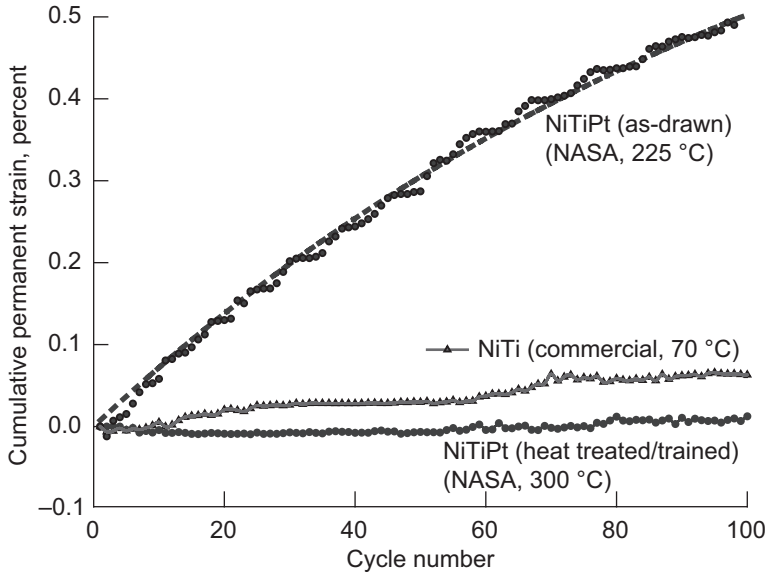


*Accumulated permanent strain as a function of the number of actuation cycles acting against a 25-ksi (172-MPa) bias stress on a 20-mil wire. The amount of permanent strain accumulated in the trained NiTiPt wire is minimal and less than that of a commercial "high-temperature" NiTi actuator wire even though the NiTiPt wire is operating at temperatures higher than 400 °F.*

After appropriate training, HTSMAs also display excellent dimensional stability during repeated actuation against a bias stress of 25 ksi, as shown in the graph. In fact, the trained NiTiPt alloy is dimensionally more stable after repeated actuation than commercial "high-temperature" NiTi alloys, even though there is a 400 °F difference in operating temperature. This dimensional stability or resistance to changes in length during use is critical for applications requiring repeated cycling, to ensure a reasonable fatigue life and to minimize drifting of the zero point in shape-memory alloy actuators (ref. 1). Further improvements in the capabilities of the NiTiPt wire are expected as this new HTSMA is carefully optimized.

**Reference**

1. Stoeckel, D.: Shape Memory Actuators for Automotive Applications. Engineering Aspects of Shape Memory Alloys, T.W. Duerig et al., eds., Butterworth-Heinemann, 1990, pp. 283–294.

**Find out more about this research:**

**Glenn's materials research:**
http://www.grc.nasa.gov/WWW/MDWeb/

**Dynalloy, Inc.:**
http://www.dynalloy.com/

**Glenn contacts:**
Dr. Ronald D. Noebe, 216–433–2093, Ronald.D.Noebe@nasa.gov; and
Dr. Santo A. Padula II, 216–433–9375, Santo.A.Padula@nasa.gov

**Authors:**
Dr. Ronald D. Noebe, Jeffrey C. Brown, Susan L. Draper, Glen S. Bigelow, and Nicholas Penney

**Headquarters program office:**
Aeronautics Research

**Programs/Projects:**
QAT

# Benchtop Demonstration of an Adaptive Chevron Completed Using a New High-Temperature Shape-Memory Alloy

Chevrons placed on either the fan or core exhaust of jet engines have been shown to be very effective in reducing noise during the takeoff of commercial aircraft. However, conventional fixed-geometry chevrons represent a tradeoff in design that reduces noise over a limited range of flight conditions but also imposes a small, but significant, performance penalty on aircraft engines. The solution would be an adaptive-geometry chevron that could mitigate noise during takeoff (possibly even more so than current fixed designs because of greater immersion into the exhaust stream) but could be retracted during cruise so as not to affect performance. However, there are several daunting challenges to developing a successful adaptive-geometry chevron, especially for core exhaust applications. These include the need for very high actuation forces, a very limited volume for actuator placement, and high operating temperatures. Initial testing indicates that these challenges may be overcome through the use of a new chevron design developed by Continuum Dynamics, Inc., that utilizes a high-temperature shape-memory alloy (HTSMA) developed and supplied by the NASA Glenn Research Center.

The first two challenges (the need for high actuation forces and the limited space for actuator placement) affect both core exhaust and fan chevron designs. These challenges were solved through an extremely innovative and original approach that combined changes in chevron design with actuator development and placement. This resulted in an overall concept with deflection performance that is at least 5 times more efficient than current approaches. The performance, or action, of the chevron is also reproducible because all movement is completely elastic. This is in contrast to current adaptive metallic chevron designs that also undergo plastic deformation or to composite designs that undergo viscoelastic-plastic behavior and microcracking. The high-temperature requirement for a core exhaust chevron design was overcome by the identification, testing, and validation of a new nickel-titanium-platinum (NiTiPt) HTSMA.

The photographs show a 0.025-in.-thick steel chevron in the neutral position and actuated with a single strand of 0.045-in.-diameter HTSMA wire. The substantial deflection achieved during the test is a reflection of the high force generation capability of the HTSMA. The demonstration represents approximately 8 percent of the stiffness of a full-scale test. Computational modeling accurately predicted successful performance of the subscale bench test and indicated that the concept is scalable to full-size components that could operate under realistic conditions using the NiTiPt alloy. Although demonstrated at room temperature for convenience, the current shape-memory alloy could be used at temperatures up to approximately 260 °C (500 °F), and higher temperature versions are under development. Consequently, with the proper placement of the shape-memory alloy, this combination of material and design could be used in the actuation of core exhaust chevrons.

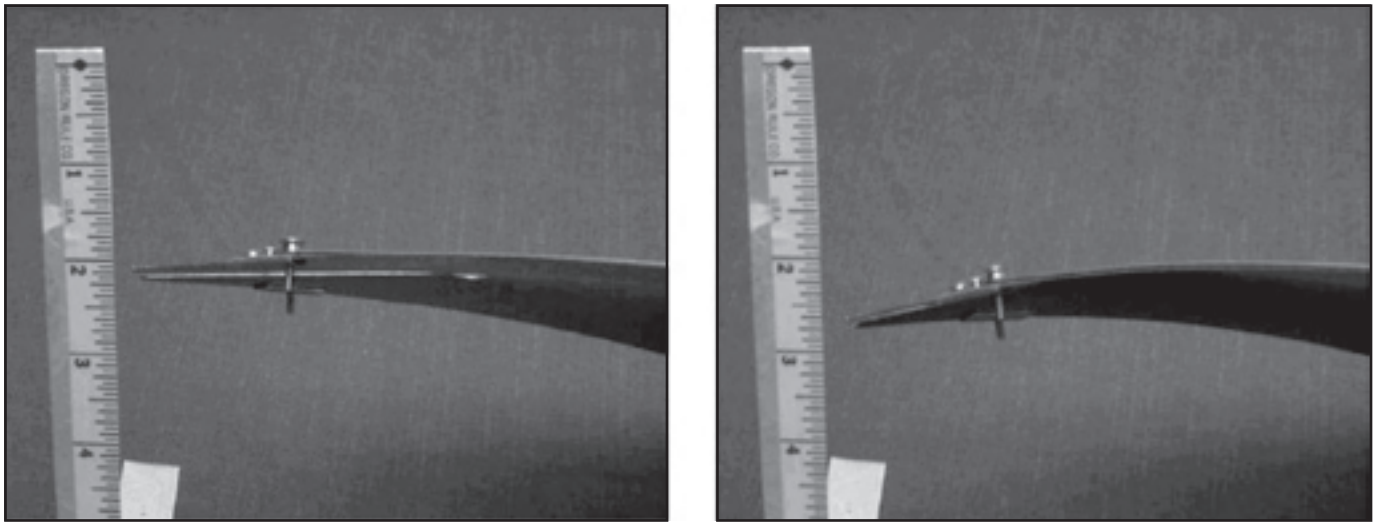

*Left: Side view of the neutral chevron position. Right: Actuated chevron showing full deflection (~0.75 in.) of the tip using a NiTiPt HTSMA.*

**Find out more about this research:**

**Continuum Dynamics, Inc.:**
http://www.continuum-dynamics.com

**Glenn's materials research:**
http://www.grc.nasa.gov/WWW/MDWeb/

**Glenn contacts:**
Dr. Ronald D. Noebe, 216–433–2093, Ronald.D.Noebe@nasa.gov; and
Dr. Santo A. Padula II, 216–433–9375, Santo.A.Padula@nasa.gov

**Authors:**
Dr. Ronald D. Noebe,
Dr. Todd R. Quackenbush, and
Dr. Santo A. Padula II

**Headquarters program office:**
Aeronautics Research

**Programs/Projects:**
QAT, Propulsion 21

# Advanced Stirling Convertor Superalloy Heater Head Developed and Demonstrated

The Department of Energy, Lockheed Martin, Infinia Corporation (formerly known as the Stirling Technology Company), and the NASA Glenn Research Center are developing a Stirling Radioisotope Generator (SRG) as an alternative to radioisotope thermoelectric generators for NASA space science missions. The 20- to 25-percent efficiency of the SRG system would reduce the required amount of radioisotope by a factor of 3 or more in comparison to radioisotope thermoelectric generators. This would significantly reduce radioisotope cost, radiological inventory, and system cost, providing efficient use of the scarce domestic supply of radioisotope resources.

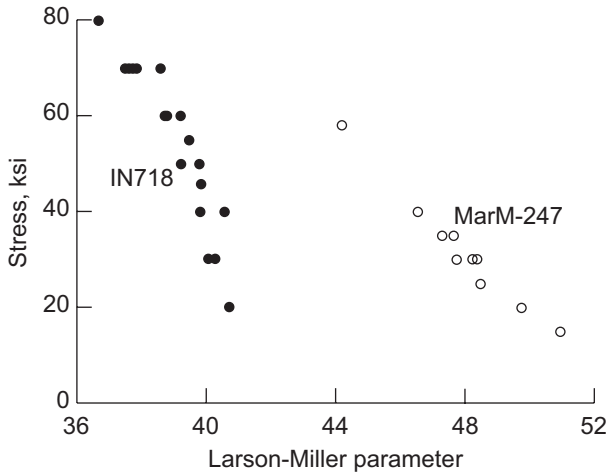


*Creep properties of the conventional heater head material, IN718 compared with the more advanced material, MarM-247. The data are plotted using a Larson-Miller parameter, which allows test data collected at different temperatures to be plotted on a single curve.*

In addition to the highly focused SRG program, NASA is spearheading an effort to develop an even higher efficiency, lower mass Stirling convertor for use with a radioisotope, reactor, or solar concentrator heat source. One of the goals for this upgraded version of the SRG is to improve performance by increasing the Carnot efficiency of the convertor. To achieve this improvement, researchers must maximize the hot-end temperature and the pressure of the working gas. Although increasing both the temperature and pressure of the working fluid will place an increased burden on all components of the convertor, the heater head will be the most severely tested. The current heater head is made from the nickel-base superalloy 718 and operates at 650 °C, which is this alloy's maximum use-temperature. Further increases in temperature will require the use of a more advanced high-temperature material.

At the NASA Glenn Research Center, over 200 material candidates were initially screened with regard to the following properties: (1) creep resistance, (2) fabricability, (3) helium gas containment, (4) long-term stability and compatibility, (5) ability to form a hermetical closeout seal, and (6) ductility and toughness (to assist in fabrication, handling, and resistance to foreign object damage). In the end, the list of candidates was narrowed to five superalloys. These five alloys were then subjected to additional testing, including creep testing under a wide variety of conditions. From these experiments, the nickel-base superalloy MarM-247 was the clear choice as the primary material for the new heater head.

One critical feature of the heater head is its thin wall thickness (<1 mm in some regions). Since thin walls are known to

affect the creep behavior of superalloys, it was necessary to produce several heats of material with different grain sizes and, thereby, determine the optimum microstructure. Further analysis of the creep data allowed a detailed reliability assessment to be performed, and it established the maximum operating temperature and stress that could be tolerated with a high confidence of success for the intended mission duration.

In additional to the mechanical properties of the heater head, some method of hermetically sealing the MarM-247 to the convertor body is required. Unfortunately, one negative consequence of MarM-247's high strength is that it cannot be joined by traditional fusion welding techniques. Also, any joining technique that requires heat input into the heater head must be compatible with the overall assembly and with the material heat-treatment procedure that is required to develop the material's high strength.

Many joining techniques were explored at Glenn, but eventually two methods emerged as the most promising. One is a brazing process that uses a braze filler metal and brazing cycle that is completely compatible with the heat-treatment schedule. The other is electrospark deposition, which is a nonfusion technique normally used for surface repair. The brazing concept was demonstrated and proven not to adversely affect the properties of the MarM-247, even after long-duration missions. The electrospark deposition technique is undergoing detailed evaluation.

Independent of the in-house effort, NASA awarded a NASA Research Announcement (NRA, NAS3–03128) to a Sunpower/Rocketdyne team to develop an Advanced Stirling Convertor (ASC). Upon the completion of Glenn's MarM-247 optimization program, the results of the material screening and optimization efforts were presented at the Space Technology and Applications International Forum. A detailed summary of Glenn's findings also were presented to the NRA team at their request. After reviewing the data, the NRA team accepted the results of Glenn's study and adopted MarM-247 as the material of choice. Since then, Glenn and the Sunpower/Rocketdyne team have collaborated on development of the ASC. In late September 2005, the team successfully operated an ASC testbed convertor using the MarM-247 heater head. The head temperature was limited to 650 °C for the first run, but subsequent runs have been performed at the design temperature of 850 °C, which is 200 °C higher than for the previous SRG design.


*The ASC developed jointly by Sunpower and Rocketdyne, complete with a fully fabricated MarM-247 heater head.*

**Find out more about this research:**

**Glenn's Advanced Materials Branch:**
http://www.grc.nasa.gov/WWW/AdvMet/webpage

**Glenn's Thermal Energy Conversion Branch:**
http://www.grc.nasa.gov/WWW/tmsb/

**Glenn's Power and Propulsion Office**
http://space-power.grc.nasa.gov/ppo/

**Glenn contact:**
Dr. Randy R. Bowman, 216–433–3205, Randy.R.Bowman@nasa.gov

**Author:**
Dr. Randy R. Bowman

**Headquarters program office:**
Science Mission

**Programs/Projects:**
RPS

# Long-Term Structural Benchmark Testing Started for Stirling Convertor Heater Heads

A major phase of structural benchmark testing began at the NASA Glenn Research Center (http://www.grc.nasa.gov) for a critical component of the 110-W Stirling Radioisotope Generator (SRG110). Durability testing of the heater head component was initiated on two test articles under prototypical environmental conditions: Glenn's special-purpose test rigs subject the heater head specimens to the design operating temperatures and pressure. Under these conditions, the primary life-limiting damage mechanism is creep deformation. The experimental data produced support the development of an analytical life-prediction methodology (ref. 1). The testing will be terminated after approximately 1 year of operation.

The SRG110 is being developed to provide electric power for multimission uses, including possible future long-duration NASA space science missions such as deep-space missions or lunar applications (ref. 2). For these uses, the heater head component must endure high temperature at low stress for a long time. The heater head is designed to minimize the effects of material creep—a slow, gradual increase in the pressure vessel diameter that could result in reduced system performance if not properly designed.

Although creep-limited components have been designed satisfactorily using material properties generated from traditional uniaxial tests, the heater head is subjected to a biaxial state of stress. To supplement the ongoing uniaxial creep tests of flight heat Inconel 718 material (ref. 3), Glenn researchers developed benchmark testing to experimentally evaluate the response to this specific biaxial stress condition. Early test data from previous benchmark testing at Glenn accelerated the creep response in short-duration tests by increasing test pressures to raise the specimens' stress levels. The current final test phase is not accelerated, and high scatter of the very small magnitude creep strains in the short term can be averaged over the extended 1-year test time.

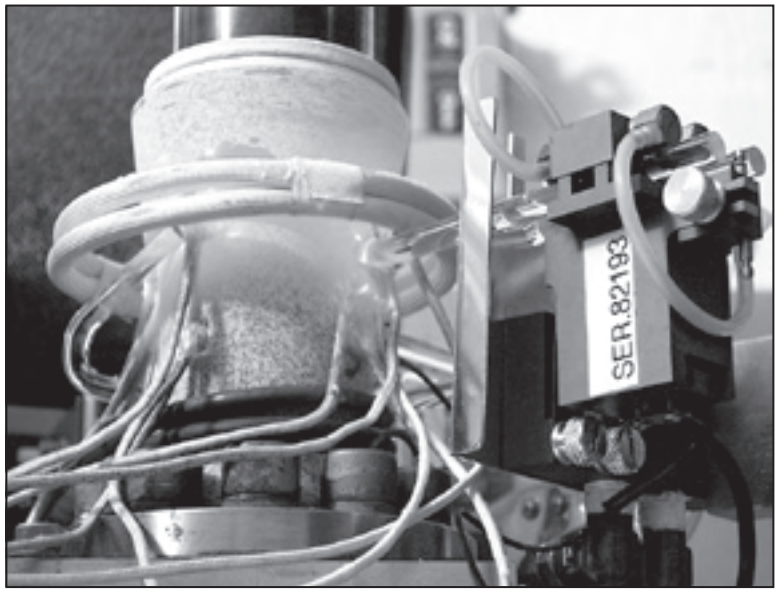


*Twelve-month test of Inconel 718 heater head with axial loading at 650 °C (1200 °F); induction heating coils and diametral extensometer quartz probes are visible.*

The current in-house testing uses two heater-head test articles fabricated to flight prototype specifications. One of these is a "full-up" specimen with structurally significant brazed-on attachments; its test includes an additional externally applied axial load to simulate actual heat source contact loading (see the photograph on this page).

The test facility is located at the Life Prediction Branch's (http://www.grc.nasa.gov/WWW/LPB/) Structural Benchmark Test Facility. The test stand (see the photograph on the following page) includes two independently operated test rigs with argon pressurization systems capable of 3000 psig. Two 3-kW induction power supplies provide even heating and temperature profiling, and a custom data-acquisition and control system is employed to safely conduct tests and record results.

The benchmark testing was performed in collaboration with Glenn's Thermal Energy Conversion Branch (http://www.grc.nasa.gov/WWW/tmsb/) as part of a Glenn in-house project supporting the development of the SRG110. NASA's Science Mission Directorate provided funding for this effort. The overall SRG110 project is managed by the Department of Energy. Lockheed Martin and Infinia Corporation are developing the SRG110 for the Department of Energy. Glenn is providing supporting technology development for the SRG110, independent verification and validation testing, and advanced technology efforts.

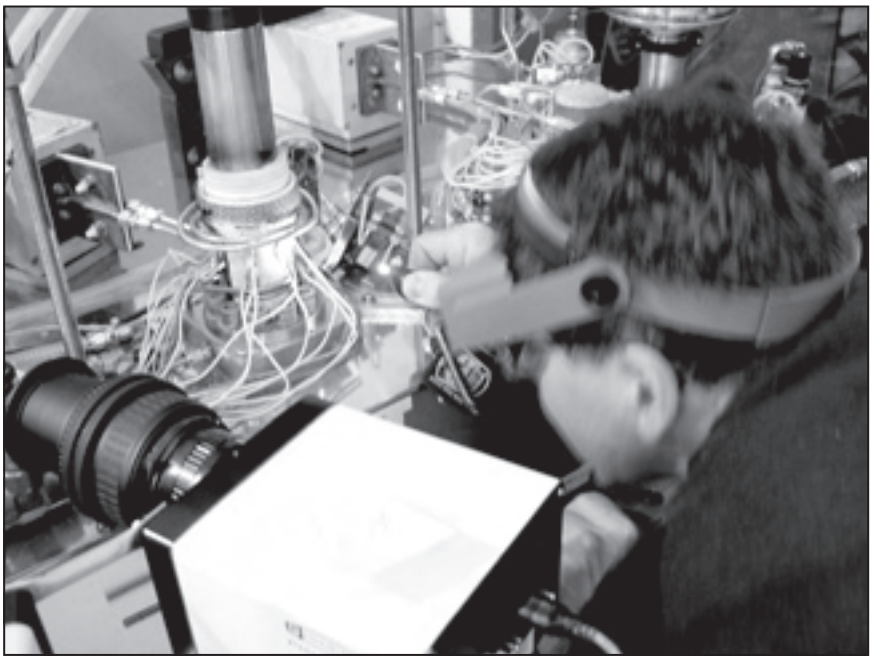

*A final check of thermocouple positions is made at the heater head structural benchmark test stand.*


**References**

1. Halford, Gary R., et al.: Structural Analyses of Stirling Power Convertor Heater Head for Long-Term Reliability, Durability, and Performance. NASA/TM—2002-211327, 2002. http://gltrs.grc.nasa.gov/cgi-bin/GLTRS/browse.pl?2002/TM-2002-211327.html
2. Thieme, Lanny G.; and Schreiber, Jeffrey G.: Supporting Development for the Stirling Radioisotope Generator and Advanced Stirling Technology Development at NASA GRC. NASA/TM—2005-213409 (AIP Conf. Proc., vol. 746, 2005, pp. 674–681), 2005. http://gltrs.grc.nasa.gov/cgi-bin/GLTRS/browse.pl?2005/TM-2005-213409.html
3. Bowman, R.R.: Long-Term Creep Assessment of a Thin-Walled Inconel 718 Stirling Power-Convertor Heater Head. Proceedings of the 36th Intersociety Energy Conversion Engineering Conference, IECEC2001–CT–33, vol. 1, 2001, pp. 435–440.


**Find out more about this research:**

**NASA Glenn Research Center:**
http://www.grc.nasa.gov/

**Glenn's Thermal Energy Conversion Branch:**
http://www.grc.nasa.gov/WWW/tmsb/

**Glenn's Life Prediction Branch:**
http://www.grc.nasa.gov/WWW/LPB/


**Glenn contacts:**
David L. Krause, 216–433–5465, David.L.Krause@nasa.gov; and
Dr. Randy R. Bowman, 216–433–3205, Randy.R.Bowman@nasa.gov

**Authors:**
David L. Krause, Dr. Gary R. Halford, and Dr. Randy R. Bowman


**Headquarters program office:**
Science Mission

**Programs/Projects:**
RPS, SRG110

# Materials Compatibility Evaluated for Advanced Heat Pipes in Space Power Thermal Management Systems

Management of the residual heat generated during power conversion in space is a critical stage for a successful space exploration mission. Under the Prometheus program, an exploratory design of space radiators using intermediate-temperature (450 to 700 K) heat pipe systems to efficiently distribute the heat within radiator panels was studied at the NASA Glenn Research Center. A heat pipe is a self-contained two-phase sealed device that can transport large quantities of heat with minimal temperature drop. This is accomplished by the evaporation of a liquid at the hotter end of the device and the condensation of the vapor at the cooler end. Specially designed wicks lined against the device wall return the condensed liquid to the evaporator section. Hundreds of these devices are planned to be major components of radiator panels for Moon, Mars, and deep-space missions.

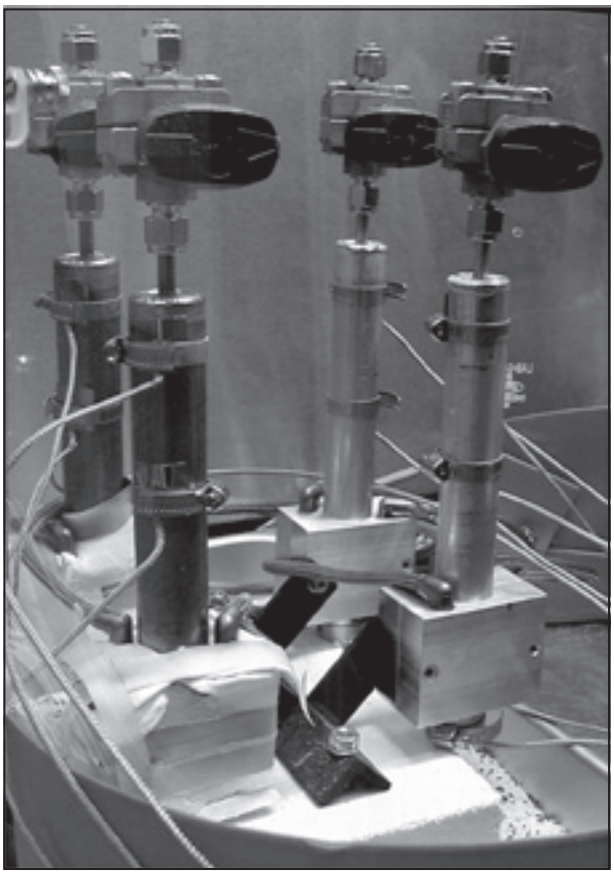

*View of the Ti (CP2) and Al-alloys testing capsules and testing station.*

Although water has been tested to about 550 K, its vapor pressure rises to a level that will require very thick container walls, resulting in heavier components. Thus, a study was conducted at Glenn to identify alternative fluids with the desired thermodynamic properties along with envelope materials that have sufficient chemical compatibility, thermal conductance, and mechanical integrity. This study resulted in the selection of the halides aluminum bromide ($AlBr_3$), antimony bromide ($SbBr_3$), and titanium chloride ($TiCl_4$). The halide choices were based on several factors, including vapor pressure, melting and boiling points, cost, availability, and handling safety. The envelope and wick metals chosen for the study were two aluminum alloys (Al–5052 and Al–6061) and commercial pure titanium grade 2 (Ti CP2) because of thermodynamics compatibility predictions and the availability, low density, and wide use of these materials in aerospace technologies. The next step was to conduct experiments to determine the chemical compatibility of selected metals for the envelope and wick with the selected halides.

Commercial pipes and rods were procured, machined, and welded to fabricate the experimental capsules. Then, assembled capsules were tested at 500 K in a specially designed test station that mimics actual heat pipe conditions. A total of five fluid/envelope combinations, with duplicates, were evaluated experimentally. The internal pipe surfaces and metallographically polished cross sections were observed by optical and field-emission scanning electron microscopy. Chemical and x-ray analyses were performed on the products and layers that formed on the inner diameter of the capsule. The compatibility studies have shown that $AlBr_3$ is not compatible with Ti (CP2), Al-6061, or Al-5052 alloys. Although thermodynamic calculations indicated that pure-Al is compatible with $AlBr_3$, the influence of alloying additions was not considered analytically. Although the results show that $AlBr_3$ was more stable than Ti (CP2) in the Al-6061 envelope, microstructural characterization revealed severe intergranular corrosion on both metal systems. Among the successful combinations, a Ti (CP2) capsule containing $TiCl_4$, and an Al-6061 capsule containing $SbBr_3$ have reached over 4000 hr of exposure at 500 K with no sign of degradation.

In summary, it was found that several advanced heat pipe fluids can be incorporated into realistic intermediate temperature heat pipes with good compatibility with the proposed envelope and wick materials.

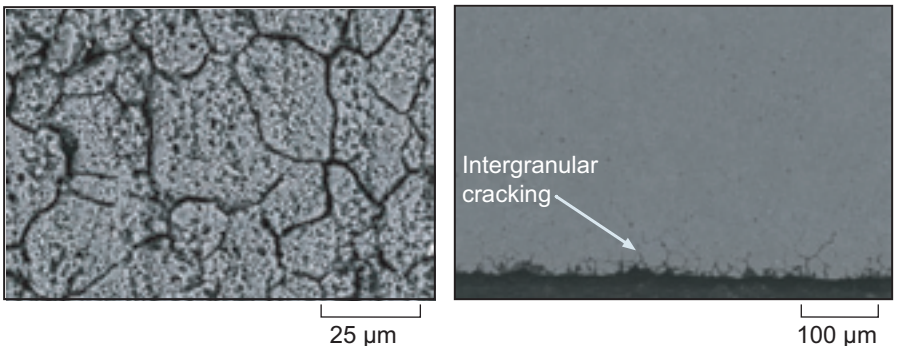


*Electron microscopy images showing intergranular corrosion attack produced on the wall of the Al-6061 alloy by $AlBr_3$ after 1100 hr of testing at 500 K. Left: Internal surface of tube midsection. Right: Cross-section view of the evaporator.*

**Bibliography**

Anderson, William G., et al.: Evaluation of Heat Pipe Working Fluids in the Temperature Range 450 to 700 K. Space Technology and Applications International Forum–STAIF 2004, 2004, pp. 20–27.

Devarakonda, A.; and Olminsky, J.K.: An Evaluation of Halides and Other Substances as Potential Heat Pipe Fluids. AIAA–2004–5575, 2004.

Locci, Ivan E., et al.: Analytical and Experimental Thermo-Chemical Compatibility Study of Potential Heat Pipe Materials. AIAA–2005–5666, 2005.

**Find out more about materials research at Glenn:**
http://www.grc.nasa.gov/WWW/MDWeb/

**University of Toledo contact:**
Dr. Ivan E. Locci, 216–433–5009,
Ivan.E.Locci@nasa.gov

**Glenn contact:**
Duane E. Beach, 216–433–6285,
Duane.E.Beach@nasa.gov

**Authors:**
Dr. Ivan E. Locci,
Dr. Angirasa Devarakonda,
Dr. Evan H. Copland, Jami K. Olminsky,
and Duane E. Beach.

**Headquarters program office:**
Space Exploration

**Programs/Projects:**
Project Prometheus

## Reaction Zones Associated With Joining Ni-Based Superalloys to Refractory Metals Studied

The NASA Glenn Research Center initiated an experimental program to join superalloys to refractory metals in response to the future need of nuclear power for electrical power generation and propulsion for future space missions. The primary goal was to understand and characterize the reaction zones that form between the refractory alloys and nickel-based (Ni-based) superalloys after joining. This will lead to the development of a model for predicting the integrity of the bond after extremely long-term thermal exposures.

Future space missions, in addition to lunar and Mars habitats, will benefit greatly from the abundant electrical power generated with heat from nuclear reactors. Certain refractory metals are ideally suited for use with nuclear reactors because of their high strength at elevated temperatures and low radiation cross sections. However, Ni-based alloys are typically employed for power generation by gas turbines because of their high strengths at intermediate temperatures and significantly lower densities than refractory metals, an important consideration for rotating hardware in gas turbines. To use both metals, in concert, for electrical power generation in space requires some type of joint that typically is held at an elevated temperature. Furthermore, this joint must maintain its integrity without maintenance for many years, possibly decades. The problem is that when refractory metals are bonded to Ni-based superalloys, brittle phases (i.e., intermetallics) can form because of interdiffusion between the two different metals. In addition, other deleterious phases or even porosity can form and threaten the integrity of the bond.

Previous work (ref. 1) had suggested that if these layers are sufficiently thin

(less than 12 μm), they will not degrade the mechanical properties of the joint. However, these layers thicken with time with the growth rate depending on the temperature and composition of the metals. The purpose of the present work was to characterize the layers for various Ni-based superalloy and refractory metal combinations at different temperatures. The thicknesses of the layers were measured, and the formation of potentially harmful phases and/or porosity was noted.

Commercially available superalloys MarM-247, Hastelloy X, Haynes 230, and Inconel 617 were diffusion bonded to various tantalum (Ta), niobium (Nb), and molybdenum (Mo) refractory alloys (T–111, FS–85, and Mo-47Re, respectively). The alloys were bonded together using a hot press to form "diffusion couples" and annealed at various temperatures. The total width of the reaction zone encompassing the intermetallic phase layers and porosity was measured using a scanning electron microscope. Other potentially deleterious features, such as significant cracking and discontinuous phase formation, were also noted. Lastly, the potentially beneficial effect of thin Ni and Mo interlayers between the two dissimilar alloys was examined.

A relatively simple reaction zone consisting of only two layers is shown in the photomicrograph. The reaction zone thicknesses for several of the couples annealed at either 1150 or 1300 K are shown in the bar chart. This figure shows that zone width is very similar for the two Ni-based superalloys, whereas the zone width is a factor of 4 greater for the FS–85 than it is for the Mo-47Re refractory alloys. The x-ray maps in the final figure show the elemental distributions between a more complex five-layer reaction zone and illustrate enrichments for some elements and depletions for others. From data similar to that in the bar chart, reaction rates were calculated. Although longer term exposures are still needed, data generated to date show that traditional diffusion models are accurate and that high-temperature exposures are valid as an accelerated test method. Future work will refine and calibrate a model to predict reaction zone widths after years and decades to determine the best superalloy-refractory metal combinations for future space missions.

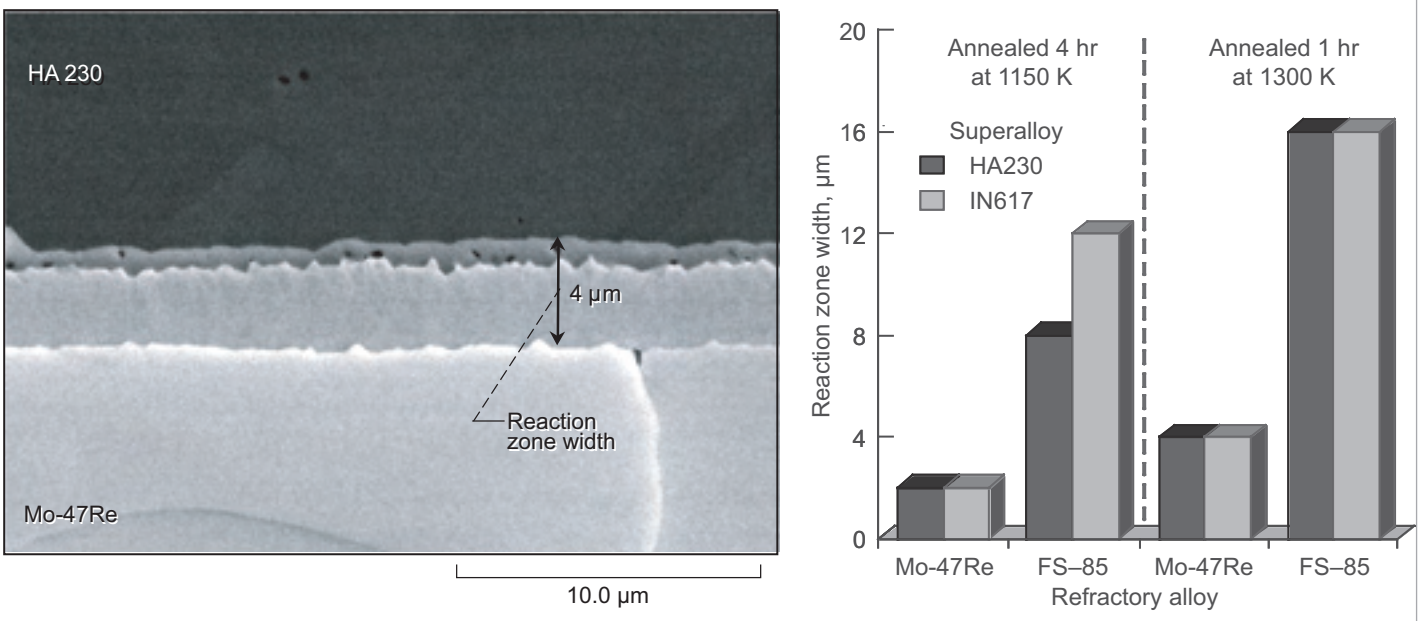


*Left: Reaction zone for HA230/Mo-47Re diffusion couple after 1 hr at 1300 K. Right: Reaction zone width for various Ni-based superalloy/refractory alloy combinations annealed at either 1150 or 1300 K.*

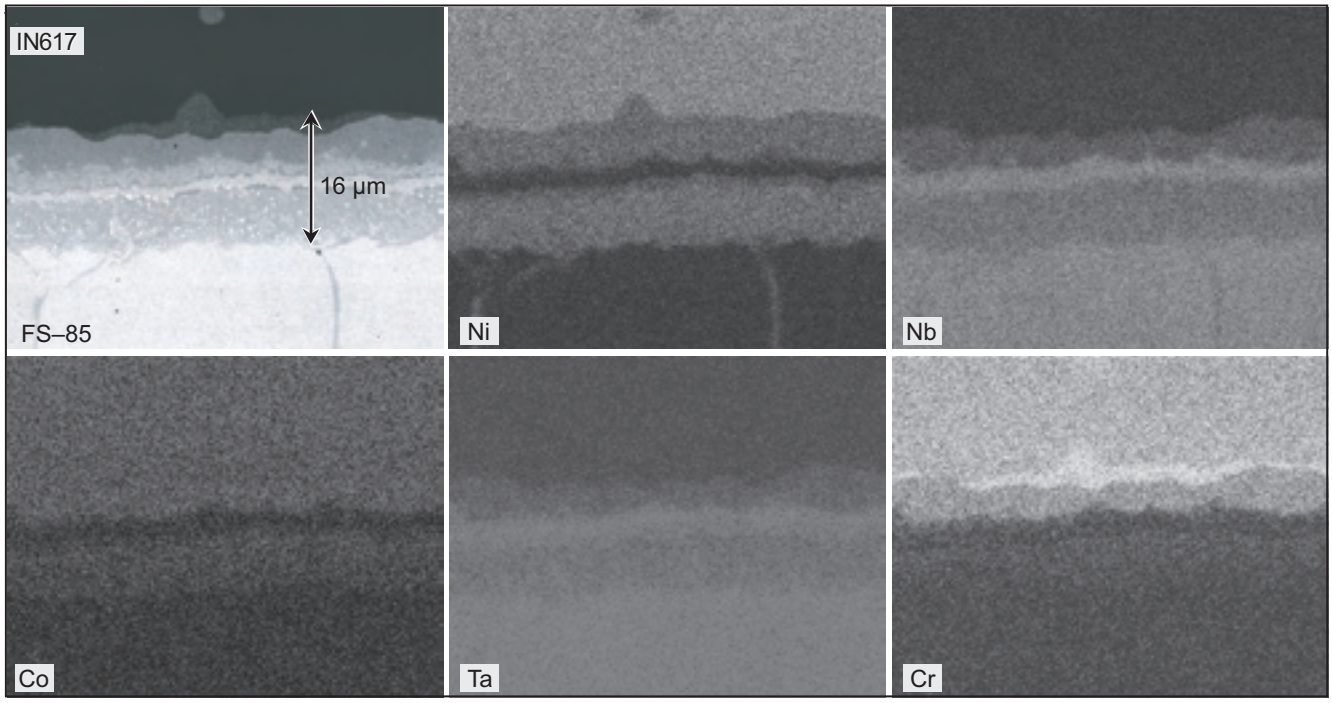


*X-ray maps showing elemental distributions in the reaction zone for a IN617/FS85 couple annealed at 1300 K for 1 hr; Co, cobalt; Cr, chromium.*

**Reference**

1. Buckman, R.W. Jr.; and Goodspeed, R.C.: Evaluation of Refractory/Austenitic Bimetal Combinations. Westinghouse Astronuclear Laboratory Report WANL–PR–(EE)–004 (NASA CR–1516), 1970.

**University of Toledo contact:**

Dr. Ivan E. Locci, 216–433–5009, Ivan.E.Locci@nasa.gov

**Glenn contacts:**

Dr. James A. Nesbitt, 216–433–3275, James.A.Nesbitt@nasa.gov; and
Frank J. Ritzert, 216–433–8199, Frank.Ritzert@nasa.gov

**Authors:**

Dr. Ivan E. Locci, Dr. James A. Nesbitt, and Frank J. Ritzert

**Headquarters program office:**

Space Exploration

**Programs/Projects:**

Project Prometheus

# Techniques Investigated to Join Advanced Materials for Future Space Exploration Missions

The next generation of power systems for future spacecraft and lunar surface systems will likely have a strong dependence on nuclear power. The design of a space nuclear power plant involves integrating the major subsystems of the reactor, the power-conversion system, and the heat-rejection system. Optimum material choices are very different for each subsystem, with likely choices for the reactor tending toward high-temperature refractory metal alloys, the power-conversion system tending toward intermediate-temperature nickel-based (Ni-based) superalloys, and the heat-rejection system tending toward titanium and carbon/carbon composites. The transitions between these three subsystems are critical points in the system, and thus joining the dissimilar metals is a key factor in determining life and performance. The NASA Glenn Research Center has, therefore, initiated a comprehensive program to evaluate the best technologies to join the dissimilar metals required for future exploration missions.

The joining of refractory metals to Ni-base alloys was considered the most significant challenge, since these joints will likely be exposed for thousands of hours at high temperatures. The refractory alloy candidates are based primarily on molybdenum (Mo), niobium (Nb), tantalum (Ta), or rhenium (Re), whereas the superalloy candidate would most likely be a wrought alloy with a significant history and pedigree. Wrought superalloys are preferred for hot duct applications because of their fabricability and weldability. Both gas- and liquid-cooled joint designs require the ducting to be hermetically sealed, accompanied by good strength at the joint, with long-term thermal stability. Conventional fusion techniques for joining were considered but were rejected since intermetallic phases and cracking are associated with the postweld zones accompanying those techniques. Thus, solid-state methods of joining the dissimilar materials provided the best opportunity to eliminate unwanted phases and cracking at the transition joint.

In collaboration with the Edison Welding Institute, Glenn researchers selected magnetic pulse welding, electrospark deposition (ESD), and inertia welding to join the refractory metals tantalum (Ta10W and T111) and molybdenum (Mo-47Re) to representative superalloys—both a wrought (Hastelloy X) and a cast (MarM-247) alloy. Inertia welding techniques were successfully developed for MarM-247 with Mo-47Re and for Hastelloy X with both Ta10W and Mo-47Re. ESD methods also were developed for Mar-M247 and Hastelloy X with T111 and Mo-47Re. Examples are shown in the photomicrographs on this page. Difficulties were encountered with efforts to develop magnetic pulse welding, but future modifications to the method appear promising.

A second class of joining process that was considered for dissimilar metals is brazing. Several different refractory metal candidates (Re, Mo-47Re, Nb-1Zr, and ASTAR 811C) were brazed to both Ni201 and Hastelloy X to assess process viability, to evaluate bond integrity, and to examine resultant microstructures at the interface. Candidate filler materials included Palni, Palco, Palniro-4, and copper (Cu) ABA. Preliminary microstructural observations showed that brazing these alloys is feasible, and the photomicrograph on the next page shows an example of a sound braze joint.

Because space missions could last for decades, it is important to evaluate and develop processes that will promote long-term bonding, strength, and phase stability. Therefore, all the successfully joined materials are scheduled for mechanical strength evaluation as well as for long-term stability testing at appropriate temperatures. Continued evaluation and optimization of solid-state and brazing options are necessary for systems that will rely on the long-term durability of a transition joint.

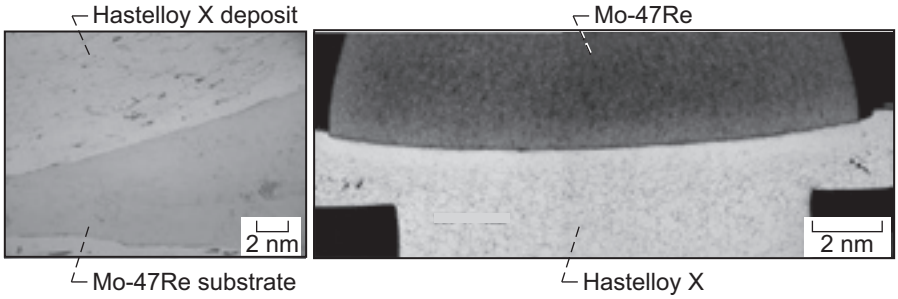


*Joint between Hastelloy X and Mo-47Re. Left: Electrospark deposition. Right: Inertia welding.*

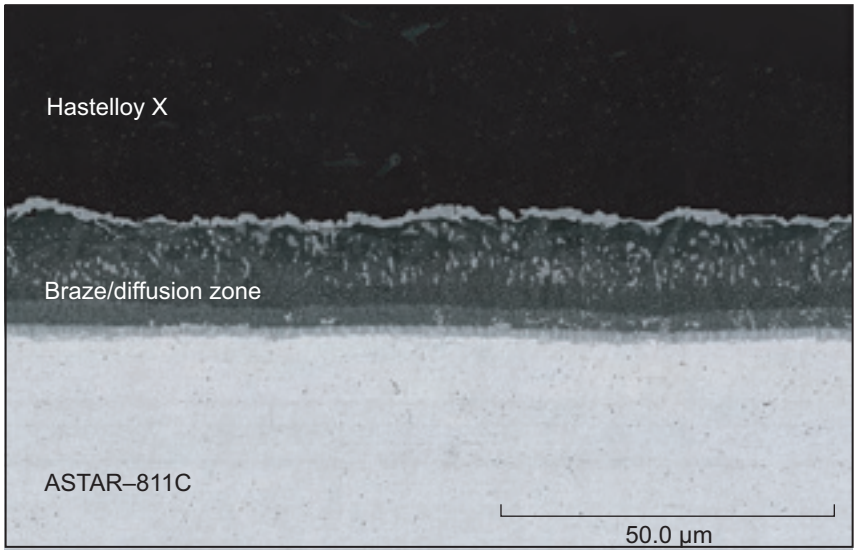


*Complex braze interface, Hastelloy X/Palni/ASTAR–811C.*

**Glenn contacts:**
Frank J. Ritzert, 216–433–8199, Frank.Ritzert@nasa.gov;
Dr. Cheryl L. Bowman, 216–433–8462, Cheryl.L.Bowman@nasa.gov; and
Dr. John Gayda, 216–433–3273, John.Gayda-1@nasa.gov

**University of Toledo contact:**
Dr. Ivan E. Locci, 216–433–5009, Ivan.E.Locci@nasa.gov

**Ohio Aerospace Institute (OAI) contact:**
William S. Loewenthal, 216–433–2697, William.S.Loewenthal@nasa.gov

**Author:**
Frank J. Ritzert

**Headquarters program office:**
Exploration Systems

**Programs/Projects:**
Project Prometheus

## Simple Test Developed to Determine the Effectiveness of Different Braze Compositions for Joining Titanium Tubes to Carbon/Carbon Composite Plates

Thermal management components based on high-conductivity carbon-fiber-reinforced carbon matrix (C/C) composites are being developed for various space exploration systems. Many of these applications require that metal tubes be joined to C/C composite plates. Typical joint tests involve the joining of flat plates to flat plates to determine the through-the-thickness tensile strength or shear strength of the joint. These traditional tests mask some of the issues involved in joining curved surfaces to flat plates. To meet this need, researchers at the NASA Glenn Research Center implemented a simple tube-plate joint tensile test to compare the effectiveness of commercial brazes for bonding titanium (Ti) tubes to C/C composite plates (see the figure below).

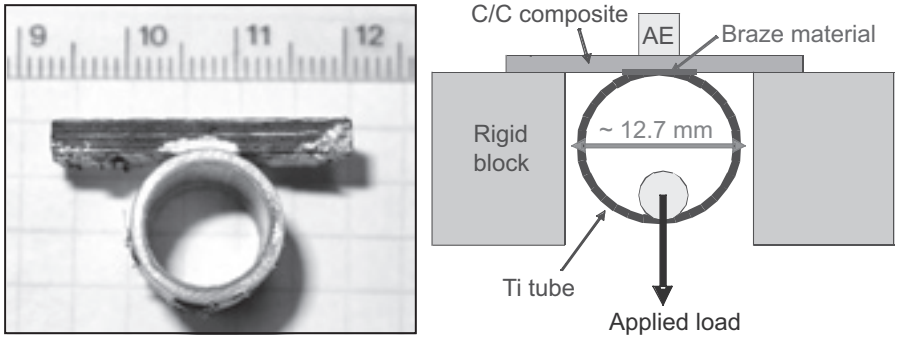


*Left: Optical photograph of specimen. Right: Schematic of tube-plate tensile test. AE, acoustic emission.*

The test consists of brazing the Ti-tube (0.5 in. in diameter by 1 in. long) to a C/C plate (1 in. long by 0.5 in. wide). The plate is set on a hollow rigid block, and the tube is pulled in tension until failure. Three braze systems (copper active braze alloy, Cu-ABA; titanium copper nickel, TiCuNi; and titanium copper silver, TiCuSil) were used to join the tube-plate structures. There were considerable differences in the load-carrying abilities of the braze systems (see the bar chart on the next page). Failure always occurred in the surface ply of the C/C composite, indicating strong bonding between the braze material and the composite; however, the load-carrying ability of the joint was controlled by the interlaminar strength of the composite itself. The Cu-ABA braze system proved to have about twice the load-carrying ability of the other two systems because the bonded area between the braze material and the C/C plate was largest for this system (see

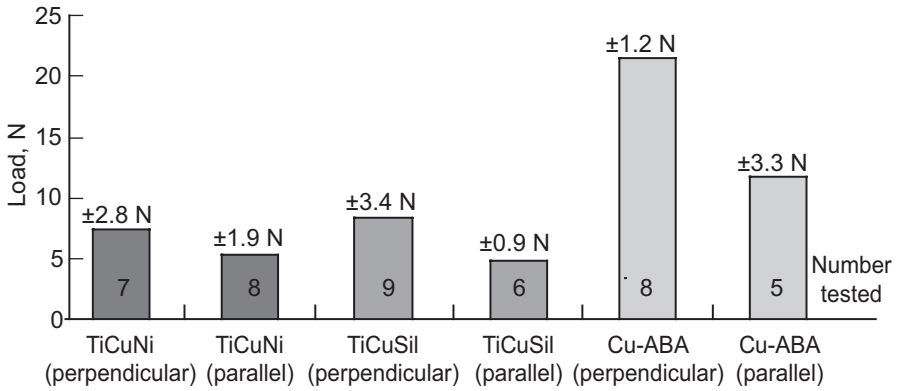


*Failure load of tube-plate tensile tests for different braze systems and different orientations of the outer fiber tows of the C/C composites; showing ± standard deviation.*

the photographs). This was because the Cu-ABA braze system had superior spreading properties around the circumference of the tube and into the pores and crevices of the surface of the C/C composite. It was also found that the orientation of the surface fiber tows had a significant effect on the load-carrying ability. The alignment of the outer tows in the photographs is perpendicular to the tube axis, which for all the systems tested, was a stronger orientation (see the bar chart) than when the fibers were oriented parallel to the tube axis.

The test is a very good way of comparing processing or structural alterations during the developmental process. For example, processing modifications, such as increasing the process load and modifying the surface of the C/C plate by grooving out channels for the Ti-tube to nest in, were compared. These modifications resulted in higher failure loads and demonstrated how this simple test could be used to evaluate process and structure changes in a meaningful, yet rapid, way.

**Bibliography**
Morscher, Gregory N., et al.: A Simple Test to Determine the Effectiveness of Different Braze Compositions for Joining Ti-Tubes to C/C Composite Plates. Mater. Sci. Eng. A., vol. 418, 2006, pp. 19–24.

**Ohio Aerospace Institute (OAI) contact:**
Dr. Gregory N. Morscher, 216–433–5512, Gregory.N.Morscher@nasa.gov

**Glenn contact:**
Dr. Andrew J. Eckel, 216–433–8185, Andrew.J.Eckel@nasa.gov

**Authors:**
Dr. Gregory N. Morscher,
Dr. Mrityunjay Singh, and
Tarah P. Shpargel

**Headquarters program office:**
Exploration Systems

**Programs/Projects:**
Project Prometheus

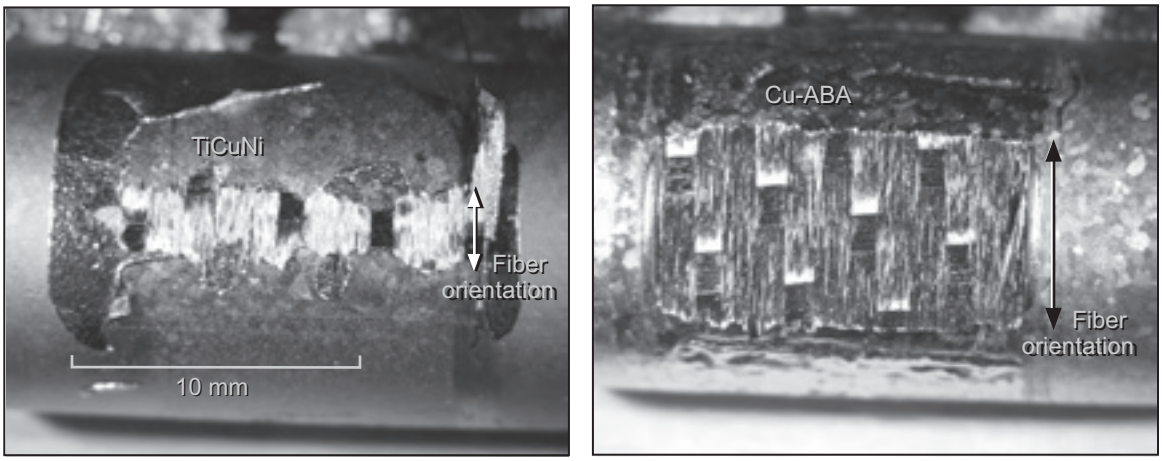


*Typical joint structure C/C fracture surfaces (arrows show length of fractures) that adhered to the titanium tube. Left: TiCuNi braze material. Right: Cu-ABA braze material.*

# Thermochemistry for Chromia Volatility Determined by the Transpiration Technique

The corrosion of chromium-containing materials in oxidizing environments containing water vapor, via the formation of volatile species, is a problem with broad technological and environmental implications. Chromium in the +6 valence state is considered to be a carcinogenic hazard. In addition, the volatility of chromium causes contamination and/or reduced lifetimes for solid oxide fuel cell interconnects, steam-methane reformer catalysts, structural steels in combustion environments, and chemical vapor deposition reactions. The thermochemistry of the volatilization reactions is not well characterized, preventing accurate understanding and prediction of the degradation processes described.

In oxidizing environments, chromium-containing materials oxidize to form chromia, $Cr_2O_3(s)$. Chromia is known to form gaseous oxide and/or oxyhydroxide species in oxidizing environments by the following three reactions:

$$\tfrac{1}{2}\, Cr_2O_3(s) + \tfrac{3}{4}\, O_2(g) = CrO_3(g) \quad (1)$$

$$\tfrac{1}{2}\, Cr_2O_3(s) + \tfrac{3}{4}\, O_2(g) + H_2O(g) = CrO_2(OH)_2(g) \quad (2)$$

$$\tfrac{1}{2}\, Cr_2O_3(s) + \tfrac{1}{2}\, O_2(g) + \tfrac{1}{2}\, H_2O(g) = CrO_2(OH)(g) \quad (3)$$

Although reaction (2) is proposed to be the reaction of greatest importance for environments of technological interest, the identity of this volatile species has not been established with certainty. Furthermore, the thermochemistry of $CrO_2(OH)_2(g)$ has been studied both theoretically and experimentally, but the resulting data are in poor agreement. For this reason, the volatility of chromia in oxygen and water vapor was studied at the NASA Glenn Research Center by the transpiration method to confirm the identity of the volatile Cr-O-H species and to determine accurate thermochemical data for this species.

The transpiration method is a well-established and versatile technique for studying gas-solid equilibria and measuring vapor pressures in the presence of large concentrations of other gases. In this study, the reactive gases oxygen and water vapor, at 1-atm total pressure, flowed over chromia at well-defined temperatures between 300 and 900 °C. The volatile species were formed in equilibrium concentrations and were transported to a cooler portion of the gas train where they condensed. The condensate was collected, and the amount of transported chromium was measured by inductively coupled plasma—atomic emission spectrometry.

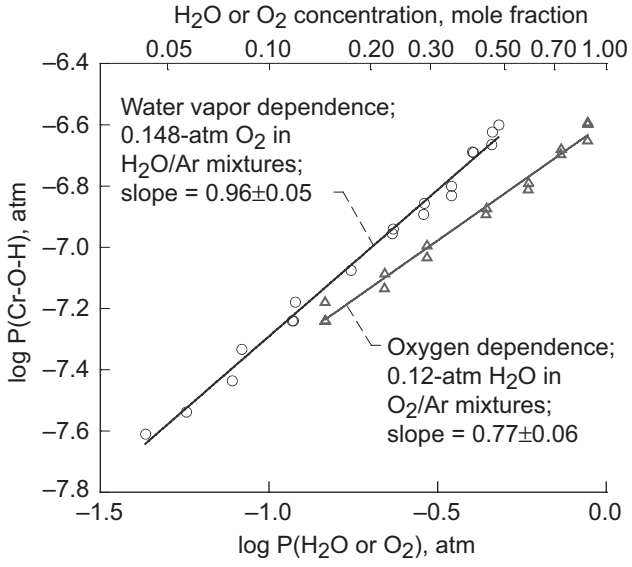


*Pressure dependence of the volatilization of $Cr_2O_3(s)$ enables the identification of volatile species as $CrO_2(OH)_2(g)$.*

The oxygen and water vapor pressure dependencies of the chromia volatilization reaction were determined at 600 °C to identify the volatile species (shown in the graph). We found that the pressure of the volatile species, $P_{Cr\text{-}O\text{-}H}$, depended on $P(O_2)^m$ and $P(H_2O)^n$, where the power law exponents were $m = 0.77 \pm 0.06$ and $n = 0.96 \pm 0.05$. These exponents are in excellent agreement with those predicted by reaction (2), m = ¾ and n = 1, indicating that $CrO_2(OH)_2(g)$ is the volatile species formed from the reaction of chromia with oxygen and water vapor at 600 °C.

Because the input rate of oxygen and water vapor is known and the output rate of volatilized chromium is measured, the equilibrium constant for the reaction, $K_p$, can be determined. $K_p$ depends on the gas species partial pressures $P$ according to the following equation:

$$K_p = \frac{P(CrO_2\,(OH)_2)}{P(H_2O) \cdot P(O_2)^{3/4}} \quad (4)$$

The variation of the equilibrium constant with temperature for reaction (2) is shown in the graph on the next page. The enthalpy, $\Delta H^\circ_{r\,861}$, and entropy, $\Delta S^\circ_{r\,861}$, for reaction (2) at the average experimental temperature of 861 K were determined from the slope and intercept of this line. The resulting thermodynamic data are $\Delta H^\circ_{r\,861}$ = 53.5±1.8 kJ/mol and $\Delta S^\circ_{r\,861}$ = –45.6±2.2 J/mol K.

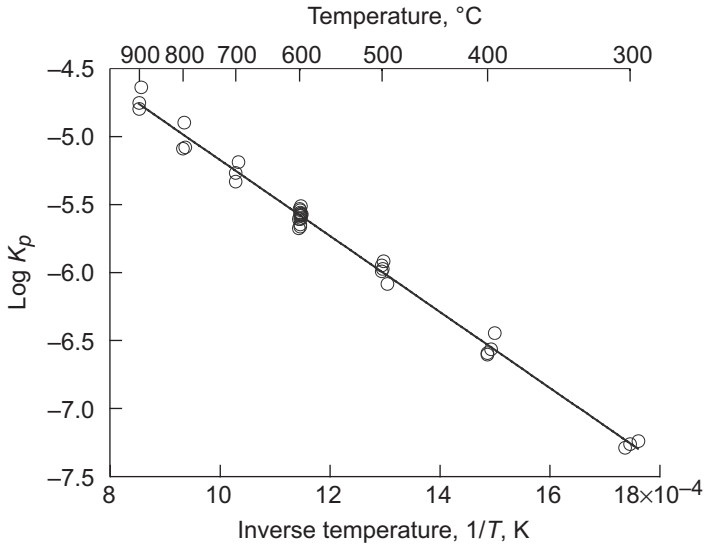


*Temperature dependence of the equilibrium constant, $K_p$, for reaction (2) enables the determination of accurate thermochemical data for $CrO_2(OH)$ (g).*

**Find out more about the research of Glenn's Durability and Protective Coatings Branch:**
http://www.grc.nasa.gov/WWW/EDB/

**Glenn contacts:**
Dr. Elizabeth J. Opila, 216–433–8904, Elizabeth.J.Opila@nasa.gov; and
Dr. Nathan S. Jacobson, 216–433–5498, Nathan.S.Jacobson@nasa.gov

**Authors:**
Dr. Elizabeth J. Opila,
Dr. Nathan S. Jacobson,
Prof. Dwight L. Myers,
Dereck F. Johnson, and Jami K. Olminsky

**Headquarters program office:**
Aeronautics Research

**Programs/Projects:**
LEAP, VSP

# Proof of Concept (Design, Fabrication, and Testing) of a Novel High-Power-Density Solid Oxide Fuel Cell Established

Solid oxide fuel cells (SOFC) have potential for a number of industries and technologies, both for industrial and NASA applications, because of their high-energy efficiency. NASA applications for SOFCs include auxiliary power units for commercial airlines, power sources for high-altitude drones, and reversible fuel cells to electrolyze water and generate power for lunar satellites and space stations and to electrolyze carbon dioxide to produce oxygen for a Mars mission. A key advantage of SOFCs is that they can be sulfur tolerant, so they can operate on any hydrocarbon fuel, most of which contain some level of sulfur.

The higher the temperature, the greater the efficiency and power output of a fuel cell. SOFCs have the potential to operate at high temperatures, from 600 to 1000 °C. However, the majority of industrial SOFC designs contain a metal interconnect between the ceramic cells that limits the operating temperatures to 600 to 700 °C. Operation at low temperature makes it more difficult for conventional SOFCs to meet the high specific power density (kilowatts per kilogram) requirements of NASA and industry applications. For example, a recent Boeing study sponsored by the NASA Glenn Research Center determined that a commercial jet auxiliary power unit requires an SOFC specific power density of 1.0 kW/kg. Present state-of-the-art SOFC developers are struggling to attain power densities of 0.1 kW/kg. An order-of-magnitude improvement in performance must be achieved. Glenn has developed a novel fuel cell and fuel cell stack design that is ideally suited to high temperatures and can achieve the high specific power densities required for aeronautics applications.

Glenn has developed both a novel cell design and a novel ceramic fabrication technique that has a predicted specific power density of 1.0 kW/kg. This design is called a bielectrode-supported cell (BSC), see the photomicrograph. It has both low volume and low weight. The BSC uses a thin ceramic interconnect rather than a metal interconnect, which makes it ideally suited to operate at high temperatures, in the 800 to 1000 °C range. Higher operating temperatures allow the BSC to take advantage of higher power density and higher efficiency, and thus

make it suited for reversibility applications, such as water and carbon dioxide electrolysis, and for sulfur tolerance.

One other aspect of the Glenn design that is critical for many NASA applications is that fully hermetic seals can be fabricated. Because the BSC all-ceramic design allows multiple cells, with seals, to be built into a stack using low-temperature assembly techniques, followed by a high-temperature sintering of the ceramic stack and seals, the product is a hermetic stack that can be leak tested prior to its application. No other design has this advantageous feature. Previous SOFC technology that was evaluated for NASA lunar and Mars missions failed because of leaking seals. We believe that Glenn's technology can be developed to deliver a stack with hermetic seals.

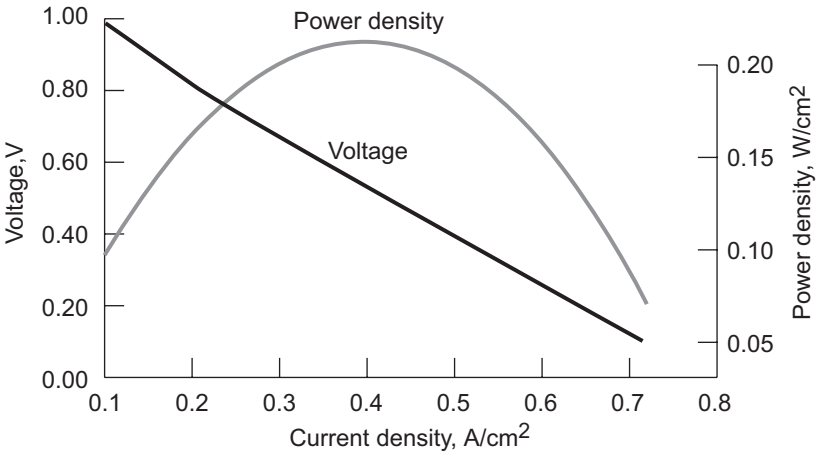


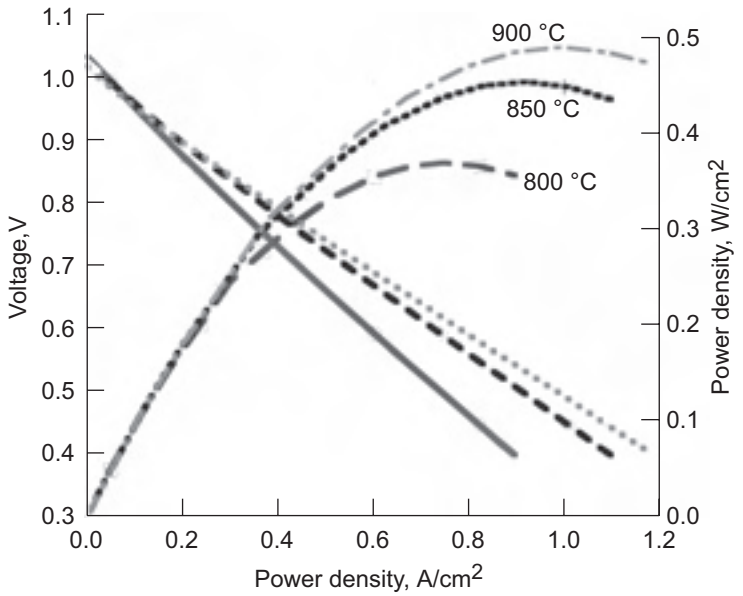


*Performance test of a single cell. Top: 1.5-cm$^2$ cell area; cell tested at 850 °C with silver electrodes; power density, 205 mW/cm$^2$. Bottom: 10-cm$^2$ cell area; cell tested at 800 to 900 °C with Ni/$LaSrFeO_3$ electrodes. Peak power density at 850 °C, 460 mW/cm$^2$. Further development is expected to drive this power density higher. The BSC cell design has inherent weight and volume savings, and we have calculated that it will be able to meet the 1-kW/kg design goals using individual cells with a performance of 300 mW/cm$^2$.*

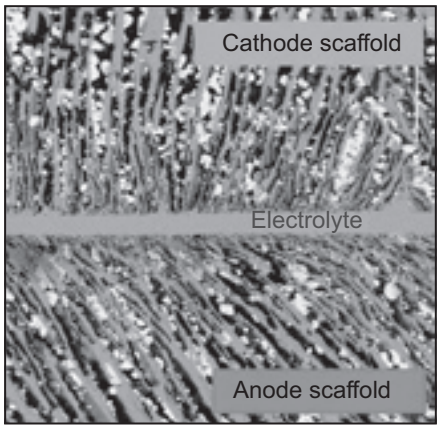


*Example zirconia ($ZrO_2$) electrolyte and $ZrO_2$ scaffolds with silver-infiltrated anode and cathode. In 2005, procedures for the infiltration of a nickel (Ni) anode and $LaSrFeO_3$ cathode, an electronically conductive oxide with the perovskite structure, were developed and tested. Alternative anode and cathode chemistries are being pursued.*

The BSC concept introduces many unique new features and fabrication techniques. Key technical challenges that were demonstrated in 2005 include (1) hermetic electrolytes demonstrated by near theoretical open-circuit voltages ($V_{oc}$) in single-cell tests, (2) active anodes and cathodes infiltrated into the cell electrode support regions by wet chemical techniques with a cell power density of 460 mW/cm$^2$ at 850 °C for 5-cm-diameter cells (see the graphs to the left), and (3) fabrication of a single repeating unit consisting of a BSC cell between dense ceramic interconnect layers.

**University of Toledo contact:**
Dr. Thomas L. Cable, 216–433–5897, Thomas.L.Cable@nasa.gov

**Glenn contact:**
Dr. Serene C. Farmer, 216–433–3289, Serene.C.Farmer@nasa.gov

**Authors:**
Dr. Thomas L. Cable,
Dr. Samuel M. Salamone, John A. Setlock, and Dr. Serene C. Farmer

**Headquarters program office:**
Aeronautics Research, VSP

**Programs/Projects:**
VSP

# Mechanical Properties of Solid Oxide Fuel Cell Seal Glass Enhanced by Boron Nitride Nanotubes

A fuel cell is an electrochemical device consisting of an electrolyte, an anode, and a cathode which continuously converts the chemical energy of a fuel directly into electrical energy. Various types of fuel cells are available, including direct methanol fuel cells, alkaline fuel cells, proton exchange membrane fuel cells, phosphoric acid fuel cells, molten carbonate fuel cells, and solid oxide fuel cells (SOFCs). The salient features of an SOFC are all-solid construction and high-temperature electrochemical-reaction-based operation, resulting in clean, efficient power generation from a variety of fuels. Solid oxide fuel cells are being considered as the premium power-generation devices for a broad range of applications, such as in portable electronic devices, automobiles, power generation, and aeronautics. SOFCs of two different designs, tubular and planar, are currently under development. Planar SOFCs offer simple manufacturing and a relatively short current path resulting in power densities and efficiencies higher than for the tubular design. However, planar SOFCs require hermetic seals to separate and contain the fuel and oxidant within the cell and to bond cell components together. The requirements for SOFC sealing materials are severe because the cells will operate at 600 to 1000 °C for thousands of hours, with sealing materials exposed to both oxidizing and reducing conditions. The seals must be chemically and mechanically compatible with different oxide and metallic cell components and should be electrically insulating. Also, they must survive cycling between room and SOFC operating temperatures.

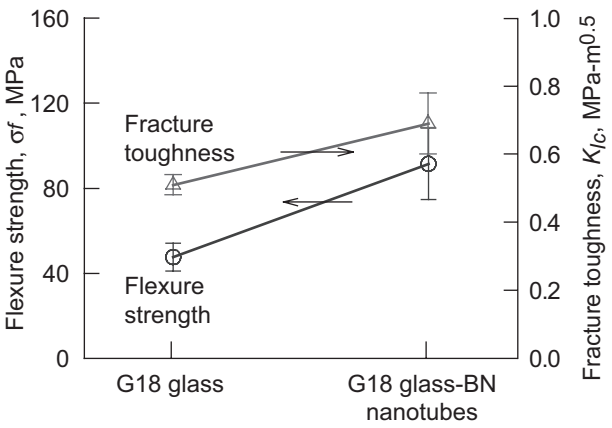


*Flexure strength and fracture toughness of glass reinforced with 4 wt% BN nanotubes. Strength and fracture toughness data for glass are also included for comparison. Error bars indicate ±1.0 standard deviation.*

Various types of seals—such as rigid seals, compressive seals, compliant seals, and hybrid seals—are being tried for SOFCs. For compliant and rigid seals, a number of glass and glass-ceramics based on borates, phosphates, and silicates are being investigated. Silicate glasses are expected to have performance superior to that of the borate and phosphate glasses. A barium calcium aluminosilicate (BCAS) glass of composition 35BaO-15CaO-5$Al_2O_3$-10$B_2O_3$-35$SiO_2$ (mol%) was developed for use as sealing material for planar SOFCs, but during thermal cycling of the SOFC, the glass seal is prone to cracking. The strength and fracture toughness of this glass need to be improved to alleviate this problem. To achieve this goal, researchers reinforced the glass with boron nitride (BN) nanotubes that were produced at the NASA Glenn Research Center. Panels of glass containing 4 wt% of the nanotubes were hot pressed and machined into test bars. Mechanical and physical properties of the glass composites—including four-point flexure strength, fracture toughness, elastic modulus, microhardness, and density—were determined at room temperature. As shown in the graph, the addition of BN nanotubes improved the flexure strength of the glass by as much as 90 percent and the fracture toughness of the glass (measured by the single-edge v-notched beam method) by 35 percent. The addition of BN nanotubes decreased the elastic modulus and microhardness.

Thus, it was demonstrated that the strength of the SOFC seal glass can be improved as much as 90 percent and the fracture toughness as much as 35 percent by reinforcing the glass with just 4 wt% of BN nanotubes. This is important because the addition of such a small amount of BN nanotubes will have little effect on the viscous behavior of the glass at the fuel-cell operating temperatures. Leak tests for the glass composite seals need to be carried out. The glass/BN nanotubes composites are expected to result in much improved seals for SOFCs. This is the first time that a glass matrix composite reinforced with BN nanotubes has been produced and that significant improvements in mechanical properties have been demonstrated.

**Bibliography**

Bansal, Narottam P.; Hurst, Janet B.; and Choi, Sung R.: Boron Nitride Nanotubes-Reinforced Glass Composites. J. Am. Ceram. Soc., vol. 89, no. 1, 2006, pp. 388–390.

Bansal, Narottam P.; and Gamble, Eleanor A.: Crystallization Kinetics of a Solid Oxide Fuel Cell Seal Glass by Differential Thermal Analysis. J. Power Sources, vol. 147, nos. 1–2, 2005, pp. 107–115.

**Glenn contact:**
Dr. Narottam P. Bansal, 216–433–3855, Narottam.P.Bansal@nasa.gov

**University of Toledo contact:**
Dr. Sung R. Choi, 216–433–8366, Sung.R.Choi@nasa.gov

**Authors:**
Dr. Narottam P. Bansal, Janet B. Hurst, and Dr. Sung R. Choi

**Headquarters program office:**
Aeronautics Research

**Programs/Projects:**
VSP, LEAP, AEFT

# Flutter and Response Studied for a Mistuned Bladed Disk With Structural and Aerodynamic Coupling

Turbomachinery blade rows are designed to contain identical blades, identically mounted, and uniformly spaced on a disk within a given blade row. When this is accomplished, the blade row is called tuned. However, minor differences in blade shape, blade structural and material properties, and blade attachments are inherently present in all bladed disks. This difference from one blade to another is referred to as mistuning. In a mistuned system, the vibration energy of the system may be concentrated in a few blades, and these blades will have a significantly higher amplitude of response than will those in a tuned rotor, resulting in higher stresses and premature fatigue failure. Hence, it is essential to understand and include the effects of mistuning on bladed disks in the process of designing turbomachinery blade rows.

The blades in a turbomachinery blade row are coupled aerodynamically through the presence of neighboring blades and/or are coupled structurally through a flexible disk, shrouds, lacing wires, or other structures. Previous studies of mistuned blade rows were based on either a simple structural model or a combined simple structural and aerodynamic model. A realistic analysis would require a complete finite element modeling and analysis of the entire blade and disk. However, such an analysis would be computationally expensive and could not be used in a design process. Reduced-order models (ROMs), where the finite element degrees of freedom are reduced to a manageable number while the essential features of the structural model are retained, have been developed to address this issue.

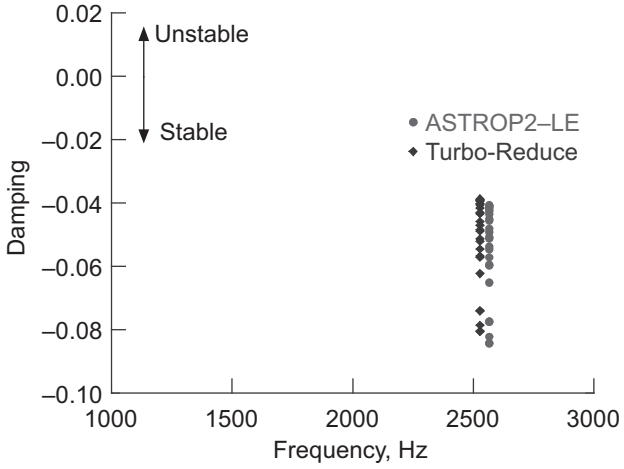


*Comparison of root locus plot-tuned rotor with and without disk flexibility for mach 0.7. ASTROP2–LE results are for a rigid disk; Turbo-Reduce results are for a flexible-bladed disk.*

In this study at the NASA Glenn Research Center, the Turbo-Reduce code, which is based on an ROM and cyclic symmetry, was used to study the effects of structural and aerodynamic coupling on flutter and response. The unsteady aerodynamic forces required for flutter analysis were calculated using the ASTROP2–LE code, an aeroelastic code formulated for a rigid disk. These unsteady aerodynamic forces were then transferred to Turbo-Reduce for use in the mistuned bladed-disk analysis. A 24-bladed rotor with a disk was used for the study. The graph on this page shows the root locus plot (damping versus frequency) obtained for the rigid disk (ASTROP2–LE) and for the flexible disk (Turbo-Reduce) for the second mode at mach 0.7. The flexibility of the disk slightly increased the damping, making the rotor more stable. The graph on the next page shows the response for a sinusoidal wake at 3125 Hz for random mistuning. For the

case considered, the mistuning increased the response amplitudes by about 50 percent, and the amplitudes at multiple frequencies were higher than those of the tuned response. This clearly shows that to avoid blade premature failures, one must incorporate the effects of flexibility and mistuning in the rotor design to accurately predict the damping levels and response amplitudes.

**University of Toledo contact:**
Dr. Tondapu R. Reddy, 216–433–6083, Tondapu.S.Reddy@nasa.gov

**Glenn contact:**
Dr. James B. Min, 216–433–2587, James.B.Min@nasa.gov

**Authors:**
Dr. Tondapu R. Reddy, Dr. James B. Min, and Jeffrey J. Trudell

**Headquarters program office:**
Aeronautics Research

**Programs/Projects:**
Aviation Safety

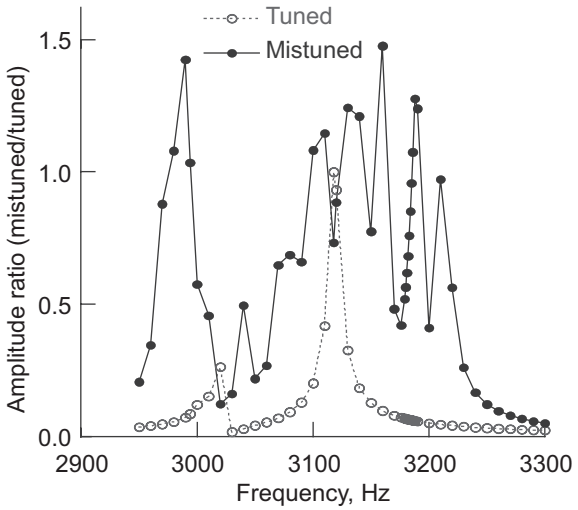


*Blade displacement response for a tuned rotor and a randomly mistuned rotor with standard deviation, 5-percent; sinusoidal wake at 3125 Hz; structural damping ratio, 0.002; number of blades, 24; disk flexibility; mach 0.7; engine order, 2E.*

## Advanced Vibration Analysis Tools and New Strategies Developed for Robust Engine Rotor Development

The adverse effects of small, random structural irregularities among rotor blades, called mistuning, can result in blade forced-response amplitudes and stresses that are much larger than those predicted for a perfectly tuned rotor. Manufacturing tolerances, deviations in material properties, or nonuniform operational wear cause mistuning; therefore, mistuning is unavoidable. Furthermore, even small mistuning can have a dramatic effect on the vibratory behavior of a rotor because it can lead to spatial localization of the vibration energy (see the photos). As a result, certain blades may experience forced-response amplitudes and stresses that are substantially larger than those predicted by an analysis of the nominal (tuned) design. Unfortunately, these random uncertainties in blade properties, and the immense computational effort involved in obtaining statistically reliable design data, combine to make this aspect of rotor design cumbersome.

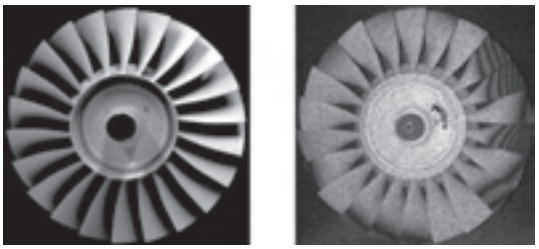

*Spatial localization of mistuned bladed disks. Left: Turbine engine rotor. Right: Localized vibration.*

The primary objective of this work was to develop advanced vibration analysis tools and new rotor development strategies to significantly improve the safety and robustness of engine rotors. Mistuning can lead to a dramatic increase in blade forced-response amplitudes and stresses. Ultimately, this results in high-cycle fatigue (HCF), which is a major safety and cost concern. In this research, the necessary steps were taken to transform a state-of-the-art vibration analysis tool, the Turbo-Reduce blade-mistuning analysis code, into an effective design tool by enhancing and extending the underlying modeling and analysis methods. This work also will aid statistical studies of forced response by reducing the necessary number of simulations.

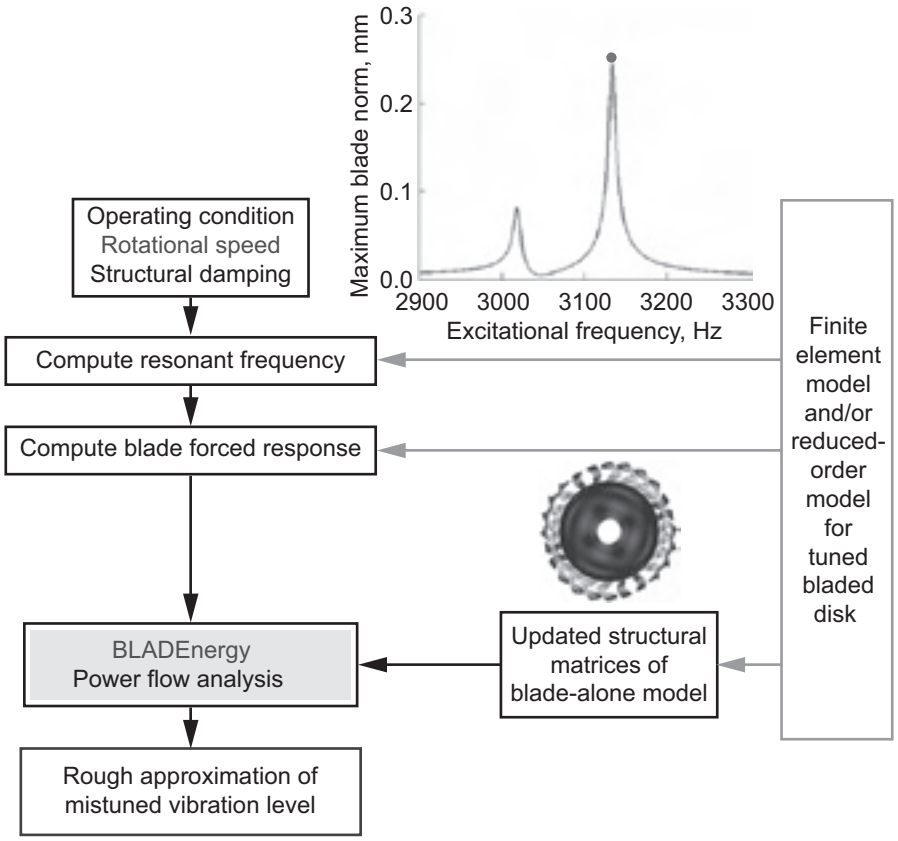


*Accelerated design analysis tool for power flow analysis.*

Several methods were investigated, including the use of intentional mistuning patterns to mitigate the harmful effects of random mistuning, and the modification of disk stiffness to avoid reaching critical values of interblade coupling in the desired operating range. The research activities for this project resulted in the following three major accomplishments:

(1) The BLADEnergy mistuning sensitivity prediction code was developed, which use quick, approximate assessment of mistuning sensitivity via power-flow analysis; and the BLADEnergy code was validated as a tool for predicting the mistuning sensitivity of bladed disks (see the diagram to the left).
(2) Disk design optimization was developed for reducing mistuned blade vibration (see the following graphs).
(3) Turbo-Reduce code features were validated for handling aerodynamic coupling (see the computational grid on the next page).

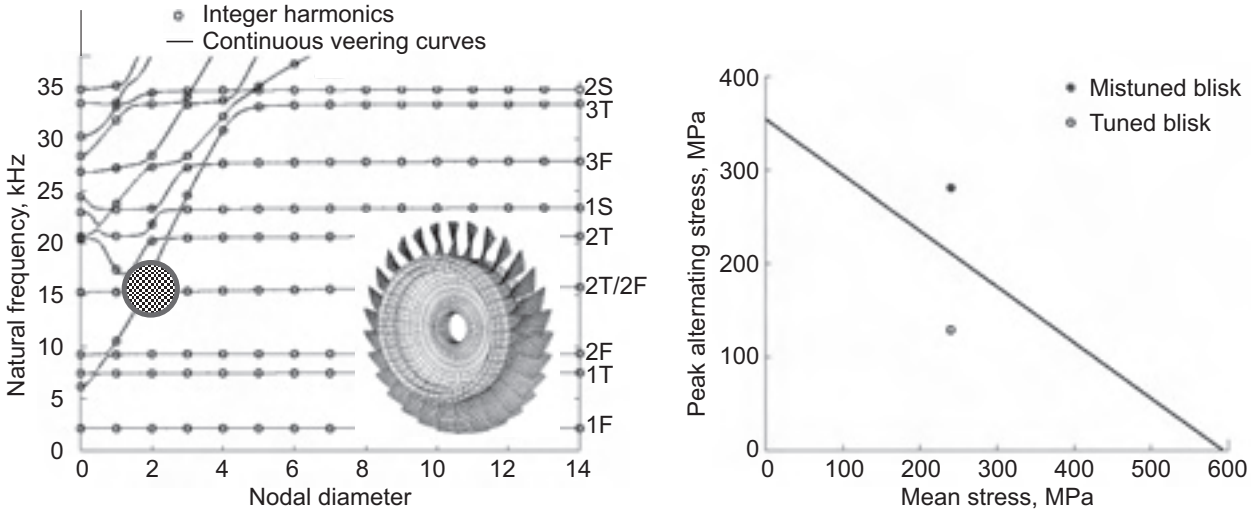


*Optimization of an industrial compressor rotor; Ti-17 material; safety factor, 2. When mistuned, the blade stress level exceeds the Goodman diagram criterion; the ideal system is below the Goodman line. 1S and 2S are the first and second stripe modes; 1T, 2T, and 3T are the first, second, and third torsional modes; and 1F, 2F, and 3F are the first, second, and third flexural bending modes.*

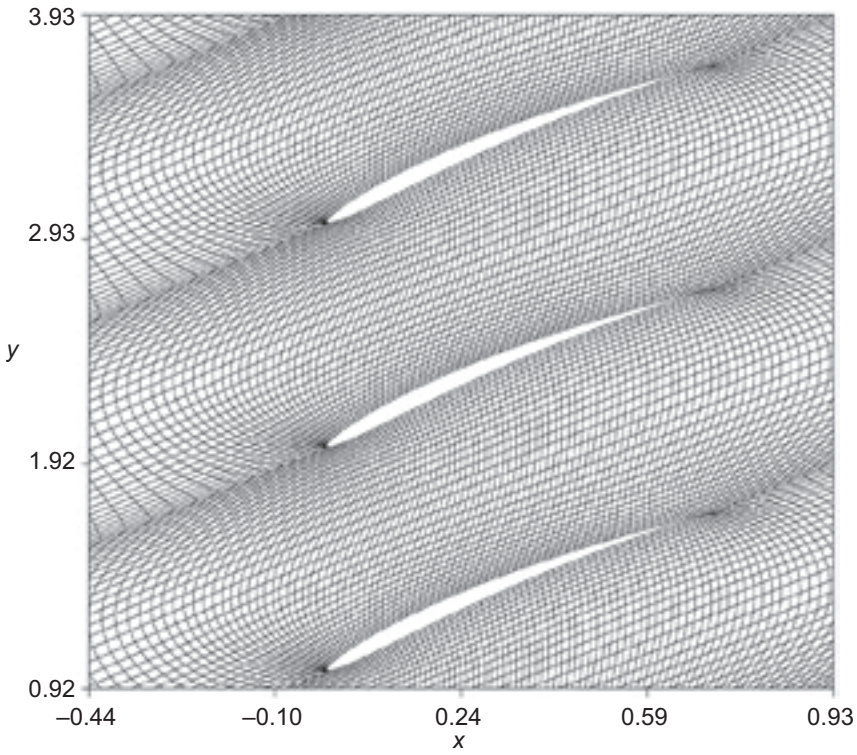


*Three-dimensional computational grids of an industrial rotor.*

This research was performed under a NASA Glenn Research Center Grant by University of Michigan researchers in collaboration with Glenn researchers.

**Bibliography**

Lim, Sang-Ho; Castanier, Matthew P.; and Pierre, Christophe: Intentional Mistuning Design Space Reduction Based on Vibration Energy Flow in Bladed Disks. ASME Paper GT2004–53873, 2004, pp. 373–384.

Baik, S.; Castanier, M.; and Pierre, C.: Assessment of Blade Mistuning Effects Via Power Flow Analysis of Tuned Bladed Disks. AIAA–2005–2027, 2005.

Reddy, T.; Min, J.; and Trudell, J.: Mistuned Bladed Disk Analysis With Unsteady Aerodynamics Using Turbo-REDUCE. AIAA–2005–2028, 2005.

**Glenn contact:**
Dr. James B. Min, 216–433–2587, James.B.Min@nasa.gov

**Author:**
Dr. James B. Min

**Headquarters program office:**
Aeronautics Research

**Programs/Projects:**
UEET

## Integral Damping Studied for Trailing Edge Blowing Fan

An integral damping approach has been studied for the trailing edge blowing (TEB) fan to reduce fan blade vibrations. The TEB fan is a unique technology demonstrator that was designed and fabricated at the NASA Glenn Research Center for testing in Glenn's 9- by 15-Foot Low-Speed Wind Tunnel. The rotor blades are constructed of a composite core with two 16-ply composite outer skins (or shells). The integral damping concept consists of a thin layer of viscoelastic material (VEM) embedded within the outer skins to significantly damp the primary bending and torsion vibration modes. Air is blown out of slots near the trailing edges of the TEB fan blades to fill in the wakes downstream of the rotating blades. This leads to a reduction in the rotor-stator interaction (tone) noise caused by the interaction of wakes with the downstream stators. The TEB fan will demonstrate a 1.6-EPNdB (effective perceived noise decibel) reduction in tone noise through wake filling. Furthermore, the reduced blade row interaction will decrease the possibility of forced-response vibrations and enable closer spacing of blade rows, thus reducing engine length and weight.

The viscoelastic material patch, approximately 0.005 in. thick, replaces the composite material of the blade skin at a selected location of the blade. The patch includes a barrier film to protect the VEM during the curing process. The location, shape, and size of the VEM patch have been varied to optimize the damping without reducing the strength of the blade. Finite-element models of the integral damped fan blade were created to analytically predict the damping, structural strength, vibration mode, and frequencies, and to optimize the VEM patch location, shape, and size. Four sets of blades with different levels of

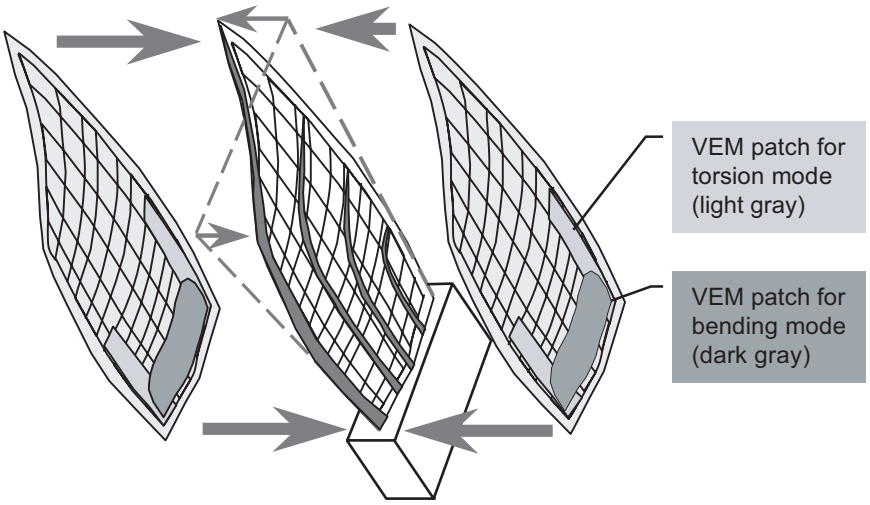


*TEB fan blade with embedded VEM damping patch.*

damping were analyzed, fabricated, and tested. The testing validated the structural analysis and demonstrated the feasibility of the integral damping approach. The optimally damped blade, which had a VEM patch size of 29 percent of the blade surface, had a resonant blade vibration amplitude that was 1.5 to 3.3 times less than that of an undamped blade.

The research described here was performed under a grant to Dr. John Kosmatka (University of California, San Diego) in collaboration with Glenn researchers. This work was supported by the Quiet Aircraft Technology Project, Dr. Joseph Grady, manager.

**Bibliography**

Ma, Zhixin; and Kosmatka, John: Structural Analysis of an Integral Damped Reduced Weight Fan Blade. Structural Systems Research Report, SSRP–04/09. Final Report submitted to NASA Grant NCC3–902, Aug. 2004.

**Glenn contact:**
Dr. Milind A. Bakhle, 216–433–6037, Milind.A.Bakhle@nasa.gov

**Authors:**
Dr. John Kosmatka and Dr. Milind A. Bakhle

**Headquarters program office:**
Aeronautics Research

**Programs/Projects:**
QAT

## Turbine Structure Investigated for the Constant-Volume Combustion Cycle Engine

The structural effects of the unsteady loading of a pulse detonation tube on a downstream turbine were investigated at the NASA Glenn Research Center as a possible basis for a hybrid aircraft engine in which the combustor would be replaced by a set of pulse detonation tubes arranged in a circumferential array. Such hybrid engines may increase fuel efficiency. Combustion would occur under constant-volume conditions rather than under the constant-pressure conditions of current conventional combustors. Also, the combustion process would consist of a sequence of detonations, rather than the deflagration that characterizes current combustors. Consequently, the flow downstream of the pulse detonation tubes is expected to have a large unsteady component. The objective of this study was to analyze the unsteady aerodynamic loading on turbine blades to evaluate its structural effects, such as increased vibration amplitudes or increased dynamic stresses, which can result in premature high-cycle fatigue failures.

This study used numerical flow-field simulation to calculate the aerodynamic loading history on turbine blades resulting from the unsteady flow created by the upstream pulse detonation tubes. A Reynolds-averaged Navier-Stokes code named TURBO was used to model the unsteady flow through the turbine, and the pulses from the detonation tubes were introduced into the flow domain through upstream boundary conditions. The flow inside the pulse detonation tubes was not modeled as part of this effort. Instead, the conditions at the exit of the tube were obtained from a separate one-dimensional calculation.

The unsteady flowfield through the turbine stage was calculated as part of a study that addressed aeroacoustics, unsteady aerodynamics, aeroelastics, performance, and heat transfer. The TURBO code was modified to generate a time history of the pressure on the blade surfaces, and the blade passage grids were partitioned to enable rapid computations using the parallel TURBO code on a computer cluster. Accordingly, the time history of pressure for individual grid blocks (that comprise the blade

surfaces of a turbine blade) had to be merged and then decomposed into Fourier components. The Fourier components with frequencies near the natural frequencies of the blade were the ones of most interest since these can cause resonant response vibrations in the blades. Large vibration amplitudes lead to large dynamic stresses that can shorten the high-cycle fatigue life.

On the structural side, a finite element model was created for the turbine blade. The structural analysis packages NESSUS (Southwest Research Institute, San Antonio, TX) and ANSYS (ANSYS, Inc., Canonsburg, PA) were used to calculate the structural dynamic characteristics of the blade. Then, the unsteady aerodynamic loading was mapped from the TURBO computational grid onto the finite element mesh and was prescribed as a forcing function (or excitation force). Calculations performed with and without the pulse detonation tubes upstream of the turbine enabled the effect of the tubes to be identified. Initial calculations only modeled the spatial distortion in total pressure and total temperature coming into the turbine vane. The detonation tubes actually produced a spatially nonuniform flow and a time nonuniform flow, but the spatial nonuniformities did not have a strong effect on the rotor blades. The unsteady flow calculations are being updated with an improved model in which the detonation tubes are included as part of the computational domain and provide an initial pulse in the flowfield that propagates through the turbine stage. This work was supported by the Constant Volume Combustion Cycle Engine Subproject (Leo Burkardt, manager) of the Low Emissions Alternative Propulsion Project.

**Glenn contact:**
Dr. Milind A. Bakhle, 216–433–6037, Milind.A.Bakhle@nasa.gov

**Authors:**
Dr. Milind A. Bakhle, Dr. James B. Min, Dr. Tondapu R. Reddy, and Dr. Dale E. Van Zante

**Headquarters program office:**
Aeronautics Research

**Programs/Projects:**
LEAP, CVCCE

## Probabilistic Creep Life Analysis of an Engine Combustor Composite Liner Performed

An engine combustor composite liner is required to operate at elevated temperatures where creep is prevalent. The creep life analysis of a combustor liner is, therefore, of great significance. The variation in material properties, thermal loading, or mechanical loading makes it mandatory to perform a probabilistic creep life analysis of an engine combustor composite liner. This work was directed by the NASA Glenn Research Center to address this important problem.

The MARC program was employed for the nonlinear creep life analysis of the composite combustor liner. The figure on the next page displays the sensitivity factors from the variation of various parameters on the life of the composite combustor liner. Clearly, the reliability of the combustor composite liner is most sensitive to thermal loads.

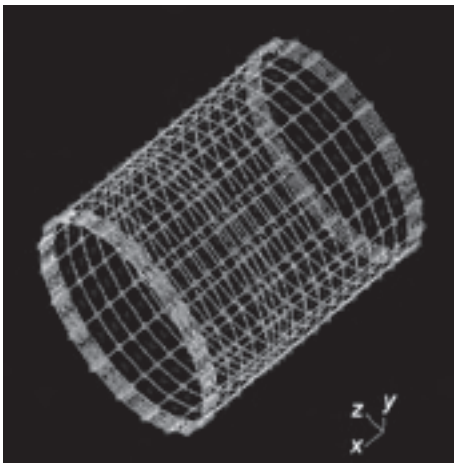


*Model of an engine combustor composite liner.*

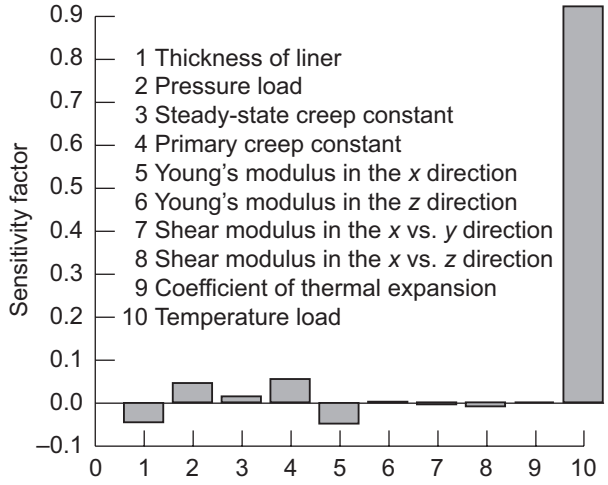


*Results from the reliability analysis.*

**Glenn contact:**
Dr. Shantaram S. Pai, 218–433–3255,
Shantaram.S.Pai@nasa.gov

**University of Akron contact:**
Prof. Vinod K. Arya, 216–433–2816,
Vinod.K.Arya@.nasa.gov

**Author:**
Prof. Vinod K. Arya

**Headquarters program office:**
Exploration Systems

**Programs/Projects:**
Exploration Systems

## Stator and Rotor Designed and Manufactured for an Ironless High-Power-Density Permanent Magnet Electric Motor for Pollution-Free Aircraft

Demonstrating a pollution-free aircraft is a NASA 21st century goal. The NASA Glenn Research Center has been investigating, both through feasibility studies and experimental research, the possibility of hydrogen-fueled aircraft that would use fuel cells or turbogenerators to produce electric power to drive the electric motors that turn the aircraft's propulsive fans or propellers. Conventional electric motors and their electronics are too heavy to use in these new systems, so Glenn is working to make motors lighter and more powerful. One new type of motor that shows promise for flight application is the ironless permanent magnet motor.

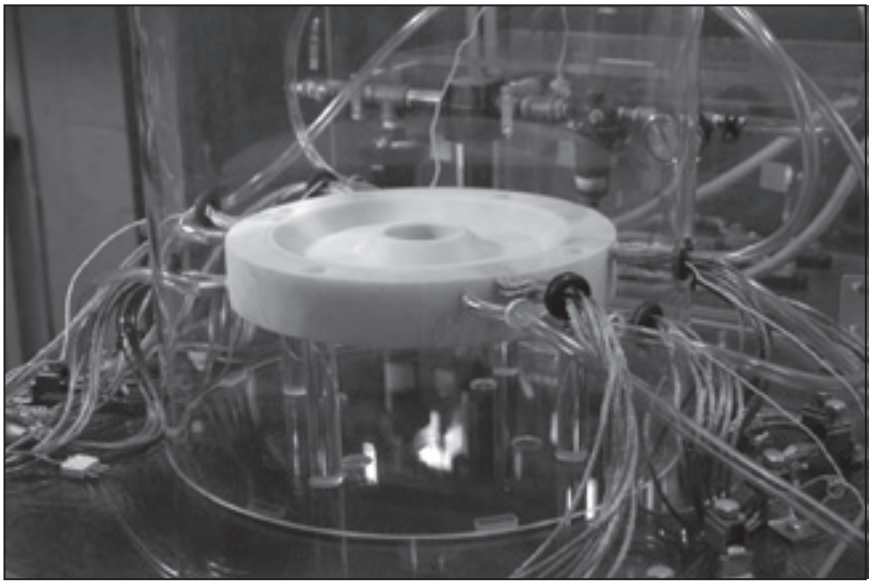

*First ironless motor pancake stator setup for determining the current density that can be achieved with this design.*

The rotating magnetic flux circuit in this device is generated using high-energy-density permanent magnets configured on the rotor in Halbach arrays. The magnets are contained by carbon-fiber composite rings. Two of these arrays working together produce a 1.2-tesla flux density at the center of a 0.5-in. gap. This eliminates the need for iron in the motor, which is heavy, lossy, and potentially very expensive. Different stator design and active cooling concepts will be investigated to obtain higher current densities. The first stator concept was designed and manufactured and is currently being tested. This stator was constructed using

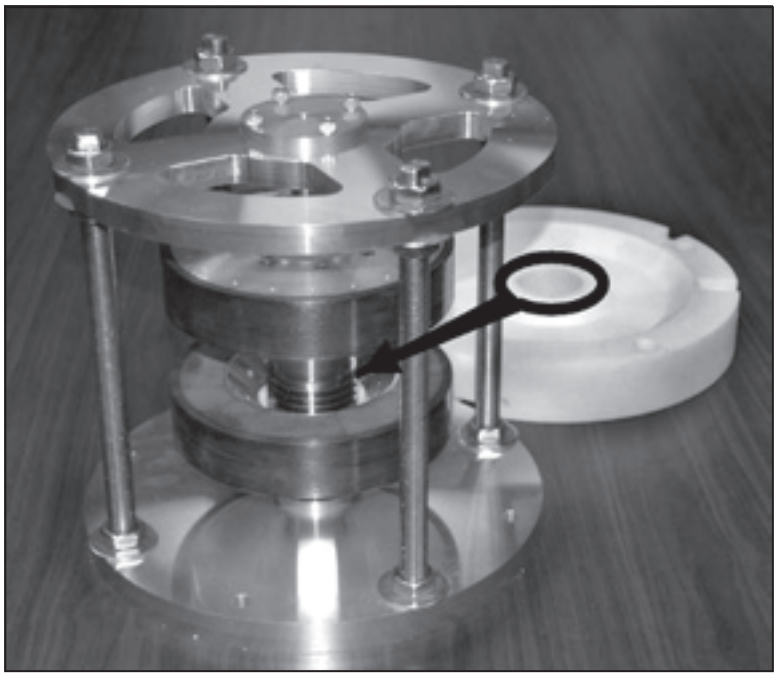

*Basic ironless Halbach permanent magnet motor hardware designed and manufactured in fiscal year 2005. The structural integrity of the rotating magnet structures shown is currently being determined.*

Litz wire interlaced with cooling passages for heat removal via forced-convection heat transfer. In addition, a rotating magnet structure is being spun up to verify its structural integrity. This work was supported by the Alternative Energy Foundation Technologies Project.

**Glenn contact:**
Andrew J. Provenza, 216–433–6025, Andrew.J.Provenza@nasa.gov

**U.S. Army Research Laboratory at Glenn contact:**
Albert F. Kascak, 216–433–6024, Albert.F.Kascak@nasa.gov

**Author:**
Andrew J. Provenza

**Headquarters program office:**
Aeronautics Research

**Programs/Projects:**
AEFT, VSP

## Bearingless Motor Demonstrated

The G4 bearingless motor is a new type of motor that was successfully demonstrated on August 16, 2005, at the NASA Glenn Research Center. This innovative motor can be applied to high-speed, long-life, or broad-temperature-range products. It combines the features of a typical permanent-magnet motor with the functions of a magnetic bearing and can be operated as a motor or a generator, transferring energy to or from a load. One unique feature of this motor is that it produces forces in the radial and axial directions, and as a result, two motors can be used to levitate a rotor system. Fault tolerance is another feature of the motor, enabling it to continue operating even after partial failure of the electronics or wiring. The fundamental scientific accomplishment is the successful motoring and levitation of a rotor in all degrees of freedom using electromagnetic control from only two magnetic actuators. Practically, this configuration brings the long-life, noncontact, broad operating temperature range and rotordynamic benefits of magnetic bearing technology to a motorized system in a compact form factor.

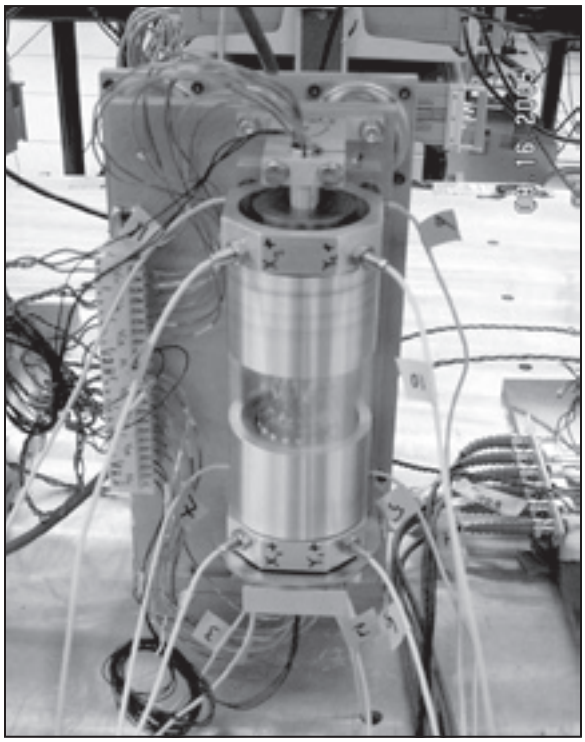

*G4 bearingless motor.*

This innovation is protected under U.S. Provisional Patent Applications 60/548,892; 60/548,893; and 60/548,894 owned by the University of Toledo. The work was performed by University of Toledo, QSS Group, Inc., Analex Corporation, and National Research Council personnel working for Glenn's Advanced Electrical Systems Branch and Structural Mechanics and Dynamics Branch. The work was funded by the Aerospace Flywheel Technology Program and the Advanced Mechanisms and Tribology Technologies for Durable Lightweight Actuation and Mechanical Power Transmission Systems (MTLAMPS) Project.

**Glenn contact:**
James F. Soeder, 216–433–5328, James.F.Soeder@nasa.gov

**University of Toledo contacts:**
Peter E. Kascak, 216–433–8408, Peter.E.Kascak@nasa.gov; and
Ralph H. Jansen, 216–433–6038, Ralph.H.Jansen@nasa.gov

**Author:**
Ralph H. Jansen

**Headquarters program office:**
Exploration Systems

**Programs/Projects:**
Energetics, MTLAMPS

## Novel Eight-Stator-Pole, Six-Rotor-Pole, Bearingless Switched-Reluctance Motor Performance Correlated With Analysis

Reliable, failsafe, robust, compact, low-cost electric motors are needed for applications where high temperature or intense temperature variations are the norm. Switched-reluctance motors have these characteristics. In addition, they are most often the natural choice of motors for operation under high rotational speeds (refs. 1 and 2). However, because of rotor eccentricity due to fabrication imperfections, conventional switched-reluctance motors suffer from vibration caused by large magnetic attraction forces on the rotor in radial directions (ref. 3). A solution to this problem is to suspend the rotor by magnetic bearings, where the vibration suppression capability of these bearings can be employed.

Methods for simultaneously levitating and rotating a switched-reluctance motor within a single stator are proposed in references 2 and 4. In these motors, the technique of differential stator windings was employed. The studies primarily used a main four-pole winding to rotate the rotor and a two-pole winding to apply radial force to the rotor, with all of the stator poles having both windings thereon. This device consisted of a 12-pole stator and an 8-pole rotor (12/8 configuration). Self-levitation (also called self-bearing) of motors has been achieved for nearly every type of electric motor, but it is very marginal in performance for switched-reluctance motors with low numbers of poles.

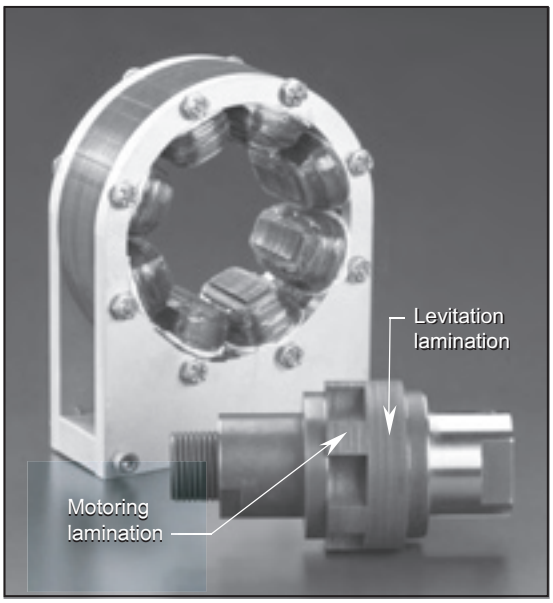


*Disassembled eight-stator-pole, six-rotor-pole (8/6) hybrid rotor.*

At the NASA Glenn Research Center, a novel eight-stator-pole, six-rotor-pole (8/6), hybrid bearingless switched reluctance motor, also known as the Morrison Motor, was developed to address the marginal performance of motors with few poles. The motor employs an alternate mode of operation in

which robust, simultaneous levitation and rotation can be attained, not only for 18/12 or 12/8 stator-pole/rotor-pole configurations, but also for 8/6 and 6/4 configurations that employ a single set of coils positioned on each stator pole. The motoring techniques described in references 2 and 4 are not applicable to 8/6 and 6/4 motor configurations because, for many positions of the shaft during rotation, there are no rotor poles in appropriate positions to apply levitating forces. In contrast, the hybrid rotor technique ensures robust bearingless operation in all four of these configurations.

The successful operation of the Morrison Motor (see ref. 5 for a detailed description) hinges on the novel hybrid rotor design depicted in the photograph on the preceding page, in which a portion of the length of the rotor lamination stack is composed of circular laminations (used for levitation) and the remaining portion is composed of castellated laminations (used for motoring).

Inserting circular laminations onto the shaft ensures that levitating force is always present as the rotor spins. The recently formulated one-dimensional magnetic circuit equations, approximating the complex topology of the magnetic field existing in and around the hybrid rotor, were employed to generate the theoretical curve depicted in the graph. The experimental and theoretical curves represent the nonlevitated static radial force on the hybrid rotor.

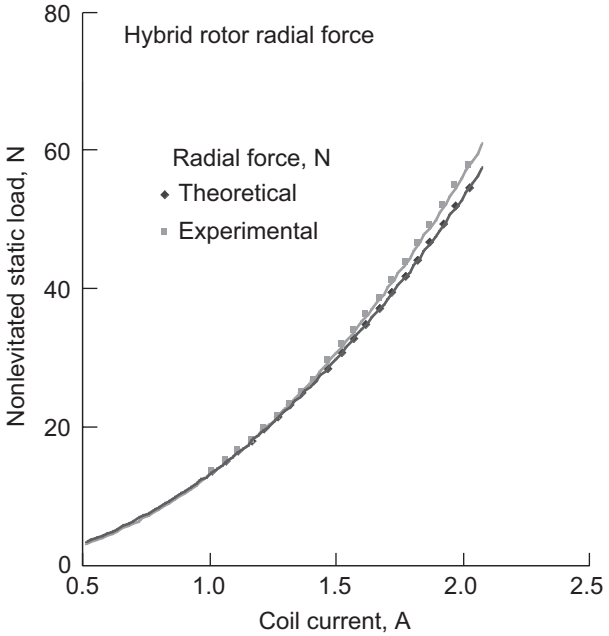


*Theoretical and experimental radial forces.*

The prototype achieved a levitated rotor speed of 6000 rpm. Future software and hardware upgrades will engender higher rotational speeds. Before this demonstration, it was not clear whether or not circular and motor laminations could coexist without grossly distorting the magnetic flux distribution, and thus seriously degrading or destroying either the levitating or motoring action. A paper describing the levitated and nonlevitated magnetic field and force characteristics of the motor is in preparation.

**References**

1. Richter, E.; and Ferreira, C.: Performance Evaluation of a 250 kW Switched Reluctance Starter Generator. Conference Record of the 1995 IEEE and the IAS'95 Meeting, 1995, pp. 434–440.
2. Takemoto, Masatsuga, et al.: A Design and Characteristics of Switched Reluctance Type Bearingless Motors. Proceedings of the Fourth International Symposium on Magnetic Suspension Technology, NASA/CP—1998-207654, 1998, pp. 49–63.
3. Miller, Timothy J.E.: Faults and Unbalanced Forces in the Switched Reluctance Machine. IEEE Trans. Ind. Appl., vol. 31, no. 2, 1995, pp. 319–328.
4. Takemoto M., et al.: Improved Analysis of a Bearingless Switched Reluctance Motor. IEEE Trans. Ind. Appl., vol. 37, issue 1, 2001, pp. 26–34.
5. Morrison, Carlos R.: Bearingless Switched Reluctance Motor. U.S. Patent 6,727,618 B1, Apr. 27, 2004.

**Glenn contacts:**
Carlos R. Morrison, 216–433–8447, Carlos.R.Morrison@nasa.gov;
Dr. Gerald V. Brown, 216–433–6047, Gerald.V.Brown@nasa.gov;
Dr. Dexter Johnson, 216–433–6046, Dexter.Johnson-1@nasa.gov;
Dr. Benjamin B. Choi, 216–433–6040, Benjamin.B.Choi@nasa.gov; and
Andrew J. Provenza, 216–433–6025, Andrew.J.Provenza@nasa.gov

**University of Toledo contact:**
Mark W. Siebert, 216–433–6012, Mark.W.Siebert@nasa.gov

**Authors:**
Carlos R. Morrison, Mark W. Siebert, and Dr. Gerald V. Brown

**Headquarters program office:**
Aeronautics Research

**Programs/Projects:**
AEFT, AFFT

**Special recognition:**
2004 R&D 100 award, U.S. Patent 6727618 B1, 2004 Space Act Award

# Performance of Switched-Reluctance Cryogenic Motor Tripled

Pollution-free flight is one of NASA's goals for the 21st century. One method of approaching that goal is hydrogen-fueled aircraft that use fuel cells or turbogenerators to develop electric power to drive the electric motors that turn the aircraft's propulsive fans or propellers. Hydrogen fuel would likely be carried as a liquid, stored in tanks at its boiling point of 20.5 K (–422.5 °F). The liquid hydrogen could provide essentially free refrigeration to cool electric motor windings before being used as fuel. Either superconductivity or the low resistance of pure copper or aluminum in liquid hydrogen could be applied to greatly increase electric current density and motor power density.

At the NASA Glenn Research Center, a testbed switched-reluctance motor with copper windings was operated in liquid nitrogen at current densities, specific torque, and specific force that would not be possible at room temperature. Coil current capacity measurements and locked-rotor torque measurements were made to guide upgrades in coil geometry and power electronics and to validate analysis methods that can be extended to liquid-hydrogen-cooled motors. These results are reported in references 1 and 2.

Changes in coil geometry and power electronics have since increased the measured torque and power output substantially. Because the phases (and even "half phases") in a switched reluctance motor operate virtually independently of each other, Glenn researchers excite the windings on just one pole pair and project the measured results to the full-motor performance (12 coils) by multiplying the torque and power produced by 6. The previously reported best projected power output (ref. 2) was 15 kW (20 hp) for the motor, which has an electromagnetic weight of 18 lb. By increasing the drive voltage and current capacity of the power conditioning and rewinding the motor coils to match the new power electronics, Glenn researchers have more than tripled the power output to 47 kW (63 hp) at 12,000 rpm with the motor submerged in liquid nitrogen. The specific power now stands at 3.5 hp/lb-EM, the specific torque at 1.5 ft-lb/lb, and the specific force at 9 lb/lb-EM (all figures based on the electromagnetic weight (EM), as is typically done for switched-reluctance motors). By "specific force" we mean the effective specific circumferential force applied to the rotor surface, a basic measure of motor performance. (It avoids the misjudgment of the relative merits of motors of different radial size which, though possessing equally effective motive features, would have differing specific torques because the rotor radii differ.) Planned upgrades to the power electronics will have only minor effects on the specific torque and force, but they may nearly double the specific power by preserving the motor's torque to higher speeds.

**References**

1. Brown, Gerald V.: Cryogenic Electric Motor Tested. Research & Technology 2003, NASA/TM—2004-212729, 2004, pp. 162–163. http://www.grc.nasa.gov/WWW/RT/2003/5000/5930brown.html
2. Brown, Gerald V.; and Siebert, Mark W.: Switched-Reluctance Cryogenic Motor Tested and Upgraded. Research & Technology 2004, NASA/TM—2005-213419, 2005, pp. 137–139. http://www.grc.nasa.gov/WWW/RT/2004/RS/RS14S-brown.html

**Glenn contact:**
Dr. Gerald V. Brown, 216–433–6047, Gerald.V.Brown@nasa.gov

**University of Toledo contact:**
Ralph H. Jansen, 216–433–6038, Ralph.H.Jansen@nasa.gov

**QSS Group, Inc., contact:**
Timothy P. Dever, 216–433–2384, Timothy.P.Dever@nasa.gov

**National Research Council contact:**
Aleksandr S. Nagorny, 216–433–6129, Aleksandr.S.Nagorny@nasa.gov

**Authors:**
Dr. Gerald V. Brown, Ralph H. Jansen, Timothy P. Dever, Aleksandr S. Nagorny, Carl J. Buccieri, and Mark W. Siebert

**Headquarters program office:**
Aeronautics Research

**Programs/Projects:**
Propulsion and Power, VSP, RAC, AEFT

# Radial Forces Derived for a Switched-Reluctance Motor for Aerospace Applications

A switched-reluctance cryogenic motor (ref. 1) is being developed for pollution-free flight, which is one of NASA's goals for the 21st century. Before a super-high-power-density motor can be developed for the next-generation all-electric propulsion system, a noncontact rotor-bearing system is necessary to circumvent the poor bearing life that ordinarily accompanies cryogenic operation.

Recently, a variety of bearingless motors—including permanent magnet, induction, and reluctance—were introduced. These motors have different characteristics and different suitable applications. Among them, switched-reluctance motors can be good candidates for the electric propulsion system because they have inherent fault-tolerance and rotor robustness at high rotational speeds (no coil windings on the rotor). In addition, this type of motor generates a high radial force in the air gap that we might be able to use for rotor levitation (bearing function).

At the NASA Glenn Research Center, a 12-stator-pole, 8-rotor-pole (12/8) switched-reluctance cryogenic motor (ref. 1) was studied for the bearingless motor. This motor does not have separate magnetic bearing coils, but only motor coils, as in a conventional motor configuration. The motor coil windings on the stator generate a radial force (bearing function) and torque (motor function) at the same time. On a stator with superimposed differential magnetic bearing coil windings on the motor coil windings, the radial force is a function of the radial force winding current and the motor current, as well as of the rotor rotational position.

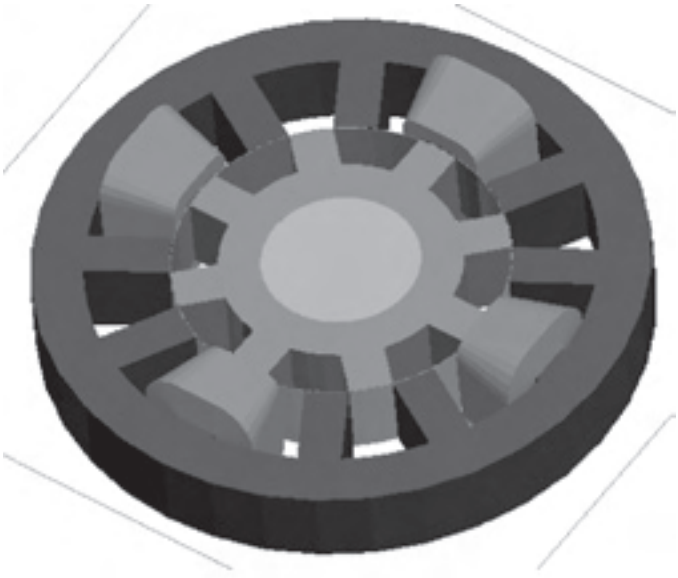

*Maxwell three-dimensional model of a 12/8 switched-reluctance motor in one phase.*

In this work, the theoretical equations of radial forces were derived from finite-element model (FEM) analysis results to express fringing fluxes neglecting magnetic saturation. This was developed early by Takemoto et al. (ref. 2) and Shuang et al. (ref. 3). We used the fringing effects based on the Maxwell FEM model shown in the illustration to derive the relationships between the radial force and current around unaligned positions. The radial equations developed using Takemoto's method and Shuang's method are compared with three-dimensional FEM results in the graph on the next page.

In the near future, we plan to develop a bearingless controller based on this radial force equation and to further investigate the radial force derivation in the magnetic saturation region. This work is supported by the Alternate Energy Foundation Technologies Project of the Low Emissions Alternative Power Project (Mark D. Klem, manager).

**References**

1. Brown, Gerald V.; and Siebert, Mark W.: Switched-Reluctance Cryogenic Motor Tested and Upgraded. Research & Technology 2004, NASA/TM—2005-213419, 2005, pp. 137–139. http://www.grc.nasa.gov/WWW/RT/2004/RS/RS14S-brown.html
2. Takemoto, Masatsuga, et al.: A Design and Characteristics of Switched Reluctance Type Bearingless Motors. Proceedings of the Fourth International Symposium on Magnetic Suspension Technology, NASA/CP—1998-207654, 1998, pp. 49–63.
3. Shuang, Ye; Zhiquan, Deng; and Yangguang, Yan: New Formulae Based on Fourier Extension for Bearingless Switched Reluctance Motors. Proceedings of the 8th International Symposium on Magnetic Bearings, Mito, Japan, 2002, pp. 53–58.

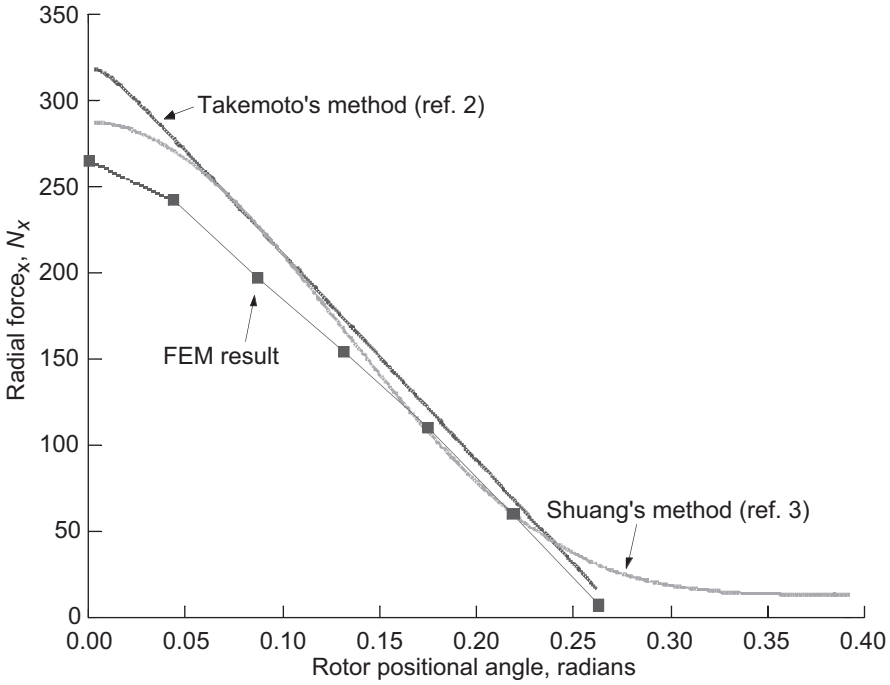


*Radial force equations developed using Takemoto's method and Shuang's method are compared with Maxwell three-dimensional FEM results. Radial force in the x-axis, Radial force$_x$, x-axis levitation current in phase a, $I_{ma}$, 8 A; motor current in phase a, $I_{sa1}$, 2 A; and y-axis levitation current in phase a, $I_{sa2}$, 2 A.*

**Glenn contacts:**
Dr. Benjamin B. Choi, 216–433–6040, Benjamin.B.Choi@nasa.gov; and
Dr. Gerald V. Brown, 216–433–6047, Gerald.V.Brown@nasa.gov

**Author:**
Dr. Benjamin B. Choi

**Headquarters program office:**
Aeronautics Research

**Programs/Projects:**
Propulsion and Power, AEFT, LEAP

## Vertical-Axis, Bearingless Switched-Reluctance Motor for All-Electric Propulsion System Demonstrated Successfully

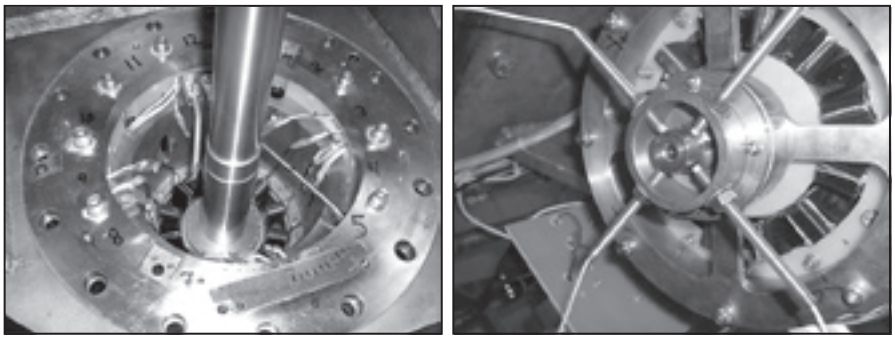

*Left: 12/8 switched reluctance motor with motor coil windings only—no magnetic bearing coil windings. Right: Bottom view of motor with x- and y-axis position probes. Motor coils generate torque and radial force at the same time.*

Before a super-high-power-density motor can be developed for the next-generation all-electric propulsion system, a noncontact rotor bearing system is necessary to circumvent the poor bearing life that ordinarily accompanies cryogenic operation. The Self-Levitation Team at the NASA Glenn Research Center developed and successfully demonstrated a bearingless motor control technology for the vertical-axis, 12-stator-pole, 8-rotor-pole (12/8) switched-reluctance motor (ref. 1). This motor does not have separate magnetic bearing coils, but only motor coils as in a conventional motor configuration (see the photograph on the left). This novel

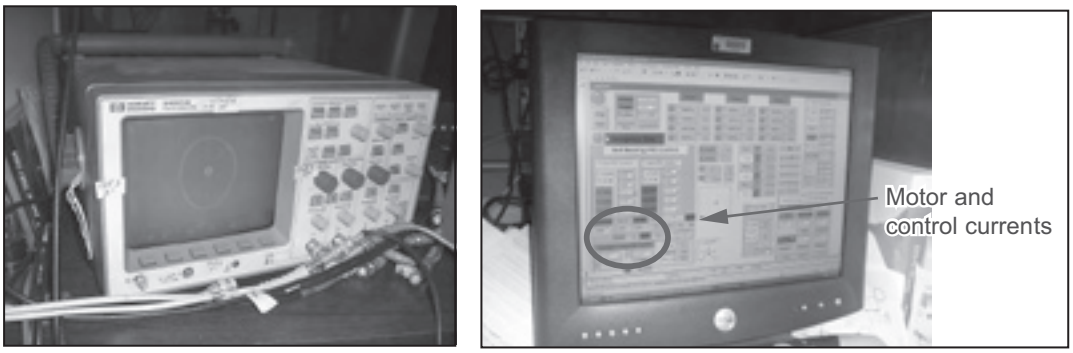


*Left: Control screen showing rotor orbit at 6000 rpm and less than 10 percent of backup bearing gap (±10 mils). Right: Computer screen showing motor and control currents. Motor speed, 6000 rpm; motor current, 4.0 A; levitation current, less than 10 percent of motor current.*

self-bearing control technology generates the required torque (motor function) and radial force (bearing function) by using the motor winding coils only (see the right photograph on the preceding page). This is believed to be a world's first for this motor type.

Two controllers were developed and tested for the bearingless motor. The first one is based on the mathematical expression of radial force using Takemoto's method (ref. 2). The other controller is relatively simple because it does not require a mathematical equation of radial force. Those two controllers are working very well, and details will be published later. As shown in the left photograph on this page, the rotor was quite stable in the operation speed range from levitation up to 6500 rpm (maximum allowable speed at that time). At the operating speed, the rotor orbit has 10 percent of back-bearing clearance. Furthermore, the required levitation current is less than 10 percent of the operating motor current (see the right photograph on this page). In the near future, a controller will be developed for a horizontal-axis bearingless motor, where we will need to generate a levitating force to counteract the rotor weight as well as for motor and bearing functions.

This technology can significantly reduce overall system weight by eliminating separate mechanical or magnetic bearing systems and the associated plumbing and electrical subsystems. It can also prepare the way for an all-electric, quiet, pollution-free aircraft propulsion system. This work is supported by the Alternate Energy Foundation Technologies Project of the Low Emissions Alternative Power Project.

**References**

1. Brown, Gerald V.; and Siebert, Mark W.: Switched-Reluctance Cryogenic Motor Tested and Upgraded. Research & Technology 2004, NASA/TM—2005-213419, 2005, pp. 137–139. http://www.grc.nasa.gov/WWW/RT/2004/RS/RS14S-brown.html
2. Takemoto, Masatsuga, et al.: A Design and Characteristics of Switched Reluctance Type Bearingless Motors. Proceedings of the Fourth International Symposium on Magnetic Suspension Technology, NASA/CP—1998-207654, 1998, pp. 49–63.

**Glenn contacts:**
Dr. Benjamin B. Choi, 216–433–6040, Benjamin.B.Choi@nasa.gov; and
Dr. Gerald V. Brown, 216–433–6047, Gerald.V.Brown@nasa.gov

**University of Toledo contact:**
Mark W. Siebert, 216–433–6012, Mark.W.Siebert@nasa.gov

**Authors:**
Dr. Benjamin B. Choi, Dr. Gerald V. Brown, and Mark W. Siebert

**Headquarters program office:**
Aeronautics Research

**Programs/Projects:**
Propulsion and Power, AEFT, LEAP

# Mission Analysis Conducted of a High-Altitude, Long-Endurance, Remotely Operated Aircraft With a High-Power-Density Electric Motor

NASA has the goal of completely eliminating the harmful emissions that are associated with current aircraft propulsion systems. An advanced electric drive with electric power generated by turbogenerators, or by fuel cells using hydrogen, is an alternative propulsion system for transport-sized aircraft that may help achieve this goal. Another NASA goal is to develop specialized unmanned aerial vehicles (UAV) to meet NASA science mission objectives. Current propulsion technology limits the endurance and range of UAVs. The NASA Glenn Research Center's High Power Density Motor (HPDM) development research team is interested in applying its technology to high-altitude, long-endurance remotely operated aircraft (HALE ROA) to enhance vehicle performance (see the figure). Consequently, a mission analysis of a HALE ROA was conducted to determine if HPDMs are a viable solution for these propulsion challenges.

The mission analysis has four major parts: (1) mission selection, (2) UAV selection, (3) matching the HPDM with mission requirements and the UAV vehicle, and (4) mission analysis. Mission selection involved examining six NASA science missions that are considered candidates for HALE ROA application. The hurricane tracker mission was selected because it may benefit the most by using a HPDM. This mission requires a UAV to fly to a developing tropical cyclone and follow the system until it makes landfall. From birth to landfall, a typical hurricane usually lasts 10 to 14 days, defining the flight endurance requirement for this particular mission.

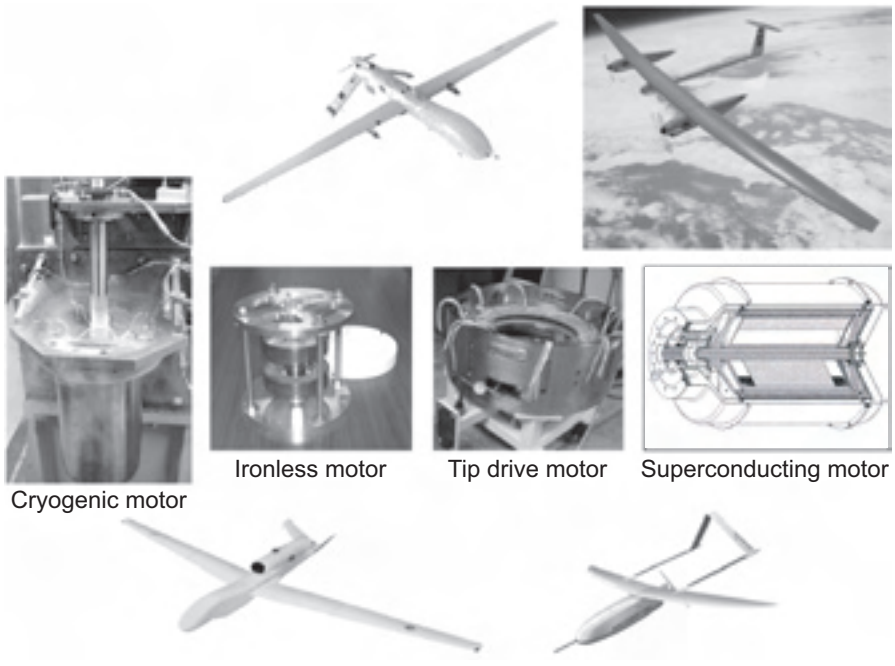


*Advanced high-power-density electric motors, such as superconducting motors, are being developed. These motors may provide electric propulsion for future HALE ROA used to support NASA science missions, such as hurricane tracking. Flight mission analyses have been conducted to determine the viability of these advanced motors.*

UAV selection was based on research performed on numerous current UAVs suitable for this mission. The Global Hawk was selected as the best candidate. Currently used by the U.S. military for high-altitude reconnaissance, with its current propulsion system, the Global Hawk can stay airborne for over 36 hr with regularity. The aircraft is large enough, strong enough, and fast enough to fly in, over, and through strong hurricanes.

The current propulsion system, the Allison Rolls-Royce AE 3007H, is a modified engine that allows the aircraft to climb to altitudes of 65,000 ft. The engine produces a maximum of 7600-lb thrust, rated at takeoff, and the HPDM design used in the analysis can produce upwards of 1000 hp, providing enough thrust to allow the redesigned aircraft to take off.

The mission analysis involved four phases of the flight profile: takeoff, cruise out to the storm, loiter over the storm until landfall, and land after the storm has made landfall. From the takeoff portion of the flight, the parameters that were most important were the required horsepower, thrust, velocity, and takeoff distance. For the cruise portion of the flight, the aircraft cruising velocity was important since it determines how fast the aircraft can reach the storm system. For the loiter phase, when the aircraft circles over or through the storm until it makes landfall, the major factors that determine the aircraft's performance are the cruise velocity and the endurance of the aircraft.

The results of the study revealed that the HPDM could not meet the minimum 10-day endurance requirement desired for hurricane tracking because of fuel-space limitations in the current Global Hawk design. The HPDM did, however, improve the UAV endurance from 48 to 130 hr, which is a very significant performance improvement. If sufficient

fuel space was available and the specific fuel consumption of the fuel cells was lowered, the proposed 240 hr could be reached. This study shows that HPDM technology could be viable for future aircraft and UAV performing civil missions like hurricane tracking. The 130-hr endurance shows that, based on the assumptions and analysis of this study, these motors will allow aircraft to fly longer while reducing harmful emissions.

**Glenn contacts:**
Dr. Dexter Johnson, 216–433–6046, Dexter.Johnson-1@nasa.gov; and Dr. Gerald V. Brown, 216–433–6047, Gerald.V.Brown@nasa.gov

**Author:**
Dr. Dexter Johnson

**Headquarters program office:**
VSP

**Programs/Projects:**
LEAP

## Thioether Tested for the High-Temperature Vapor/Mist Phase Lubrication of Bearings and Gears

In the design of future high-speed jet engines, whose operating temperatures will most likely exceed 400 °C, the choice of a lubricant and lubrication method will be of considerable concern. Because of the thermal limits of conventional liquid lubricants, vapor/mist phase lubrication (VMPL) has received attention over the past decade as an alternative approach for high-temperature lubrication.

VMPL is a unique lubrication technology where a small quantity of an organic liquid lubricant is either vaporized or misted into a high-velocity stream of air. The air-lubricant stream is directed toward bearings and/or gears. This technology has substantial potential for near-term use as an emergency backup system for loss-of-oil situations in aircraft and could serve, with further refinements, as the primary lubrication system for advanced aircraft of the future.

Nearly all previous work, including that by NASA and the Air Force, involving VMPL focused on the use of organophosphorous oils. Although these oils adequately lubricated bearings and gears, it was found that the oils reacted excessively with the bearing and gear surfaces, leading to unacceptable wear rates and erratic temperature spikes. Research at the NASA Glenn Research Center identified a thioether lubricant that provides outstanding lubrication with no detectable wear of the bearing and gear components and elimination of the temperature spikes.

A series of tests were concluded this year that involved the lubrication of a spur gearbox rig using the thioether as the vapor/mist phase lubricant. Two spur gears were loaded against each other in excess of 1-GPa pressure to ensure boundary lubricating conditions, and they were operated at 10,000 rpm. The thioether was delivered to the spur gears as a fine mist or fog at a rate of only

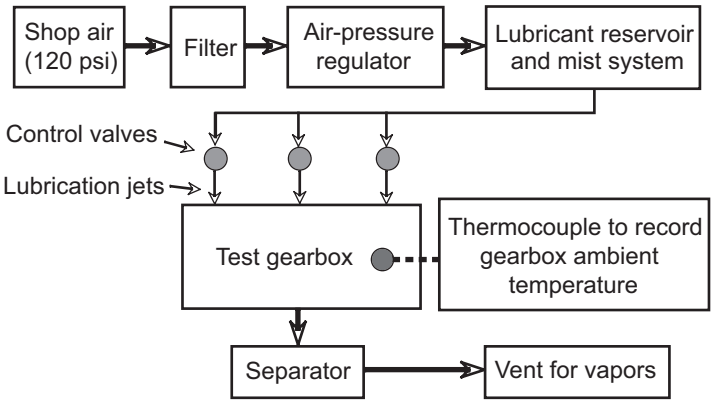


*Vapor/mist phase lubrication system.*

10 ml/hr. After 30 hr of running time, the spur gears were examined for wear. Even under these severe operating conditions, no detectable wear was found.

These tests show that VMPL technology using the thioether has immediate application as an emergency backup lubrication system where weight and size constraints can be minimized aboard aircraft and has excellent potential as the primary lubrication system for future advanced aircraft where conventional liquid lubricants cannot be used.

**Find out more about the research of Glenn's Mechanical Components Branch:**
http://www.grc.nasa.gov/WWW/5900/5950/

**Glenn contact:**
Dr. Wilfredo Morales, 216–433–6052, Wilfredo.Morales-1@nasa.gov

**Authors:**
Dr. Wilfredo Morales,
Dr. Robert F. Handschuh, and
Dr. Timothy L. Krantz

**Headquarters program office:**
Aeronautics Research

**Programs/Projects:**
Aviation Safety, Rotorcraft

## Influence of Speed and Load on High-Speed Helical Gear Trains Investigated

High-speed, heavily loaded, and lightweight gearing components are commonplace in rotorcraft systems. These systems are expected to deliver high power from the gas turbine engines to the high-torque, low-speed rotor. The gearing systems in these extreme-duty applications can have thermal behavior problems because of high pitch line velocities that approach 25,000 ft/min.

A significant number of tests with varying speeds and loads were conducted on a full-scale, aircraft-quality, high-speed helical gear train. These tests validated the effects of gear shrouding and lubricant jet pressure on the thermal and mechanical performance of this gear system.

Because of the high speed, the thermal behavior of mechanical components can change a design that is successful from a load-capacity (bending and contact stress) viewpoint into a thermally induced failure (because of high operational temperatures, gear tooth scoring, and high drive system losses). In rotorcraft drive systems, such as those of tiltrotors, a helical gear train is used to separate the parallel engine and rotor shafting on the aircraft. This part of the drive system operates at very high rotational speeds and carries the full power of the engine during operation. In this type of arrangement, several idler gears are used to transmit power between the engine and the rotor shaft centerlines. Since these gears have two thermal cycles per revolution and are extremely lightweight (low heat-carrying capacity), the successful operation of the system in all possible normal and emergency conditions can be difficult. The test facility at the NASA Glenn Research Center is full scale and can operate to 15,000 rpm (to simulate the engine input rotational speed) and at power levels to 5000 hp. The test facility is being used to assess performance improvements for normal and emergency lubrication operation.

*Helical gear train test components.*

The current test program investigated the effects of gear shrouding and lubricating jet pressure on the performance of this high-speed helical gear train. The temperature increase in the lubricant and power loss on the gearing system as a function of these variables is shown in the graphs on the next page. Test data are shown for two speeds (12,500 and 15,000 rpm, for forward flight and hover conditions, respectively), whereas the load on the system was maintained at

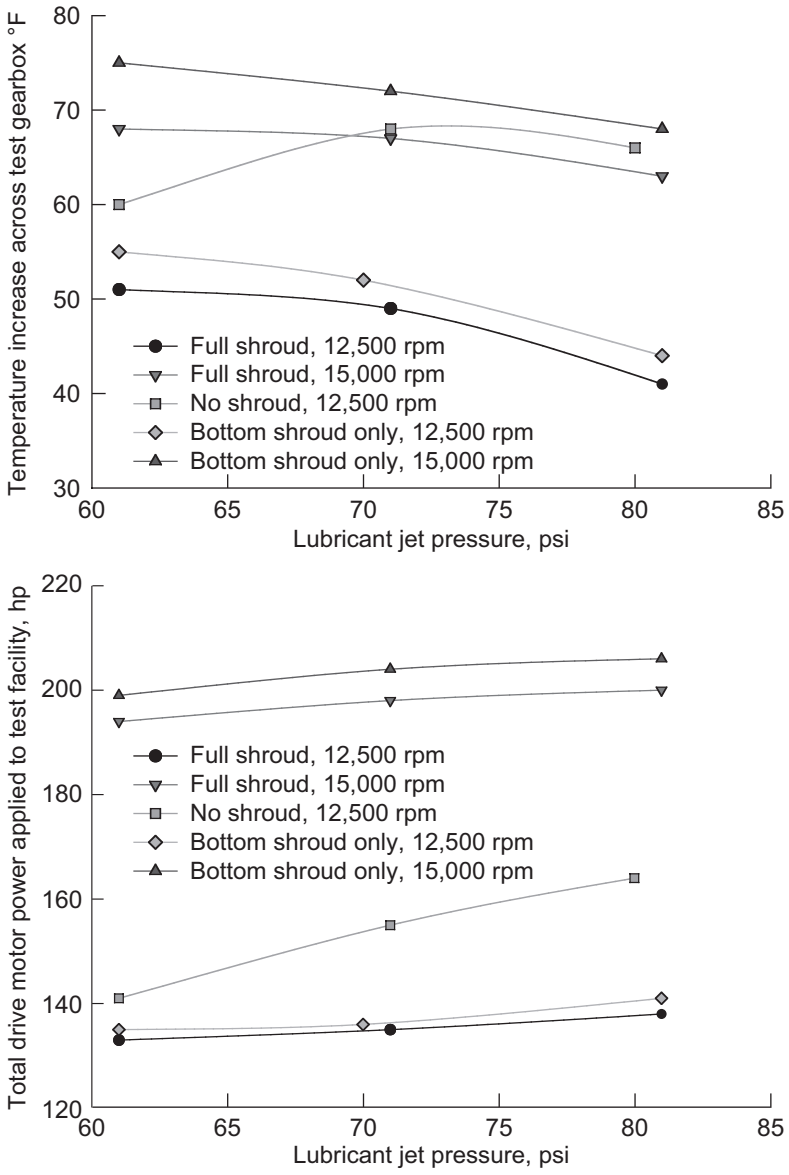


*Top: Effect of lubricant jet pressure, input shaft speed, and shrouding on the temperature increase across the test gearbox. Bottom: Effect of lubricant jet pressure, input shaft speed, and shrouding on the power to drive the test facility.*

similar conditions (approximately 33 percent of full conditions). Both measured parameters, the temperature increase across the test gearbox and the amount of power to drive the entire facility, were affected by the shrouding and the lubricant jet pressure. At either speed condition, the full shroud case was the best over all the speed and load conditions except when the flow was reduced to approximately 60 psi. Using just the bottom half of the shrouds resulted in a high temperature increase across the test gearbox. The no-shroud condition could not be conducted at 15,000 rpm because of operational instability thought to be due to interactions between the lubricant and the bull gear that affected the proper scavenging of the lubricant. A similar trend is shown for the amount of power supplied to the entire test facility for shroud, bottom-half-shroud, and no-shroud conditions. Full-shrouded gears require the least amount of drive motor power for the tests conducted.

**Find out more about Glenn's Mechanical Component's Branch:**
http://www.grc.nasa.gov/WWW/5900/5950/

**U.S. Army Research Laboratory at Glenn contact:**
Dr. Robert F. Handschuh, 216–433–3969, Robert.F.Handschuh@nasa.gov

**Author:**
Dr. Robert F. Handschuh

**Headquarters program office:**
Aeronautics Research, VSP

**Programs/Projects:**
VSP

# Damage Tolerance of Gears Demonstrated for Application to the Space Shuttle Rudder/Speed Brake Safety Assessment

Space shuttle orbiters use geared actuators to control the rudder/speed brake and body flap panels that are used for flight control and steering. Therefore, the gears used to position the panels are safety-critical components. Inspection of gears from flight units revealed unexpected damage to the gear working surfaces. Working as part of the NASA Safety Engineering Center's (NESC) Independent Assessment Team, a project was executed to determine whether or not gears with defined levels of damage are fit for service.

The first two steps of the project were to establish the root cause of the damage and to replicate the damage on gear test specimens. Experiments were done using NASA Glenn Research Center's Spur Gear Test Rigs, which were specially modified for this project. The rigs were arranged to give a controlled dithering (back-and-forth) motion to a set of gears representative of those used on orbiters. The test gears had damage fully representative of that found on the flight hardware. The damage on the working surfaces of the gears was identified as a form of fretting damage. Thus, it was established that the observed fretting damage on flight hardware was caused by many repetitions of a small-amplitude dithering motion with relatively small loads.

The third step of the project was to investigate the damage tolerance of gears having fretting damage. Test gears were subjected to fretting motions to impart fretting damage and then subjected to motions and loads representative of flight control requirements. After the damaged gears were exercised to simulate flight requirements, the residual strengths of the test gears were determined using a newly devised and commissioned single-tooth bending fatigue test rig. Both the damaged test gears and new gears were tested to failure to determine and compare the fatigue lives and failure modes. Several tests were done since gear bending fatigue is a probabilistic phenomenon requiring multiple tests to properly establish fatigue lives. The testing demonstrated that the bending fatigue lives of the undamaged and damaged gears were similar. Most importantly, both the new gears and the damaged gears failed at the base of the gear tooth, away from the fretting damage that was located on the contacting-flank portion of the gear teeth (see the photograph). We concluded that the fretting damage did not reduce the low-cycle-fatigue lives of the gears.

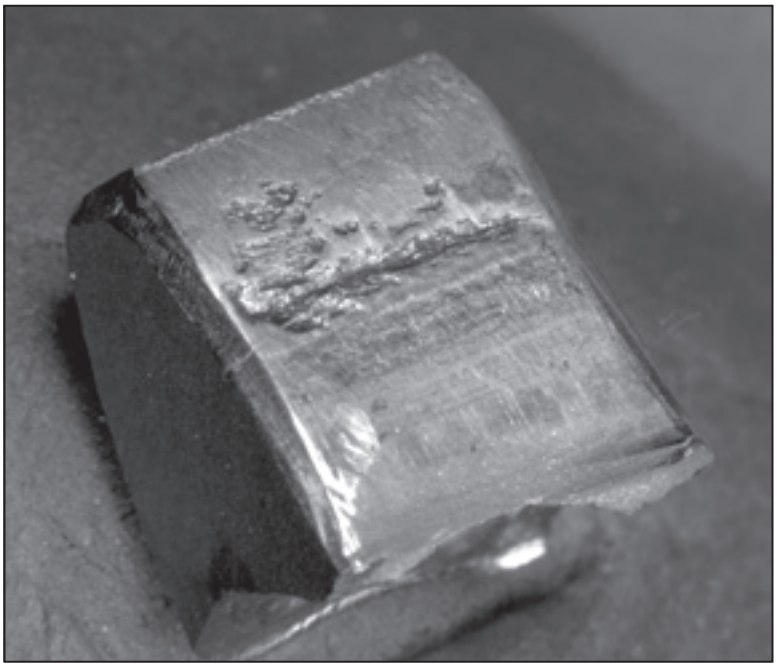

*Gear tooth with fretting and pitting damage tested to failure using the single-tooth bending test method.*

This gear testing devised and executed at Glenn demonstrated the damage tolerance of gears with fretting damage. The project and the demonstrated results were a key part of the NESC Rudder/Speed Brake Gear Margins Independent Technical Assessment supporting the safe return to flight of the space shuttle.

**Find out more about this research:**

**Glenn's Mechanical Components Branch:**
http://www.grc.nasa.gov/WWW/5900/5950/

**NESC:** http://nesc.nasa.gov/index.cfm?linkfrom=home

**U.S. Army Research Laboratory at Glenn contacts:**
Dr. Timothy L. Krantz, 216–433–3580, Timothy.L.Krantz@nasa.gov; and
Dr. Robert F. Handschuh, 216–433–3969, Robert.F.Handschuh@nasa.gov

**Glenn contact:**
Dr. Bradley A. Lerch, 216–433–5522, Bradley.A.Lerch@nasa.gov

**Author:**
Dr. Timothy L. Krantz

**Headquarters program office:**
NESC

**Programs/Projects:**
NESC, Orbiter Rudder/Speed Brake Gear Margins Independent Technical Assessment

# Space Shuttle Power Drive Unit Gears Tested for Scuffing

In support of space shuttle return-to-flight efforts, gear-scuffing tests were conducted by the Mechanical Components Branch at the NASA Glenn Research Center. A new test gear box was designed, fabricated, and installed in Glenn's Gear Noise Test Facility to test flight gears from the shuttle rudder/speed brake power drive unit (PDU). Failure of these gears during flight could jam the rudder/speed brake, which is needed for steering and landing the shuttle, and cause a catastrophic failure. The objectives were to recreate scuffing damage similar to that found on the flight gears at conditions expected during back-drive, to document conditions that induce scuff, to demonstrate that scuffed PDU flight gears can be operated long enough to complete a shuttle mission, and to quantify the scuffing and tooth wear.

Scuffing-like damage was found on the tooth surfaces of gears 5 and 6 of the shuttle rudder/speed brake PDU 2 after a transient back-driving event occurred in flight. Tests were conducted using a pair of unused space flight gears in a bench test setup (see the photograph) at operating conditions up to 2866 rpm and 1144 in.-lb at the input ring gear and 14,000 rpm and 234 in.-lb at the output pinion gear. This corresponds to a power level of 52 hp.

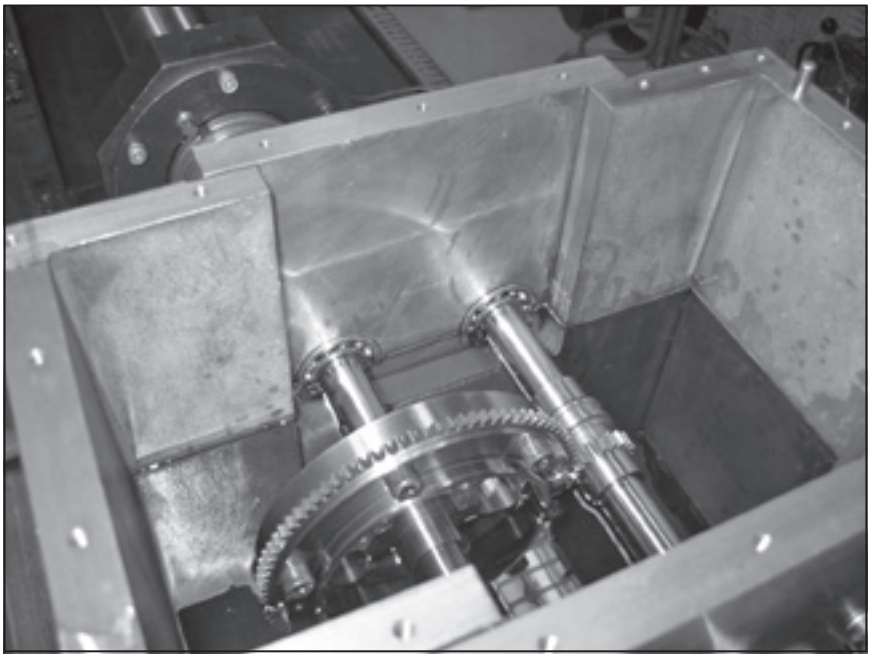

*Space shuttle rudder/speed brake PDU flight gears installed in a test gear box for scuffing tests at Glenn.*

This test condition exceeds the maximum estimated conditions expected in the back-driving event that was thought to produce the scuffing damage. Some wear marks were produced, but they were much less severe than the scuffing damage produced during shuttle flight. These tests gave confidence to the Shuttle Project Office to proceed with the launch of space shuttle flight STS–114. If a future shuttle flight includes a back-driving event that produces gear scuffing, Glenn's bench test rig could be used to assess the remaining life of gears that were scuffed in flight. Such an approach provides the most direct assessment method short of system-level testing.

**Find out more about the research of Glenn's Mechanical Components Branch:**
http://www.grc.nasa.gov/WWW/5900/5950/

**Glenn contacts:**
Margaret P. Proctor, 216–977–7526, Margaret.P.Proctor@nasa.gov; and
Fred B. Oswald, 216–433–3957, Fred.B.Oswald@nasa.gov

**Authors:**
Margaret P. Proctor, Fred B. Oswald, and Dr. Timothy L. Krantz

**Headquarters program office:**
Space Operations

**Programs/Projects:**
Shuttle Project Office

# Environmental Seals of the Space Shuttle Main Landing Gear Door Investigated

During the investigation into the loss of the *Space Shuttle Columbia* (STS–107), the Columbia Accident Investigation Board requested an investigation into the main landing gear (MLG) door environmental seals. Visual inspections of the seals on *Space Shuttle Discovery* (OV–103) revealed that the seals were permanently deformed, which necessitated their replacement. In addition, constant-height shims were added to the MLG doors to ensure that the proper compression was applied to the seals. However, the shims caused the newly installed seals to generate excessive loads that prevented full closure of the doors. The NASA Johnson Space Center requested that the NASA Glenn Research Center perform compression tests and leakage evaluations of the seals to obtain data to guide seal installation and maintenance as well as to aid in closing the MLG doors. The MLG door environmental seal is shown in the photograph to the right.

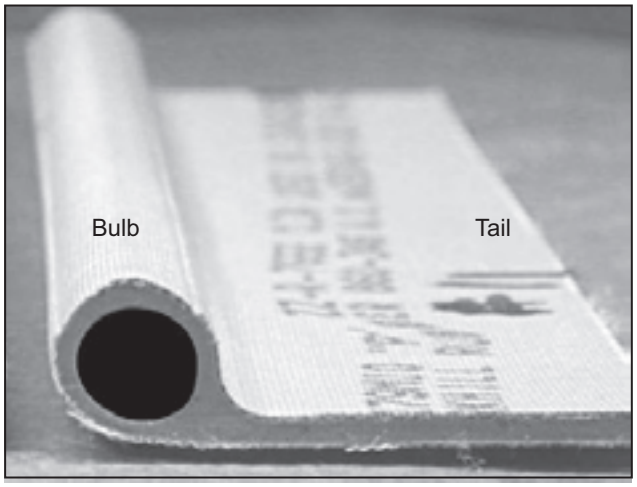


*Orbiter MLG door environmental seal sample with bulb and tail sections labeled.*

Three seal-installation variables were examined as potentially contributing to the excessive loads generated by the replacement MLG door seals: the presence of a groove adjacent to the seal bulb, the loading speed of the seal bulb, and excess room-temperature vulcanizing (RTV) rubber bonding agent applied under the seal bulb. The following figure presents the loads generated by the seal at 63-percent compression for each installation variable and its respective control case. The groove and the loading speed of the bulb had no significant effect on seal loading, whereas excess RTV rubber under the seal bulb dramatically increased the load generated by the seal. The figure also shows two photographs of a fully compressed seal, one showing a seal with excess RTV rubber under the bulb and the other showing the control case.

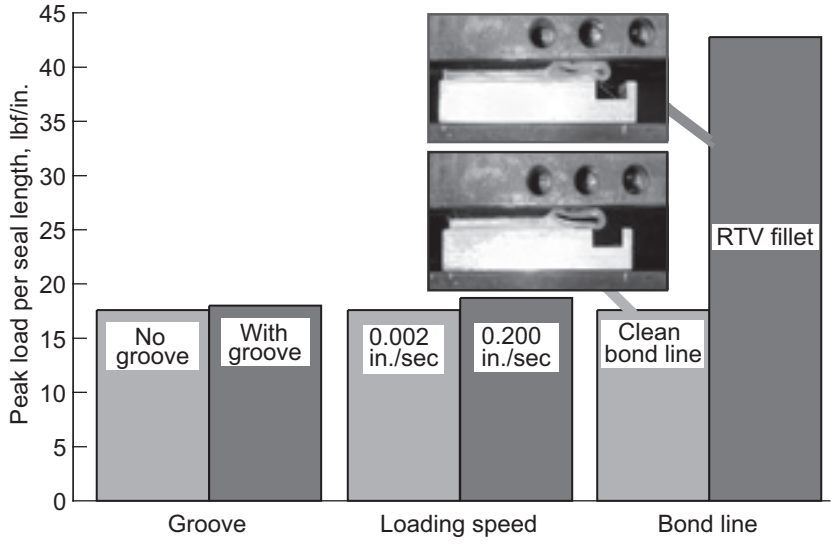


*Peak loads generated by the MLG door environmental seal for three seal installation variables with respective control cases.*

The figure on the next page presents results from leakage tests performed at discrete compression levels with a pressure drop of 2 psig across the seal. The bulb-first and tail-first seal orientations indicate the location of the high-pressure side of the seal and simulate the pressure loading during orbiter reentry and ascent, respectively. At 0-percent compression (i.e., the seal touching the opposing surface without bulb compression), the leakage rates measured from the two seal orientations differed by two orders of magnitude. The tail-first case with 0-percent compression demonstrated seal leakage in excess of the 3-SCFM[1]-of-seal certification limit. Imposing compression upon the seal bulb reduced the leakage rate sufficiently to meet the requirements and also reduced the difference in leakage measured between the two seal orientations.

Using Glenn's test data and recommendations, shuttle technicians were able to close *Discovery*'s MLG doors. The starboard MLG door was successfully closed after technicians removed excess RTV rubber from under the bulb of the

[1]Standard cubic feet per minute.

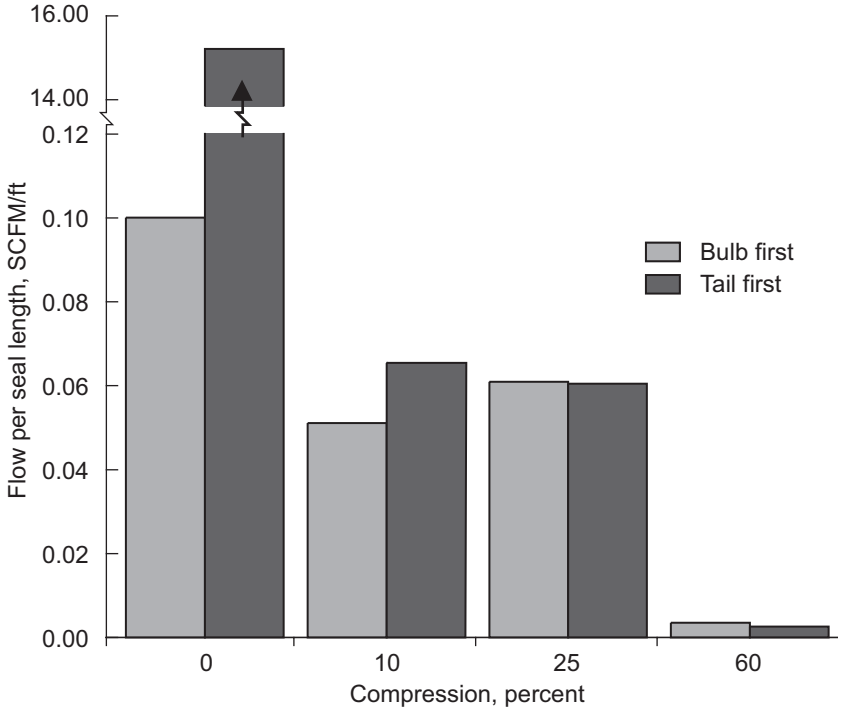


*Leakage rates measured across the MLG door environmental seal for discrete compression levels for both bulb-first and tail-first orientations. The pressure drop across the seal was 2 psig.*

newly installed environmental seals. Successful closure of the port MLG door required further minor modifications in addition to the removal of the excess RTV rubber. Flow tests performed at Glenn demonstrated that when installed and maintained at an appropriate compression level, leakage rates across the seals meet the requirements in the certification drawings.

**Find out more about this research:**

**Structural seals and thermal barriers research at Glenn:**
http://www.grc.nasa.gov/WWW/structuralseal/

**Glenn's Mechanical Components Branch:**
http://www.grc.nasa.govWWW/5900/5950/

**Glenn contacts:**
Joshua R. Finkbeiner, 216–433–6080, Joshua.R.Finkbeiner@nasa.gov;
Patrick H. Dunlap, Jr., 216–433–3017, Patrick.H.Dunlap@nasa.gov; and
Dr. Bruce M. Steinetz, 216–433–3302, Bruce.M.Steinetz@nasa.gov

**University of Toledo contact:**
Jeffrey J. DeMange, 216–433–3568, Jeffrey.J.DeMange@nasa.gov

**Authors:**
Joshua R. Finkbeiner, Jeffrey J. DeMange, Patrick H. Dunlap, Jr., and Dr. Bruce M. Steinetz

**Headquarters program office:**
Space Operations

**Programs/Projects:**
Space Shuttle

## Tradeoffs of Various Concepts for Planetary Vehicle Drives Studied

Exploration of the planets and moons of the solar system will require several types of vehicles, including manned and unmanned rovers, construction vehicles, and mining vehicles. These vehicles will need mechanical drives that are lightweight, efficient, reliable, and long-lived, even as they operate under harsh conditions involving temperature extremes, rough terrain, hard vacuum, and abrasive dust.

Space mechanisms design requirements are strongly application-specific. Factors that will influence rover vehicle drive design decisions include the speed, torque, weight and space allowances, temperatures, lubrication, challenges of the environment, and requirements for efficiency, life, and reliability. In addition, heat dissipation can be a problem for high-power drives, especially if solid lubricants are used.

This study at the NASA Glenn Research Center considered classical gear designs, including simple spur and helical stages and combinations of simple stages such as epicyclic (planetary) transmissions, including compound planetary and differential transmissions and harmonic drives. Each of these types has specific advantages and challenges.

The study also considered novel concepts, such as traction drive transmissions and hybrid traction-gear transmissions. Novel concepts need additional development work to establish their reliability and suitability for particular missions.

Very high gear ratios are available by cascading transmission stages. The stages

DESIGN TRADEOFFS FOR PLANETARY ROVER PARALLEL-AXIS TRANSMISSIONS

| Advantages | Challenges |
|---|---|
| **Spur and helical gear pairs** | |
| Highest mechanical efficiency (>98 percent)<br>Relatively inexpensive<br>Compatible with dry lubricants | Offers only a moderate speed ratio per stage<br>Requires many stages for high ratios<br>Helical gears have thrust load<br>Requires shaft offset (except reverted train) |
| **Harmonic drives** | |
| Space qualified<br>High reduction in one stage<br>Can be hermetically sealed<br>Near-zero backlash | Limited life of wave generator bearing<br>Moderate efficiency (<80 percent)<br>Not very suitable for dry lubrication |
| **Simple planetary gear train** | |
| High efficiency (>90 percent)<br>Compact, close-coupled design<br>Much experience in aeronautics<br>Distributed loading of gears and bearings<br>Compatible with dry lubricants | Complex (many components)<br>Requires multiple stages for high ratio |
| **Compound planetary gear train** | |
| High efficiency (>90 percent)<br>Distributed loading of gears and bearings<br>Compatible with dry lubricants | Complex (many components)<br>Moment loads on planet bearings |
| **Differential planetary gear train** | |
| High ratio (500:1) possible in a single stage<br>Distributed loading of gears and bearings<br>Compatible with dry lubricants | Complex (many components)<br>Low efficiency, especially for high ratio |
| **Traction drive** | |
| High efficiency (>94 percent)<br>High ratio (250:1)<br>Smooth operation (low noise/ripple)<br>Compatible with dry lubricants | Complex (many components)<br>High weight (30-percent higher than planetary)<br>Possible surface durability problems<br>Needs technology development |

need not be of the same type. For example, the 1500:1 ratio used on the Mars Exploration Rover was obtained with an 18.8:1 planetary first stage and an 80:1 harmonic-drive second stage. Staging can optimize the performance of a transmission. The Mars Exploration Rover benefits from the high torque to weight of the harmonic-drive output stage while avoiding problems from the limited life of the input bearing of the harmonic drive.

Some of the general characteristics are summarized in the table.

The graph relates the mass to the output torque of high-ratio, space-rated drives from four commercial vendors. The drives include 80:1 and 160:1 harmonic drives, two-stage planetary units with ratios from 61:1 to 114:1, and miscellaneous drives with ratios up to 17933:1.

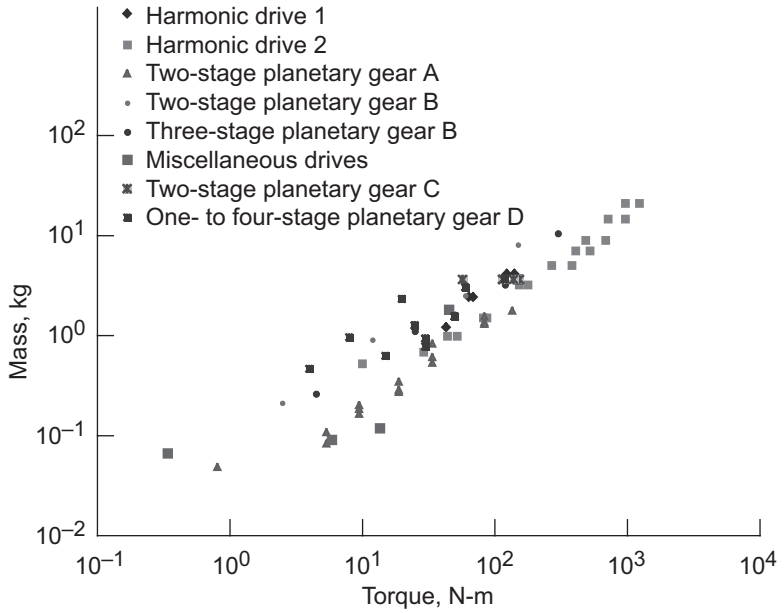


*Mass of high-ratio transmissions from four commercial vendors as a function of the output torque. Curve-fitting mass M versus torque T yields $M = 0.0678T^{0.7782}$, where M is in kilograms and T is in newton-meters.*

**Find out more about this research:**

**Space Mechanisms Project:**
http://www.grc.nasa.gov/WWW/spacemech/

**Glenn's Mechanical Components Branch:**
http://www.grc.nasa.gov/WWW/5900/5950/

**Glenn contact:**
Fred B. Oswald, 216–433–3957,
Fred.B.Oswald@nasa.gov

**Author:**
Fred B. Oswald

**Headquarters program office:**
Exploration Systems

**Programs/Projects:**
MTLAMPS

# Modeling of Nonmetallic Inclusions in Powder Metallurgy Alloys Improved

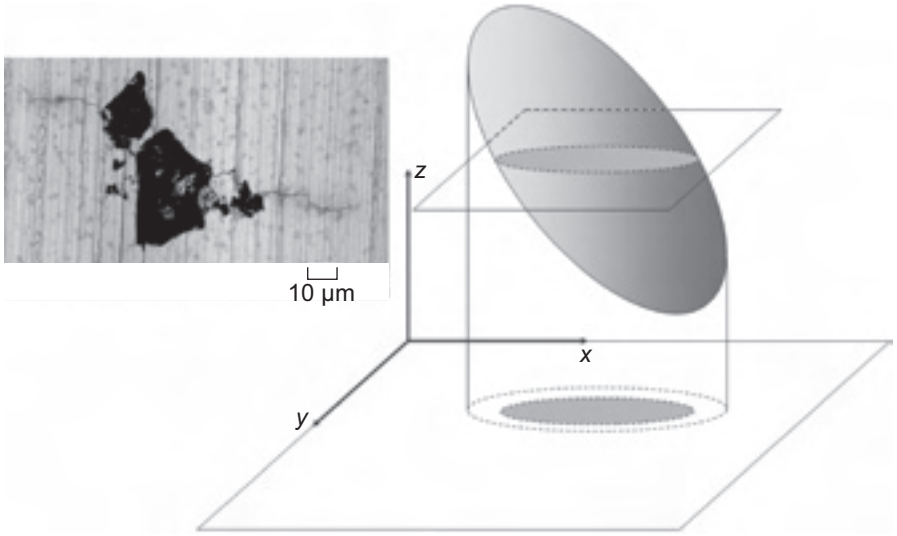


*Projected area of an ellipsoidal representation of an inclusion. Inset photograph displays cracks propagating from noncoplanar asperities.*

Inclusions can cause early and catastrophic fatigue failure in powder metallurgy alloys. They act as sites for premature crack initiation, bypassing the typically long period of slow crack growth. To study this phenomenon, researchers conducted a test program at the NASA Glenn Research Center involving specially prepared powder metallurgy alloy test specimens with controlled inclusions. Because inclusions tend to be small and relatively rare in current production powder, inclusions of known size distributions were introduced to the precursor powder to ensure that a prescribed average number would occur on the surface of the fatigue test samples. A geometric model was devised at Glenn so that the inclusions could be modeled as crack-initiating defects. It models the inclusions as ellipsoids that can have three different dimensions (semi-axes) and random orientation.

In examining the fracture surfaces of failed "seeded" specimens, we found that the expected maximum cross section of an inclusion was not always an accurate predictor of the starting crack size. Geometric simulations based on the maximum-cross-section assumption predicted size distributions that have smaller means and less scatter than the size distributions observed on fracture surfaces. We also observed that cracks tend to grow from the corners of inclusions and do not always initiate in the same plane (see the top right figure).

These observations led to an alternate assumption that the projected area of the inclusion may be a more accurate predictor of the crack-initiation area. Consequently, a closed-form solution

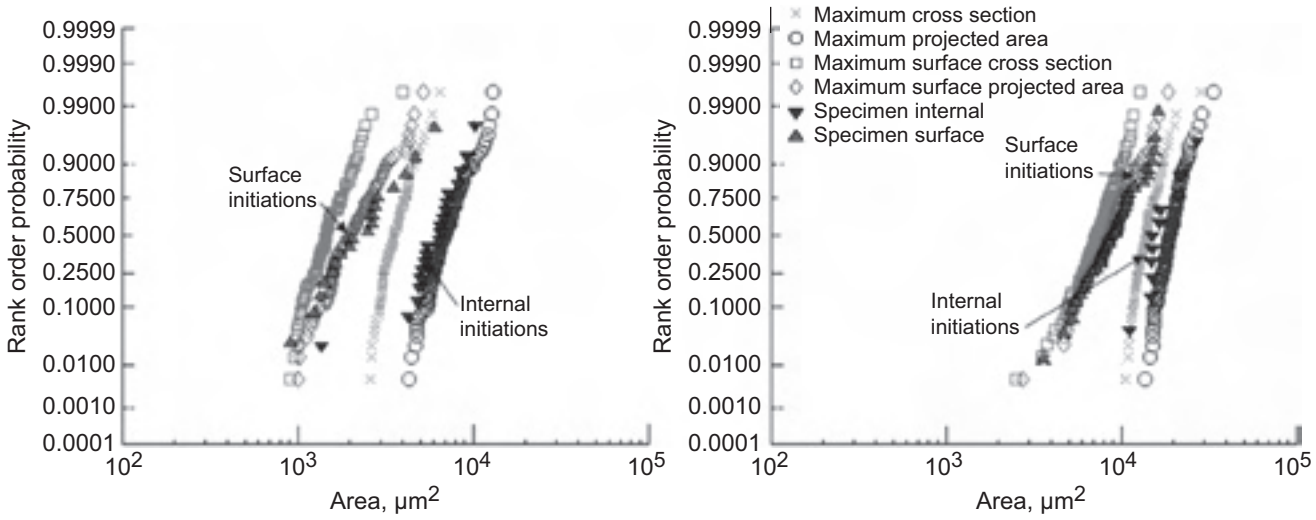


*Comparison of fracture surface failure-initiating inclusion areas with simulated maximum cross section and projected area for*
□
*Left: Ram 90–270+325 (mesh size). Right: Alcoa T64–140+170 (mesh size).*

for the projected area of a randomly oriented arbitrary ellipsoid was derived. Simulations based on the projected-area assumption showed improved correlation with the observed fracture surface area distributions.

**U.S. Army Research Laboratory at Glenn contact:**
Pete Bonacuse, 216–433–3309, Peter.J.Bonacuse@nasa.gov

**Glenn contacts:**
Jack Telesman, 216–433–3310, Ignacy.Telesman@nasa.gov; and Tim Gabb, 216–433–3272, Timothy.P.Gabb@nasa.gov

**Ohio Aerospace Institute (OAI) contact:**
Pete Kantzos, 216–433–5202, Pete.T.Kantzos@nasa.gov

**Author:**
Peter J. Bonacuse

**Headquarters program office:**
Aeronautics Research

**Programs/Projects:**
Aviation Safety

## Design of an Airliner-Stabilizer Optimized Through Component Mode Synthesis

A design synthesis methodology was developed at the NASA Glenn Research Center to optimize the composite stabilizer of an airliner. The stabilizer was separated into components, including the spars, the webs or stiffeners, composite face sheets, the elevator, and the carry-through frame. Each component was optimized for its free-body reactive loads. The entire stabilizer was synthesized from the optimized components. The design synthesis used the commercial MSC/Nastran code (MSC Software Corporation, Santa Ana, CA) as the analysis tool and Glenn's testbed CometBoards as the optimizer. The stabilizer, made of 80-percent composite material and 20-percent metal, was subjected to over 500 load conditions. A reduced set of critical load cases was extracted for design calculation on the basis of a strain energy criterion, which was also validated from a probabilistic sensitivity analysis.

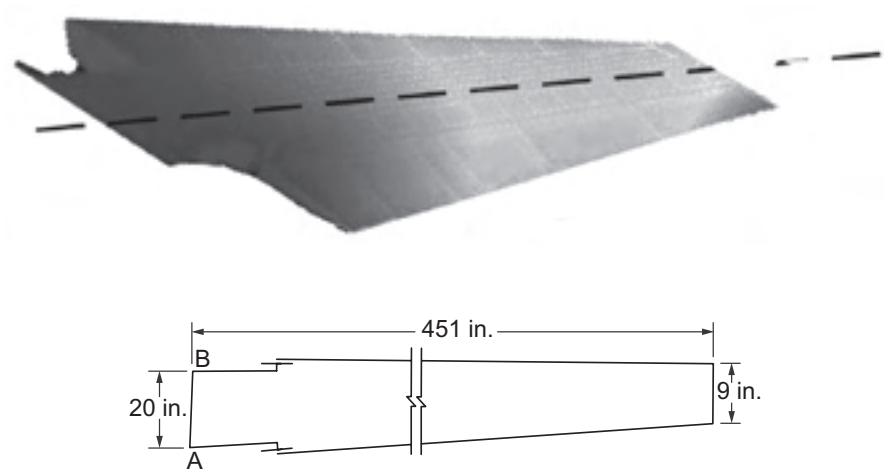


*Top: Aircraft stabilizer—symmetrical half. Bottom: Central spar made of six different materials.*

Stress, vibration, and frequency analyses were performed for a finite-element model that contained about 20,000 elements and 80,000 degrees of freedom. The analysis exhibited interactions between the local frequency and buckling modes. The bar chart on the next page illustrates the optimization of a component design, considering the central spar as an example. The optimum solution was generated for the minimum-weight condition for strength (with a 20-ksi stress allowable), for stiffness (with the displacement limitation in the 12- to 24-in. range), and for a 0.70-Hz frequency constraint for the set of free-body loads. The initial design with a weight of 78 lbf contained an infeasible strength constraint. Optimum solutions for different constraint scenarios, which used constraint and design variable formulations as well as the cascade optimization algorithm available in CometBoards, are shown in the bar chart. The optimization process reduced weight by 10 to 15 percent by readjusting the design parameters.

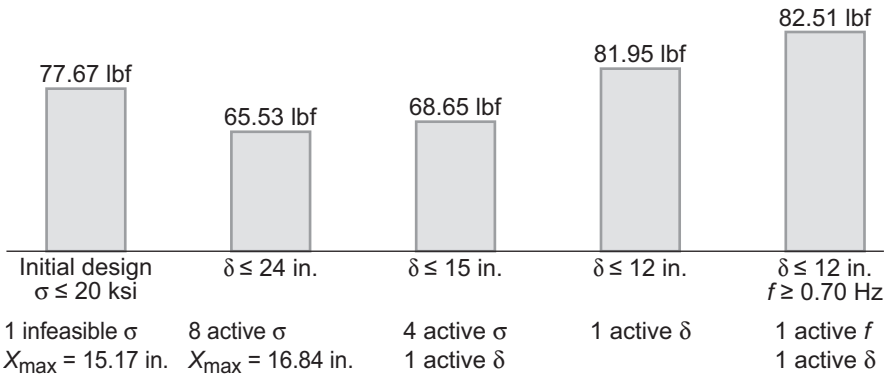


*Optimum solutions for different constraint scenarios; σ, stress; δ, displacement; and f, frequency; $X_{max}$, maximum allowed displacement.*

**Bibliography**
Patnaik, Surya N.; Guptill, James D.; and Hopkins, Dale A.: Subproblem Optimization With Regression and Neural Network Approximators. Comp. Methods Appl. Mech. Eng., vol. 194, nos. 30–33, 2005, pp. 3359–3373.

**Glenn contact:**
Dale A. Hopkins, 216–433–3260, Dale.A.Hopkins@nasa.gov

**Authors:**
Dr. Surya N. Patnaik, Dale A. Hopkins, and Dr. Shantaram S. Pai

**Headquarters program office:**
Aeronautics Research

**Programs/Projects:**
UltraSafe, UEET, HSR

## Multimechanism Viscoelastoplastic Model Used to Characterize and Predict High-Temperature TIMETAL 21S Cyclic and Cyclic-Relaxation Deformation Behavior

Cyclic-and time-dependent behavior can significantly affect the life of aerospace propulsion components. Consequently, one needs an accurate constitutive model that can represent both reversible and irreversible behavior under such loading conditions. To accomplish this, researchers at the NASA Glenn Research Center adopted a complete-potential-based framework, wherein strain, stress, and the thermodynamic functions (stored energy and dissipation) are appropriately partitioned to form a general viscoelastoplastic, multimechanism, deformation model (see ref. 1). This framework, named Generalized VIscoelastoplasticity with Potential Structure (GVIPS), attempts to capture the underlying physical processes associated with microscopic defects (e.g., dislocations, grain boundaries, and voids in metals) and their complicated interactions, which span an entire spectrum of time and length scales, through the introduction of a multiplicity of mechanisms in the mathematical description. The use of multimechanisms in the GVIPS-class formulation enables the specialization of this general model into simpler (more restricted in scope) formulations—for example, purely elastic, linear viscoelastic, classical rate-independent elastoplastic—as well as more elaborate forms of hereditary descriptions—involving such phenomena as viscous effects, nonlinear hardening, dynamic recovery, thermal/static recovery, relaxation, ratcheting, or shakedown phenomena under load cycles.

Previously, a six-mechanism viscoelastic and a three-mechanism viscoplastic GVIPS model was characterized with three constant total-strain-rate ($\dot{\varepsilon}$= $10^{-4}$, $10^{-5}$, and $10^{-6}$ 1/sec) tensile tests, three constant-load creep tests, one three-step creep test, three relaxation histories, and a single fully reversed hysteresis loop. The predictive ability was then validated with multiple-step relaxation tests and a creep-plasticity interaction test (see ref. 2). Recently, the predictive capabilities of this original model and its higher fidelity counterparts (i.e., ones with additional viscoplastic mechanisms) were examined in the context of 12 specifically designed cyclic tests at 650 °C, with and without mean stresses (wherein significant ratcheting can take place). In addition, three complex cyclic-relaxation

history tests, also performed at 650 °C, were reserved for validation purposes. The details of these experiments are discussed in reference 3. The motivation behind the selection of this specific test matrix was to gain insight into the appropriate functional forms to be taken for flow and hardening as well as to identify the appropriate state variables and material parameters to best describe the path and history dependence of TIMETAL 21S.

The graphs show representative predictive results obtained for multiple cycles of one of the three complex cyclic-relaxation histories reserved for validation purposes, given a six-mechanism reversible and a seven-mechanism irreversible viscoelastoplastic model. The corresponding material parameters were obtained using tensile, creep, relaxation, and fully reversed cyclic data and mean stress cyclic ratcheting characterization tests. Clearly, the model can accurately predict these complex cyclic-relaxation histories. Note that the top graphs illustrate the stress-strain response corresponding to three block loading histories consisting of two interrupted cycles followed by 50 uninterrupted cycles each. The bottom graphs show the subsequent material response for three similar block loading histories; however, in this case the interrupted cycles are reversed from those in on the top. A specially designed and developed python script for ABAQUS (ABAQUS, Inc., Providence, RI) was required to obtain the more complex load histories in which the control variable and target variable differ in character (e.g., strain-controlled, stress-limited; or stress-controlled, strain-limited).

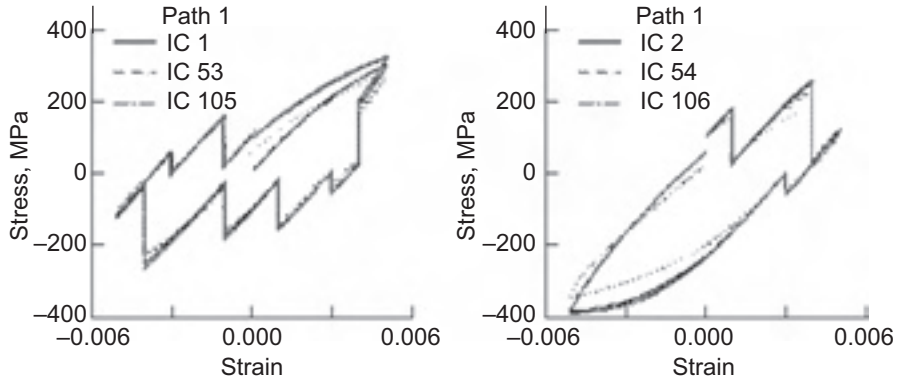


*Strain-controlled, strain-limited, complex cyclic-relaxation block histories conducted at 650 °C (i.e., path 1). IC 1 (as are IC 53 and IC 105) is an interrupted cycle (IC) containing eight 2-hr relaxation histories. This is then followed immediately by a second cycle (IC 2) that has four 2-hr relaxation histories (similar cycles are IC 54 and IC 106). Note that between each set (e.g., IC 1 + IC 2 and IC 53 + IC 54) 50 uninterrupted strain-controlled, strain-limited (±0.005 in/in) cycles are performed.*

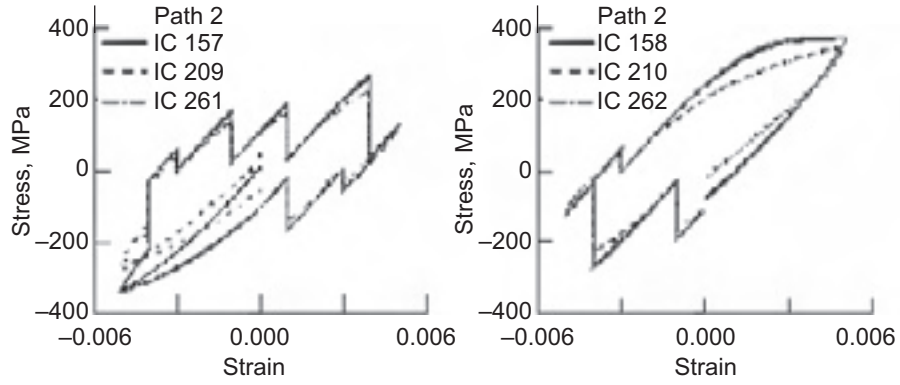


*Strain-controlled, strain-limited, **reversed** complex cyclic-relaxation block histories conducted at 650 °C (i.e., path 2) that had prior histories related to path1 in the top graphs. IC 157 (as are IC 209 and IC 261) is an interrupted cycle (IC) containing eight 2-hr relaxation histories. This is then followed immediately by a second cycle (IC 158) that has four 2-hr relaxation histories (similar cycles are IC 210 and IC 262). Note that between each set (e.g., IC 157 + IC 158 and IC 209 + IC 210), 50 uninterrupted strain-controlled, strain-limited (±0.005 in/in) cycles are performed.*

**References**


1. Saleeb, A.F., et al.: A General Hereditary Multimechanism-Based Deformation Model With Application to the Viscoelastoplastic Response of Titanium Alloys. Int. J. Plasticity, vol. 17, no. 10, 2001, pp. 1305–1350.
2. Saleeb, A.F.; and Arnold, S.M.: Specific Hardening Function Definition and Characterization of a Multimechanism Generalized Potential-Based Viscoelastoplasticity Model. Int. J. Plasticity, vol. 20, no. 12, 2004, pp. 2111–2142.
3. Lissenden, Cliff J.; Doraiswamy, Devaraj; and Arnold, Steven M.: Experimental Investigation of Cyclic and Time-Dependent Deformation of Titanium Alloy at Elevated Temperature. Int. J. Plasticity, 2005.



**Glenn contact:**
Dr. Steven M. Arnold, 216–433–3334, Steven.M.Arnold@nasa.gov

**Authors:**
Dr. Steven M. Arnold, Prof. Atef F. Saleeb, Lynn M. Powers, and Cliff J. Lissenden


**Headquarters program office:**
Aeronautics Research

**Programs/Projects:**
Aviation Safety, CEV, NGLT

# Software Tool Developed to Integrate Probabilistic Structural Analysis With the Simulation of Manufacturing Processes


*Probabilistic analysis of deformation resistance annular welding (Probdraw).*

A prototype software tool was developed at the NASA Glenn Research Center to integrate manufacturing process modeling and probabilistic structural analysis. Two manufacturing processes were considered: a powdered-metal forging process and annular deformation resistance welding (ADRW). Interface modules were developed that automatically transfer IGES files or convert CDB files from ANSYS computer-aided design (ANSYS, Inc., Canonsburg, PA) models to the DEFORM manufacturing process simulation code (Scientific Forming Technologies Corporation, Columbus, OH). Other modules handle such tasks as setting up probabilistic input data. These modules utilize graphical user interfaces to specify input parameters that are subsequently transferred to NESTEM, a NASA-sponsored probabilistic finite-element analysis code. Although the prototype represents a work in progress, some example problems have already been solved.

Present-day structural analysis performs either a deterministic or probabilistic calculation based on either a fixed set of mechanical properties and process parameters or the same properties and parameters with assumed distributions, respectively. The distribution characteristics of these variations are not necessarily reflective of the actual variation that may arise in practice. Probably the single most important factor influencing these variations comes from the manufacturing processes. For example, processes such as welding, casting, and forging can cause large variations in the resulting mechanical properties because of the operational variations in these processes, as well as variations in the materials themselves. Therefore, having a quantitative understanding of these processes and integrating the resulting information into a probabilistic calculation environment could lead to a much more realistic prediction of the structural response of a mechanical component in service. Specifically, this could lead to a more realistic assessment of the sensitivities of the mechanical properties and response, and of how they are affected by variations in the manufacturing process.

Resistance heating is used for many different manufacturing processes, including the welding of two parts. However, joining parts by this process has been restricted primarily to the flat-sheet components used in automotive and aerospace applications. In welding tubular products, a conventional welding process may burn holes unless very precise control is in place. Also, round parts may need to be fixtured or turned during the joining process, increasing cost and time substantially.

ADRW takes advantage of the resistance heating process used in resistance spot welding, but it uses an annular electrode to handle tubular products. By using resistance heating, it raises the temperature of the joining surfaces locally to a high fraction of the homologous temperature. It also allows substantially high pressure to be applied at the joining so that the two joining surfaces can slide past each other, creating a solid-state bond instead of the fusion nugget in spot welding that signifies melting and solidification. Even though this is a recently developed welding process, it has been used successfully to join tubes to solids: various sizes of sheet metals and tubes made of mild steel, stainless steel, and some nickel-based superalloys. The process has been shown to create leak-tight joints with superior strength at a much more rapid pace than with conventional welding methods.

Two separate interfaces, Forgprob and Probdraw, were developed at Glenn to connect the forging code DEFORM and ADRW process modeling with NESTEM. These interfaces enable users to quantify the influences of uncertainties in the variables associated with these two manufacturing processes. This quantified information is very critical for designers. Although designers traditionally account for these effects via factors of safety, the outcome of such factors remains unquantified. Probdraw is illustrated in the figure. The architecture of the two interfaces is basically the same.

**Glenn contact:**
Dr. Shantaram S. Pai, 216–433–3255, Shantaram.S.Pai@nasa.gov

**N&R Engineering contact:**
Dr. Vinod K. Nagpal, 440–845–7020, vnagpal@nrengineering.com

**Author:**
Dr. Arun K. Bhattacharya

**Headquarters program office:**
Exploration Systems

**Programs/Projects:**
Exploration Systems

# Progressive Failure Analysis Capability for Composite Stiffened Panels Developed

A new progressive failure analysis capability for stiffened composite panels was developed at Collier Research Corporation and the NASA Glenn Research Center. It combines Collier's HyperSizer (ref. 1) stiffened panel design software with Glenn's Micromechanics Analysis Code with Generalized Method of Cells (MAC/GMC) (ref. 2). MAC/GMC discretizes a composite material's microstructure into a number of subvolumes and solves for the stress and strain state in each while providing the homogenized composite properties. As a result, local failure criteria can be employed to predict local subvolume failure and the effects of these local failures on the overall composite response. When combined with HyperSizer, MAC/GMC represents the ply-level composite material response within the laminates that constitute a composite stiffened panel. The effects of local subvolume failures can then be tracked as loading on the stiffened panel progresses.

Progressive failure occurs when a structure experiences a significant amount of damage prior to final failure. The life of the structure is, therefore, not accurately represented by the point at which failure initiates, rather, failure progresses from initiation to final failure in some way. Clearly, in order to predict the life of such a structure, a methodology that tracks the failure progression is needed. This type of methodology has been enabled for arbitrary composite laminates and stiffened panels via the

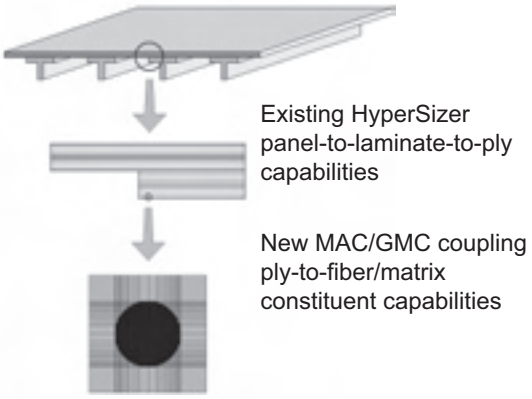


MAC/GMC repeating unit cell representing a continuous fiber composite

*T-stiffened panel-to-ply-to-micromechanics simulation now available within HyperSizer in the context of time-dependence and progressive failure. On the basis of the panel-level loads, HyperSizer determines the laminate- and ply-level stresses and strains, which are passed to MAC/GMC. MAC/GMC then determines fiber- and matrix-level stresses and strains and can predict local damage and failure, the effects of which are then passed back to the higher scales. Thus, the effects of local damage progression on the panel-level response can be simulated.*

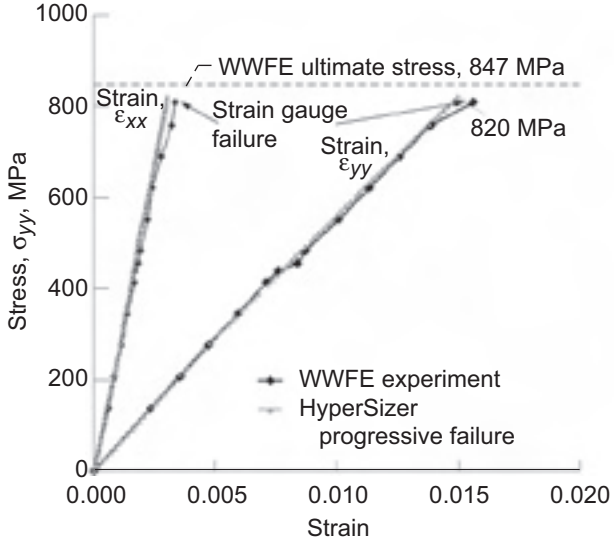


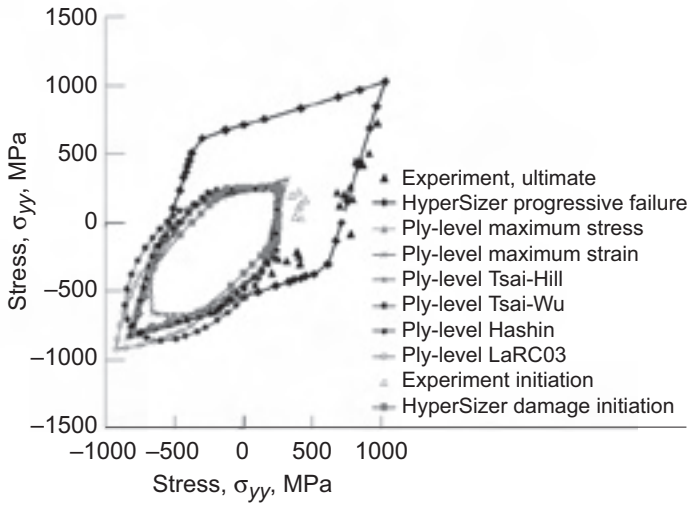


*These two plots compare predictions of the described analysis technology with experimental results from the literature. Left: Biaxial stress-versus-strain response of the laminate; curves representing both midplane strains, $\varepsilon_{xx}$ and $\varepsilon_{yy}$ are plotted against the stress $\sigma_{yy}$. The curves are nonlinear because of progressive damage, and the model and experiment match very well. The ultimate strength of the laminate in the experiment was 847 MPa, whereas the model predicted 820 MPa. Right: Several failure envelopes plotted on $\sigma_{yy}$ versus $\sigma_{xx}$ axes. The predicted ultimate failure envelope matches well with the experimental data, whereas the predicted failure initiation is somewhat inside the associated experimental data and well within the experimental and predicted ultimate failure envelopes. The envelopes that represent common first-ply failure criteria (maximum stress, maximum strain, Tsai-Hill, Tsai-Wu, Hashin, and LaRC03) are well inside the experimental ultimate failure envelope in the tensile regime and closely match the HyperSizer-predicted initiation curve. In compression, all the failure envelopes match reasonably closely.*

combination of HyperSizer with MAC/GMC. MAC/GMC can provide the ply-level composite material properties to HyperSizer, from which HyperSizer can determine laminate- and panel-level properties (see the illustration on the preceding page). Furthermore, because MAC/GMC localizes to the level of the fiber and matrix constituents, microscale failures can be predicted given ply-level stresses and strains from HyperSizer. The new ability of HyperSizer to apply loading to a stiffened panel incrementally (i.e., time-dependent loading) has now enabled progressive failure analysis based on local failures predicted within MAC/GMC while eliminating the stiffness contribution of the failed regions within the fiber and matrix constituents.

Example results are shown in the graphs on the preceding page for a quasi-isotropic $[0/\pm45/90]_s$ AS4 graphite/3501–6 epoxy composite whose response was tested as part of the World Wide Failure Exercise (ref. 3). In the graph on the left, the HyperSizer—MAC/GMC progressive-failure prediction matches well with the nonlinearity in the experimental laminate stress-strain curves, while matching the ultimate failure stress within approximately 3 percent. The graph on the right shows that the predictions agree well with the full normal stress experimental failure envelope. Furthermore, in contrast to common ply-level failure criteria (which significantly underpredict ultimate failure), the current progressive failure methodology enables the prediction of both damage initiation and ultimate failure envelopes. The graphs on this page show similar results for a T-stiffened $[0/\pm45/90]_s$ AS4 graphite/3501–6 epoxy composite panel (see the illustration on the preceding page). Although no experimental results are available in this case, the progressive failure capabilities of the new analysis tool are illustrated.

**References**

1. HyperSizer Structural Sizing Software. Collier Research Corp., Hampton, VA, 2005.
2. Bednarcyk, Brett A.; and Arnold, Steven M.: MAC/GMC 4.0 User's Manual—Keywords Manual. NASA/TM—2002-212077/VOL2, 2002.
3. Soden, P.D.; Hinton, M.J.; and Kaddour, A.S.: Biaxial Test Results for Strength and Deformation of a Range of E-Glass and Carbon Fibre Reinforced Composite Laminates: Failure Exercise Benchmark Data. Comp. Sci. T., vol. 62, 2002, 1489–1514.

**Find out more about this research:**

**ImMAC (integrated multiscale Micromechanics Analysis Code) Software Suite:**
http://www.grc.nasa.gov/WWW/LPB/mac/

**Hypersizer product profiles:**
http://www.hypersizer.com/Products/products.htm

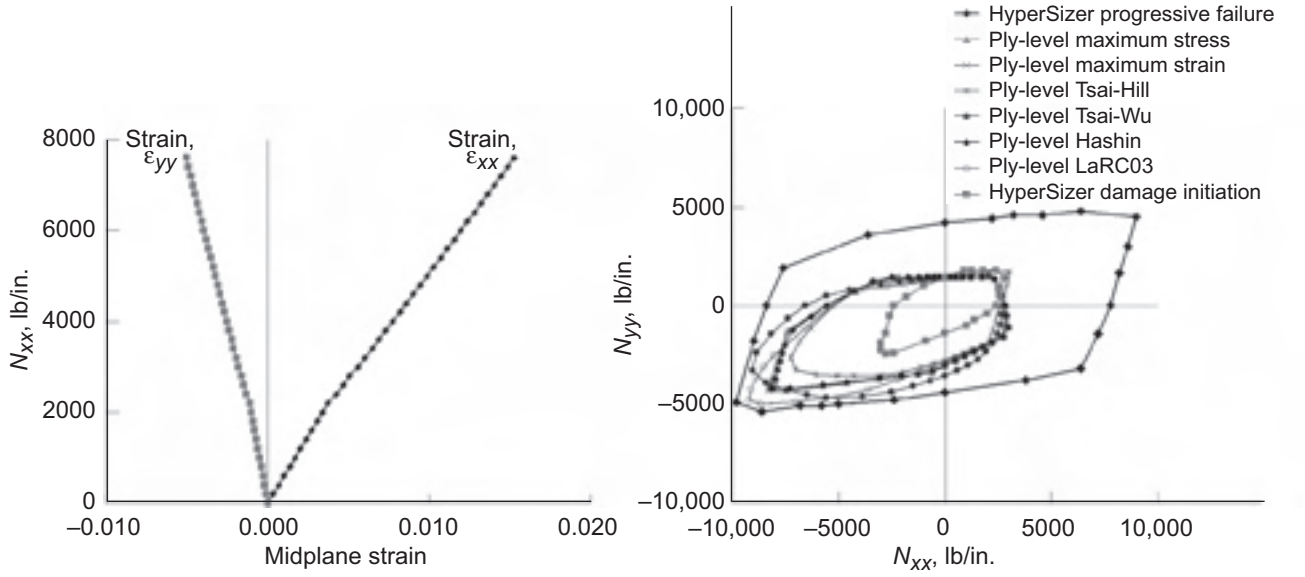


*Two plots for a T-stiffened panel—one representing deformation and the other representing failure envelopes. No experimental data are plotted in this case. Left: Midplane strains $\varepsilon_{xx}$ and $\varepsilon_{yy}$ plotted versus the panel-force resultant $N_{yy}$. Nonlinearity due to damage is evident. Right: HyperSizer damage initiation and ultimate failure envelopes are plotted with the initiation envelope falling well within the ultimate failure envelope, even in the compressive regime. The common first-ply failure criteria (maximum stress, maximum strain, Tsai-Hill, Tsai-Wu, Hashin, and LaRC03) are between the predicted initiation and ultimate failure envelopes in the compressive regime and close to the predicted initiation envelope in the tensile regime.*

**Ohio Aerospace Institute (OAI) contact:**
Dr. Brett A. Bednarcyk, 216–433–2012, Brett.A.Bednarcyk@nasa.gov

**Glenn contact:**
Dr. Steven M. Arnold, 216–433–3334, Steven.M.Arnold@nasa.gov

**Authors:**
Dr. Brett A. Bednarcyk, Phillip W. Yarrington, Craig S. Collier, and
Dr. Steven M. Arnold

**Headquarters program office:**
Aeronautics Research, Science Mission

**Programs/Projects:**
Cross-Enterprise Technology Development, CEV, NGLT

**Special recognition:**
The new capability described is part of the ImMAC software suite, winner of Glenn's 2005 Software of the Year award and second place winner of the NASA 2005 Software of the Year award.

# ENGINEERING AND TECHNICAL SERVICES

## ENGINEERING SYSTEMS

## Hybrid Power Management Program Developed a Fuel-Cell-Powered Utility Vehicle

In fiscal year 2005, the NASA Glenn Research Center initiated the development of a fuel-cell-powered utility vehicle as a way to reduce pollution in industrial settings, reduce fossil-fuel consumption, and reduce operating costs for transportation systems. The utility vehicle provides an inexpensive approach to advance the state of the art in electric vehicle technology in a practical application.

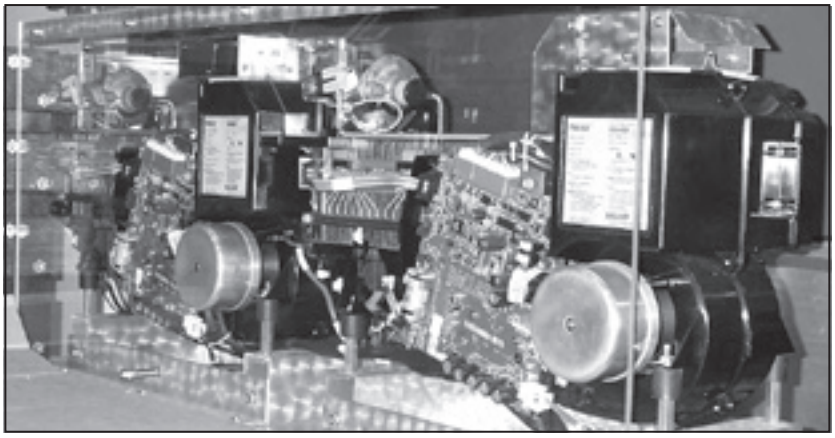

*Hybrid Power Management Program applied to the fuel-cell-powered utility vehicle project. Top: Fuel-cell-powered utility vehicle. Bottom: PEM fuel cells installed in utility vehicle.*

The project transfers space technology to terrestrial use via nontraditional partners, and it provides power system data valuable for future aeronautics and space applications. The work was done under the Hybrid Power Management Program, which includes the Hybrid Electric Transit Bus. The Avionics, Power and Communications Branch of Glenn's Engineering Systems Division initiated the Hybrid Power Management Program for the Technology Transfer and Partnership Office. The program is the innovative integration of diverse, state-of-the-art power devices in an optimal configuration for space and terrestrial applications. The appropriate application and control of the various power devices significantly improves overall system performance and efficiency. Applications include power generation, transportation systems, biotechnology systems, and space power systems.

The basis of this project is a dedicated state-of-the-art electric utility vehicle. A unique aspect of the project is the use of hydrogen-powered proton-exchange-membrane (PEM) fuel cells as the primary power source. There are large transient loads associated with electric vehicles that require a very large primary energy source, or an energy storage system. The energy storage system can consist of devices such as batteries, flywheels, or ultracapacitors. State-of-the-art symmetric ultracapacitors were used for this application. Ultracapacitors are ideal for applications such as electric vehicles where long life, maintenance-free operation, and excellent low-temperature performance are essential. The ultracapacitors were interconnected in an innovative configuration to minimize interconnection impedance. The combination of PEM fuel cells and ultracapacitors provides a power source with excellent energy and power density.

Large transient loads shorten the life of PEM fuel cells significantly, but using ultracapacitors in conjunction with PEM fuel cells reduces the transients applied to the fuel cell and lengthens the life of the cells appreciably.

Another unique aspect of the project is the use of metal hydride hydrogen storage. Hydrogen is traditionally stored as a compressed gas or as a cryogenic liquid. Both of these storage methods have shortcomings that present problems for the use of hydrogen as a ubiquitous fuel gas. Hydride hydrogen is a safe, efficient, low-pressure solid form of hydrogen.

Innovative features, such as multiple power sources and regenerative braking through ultracapacitor energy storage, are planned. Regenerative braking recovers much of the kinetic energy of the vehicle during deceleration. The fuel-cell-powered utility vehicle can provide excellent performance, and the implementation of fuel cells in conjunction with ultracapacitors in the power system can provide significant reliability and performance improvements.

**Bibliography**

Eichenberg, Dennis J.: Baseline Testing of the Club Car Carryall With Asymmetric Ultracapacitors. NASA/TM—2003-212705, 2003. http://gltrs.grc.nasa.gov/cgi-bin/GLTRS/browse.pl?2003/TM-2003-212705.html

Eichenberg, Dennis J.: Baseline Testing of Ultracapacitors for the Next Generation Launch Technology (NGLT) Project; Revised. NASA/TM—2004-213344/REV1, 2005. http://gltrs.grc.nasa.gov/cgi-bin/GLTRS/browse.pl?2005/TM-2004-213344-REV1.html

Eichenberg, Dennis J.: The Fuel Cell Powered Club Car Carryall. NASA/TM—2005-214024, 2005. http://gltrs.grc.nasa.gov/cgi-bin/GLTRS/browse.pl?2005/TM-2005-214024.html

**Glenn contact:**
Dennis J. Eichenberg, 216–433–8360, Dennis.J.Eichenberg@nasa.gov

**Author:**
Dennis J. Eichenberg

**Headquarters program office:**
Aeronautics Research

**Programs/Projects:**
Exploration Systems

## Versatile Modular Modeling Framework Completed and Validated for Multibody Mechanics

Recent developments in advanced concepts of space power and vehicle control subsystems at the NASA Glenn Research Center motivated the formulation of a modeling framework for assessing the performance of subsystems and their potential disturbances on the main system, such as the spacecraft or space vehicle, especially those due to rotating machinery and actuators. The framework is a simulation template (e.g., see the diagram on the next page) for modeling subsystems, vehicle motions, and their mutual interactions implemented as modularized functional interfaces. This is an efficient way to build up models in an orderly fashion to different levels of complexity for different phases of the conceptual design of components and systems, as well as for hardware and control developments.

The simulation framework includes a reliable, reduced-order model of rotor dynamics and other parametric models of different types of passive or actively controlled bearings. These models effectively represent rotor stability and the control of rotating machinery in a wide range of applications. In addition, they can simulate rotor dynamics as relative motions, allowing for large angular displacements or linear displacements of the carrying vehicle, such as in spinning or docking maneuvers.

In spite of various simplifications made on component models or the use of simple functional parametric representations for subsystems, actuators, or support-structures compliance, accurate simulation results with such models can be achieved with test data. A part of this model had been used for real-time monitoring and for active compensation for rotor or bearing imbalance. An adaptive scheme to compensate for rotor imbalance and sensor distortions based on that model significantly improved the robustness and performance of magnetic-bearings control for flywheels (ref. 1). This framework had been thoroughly validated on various test-rig models, including a rotor on gas-foil bearings of a closed-Brayton-cycle power-conversion unit (see the photograph on the next page) tested to its top speed of 65,000 rpm on a base suspended with cables. The model validation results for this challenging case matched well with test data on both the time-domain and frequency-domain (refs. 1 and 2).

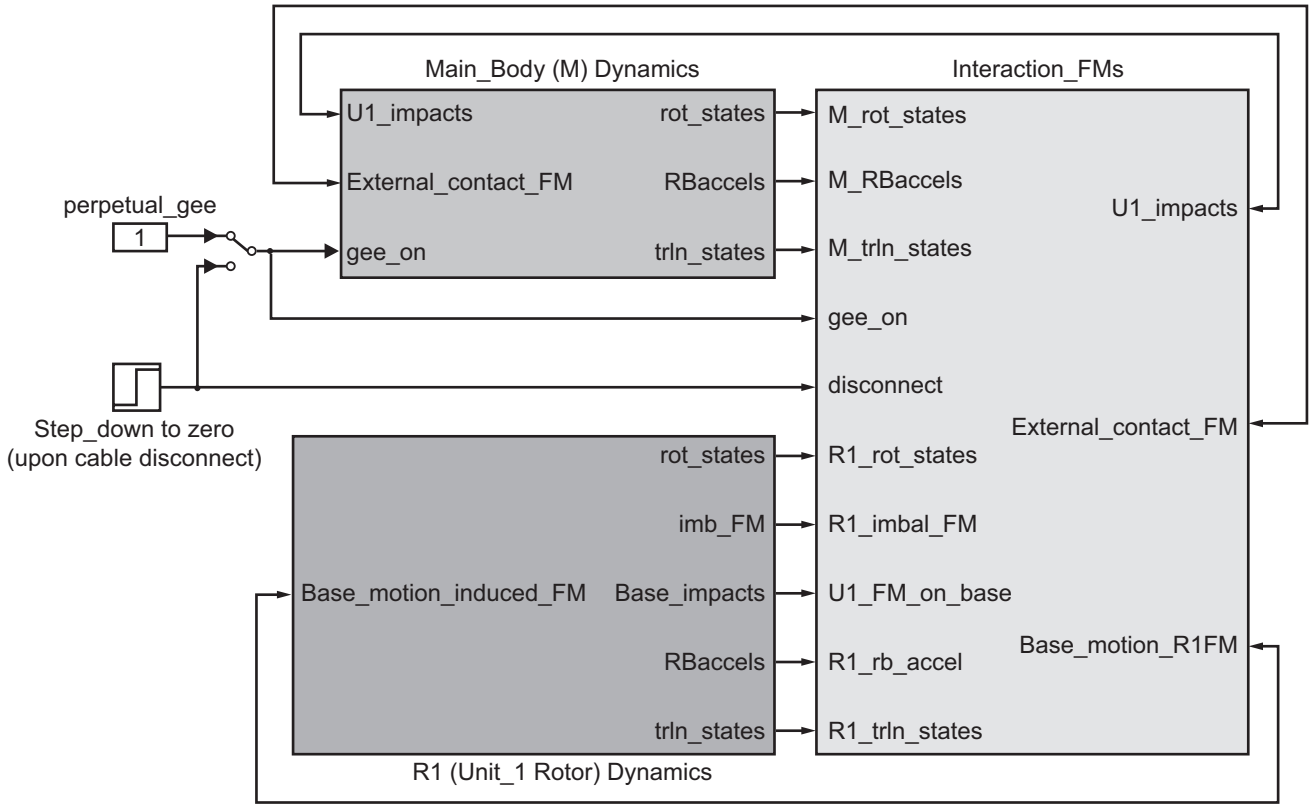


*Top level simulation diagram illustrating the modular modeling framework as applied to a flexible body (whose dynamics are represented in the box "Main_Body (M)") carrying a rotor unit (shown in "R1 (Unit1_Rotor)"). The dynamics of "M" and "R1" and their interactions ("Interaction FMs") are dependent on whether "M" is grounded or in free fall ("gee_on" is 1 or 0, respectively).*

This versatile, reduced-order modeling framework is useful for system stability analysis, vibration prediction, and control stability verification, such as in the future development of systems and subsystems for the Crew Exploration Vehicle. It can also be tailored for real-time hardware-in-the-loop simulations for system analyses and developments.

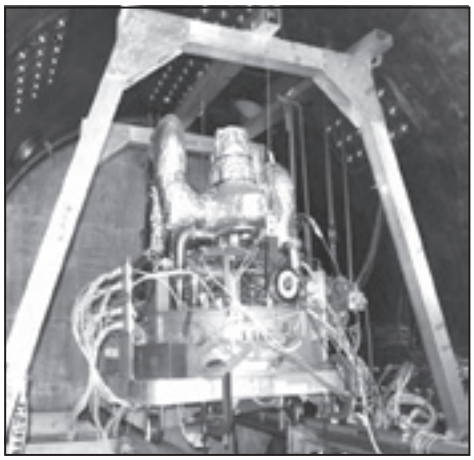

*Test rig for model validation with a high-speed, closed-Brayton-cycle power-conversion unit operated on a base suspended by cables for vibration isolation.*

**References**


1. Le, D.K.: A Versatile Reduced-Order Model for Rotating Machinery Vibration Monitoring and Control. Internal document, available from the Diagnostics and Data Systems Branch, NASA Glenn Research Center, 2005 (to be published as a NASA TM).
2. Ludwiczak, Damian R., et al.: Validation of a 2 kWe Closed-Brayton-Cycle Power Conversion System Mechanical Dynamics Model. Space Technology & Applications International Forum, Albuquerque, NM, Feb. 2005.



**Glenn contact:**
Dr. Dzu K. Le, 216–433–5640, Dzu.K.Le@nasa.gov

**Author:**
Dr. Dzu K. Le


**Headquarters program office:**
Exploration Systems

**Programs/Projects:**
CLV, CEV

# Acoustic Emission Verification Testing of Fluids and Combustion Facility Flight Racks Conducted at Glenn's Acoustical Testing Laboratory

NASA Glenn Research Center's Acoustical Testing Laboratory (ATL) provides a comprehensive suite of acoustical services for developers of science experiments manifested for the International Space Station. Since the ATL's opening in September 2000, its primary customer has been the Fluids and Combustion Facility (FCF), a two-rack microgravity research facility developed at Glenn. In support of FCF's low-noise design effort, the ATL provided acoustic emissions testing of sound-source components, subassemblies, and partially populated racks. The iterative design and test process enabled the FCF acoustics team to understand and continually track the acoustic emissions of components and subassemblies as they were successively incorporated into higher level hardware packages. This effort culminated in the final acoustic emission verification tests on the FCF Combustion Integrated Rack and Fluids Integrated Rack in the spring of 2005.

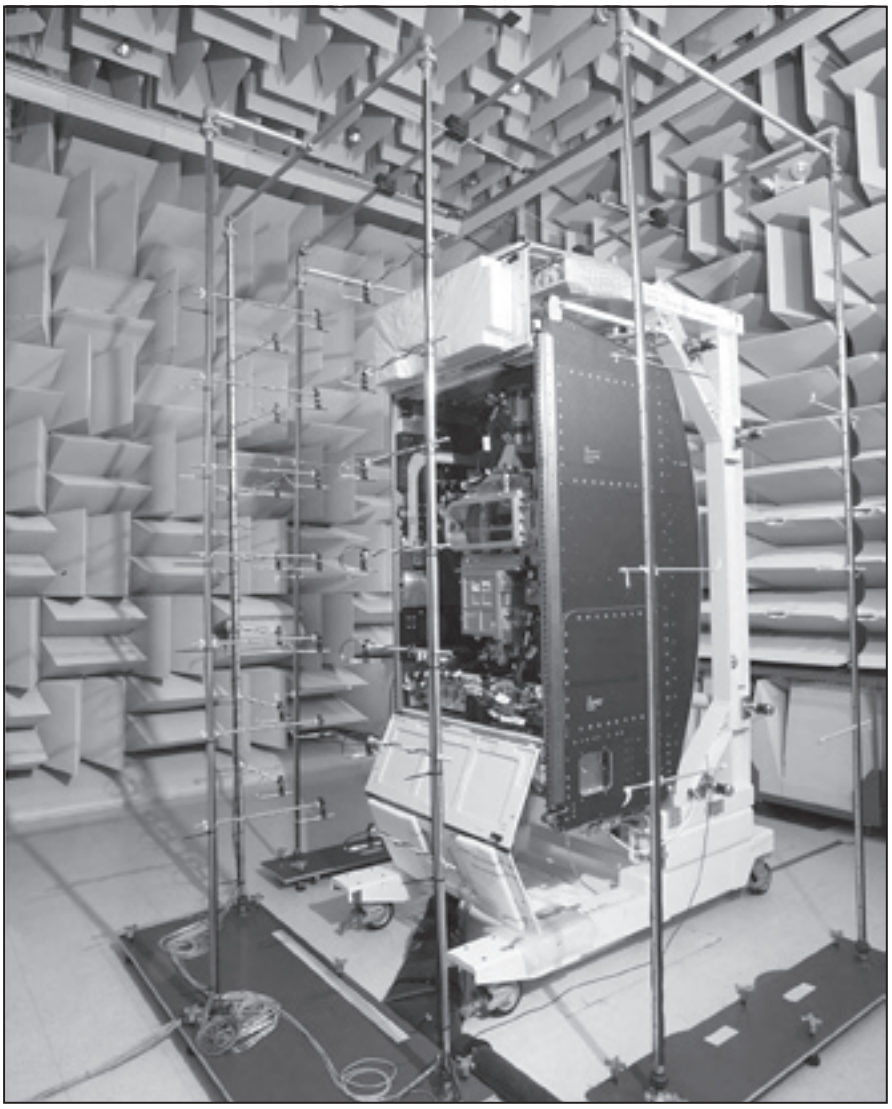

*Fluids Integrated Rack of the FCF, shown with front microphone array during acoustic emissions verification testing in Glenn's ATL.*

The primary objective of these tests was to determine the acoustic emissions of the racks so that they could be compared with the limits specified in NASA SSP 57000 (ref. 1) for both continuous and intermittent acoustical noise. The secondary objective of these tests was to provide data to support test-correlated analytical acoustic models of the racks that could be used to accurately assess the predicted acoustic emissions of Combustion Integrated Rack and Fluids Integrated Rack configurations after future on-orbit modifications.

The SSP 57000 requirements provide little guidance in the way of measurement methodology or measurement uncertainty. ATL staff selected the procedures and uncertainty estimates in ISO 11201 (ref. 2) as the method for sound pressure level determination because ISO 11201 standardizes many of the elements of NASA SSP 57000. ATL's preparation for the rack-level acoustic emissions verification tests spanned a 2-year period and involved the development of detailed procedures for testing in accordance with ISO 11201. This included the implementation of two stationary microphone arrays, which represented the optimum accommodation of the maximum number of microphones and data channels available, the desired level of measurement accuracy, and the total amount of testing time available.

The ATL's ISO 17025-compliant quality system is accredited by the National Voluntary Laboratory Accreditation Program (NVLAP Code 200557–0) for sound power level testing per ISO 3744 and

ANSI S12.54 and is the only NVLAP-accredited acoustical testing laboratory in NASA. In December 2004, the ATL became the only laboratory in the United States to receive accreditation for ISO 11201.

**Find out more about Glenn's Acoustical Testing Laboratory:**
http://www.grc.nasa.gov/WWW/AcousticalTest/

**References**


1. Pressurized Payloads Interface Requirements Document. International Space Station Program, NASA SSP 57000 Rev. G, Sept. 2003.
2. Acoustics—Noise Emitted by Machinery and Equipment—Measurement of Emission Sound Pressure Levels at a Work Station and at Other Specified Position—Engineering Method in an Essentially Free Field Over a Reflecting Plane. First ed., ISO 11201, 1995.



**Glenn contact:**
Beth A. Cooper, 216–433–3950,
Beth.A.Cooper@nasa.gov

**Authors:**
Beth A. Cooper and Paul J. Passe


**Headquarters program office:**
Space Operations

**Programs/Projects:**
FCF

# NASA HEADQUARTERS PROGRAM OFFICES

Aeronautics Research

Exploration Systems

HSRT—Human System Research and Technology

In-Space Propulsion

NESC—NASA Engineering Safety Center

Office of Safety and Mission Assurance

Office of Space Flight

Orbiter Project Office

Science Mission

Space Exploration

Space Operations

Space Shuttle

TTPO—Technology Transfer and Partnership Office

Vehicle Systems

VSP—Vehicle Systems Program

# PROGRAMS AND PROJECTS

Advanced communications, navigation, and surveillance architectures and system technologies

Advanced EVA—Advanced Extravehicular Activities

Advanced Space Technology

Advanced Systems and Technology Program

AEFT—Alternate Energy Foundation Technologies

AFCPS—Aircraft Fuel Cell Power Systems

AFFT—Alternate Fuels Foundation Technologies

Applications where electric propulsion is used

ASTP—Advanced Space Transportation Program

Aviation Safety

BEGIN—Bioscience and Engineering Glenn Initiative

CEV—Crew Exploration Vehicle

CLV—Crew Launch Vehicle

Columbia Accident Investigation

Constellation Systems

Cross-Enterprise Technology Development

CVCCE—Constant Volume Combustion Cycle Engine

Deep space robotic science exploration missions

Discovery

Earth Science

Electric Propulsion

Energetics

Energetics Legacy Program

Energy Storage Project

ESR&T—Exploration Systems Research and Technology

Europa Lander

Exploration Systems

Exploration Technology Development Program

FCF—Fluids and Combustion Facility

Future Propulsion Systems Research

Glenn's IR&D—Glenn's Independent Research & Development

GMI—Glennan Microsystems Initiative

High-conductivity, low-weight applications such as electromagnetic shielding enclosures and ground planes

HSR—High-Speed Research

Human Health and Performance

ICP—Intramural Call for Proposals

In-Space Systems

Ion propulsion

IR&D—Independent Research & Development

ISS—*International Space Station*

JWST—James Webb Space Telescope

LEAP—Low Emissions, Alternative Power Project

Life Support & Habitation

Low-emission combustors

Lunar landers

Mars orbiters and landers

Microgravity Science

Mission Operation and Integration

MTLAMPS—Advanced Mechanisms and Tribology Technologies for Durable Lightweight Actuation and Mechanical Power Transmission Systems

National Reconnaissance Office Director's Innovation Initiative

NEDT—NASA Engineering Design Team

NEPAG—NASA Electronic Parts Assurance Group

NEPP—NASA Electronic Parts and Packaging

NESC—NASA Engineering Safety Center

New Frontiers

NGLT—Next Generation Launch Technology

Nuclear power systems for electric propulsion or surface power

Nuclear Radioisotope Power System Development

Nuclear Technology and Demonstration

Orbiter Rudder/Speed Brake Gear Margins Independent Technical Assessment

Power, Propellants, and Chemical Systems

Power Systems R&T

Project Prometheus

Prometheus Nuclear Systems and Technologies project

Propulsion and Power

Propulsion 21

QAT—Quiet Aircraft Technology

RAC—Revolutionary Aeropropulsion Concepts

RASER—Revolutionary Aerospace Engine Research

Revolutionary System Concepts for Aeronautics

Rotorcraft

RPS—Radioisotope Power Systems

R&T—research and technology

RTF—Return to Flight

Satellite Missions

SBIR—Small Business Innovation Research

SCDS—Space Communications and Data Systems Project

Science Mission

Shuttle Orb□

Shuttle Project Office

Space Operations Mission Directorate

Space Shuttle

Space Shuttle Orbiter

Spacecraft Propulsion

SRG110—Stirling Radioisotope Generator 110

TTPO—Technology Transfer and Partnership Office

UEET—Ultra-Efficient Engine Technology

UltraSafe—Ultra Safe Propulsion

Vehicle Systems

VSP—Vehicle Systems Program

# INDEX OF AUTHORS AND CONTACTS

Both authors and contacts are listed in this index. Articles start on the page numbers following the names.

# REPORT DOCUMENTATION PAGE

*Form Approved*
*OMB No. 0704-0188*



| 1. AGENCY USE ONLY (Leave blank) | 2. REPORT DATE | 3. REPORT TYPE AND DATES COVERED |
|---|---|---|
| | May 2006 | Technical Memorandum |

**4. TITLE AND SUBTITLE**

Research & Technology 2005

**5. FUNDING NUMBERS**

None

**6. AUTHOR(S)**

**7. PERFORMING ORGANIZATION NAME(S) AND ADDRESS(ES)**

National Aeronautics and Space Administration
John H. Glenn Research Center at Lewis Field
Cleveland, Ohio 44135–3191

**8. PERFORMING ORGANIZATION REPORT NUMBER**

E–15297

**9. SPONSORING/MONITORING AGENCY NAME(S) AND ADDRESS(ES)**

National Aeronautics and Space Administration
Washington, DC 20546–0001

**10. SPONSORING/MONITORING AGENCY REPORT NUMBER**

NASA TM—2006-214016

**11. SUPPLEMENTARY NOTES**

Responsible person, Cynthia L. Dreibelbis, organization code X, 216–433–2912.

**12a. DISTRIBUTION/AVAILABILITY STATEMENT**

Unclassified - Unlimited
Subject Categories: 01 and 31

Available electronically at http://www.grc.nasa.gov/WWW/RT/
This publication is available from the NASA Center for AeroSpace Information, 301–621–0390.

**12b. DISTRIBUTION CODE**

**13. ABSTRACT (Maximum 200 words)**

This report selectively summarizes NASA Glenn Research Center's research and technology accomplishments for fiscal year 2005. It comprises 126 short articles submitted by the staff scientists and engineers. The report is organized into three major sections: Programs and Projects, Research and Technology, and Engineering and Technical Services. A table of contents and an author index have been developed to assist readers in finding articles of special interest. This report is not intended to be a comprehensive summary of all the research and technology work done over the past fiscal year. Most of the work is reported in Glenn-published technical reports, journal articles, and presentations prepared by Glenn staff and contractors. In addition, university grants have enabled faculty members and graduate students to engage in sponsored research that is reported at technical meetings or in journal articles. For each article in this report, a Glenn contact person has been identified, and where possible, a reference document is listed so that additional information can be easily obtained. The diversity of topics attests to the breadth of research and technology being pursued and to the skill mix of the staff that makes it possible. For more information, visit Glenn's Web site at http://www.nasa.gov/glenn/. This document is available online (http://www.grc.nasa.gov/WWW/RT/). For publicly available reports, visit the Glenn Technical Report Server (http://gltrs.grc.nasa.gov).

| 14. SUBJECT TERMS | 15. NUMBER OF PAGES |
|---|---|
| Aeronautics; Aerospace engineering; Space flight; Space power; Materials; Structures; Electronics; Space experiments | 212 |
| | 16. PRICE CODE |

| 17. SECURITY CLASSIFICATION OF REPORT | 18. SECURITY CLASSIFICATION OF THIS PAGE | 19. SECURITY CLASSIFICATION OF ABSTRACT | 20. LIMITATION OF ABSTRACT |
|---|---|---|---|
| Unclassified | Unclassified | Unclassified | |